

POLITECNICO DI TORINO



Tesi Magistrale

**Development and testing of innovative solar panels with deployable
structure for ARAMIS satellite platform**

Tutor

Prof. Leonardo M.Reyneri

Author

Giuseppe Bruni

March 2016

Acknowledgements

First of all, I express my most heartfelt gratitude to my supervisor Professor Leonardo M. Reyneri. It is said that we are the result of all the experiences that we have lived, and the experience in the ARAMIS team, beside the Professor Reyneri was for me, an important opportunity for professional growth and a strong impetus to continue the work in the space field. It is from people like the Professor Reyneri that I have received the most important gift that a student can receive from a teacher, the knowledge, the art of using the tools provided by science to do engineering. A study period is also possible if you approach it in a serene environment and full of motivations. In this regard, my deepest thanks go to my family, to my parents who have supported me and motivated during my college studies. To my irreplaceable and splendid sister and to my great friends also I extend my most sincere thanks, because it is thanks to them that the moments of the hardest studies they were able to lighten up and have been dealt with more safety and tranquillity.

Torino, March 11th, 2016

Giuseppe Bruni

Summary

The small satellites like the ARAMIS platforms [1] are solutions growing low cost and small size, to realize several kind of satellite applications. The ARAMIS is a new approach to the CubeSat designing. It is characterized by the particular designing of the side faces of a CubeSat. These implement PCB boards that realize all the basic features of a satellite platform as reaction wheels, magnetorquer, power management systems and so on. Thus, the PCBs represent also the physical tiles of the lateral faces of the CubeSat. In this way the inner space of the CubeSat will be completely employed all to accommodate a payload. The ARAMIS systems are based on a completely modular approach. All tiles are designed to be easy assembled with interfaces of interconnections realised in standard way. An ARAMIS structure can also be implemented using different format of CubeSat as 1U, 2U, 3U [1], or other more complex formats as the 2x2x2U [1]. They are able to bring on board, payloads like small telescopes or cameras, antennas, remote sensing instruments, small radios telescopes and so on. Many of these payload applications are characterized by a high working power consumption. Just think a remote sensing application that uses ecodoppler techniques to trace the altimetry profile of the earth surface or atmospheric moisture and ionization ones. These instruments usually require high power transmitters and receivers equipment, in order to send and receive the eco signal. So, for these particular high power instruments the only outer tile surfaces of a 1U ARAMIS CubeSat, cannot be large enough to mount a number of solar panels able to provide enough power to the payloads and the satellite subsystems. Furthermore there are situations where the radiation efficiency of the sun is low. It is the case of a space mission much farther from the sun.

So, in all these situations where a large surface of solar arrays needs, they are very useful the arrays of solar panels mounted on deployable mechanicals structures that at launch, for reasons of space, are closed filling a small space. Once in orbit, the structure is deployed increasing the total satellite surface exposed to the sun. In this way, more surface of solar panels can produce more power to supply high power consumption applications.

The main application of the deployable structures is for use in space. Launch vehicles are limited in space and every other kilogram of weight added represents a problem for the launch, mainly in terms of costs. Since a space application is characterised by the not possibility to repair a system, the high cost of a failure leads the space industry to be conservative in the use of its applications or devices, including deployable mechanical structures. In this way, for each for each structure of new concept, the space industry is prevented to the immediate qualification or validation the new systems.

For the market of the nanosatellites nowadays we have been realizing a large amount of deployable structures of solar panels. These structures are deployed in different ways. Generally an elastic mechanical element is used to charge a structure that is suddenly opened when sealing element is released. This is the case of the system developed for example by the Clyde Space company [2].

The designing of a deployable mechanical structure of solar panels compatible for ARAMIS platforms is the target of my work. The thesis discusses in details the mechanical and electrical design, the compatibility of the shape for ARAMIS, its simulations and tests. In addition are explained in details: how the problems of spaces are solved, the electromechanical deployment system and the choice of the employed materials. Are further provided an analysis of opening for a structure of three elements, its thermal analysis and its orbital spin analysis.

The thesis covers also the designing of a board of test for the management of the opening control for a deployable solar panels structure. A specific board is designed. The control circuit of the opening phase is designed on the outer plate element of a reaction wheel tile. In this way, this element will implements on

board also part of the mechanical system of opening of the deployable solar panels structure. The outer plate element is chosen because it is a worst case for the realization of a support tile for the deployable solar panel structure, since it has only one side that can be covered by components and it presents several holes that reduce the space for the circuits. Finally the outer plate board represents a reference model to implement the compatibility interface of the 1B111E, on others different types of ARAMIS tiles. About opening system, particular attention is done to a system of electrical thermal fusers used to detach the fixing wire that maintains the tails of the deployable structure folded during the launch and before the in orbit deployment. The last part of the discussion deals the management software of the outer plate board.

The UML is use to describe the main operation and the design phases. All main blocks are introduced with the corresponded UML class. All these classes are related to the 1B111E and the Bk1B213A1 sections of the ARAMIS project [1] of Polytechnic of Turin.

Contents

Summary.....	iii
List of Acronyms	viii
List of Figures.....	ix
List of Tables.....	xii
1 Introduction.....	1
1.1 Problem Statement	1
1.2 Proposed Solutions.....	2
1.3 Thesis Organization	3
2 Specifications.....	4
2.1 Functional Specifications.....	4
2.2 Mechanical Specifications	4
2.2.1 P-POD Compatibility	5
2.2.2 Bk1B111E20 Top and Bottom definition	8
2.2.3 Bk1B111E20 Tiles Configurations	8
2.2.4 Bk1B111E20 Solar cells configurations.....	11
2.2.5 1B111E Deployable Structure configurations.....	12
2.2.6 Bk1B111T Thermal fuser	14
2.3 Electrical Specifications	15
2.3.1 Solar Cells.....	16
2.4 Thermal & Attitude Specifications.....	20
3 Deployable Solar Panels System Architecture.....	21
3.1 1B111E Deployable Panel 1U	21
3.1.1 Bk1B111E20 Standard Tile.....	22
3.2 Bk1B213A1 Outer Plate	23
4 1B111E Mechanical Design.....	25
4.1 Introduction.....	25
4.2 Bk1B111E20 & Bk1B111E10 Design	25
4.3 Side Blocks Design	29
4.4 Hinges Design	30
4.5 Bk1B111E9 Hinges Pin Design	33
4.6 1B111E Deployment System	33
4.6.1 Springs Design.....	34
4.7 Mechanical Model.....	34
4.8 Mechanical Simulations.....	35

4.8.1	Opening Simulation	36
4.8.2	Natural Frequency	40
4.8.3	Vibrations analysis	43
5	Bk1B111E1 Electrical Design	47
5.1	Introduction	47
5.2	Bk1B111E20 connector & resistances of configuration	48
5.3	Bk1b111E1 Traces design	51
6	1B111E Thermal and Orbital Spin Analysis.....	54
6.1	Introduction.....	54
6.2	1B111E Thermal Model	54
6.2.1	Single tile Thermal Resistance	54
6.3	1B111E Thermal Analysis.....	56
6.3.1	Absorbed Radiation into the tile	56
6.3.2	Radiation sources	56
6.3.3	Thermal equilibrium equation.....	58
6.4	1B111E Thermal Simulation	60
6.5	1B111E Spin Analysis	65
7	Bk1B111T Thermal Fusers Design	69
7.1	Introduction.....	69
7.2	Sealing Wire.....	69
7.2.1	Strength Analysis	69
7.3	Bk1B111T Thermal Fuser Analysis.....	70
7.4	Bk1B111T Thermal Simulation	75
7.5	Bk1B111T Electrical Design.....	78
8	Bk1B213A1 Outer Plate board Desing.....	84
8.1	Introduction.....	84
8.2	Bk1B213A1 System Design	84
8.2.1	Bk1B4221W Tile Processor 4M.....	85
8.2.2	Analog Multiplexer	87
8.2.3	Circuit Power Management.....	87
8.3	Bk1B213A1 Power Consumption Estimation	88
8.4	Bk1B213A1 Management Software	90
8.4.1	Software Operation	90
8.4.2	Main classes.....	93
9	Chapter	97
9.1	Conclusion	97

9.2	Circuit Diagrams	99
9.2.1	1B111E1 Standard Tile PCB	99
9.2.2	1B111E2 Flex PCB	101
9.2.3	1B11110 Lateral Support PCB.....	103
9.2.4	Bk1B213A1 Outer Plate Test Board.....	105
9.3	PCB Layouts	114
9.3.1	1B111E1 Standard Tile PCB	114
9.3.2	1B111E2 Flex PCB	116
9.3.3	1B11110 Lateral Support PCB.....	116
9.3.4	Bk1B213A1 Outer Plate Test Board.....	117
9.4	Mechanical Sheets.....	119
9.5	Simulation Models of the electric components for hSPICE	129
9.6	MatLab Scripts	130
9.7	SolidWorks ARAMIS materials library.....	133
9.8	BK1B213A1 Management Software	138
9.8.1	Bk1B111X_CubeSat_Thermal_Fuser <<SW>>	138
9.8.2	Bk1B133CS_Temperature_Sensor <<SW>>	139
9.8.3	MuxControl <<SW>>.....	141
9.8.4	Bk1B213A1_main <<SW>> <<main>>	144
	Bibliography.....	149

List of Acronyms

ADC	Analog to Digital Converter
COTS	Commercial-Off-The-Shelf
FEA	Finite Element Analysis
JTAG	Joint Test Action Group
LEO	Low Earth Orbit
LV	Launch Vehicle
NTC	Negative Temperature Coefficient
OBC	On Board Computer
SAR	Synthetic Aperture Radar
SMD	Surface Mount Technology
PCB	Printed Circuit Board
PDB	Power Distribution Bus
P-POD	Poly Pico-satellite Orbital Deployer

List of Figures

Figure 1: 1B111E Functional Specifications.....	4
Figure 2: Bk1B213A Functional Specifications	4
Figure 3: 1B111E Mechanical Specifications.....	5
Figure 4: Bk1B213A Mechanical Specifications.....	5
Figure 5: Poly Picosatellite Orbital Deployer (P-POD) and cross section	6
Figure 6: ARAMIS CubeSat slide into the P-POD	6
Figure 7: P-POD cross section.....	7
Figure 8: P-POD rail cross section zoom	7
Figure 9: ARAMIS CubeSat Skeleton Tile	9
Figure 10: ARAMIS Tile Full Fixing Compatible.....	9
Figure 11: Bk1B111E20 Tiles Configurations.....	10
Figure 12: Standard tile configurations. BOTTOM side view (a) Config. A (b) Config. B (c) Config. Aw.....	10
Figure 13: Standard tile configurations. BOTTOM side view (a) Config. Af (b) Config. Bf.....	11
Figure 14: 2.2.5 Deployable Structure configurations.....	12
Figure 15: Deployable Structure configuration AAAf. Af is the last right.....	13
Figure 16: Deployable Structure Configuration Assembling Example.....	13
Figure 17: Bk1B111T (a) Cross section showing an example of tiles fixed with the wires in CuBe (b) Thermal Fuser Model.....	15
Figure 18: 1B111E Electrical Specifications.....	15
Figure 19: Bk1B213A Electrical Specifications	16
Figure 20: Single solar cell P-V characteristics.....	16
Figure 21: Current-Voltage characteristic of a single cell.....	17
Figure 22: Two solar cells connected in series (a) Schematic (b) Current and power vs voltage.....	18
Figure 23: Current and Power vs Voltage of 4 cells connected in series.....	19
Figure 24: Current and Power vs Voltage of 6 cells connected in series.....	19
Figure 25: 1B111E Thermal & Attitude Specifications.....	20
Figure 26: Deployable Solar Panels System Architecture.....	21
Figure 27: 1B111E Deployable Panel 1U.....	21
Figure 28: Bk1B111E20 Standard Tile.....	22
Figure 29: Example of standard tile with hinges already fixed (a) Bottom of the Bk1B111E12_A configuration (b) Top of the Bk1B111E12_A configuration.....	23
Figure 30: Bk1B213A1 Outer Plate.....	24
Figure 31: Bk1B111E20 Deployable Standard Tile.....	25
Figure 32: Cross section of a centre of a standard tile (a) Solar cells placed in asymmetric layout (b) Solar cells placed in symmetric layout.....	26
Figure 33: Von Mises stress plot and standard tile Bk1B11120 deformation (a) Solar cells in symmetric layout (b) Solar cells in asymmetric layout.....	27
Figure 34: Von Mises stress plot and standard tile Bk1B11120 deformation using lateral supports Bk1B111E10.....	28
Figure 35: Side Blocks elements.....	29
Figure 36: Side block (a) Example of a side block on tiles (b) Cross section of a side block on tiles.....	29
Figure 37: Side Block for base support tile.....	30
Figure 38: Types of Hinges.....	30
Figure 39: Two hinges connected between them.....	30
Figure 40: Tile Hinge (a) Mechanical locking of rotation (b) Mechanical board stop	31

Figure 41: ARAMIS side tile hinges fixing example (a) INTA & INTB (b) EXTA & EXTB	32
Figure 42: CubeSat 1U (a) 1U with 4 1B111E structures completely deployed (b) 1U 1B111E structures completely folded.....	33
Figure 43: Bk1B111E9 Hinge Pin.....	33
Figure 44: Torsion Spring scheme.	34
Figure 45: 1B111E Structure Mechanical Model.....	35
Figure 46: “Bad Opening” displacements of tails due to damping (a) Bottom tile (b) Central tile (c) Upper tile	37
Figure 47: “Good Opening” displacements of tails due to damping (a) Bottom tile (b) Central tile (c) Upper tile.....	38
Figure 48: X and Y displacements from centre of mass (a) Vertical displacement (b) Horizontal displacement.	39
Figure 49: Main frames of the opening phase.	40
Figure 50: 1B111E structure model of natural frequencies simulation (a) Top view (b) Bottom view.....	41
Figure 51: Plots of deformations exaggerated at resonance frequencies (a) Freq 1 (b) Freq 3 (c) Freq 4 (d) Freq 6 (e) Freq 7 (f) Freq 9 (g) Freq 10 (h) Freq 11 (i) Freq 13.	42
Figure 52: Standard tile model of dynamic harmonic simulation.	43
Figure 53: Vibrations stress spectrum during launch.....	44
Figure 54: Plots of deformations exaggerated at resonance frequencies (a) Freq 1 (b) Freq 4 (c) Freq 7 (d) Freq 8, 9 (e) Freq 10 (f) Freq 12, 13.....	45
Figure 55: Plot of deformation exaggerated at resonance frequency 4.	46
Figure 56: Bk1B111E1 PCB of the standard tile.....	47
Figure 57: 1B111E structure sun exposures (a) Full side exposure (b) Partial side exposure.....	47
Figure 58: Bk1B111E2 Flexible PCB.	48
Figure 59: Flexible PCB 1B111E2 connected (a) Front (b) Back.....	49
Figure 60: 1B111E Structure Power channels (a) The two channels (b) Cells connections along two channels (In Red the side of channel B).....	49
Figure 61: Flexible PCB (a) PCB folded (b) Single flexible PCB connection.....	50
Figure 62: One side power channel closed on 0 Ohm resistor.....	50
Figure 63: Cross section of a three tile structure along a points of high density of components.	51
Figure 64: PCB copper trace.	52
Figure 65: Tf of a copper trace as function of its width W.	52
Figure 66: Single tile model (a) Cross section (b) Thermal circuit model.....	55
Figure 67: CubeSat worst case of exposition to radiations in LEO orbits.....	57
Figure 68: Radiated Energy from tile.....	58
Figure 69: Radiation Model.	60
Figure 70: Orbit elevation.....	60
Figure 71: Horizon view angle.	61
Figure 72: Approximation of the distances.	62
Figure 73: Final diameter of disk.	62
Figure 74: Heating phases (a) Initial Condition (b) 1 min (c) 2min (d) 4 min (f) 8 min (g) 15 min.....	64
Figure 75: Temperature profile in the symmetric centre of the tile.	64
Figure 76: Standard tile model with two different gradient of colours between the edges (a) Single tile (b) Entire model structure	65
Figure 77: Centre of mass of a satellite with two 1B111E structure deployed.....	67
Figure 78: Time to reach ω_0 spin.	67
Figure 79: Bk1B111T Thermal Fuser.....	69
Figure 80: Thermal model structure of a fuser	71

Figure 81: Thermal circuit of the thermal fuser.	72
Figure 82: Simplification due to symmetry	72
Figure 83: Circuit reduction (a) Equivalent Norton (b) Equivalent Thevenin.	73
Figure 84: Simulation thermal model structure of a fuser.	76
Figure 85: Temperature profile of the tin of soldering.	76
Figure 86: Heating phases of the thermal fuser (a) Initial conditions (b) 2 sec (c) 10 sec.	77
Figure 87: Heating phases of the thermal fuser along the horizontal central axis (a) Initial conditions (b) 2 sec (c) 10 sec.	78
Figure 88: Driver circuit of the Thermal Fuser.	79
Figure 89: Thermal fuser circuit SPICE simulation.	80
Figure 90: Temperature control of the thermal fuser.	81
Figure 91: Thermal fuser layout.	81
Figure 92: Worst case of the temperature reached by the trace of heating due to current of the thermal fuser.	82
Figure 93: Linearization circuit of the NTC (a) Linearization circuit scheme (b) R(T) response of the NTC (c) Output response V(T) and P(T) of the linearized circuit.	83
Figure 94: Block diagram of the BK1B213A1.	85
Figure 95: Bk1B4221W Time Processor 4M V1.	85
Figure 96: Functional block of the MUX.	87
Figure 97: Final mounted system of an Outer Plate board and a 1B111E structure (a) Inner side (b) Back (c) Front.	90
Figure 98: Use Case Diagram of the Outer Plate.	90
Figure 99: Opening Phase Algorithm.	92
Figure 100: Thermal Fusers and NTC sensors classes.	93
Figure 101: MUX class.	94
Figure 102: Class of the "main()" of the software.	95
Figure 103: Outer Plate main class.	95
Figure 104: (a) Example of transversal deployment (b) Example of implantation of micro strip antennas. ...	97
Figure 105: (a) 3U CubeSat Configuration (b) 2x2x2U CubeSat Configuration.	98

List of Tables

Table 1: Simulation parameters of two cells in series.....	18
Table 2: Max output power summery table.....	20
Table 3: Torsion springs simulation parameters	37
Table 4: Natural Frequencies Simulation Details.	41
Table 5: Natural frequencies of the structure.	42
Table 6: Vibbration analysis simulation details.	44
Table 7: Resonance frequencies of the standard tile.	45
Table 8: Summery of the final result for the vibration analysis.	46
Table 9: Wire Material analysis.	70
Table 10: Parameters used for thermal fuser.	74
Table 11: MCU pin configuration.....	87
Table 12: BK1B111T total power consumption.....	88
Table 13: Alluminuim Alloy 1060.....	133
Table 14: Copper	133
Table 15: FR4	133
Table 16: Flexible PCB polymer	134
Table 17: Solar Panel Glass.....	134
Table 18: Panel Resin.....	134
Table 19: Germanium (Ge)	135
Table 20: Gallium arsenide (GaAs)	135
Table 21: Copper beryllium (CuBe) alloy 260.....	135
Table 22: Low melting temperature tin, Indalloy_1E_118°C	136
Table 23: Ceramic.....	136
Table 24: Generic Rubber	136
Table 25: Generic stiff body.....	137

1 Introduction

The 1B111E is an innovative modular and deployable structure for arrays of solar panels. It is conceived in order to be low cost using COTS components. These ones have been used for AraMiS project implementation which are low cost and easily available from the market. 1B111E is designed to be fixing compatible for different 1U ARAMIS tiles¹. Strict space, size and weight requirements have been met. The whole 1B111E deployable solar panels structure is completely modular, each tile array can be composed by different number of deployable tiles but since there are limits of size for the P POD module [3], the 1B111E is intended as a structure composed of three tiles in 1U format. For this reason the 1B111E is simulated and tested for a structure of maximum 3 tiles.

The entire structure starts folded on launch, in this way it is charged by mechanical elastic elements. Once deployed in orbit, the mechanical opening is performed by the melting of the tin soldering for the sealing wires, by means of thermal fusers. Once the deployable solar panels structure is fixed to an ARAMIS CubeSat side tile and an appropriate hinge based system is employed to deploy the array of tiles.

The standard tiles are called Bk1B11120 and each of them have the both sides covered by two solar cells such as GaAs CESI-TJ-CTJH-SolarCell-70x40 with an efficiency of 26%. Each tile has a symmetric PCB layout and they can be connected to each other according to a configuration of the tile and according to a configuration of the structure of tiles. Each configuration is designed in order to have two different power channels, one for each side. In this way for each one, all panels are connected together in a single power channel. The two channels are useful because only one side at a time can be exposed to sun then the panels in shadow would represent a loss due to the drops voltage of the diodes. A double side covered by solar panels gives in particular the possibility to maintain a spin constant for a continuous pointing of the earth surface, just because at least one side of solar panels will be always sunlit.

The Weight of each tile is kept low, using a thin board tile and lightweight materials for the mechanical parts.

The thermal fusers for the opening are designed on the outer plate tile of a reaction wheel side tile, called Bk1B213A. This represent a model for all types of tiles that have to be compatible with the 1B111E structure. So, an ARAMIS CubeSat side tile that has to be designed in order to be compatible to the 1B111E, has to implement thermal fusers, and these have to be compliance to a specific layout for the external side. On the same outer plate board, it is implemented the management circuit of the opening phase. It is microcontroller based. The controller manages the thermal fusers, controlling that they do not cause problems for the other components.

For the purpose of this thesis, the Bk1B213A outer plate represents the base tile where a deployable solar panel structure 1B111E will be fixed. It is chosen the outer plate element because it is a possible tile element that will mount the deployable solar panels structure. It is also a worst case of realization, because the outer plate board will be covered by a large number of alignment holes with one side almost completely covered by a ring of a magnetic circuit. This ring reduces further the area that can be covered by the electric components.

1.1 Problem Statement

The main goal of the thesis is the design and implementation of the deployable solar panels structure 1B111E. It is modular and fully compatible for the 1U ARAMIS tiles. Another target is the reduction of the weight, cost

¹ A 1U tile is a standard tile of size 98x82,6 mm, thus in all the discussion of the thesis the 1U is related to this format.

and especially the space occupation in such a way to allow insertion inside the P POD module [3] without any problems. The deployable structure should meet requirements of the mechanical deployment and of the stress of vibration for the launch intents.

Another part of the thesis covers in details the electronic opening system of the deployable solar panels structure. The electronic opening system will be designed following several requirements, as the avoiding to the detachment of small parts into orbit and the achieving high temperatures by the fusers. An ARAMIS side tile for a 1U CubeSat is also designed and implemented, the Bk1B213A. This one is the outer plate of a reaction wheel module. It should embed part of the deployable solar panels opening system, the electronic opening system, and the opening control circuit. So the outer plate represents a reference layout for all tiles that want to be compatibles with the 1B111E deployable solar panels structure. The management software of the Bk1B213A is finally introduced in section 9.8.

Analysis mechanical, thermals, of spin and simulations in space environment are described into the chapters. Are also described studies of opening, vibrations analysis and simulations in launch environment.

1.2 Proposed Solutions

The 1E111E deployable structure is designed starting from ARAMIS type platform. So it follows its approach of scalability and modularity. It is an assembling of several reconfigurable Bk1B111E20 standard tiles, they are different only for configuration. They are assembled together in such a way to compose a deployable solar panels structure able to be fixed on a compatible 1U ARAMIS standard tile (98x82,6 mm). A complete 1B111E structure of three Bk1B111E20 tiles, exposes two different sides of solar arrays, each of them represent a single electric power channel. The Bk1B111E20 tiles of the deployable solar panels structure is designed using COTS component selected on the basis of minimum dimensions, less weight and lower price. These components obviously are chosen in order to guarantee its working conditions under proper safety margins to allow safe operations in the harsh space environment. Mechanical elements like hinges, pins, the Bk1B111E1 boards, the sealing wires are chosen using lightweight but strong materials taking into account their young module and tensile strength for stress issues. Their shapes instead are designed taking into account their deformations for vibrations issues during launch. The tensile strength is particular important for the sealing wires because during launch these must have enough tensile strength to withstand high acceleration and vibrations caused by the launch vehicle.

Since the 1B111E structure starts folded, mechanical springs are employed to maintain the structure in charge. The base of the sealing wires is represented by the external side ARAMIS tile on which the deployable solar panels structure is mounted. This tile has to be compatible with the 1B111E structure and in this thesis, the Bk213A Outer Plate board of a reaction wheel tile is designed just for this purpose.

The thesis is enriched with a management software designed for the management of the circuit of the Bk1B213A. It is written in C++ and it is designed taking into account its possible implementation in a real mission situation, where the commands are received from a ground station to open the 1B111E structure.

The whole structure is analysed and simulated using Solid Works Tools. The tool Flow Simulation is used especially for Thermal analysis: transient and at steady state. The Studies tools instead are used for motion, natural frequencies and vibrations analysis. With respect the calculation mode, the simulations in Solid Works use FEA (Finite Elements Analysis) algorithms that provide a reliable numerical technique for analysing engineering designs. The simulation approach followed is based on continues iteration between analytic computations and the simulation results. In this way the simulations are meticulously verified and validated with a matching with analytics analysis. This approach is widely used between the numeric engineers and allows to validate the simulation models. This validation is useful in case of small variations in the project: if small changes are dome to the design, the analysis of the system behaviour can be performed in fast way by means of its simulation model validated, avoiding the performing again of all analytics computations. All the

features of the SolidWorks tools and the deployable solar panels structure models used are described in details in the followings chapters. For the Flow Simulation Tool, the main guide is followed [4]. A reference guide of tutorials is also used [5]. About the tools of the Studies, all information are taken by SolidWorks online guide [6].

In the various analysis that are proposed, the MatLab software it is employed to make calculations and to get plot diagrams. All scripts are attached to the final chapter.

1.3 Thesis Organization

This thesis will deal with the design and development of the 1B111E deployable structure of solar panels for ARAMIS platform. The Mechanical aspects, those electrical and of space, are described and analysed using also tools of simulations by SolidWorks. An electronic opening system is also designed and the Bk1B213A ARAMIS side tile of a reaction wheel is further developed in order to embed the electronic opening system, the sealing interface of the 1B111E structure and its opening control circuit that is based on a set of thermal fusers called Bk1B111T.

Chapter 2 deals all the specifications of the 1B111E and the Bk1B213A1. All the specifications are divided into categories and category of specifications is divided between the 1B111E and the Bk1B213A1 specifications separated. Functional, Mechanical, Electrical, Thermal and Spin specifications are considered. The specifications of the 1B111E and Bk1B213A1 are enumerated separately.

Chapter 3 deals the initial description of the Complete System Architecture, composed by the two main arguments of the thesis, the 1B111E and the Bk1B213A1. The UML is used to describe the system.

Chapter 4 deals with the mechanical design and the analysis of a 1B111E structure, composed of three tiles. After a first overview, will be described all mechanical design aspects and will be provided a study of opening completed by a simulation. A mechanical simulation for the natural frequencies investigation will be provided. Finally it is performed a dynamic vibration study, to estimate the behaviour of the structure to the launch accelerations.

In Chapter 5 is discusses of the electrical design of the 1B111E structure. The Spice simulation and the circuit analysis will be provided.

Chapter 6 deals the thermal analysis of the system. Thermal simulations are provided in order to enhance the prediction of the thermal behaviour in orbit. In chapter is further provided the spin analysis in orbit. This is done in order to estimate how much the system is affected by the radiation pressure.

Chapter 7 is dedicated to the Bk1B111T design. Thermal models of the fusers and simulations will be provided. It is also introduced and simulated the electric driver for the management of the thermal fusers.

Chapter 6 discusses the design of the Bk1B213A1 Outer Plate tail. This is an element that will compose a reaction wheel tile. The chapter deals the realization of the whole circuitry able to realize the electronic opening system and the interface where the 1b111E structure will be connected. For the same tile it is developed the management software.

Chapter 7 contains the conclusions of the thesis work, and all the technical sheets, the PCBs layouts, the MatLab scripts used, the various libraries used for SPICE and SolidWorks simulators and the firmware code of the Bk1B213A1.

2 Specifications

This chapter deals the main specifications for the 1B111E and the Bk1B213A designed. These are related to the implementation of the systems on a 1U CubeSat satellite. In order to better describe all specifics and the requirements met, in the following paragraphs the specifics are divided for categories and are listed using simple tables. Special sub-paragraphs are used to describe specifications that need more details to be described.

2.1 Functional Specifications

The functional specifications involves all the specifics related to the functional operations of the 1B111E deployable structure and the Bk1B213A Outer Plate. The table Figure 1 shows the functional specifics of the 1B111E. The table Figure 2 shows the functional specifics of the Bk1B213A.

Functional specifications of the 1B111E.		
Enumeration of specification	Specification Type	Specification
1	Functional	The 1B111E can be composed with a maximum number of Bk1B111E20 tiles of 3. This for P-POD standard compatibility.
2	Functional	The 1B111E is capable to deploy a structure of three Bk1B11120.
3	Functional	The Bk1B11120 tiles of the 1B111E can be realise implementing different types of devices or system applications, from solar cells to systems of antennas.
4	Functional	The Bk1B111E20 tiles can be mounts two GaAs CESI-TJ-CTJH-SolarCell-70x40 for each side.
5	Functional	The 1B111E System can be composed with a hybrid composition of Bk1B111E20 tile implementing different applications.

Figure 1: 1B111E Functional Specifications.

Functional specifications of the Bk1B213A.		
Enumeration of specification	Specification Type	Specification
1	Functional	The Bk1B213A1 is software programmable.
2	Functional	The Bk1B213A1 can mounts 8 thermal fusers Bk1B111T.
3	Functional	The Bk1B213A1 is software compatible with the ARAMIS project specifics.

Figure 2: Bk1B213A Functional Specifications .

2.2 Mechanical Specifications

The mechanical specifications involves all the specifics related to the mechanical system of the 1B111E deployable structure and the Bk1B213A Outer Plate. The table Figure 3 shows the mechanical specifics of the 1B111E. The table Figure 4 shows the mechanical specifics of the Bk1B213A.

Mechanical specifications of the 1B111E.		
Enumeration of specification	Specification Type	Specification
6	Mechanical	The Bk1B111E20 has size of 98x82.6x0.4mm, compatible with a standard of a 1U format.
7	Mechanical	The 1B111E can be folded into space of thickness less than 5mm.

8	Mechanical	The 1B111E is deployed in accordion way.
9	Mechanical	The 1B111E deployment occurs in longitudinal way and is deployed in perpendicular way respect the face surface of the Bk1B213A1 base tile.
10	Mechanical	The opening of the 1B111E occurs in less than 5 second.
11	Mechanical	The hinges, the pin and the side blocks are made in Copper material
12	Mechanical	The hinges, the pins and the side block are mounted by soldering of tin, on the specifics pads.
13	Mechanical	Specifics hole of alignment are present on the Bk1B111E20 tile for the side blocks and the hinges.
14	Mechanical	The maximum strength of the sealing wires is about 700 N.
15	Mechanical	The 1B111E is robust to the spectre of vibrations of launch for the ESA and Dnepr standards.
16	Mechanical	The 1B111E structure has a natural critical frequency located around the 528Hz, with a considered modal damping for the structure of 0,04.
17	Mechanical	The hinges have a mechanical stops tab.
18	Mechanical	A Bk1B111E20 has an estimated weight of 25g.
19	Mechanical	A complete 1B111E structure has an estimated weight less of 100g.
20	Mechanical	A Bk1B111E20 has a symmetrical PCB layout.
21	Mechanical	The Bk1B111E10 lateral supports are soldered on the Bk1B111E20 by means of tin.

Figure 3: 1B111E Mechanical Specifications.

Mechanical specifications of the Bk1B213A.		
Enumeration of specification	Specification Type	Specification
4	Mechanical	The Bk1B213A1 has size of 98x82.6x0.4mm, compatible with a standard of a 1U format.
5	Mechanical	The Bk1B213A is fixing compatible with the shape of the Reaction Wheel Tile.
6	Mechanical	The Bk1B213A is mechanically compatible with the 1B111E deployable structure.
7	Mechanical	The Bk1B213A1 is compatible with a screw fixing with all the face types of a 1U CubeSat.
8	Mechanical	The sealing wires are soldered to the Bk1B111T by means of tin in with a melting temperature of 120C°.
9	Mechanical	Specifics hole of alignment are present on the Bk1B213A1 tile for the t type side blocks and the hinges.
10	Mechanical	The Bk1B213A1 has an inner metal ring, used for the magnetic circuit of the reaction wheel.
11	Mechanical	The Bk1B213A1 has an inner Teflon ring, used as a mechanical shim for the mounting with the inner plate tile of the reaction wheel.

Figure 4: Bk1B213A Mechanical Specifications.

2.2.1 P-POD Compatibility

The launch is a very critical stage. The failures of the CubeSat, the P-POD itself, or the hardware interface they can damage the LV (Launch Vehicle) or a primary payload and put the entire CubeSat Program in jeopardy. The P-POD ensure the safety of the CubeSat and protects the LV, the primary payload and other

CubeSats. The P-POD is a rectangular box with a door and a spring mechanism used to release the inner CubeSats.

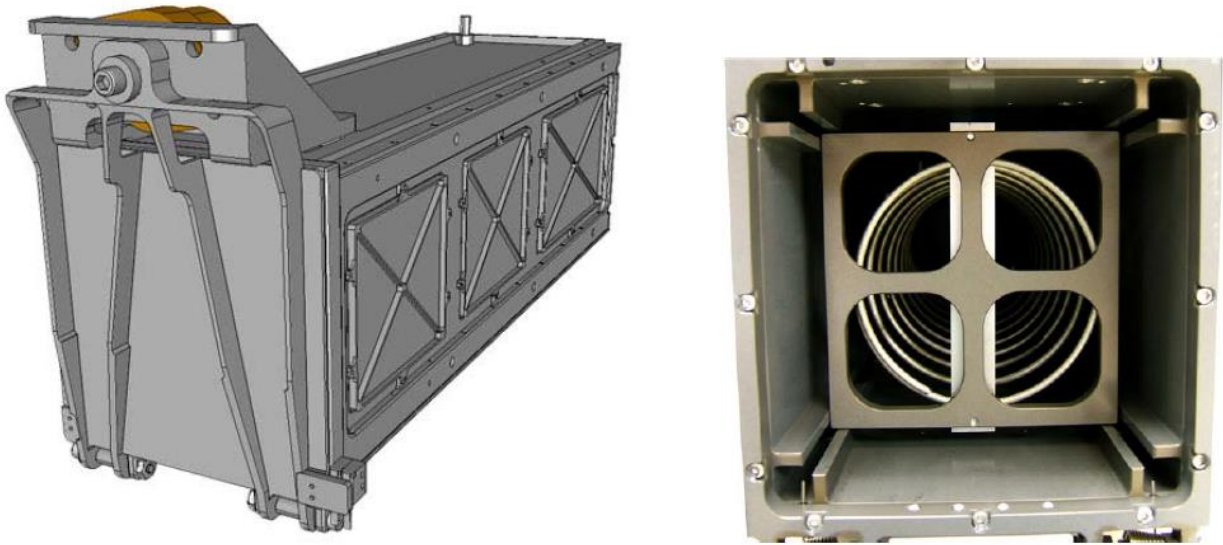


Figure 5: Poly Picosatellite Orbital Deployer (P-POD) and cross section

These ones are inserted into the box and stay closed until the launch vehicle reaches the orbital altitude and the release point. The P-POD door is opened by a signal from the LV and then the CubeSats are pushed out by a spring. They slide along a series of rails during ejection into orbit. The CubeSats shall be compatible with the P-POD to ensure safety and success of the mission. The deployable solar panles structure is designed in such a way to be entirely compatible with the P-PODs standard specifics [3]. Figure 6 shows how an ARAMIS CubeSat with four sides covered by a deployable solar panles structure of 3 tiles is inserted and slides into the P-POD.

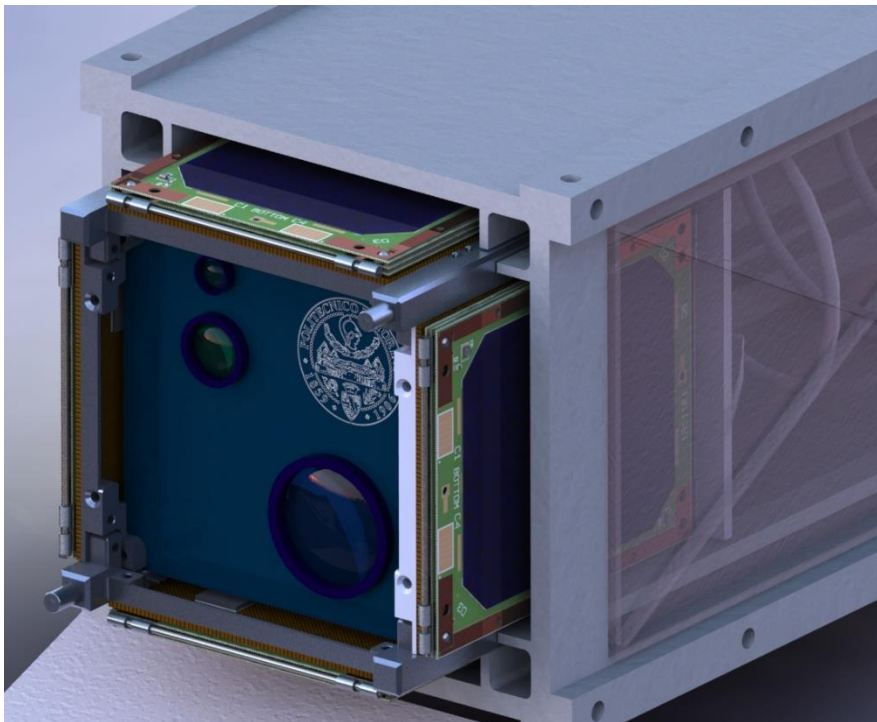


Figure 6: ARAMIS CubeSat slide into the P-POD

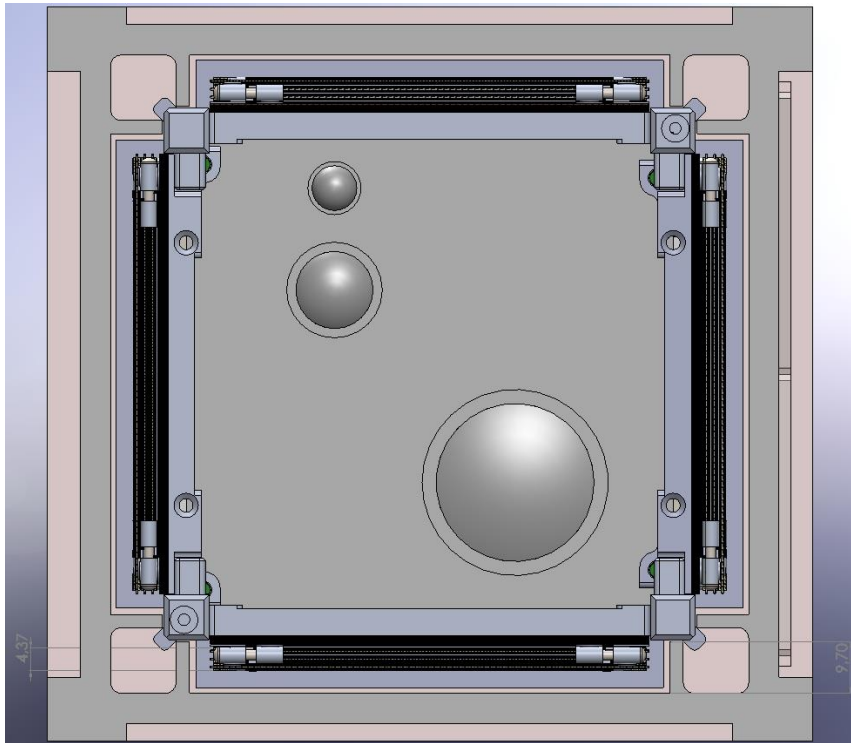


Figure 7: P-POD cross section

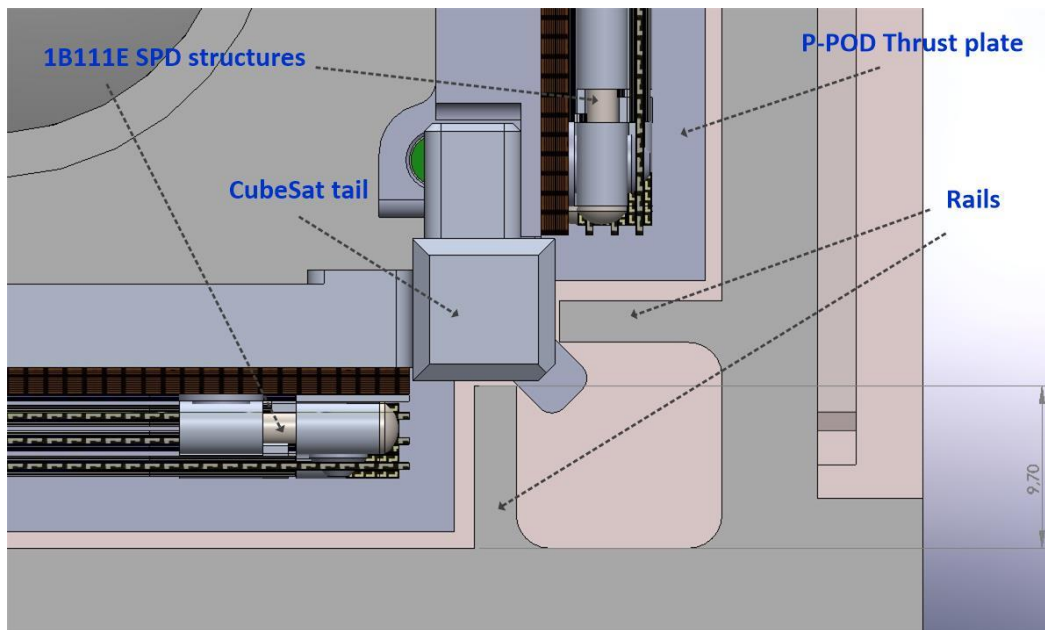


Figure 8: P-POD rail cross section zoom

The P-POD structural part that affects the deployable solar panels structure design is the space deep about 9,70mm, between two angular rails (see Figure 8). From P-POD specifics, within this space all components must not exceed the thickness of 6.5mm normal to the surface of 100mm of the CubeSat. This surface is the bottom one of a main beam of the chassis of the CubeSat. It is indicated in Figure 8 as "CubeSat tail". In Figure 7 is shown how a structure of 3 tiles folded is kept quite under 6.5mm of thickness requirement (about 5mm estimated). In this way are maintained safety margins during slipping of release.

2.2.2 Bk1B111E20 Top and Bottom definition

In order to better define the meaning of the configurations described in the paragraphs 2.2.3 and 2.2.4, it has to be defined a notation for the TOP and the BOTTOM side of the Bk1B111E20. The notation used, follows the same one used for the Bk1B111E1 PCB layouts. It means that the TOP layout of the Bk1B111E1 PCB, exactly correspond to the TOP side of the Bk1B111E20. The same is for the BOTTOM side. Appropriate labels are used on the two sides of the Bk1B111E1, to identify its relative TOP and the BOTTOM sides.

As it is also described in the section 3.1.1, the TOP side of the Bk1B111E1 has a particular meaning. It corresponds to the starting connection of the series of the BK1B111E20. The starting connection is intended as the global anode of the series of the two couple of cells mounted on a Bk1B111E20. The electric specific of section 5.2 integrate a description of the circuit network created by the connection of three Bk1B111E20 tiles.

2.2.3 Bk1B111E20 Tiles Configurations

In chapter 4.2 the Bk1B111E20 Standard Tile is introduced. This basic tile can be configured in such a way to fix on it hinges in different orientations. This capability gives the simplification to obtain different type of structures using the same Bk1B111E1 PCB board without design a different PCB for each configuration of tile. The issue of the different configurations for the standard tile, arises because the skeleton of the chassis of the 1U CubeSat has three different types of faces where an external tile can be screwed (In such a way the faces of the CubeSat are equals in couple).

The Figure 9 shows the main skeleton of the chassis of a 1U CubeSat. The side differences are related to the three types of central spacings between the holes of screwing for the lateral tiles. Considering as chassis TOP, the face that contains the springs of the kill switch component² (see Figure 9), each side of the skeleton chassis is labelled with respect to a system of axis. Three colours are used for the axes. In this way can be identified the three types of faces whose differ about the central spacing of the fixing holes. The arrows that point the holes of screwing belonging to same face type, are coloured with same colour notation of the axes. So, the axes meaning is: for each axis direction, the two perpendicular faces are of the same type. Two faces of the same type have the same central spacings between their screwing holes.

To better understand the question, let's suppose that I want to mount the same tile that is also designed to be compatible with all three sides. This tile should have three holes on each angle, as is shown in Figure 10.

² The kill switch component is the main power starter of the entire satellite system. It is directly connected to the PDB of the satellite. It is used during the phase of releasement of the CubeSat from the P-POD. During the time that the satellite is within the P-POD, the kill switch is opened and the PDB is disconnected from the satellite systems. When the CubeSat is pushed away from the P-POD, the springs of the kill switch attach it. The kill switch thus is closed, connecting the PDB. In this way the power supply can be provided to the satellites systems only after that the dangerous period of the launch is terminated.

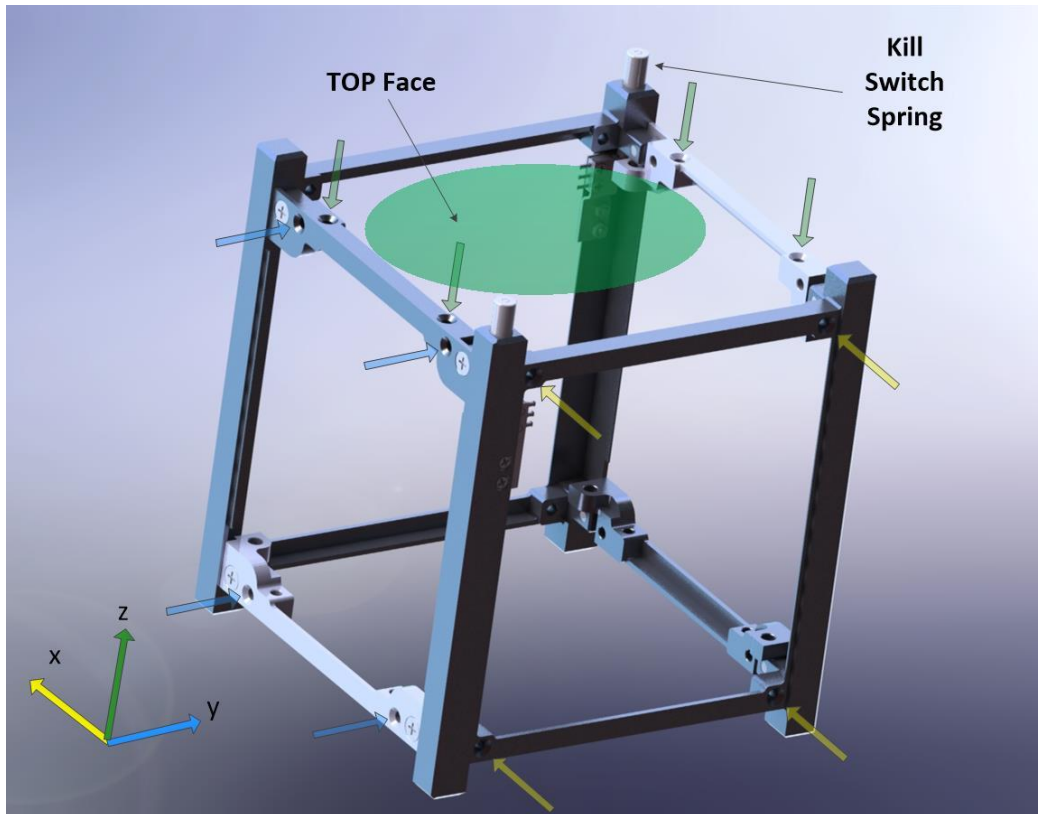


Figure 9: ARAMIS CubeSat Skeleton Tile

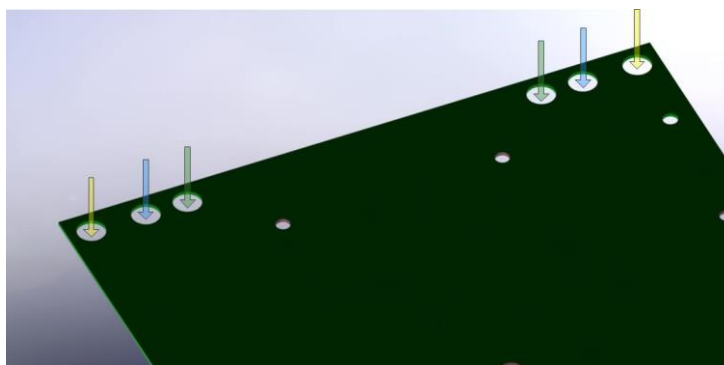


Figure 10: ARAMIS Tile Full Fixing Compatible

In Figure 10, each arrow coloured is correlated with the same colours of the arrows in Figure 9. On the board the arrows show which ones holes to use to fix the tile depending on which CubeSat face it has to be screwed.

Once a notation for the faces is defined, it is to be considered that the hinges that connect a 1B111E structure to a 1U ARAMIS lateral tile, are designed in order to be both soldered and screwed on the tile³. As will be clearer in chapter 2.2.5, since the screwing mean the realization of different spacings of the connections of the hinges, and its place of mounting is designed to be fixed and standard, the use of a single hinges configuration for the Bk1B111E20 tile, would have led to several problems of symmetry. To solve these issues are designed the different configurations of placement for the hinges on Nk1B111E20 tile. Once defined a top and bottom side for the standard tile, five main configurations have been provided:

³ The choice to perform also a screwing of the hinges has been done because the connection between the deployable solar panels structure and a 1U ARAMIS side tile is a weakness point. It is the point of the structure mainly affected by stress. During an attitude manoeuvre, due to its inertia the entire weight of a 1B111E deployable solar panels structure falls on the point of connection with the side tile of the CubeSat.

- Bk1B111E12_DepTile_A_Config
- Bk1B111E13_DepTile_Af_Config
- Bk1B111E14_DepTile_Aw_Config
- Bk1B111E15_DepTile_B_Config
- Bk1B111E12_DepTile_Bf_Config

In Figure 11 shows the UML class diagram for the Deployable Structure configurations.

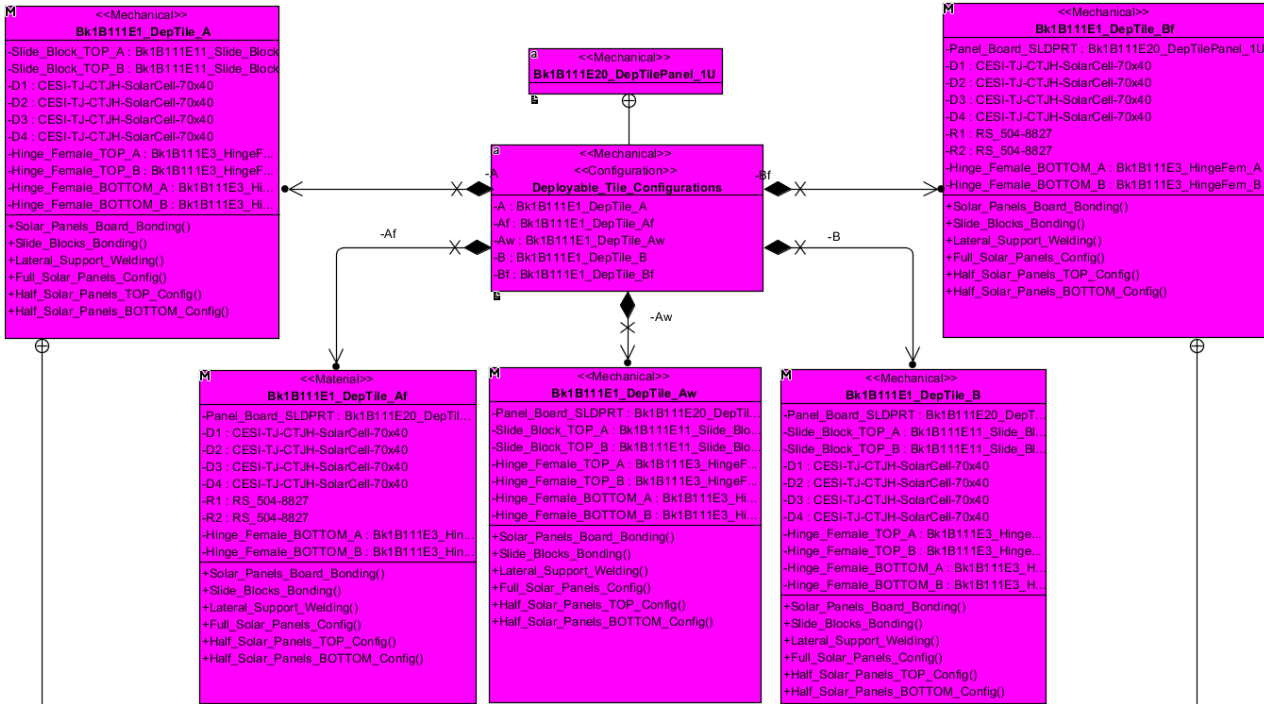


Figure 11: Bk1B111E20 Tiles Configurations.

Basically only three types of mechanicals configurations are done, A, Aw and B as have been easily labelled.

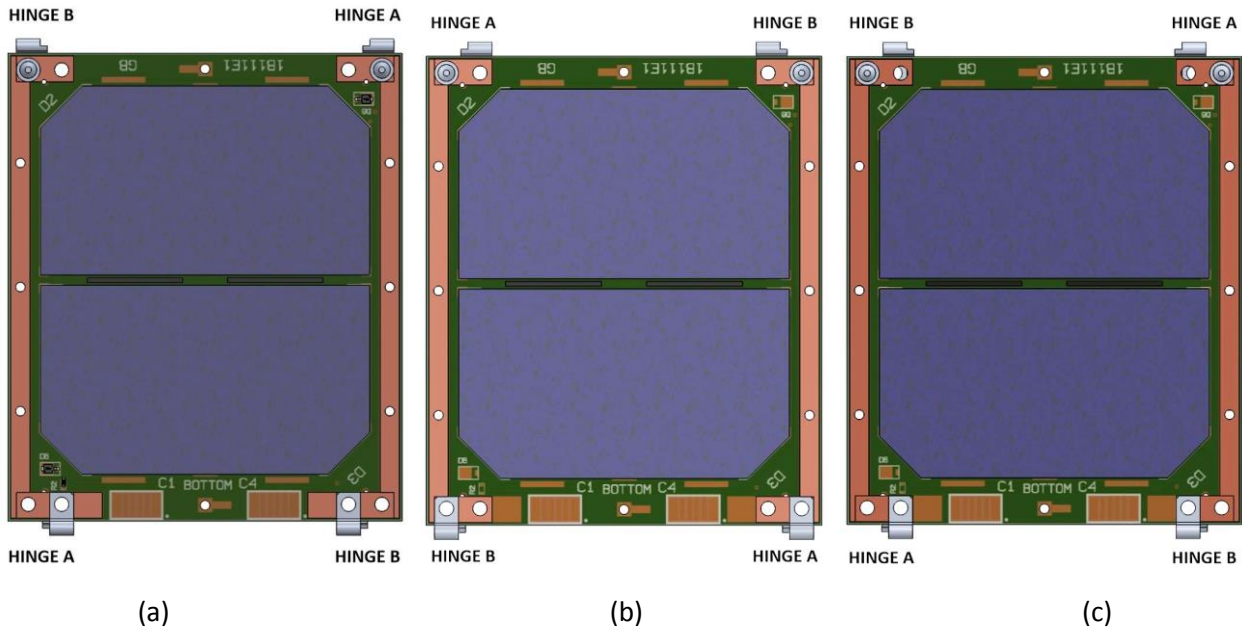


Figure 12: Standard tile configurations. BOTTOM side view (a) Config. A (b) Config. B (c) Config. Aw.

In the Aw label, the w stays for wheel. In fact this kind of tile configuration is a special configuration designed to be compatible to the fixing with the outer plate tile of the Bk1B213A reaction wheel⁴, or more in general for the 1U ARAMIS side tile with the fixing holes indicated with the dark green arrows in Figure 10. The f in the Af and Bf labels, stays for final tile. In fact Af and Bf are the terminal tiles at the end of a complete deployable solar panels structure. These configurations are similar to the A and the B ones, but the terminal hinges and two side blocks are not necessary, so these ones are not fixed. In this way the whole thickness of the terminal tile and then of a deployable solar panels structure is reduced. Furthermore, the terminals tiles will have also an electrical difference, respect to the A and B configurations. Af and Bf will close the circuit of the two power channels using R1 and R2, that are 00hm resistors. For more details about electrical specifics see chapter 5. The Hinges are all fixed by means of soldering on apposite pads, created on the angles of the PCB of the standard tiles.

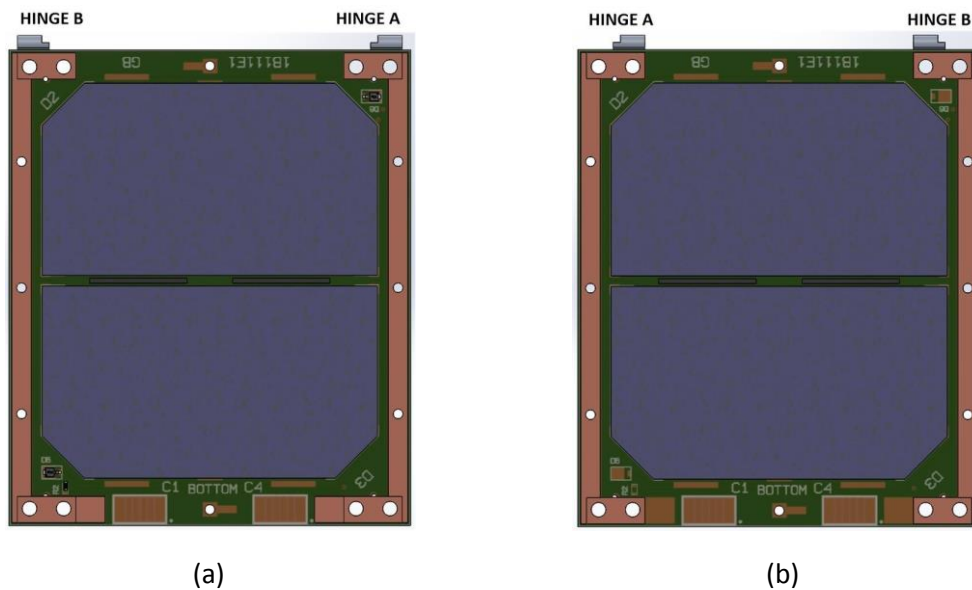


Figure 13: Standard tile configurations. BOTTOM side view (a) Config. Af (b) Config. Bf.

2.2.4 Bk1B111E20 Solar cells configurations

The Bk1B111E20 can be configured also for the number of solar cells. Three configurations are possible for a single Bk1B111E20:

- Full_Solar_Panel_Config_()
- Half_Solar_Panel_TOP_Config_()
- Half_Solar_Panel_BOTTOM_Config_()

With the first configuration all the four solar cells are mounted on a single Bk1B111E20 tile. The half configurations are related to the mounting of a single couple of solar cells. The couple of cells that is mounted, obviously must to be fixed on the same Bk1B111E20 side, in order to be connected in serial manner. In this way, the Half TOP configuration is related to the mounting of the couple of cells of the TOP side of the Bk1B111E20. Instead the Half BOTTOM configuration is related to the mounting of the couple of cells of the BOTTOM side of the Bk1B111E20.

⁴ Really, the Aw is not only for the reaction wheel module, but for all types of tiles that have to be fixed on the holes with the smaller spacing. In a first study has been used the reaction wheel as example because it is a module that surely, for conformity with the 3 axis of space, it must to be mounted on all types of side, then using all types of holes.

Using the UML description, these configurations can be possible for each type of the Bk1B11E20 tile configurations. In this way in the class diagram of Figure 11, these configurations are inserted as operation of the classes of the Bk1B11E20 configurations.

2.2.5 1B111E Deployable Structure configurations

The configurations for a standard tiles A, Aw, Af, B, Bf are all employed and combined to create further configurations of deployable structures. Since standards tiles are modular, theoretically it's possible to create structure deployable with an indefinitely number of tiles. But for the P-POD space limits, in order to stay under the tolerance margins, the deployable structures are composed all in number of maximum three tiles. Since a 1U aluminium chassis exposes three kind of faces with three types of spacings between fixing holes (as it is described in section 2.2.3), also three main configurations for the deployable structure are designed. These configurations are in strict relation with the configurations for a single Bk1B11E20 and are designed one for each type of face. The three configurations of Bk1B11E20 tiles are:

- Bk1B11E17_DepStruct_AAaf_Config
- Bk1B11E18_DepStruct_AwAAf_Config
- Bk1B11E19_DepStruct_BBBf_Config

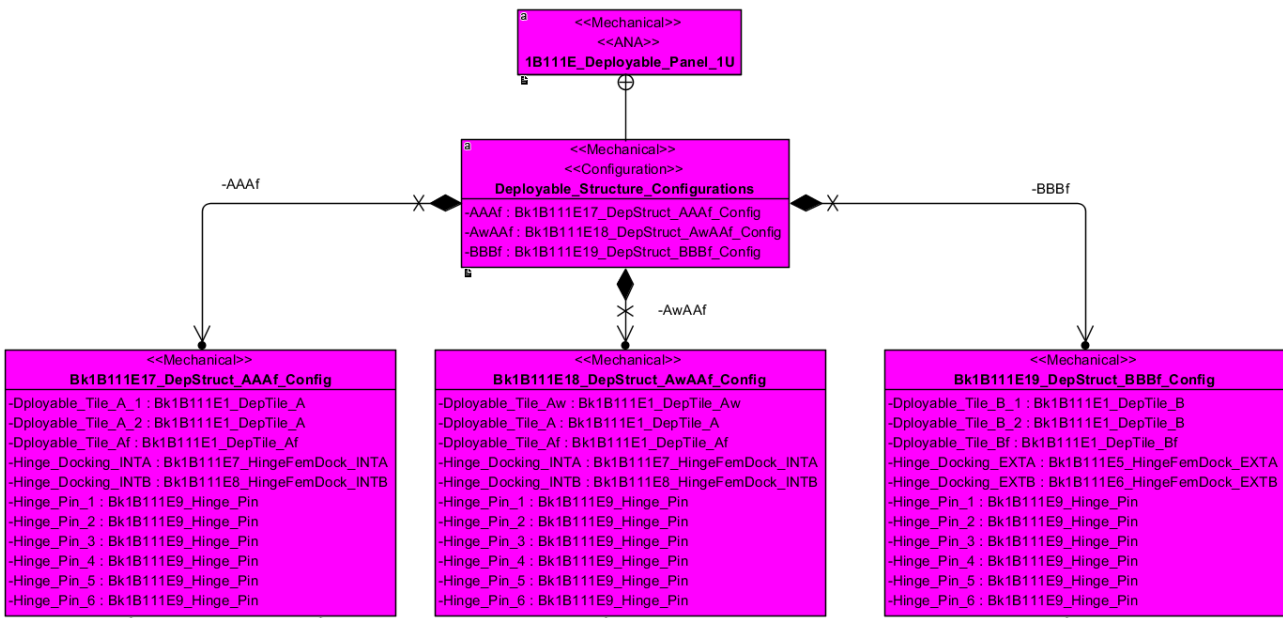


Figure 14: 2.2.5 Deployable Structure configurations.

The names of the configuration are labelled following a notation in order of mounting: starting from left to right, it means to go from the tile surface of the side of the CubeSat, to the terminal tile of the deployable solar panels structure. So, the configuration AAaf, means a structure composed by three tiles: starting from the side of the CubeSat, the first standard tile is the A, the second is A and the terminal configuration is Af. The Figure 15 shows the example of the AAaf configuration. Its orientation left-right reflects the previous description.

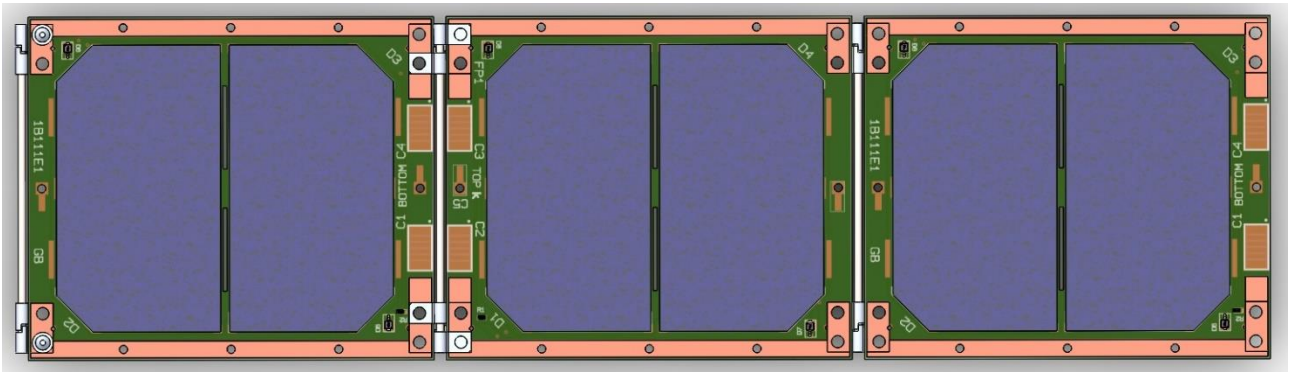


Figure 15: Deployable Structure configuration AA Af. Af is the last right

The assembling sequence is designed for each configuration of deployable structure in order to expose the top side of the first standard tile toward the surface of the 1U ARAMIS side tail. Sequentially, other tails are fixed one to each other alternating its bottom and top sides as is shown in the Figure 16, where a deployable solar panels structure of three tiles is shown completely deployed.

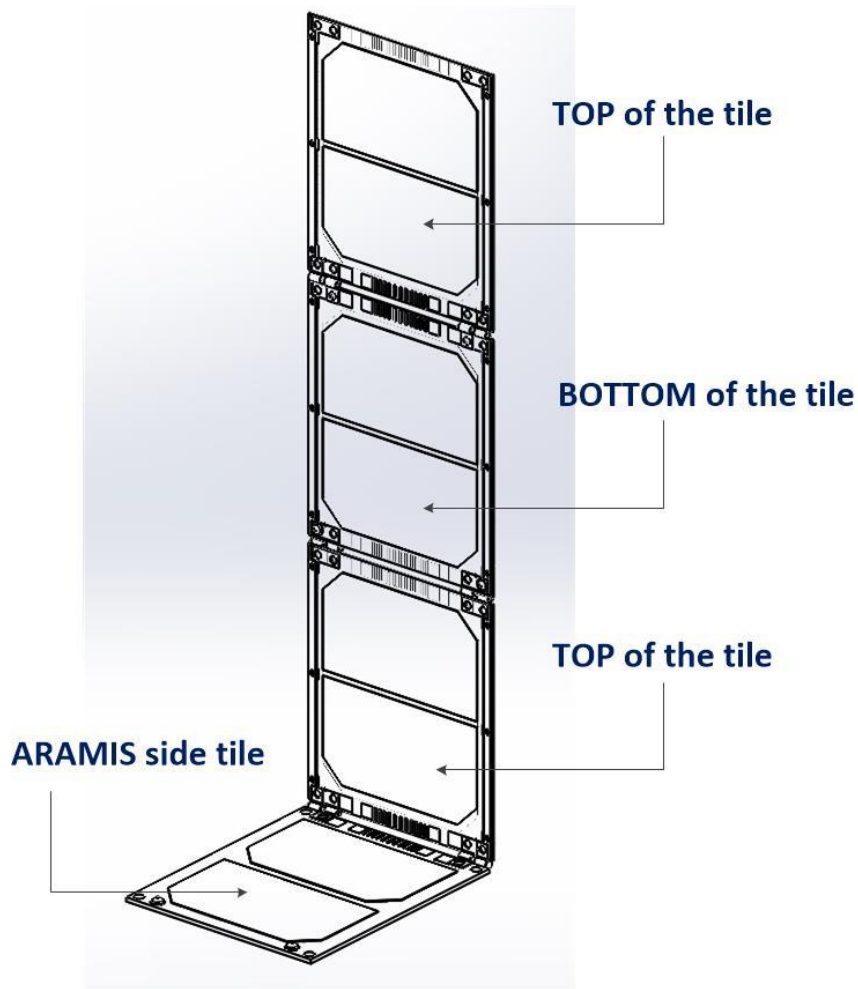


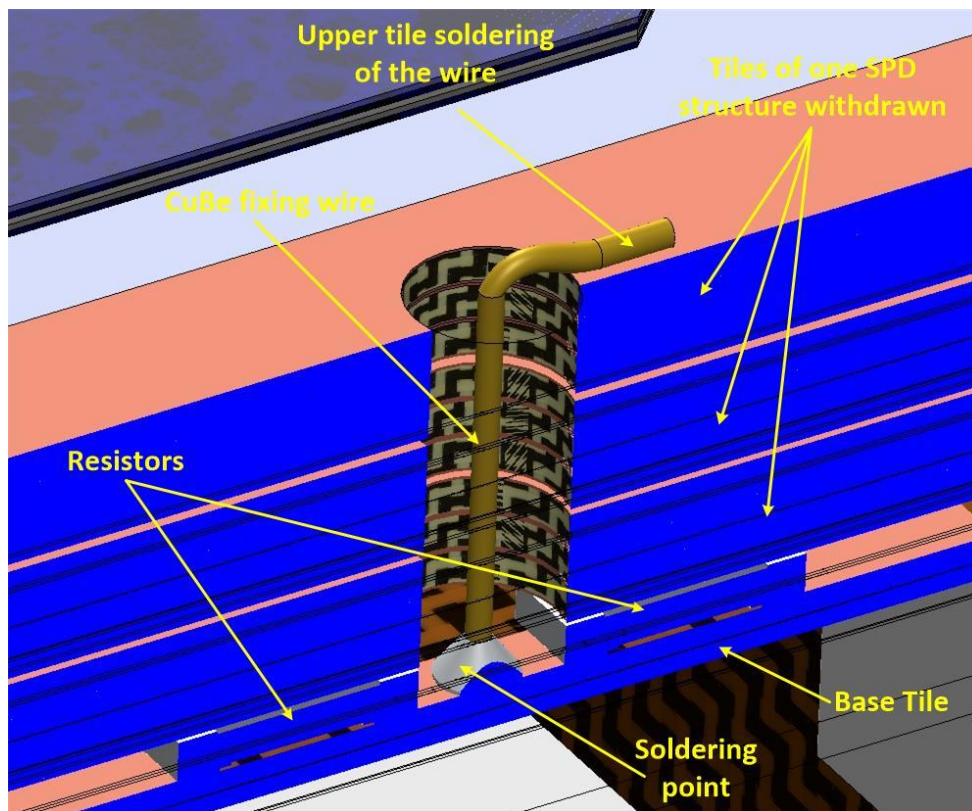
Figure 16: Deployable Structure Configuration Assembling Example

The PCBs and the connectors between the standard tiles are designed in order to create a separate power channel on both deployable solar panels structure sides. Until the deployable solar panels structure is composed using standard tiles connected in alternate configurations, the structure can theoretically grow indefinitely. The limits in the number of standard tiles are imposed by the space occupation, by the weight, by the torques of the springs, by the PCB traces length, by the bouncing during the opening phase, by the

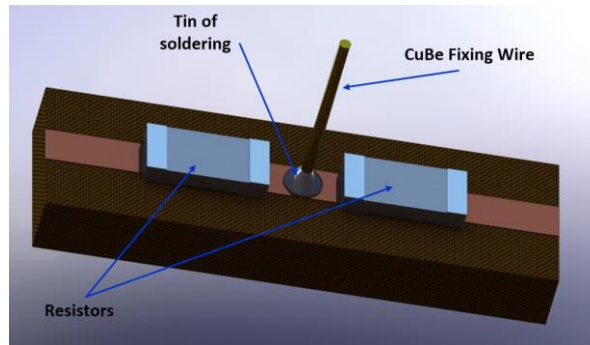
inducted vibration due to its damping and finally by the spin problems induced by the pressure of radiation incident on the wide surfaces.

2.2.6 Bk1B111T Thermal fuser

Once fixing wires are defined, the only obstacle remained is the designing of the technique to detach the fixing wires from the base tile. This system must not consume high power, it must not produce high temperatures and absolutely it must not cause the detachment of floating parts in orbit. The first solution analysed, was the direct fusion of the wires, by means of a high current flowing through them. The problem with this solution was the high power consumption and the high volume occupied by the driving circuitry for the current. A second solution was conceived to reduce melting temperature of the fixing element thus reducing the power consumption. This solution was the thermal fusion of sealing wires in nylon, by means of the heat generated from a resistor. The problem of the solution with nylon was the too low tensile strength of this material and the difficulty to paste the wire on resistor and on tiles, because the nylon is not possible to be soldered. Finally, a good trade-off between power consumption and good proprieties of tensile strength was found using wires in Copper Beryllium that are detached in an innovative way: even if copper beryllium material has a low melting temperature respect other metals or alloys, It is not yet sufficiently low, to permit the use of a low melting current, in this way the innovative solution considered, is melt its tin of soldering. Since the copper beryllium can be soldered using tin, the goal is just to use a tin with low melting temperature to realize the fixing soldering of the wires. In this way a simple circuit constituted by resistors can be designed to heat the points where the wires are soldered, causing the melting of the tin and permitting the detachment of the wires. Since the tin used has a low melting temperature, it is not required a high power consumption to fuse the tin. The Figure 17 (a) shows how the CuBe wires are used to maintain a 1B111E structure folded. The Figure 17 (b) shows the model of the thermal fuser.



(a)



(b)

Figure 17: BK1B111T (a) Cross section showing an example of tiles fixed with the wires in CuBe (b) Thermal Fuser Model.

2.3 Electrical Specifications

The electrical specifications involves all the specifics related to the electrical system of the 1B111E deployable structure and the Bk1B213A Outer Plate. The table Figure 3 shows the electrical specifics of the 1B111E. The table Figure 4 shows the electrical specifics of the Bk1B213A.

Electrical specifications of the 1B111E.		
Enumeration of specification	Specification Type	Specification
22	Electrical	A complete 1B111E structure is composed by two independent power channels for each side. Each channel is a connection in series of the solar cells of the Bk1B111E20 tiles.
23	Electrical	The maximum power provide by a Bk1B111E20 tile is about 1,97w of power with a voltage of 4,4V, for each power channel.
24	Electrical	The maximum power provide by two series of Bk1B111E20 tiles is about 3,94w of power with a voltage of 8,8V, for each power channel.
25	Electrical	The maximum power provide by a 1B111E is about 5,9w of power with a voltage of 13,2V, for each power channel.
26	Electrical	A complete 1B111E structure provide a maximum current of 0,45A
27	Electrical	The 1B111E structure is electrically compatible with the Bk1B213A1 tile connection.
28	Electrical	The Bk1B111E20 can be configured in Half or Full cells configurations.
29	Electrical	The 1B111E ha a symmetric and standard interface of electrical connection.

Figure 18: 1B111E Electrical Specifications.

Electrical specifications of the Bk1B213A.		
Enumeration of specification	Specification Type	Specification
12	Electrical	The Bk1B213A1 is electrically compatible with the direct supply connection to the ARAMIS PDB of 14V.
13	Electrical	The Bk1B213A is electronically compatible with the 1B111E deployable structure.

14	Electrical	The entire opening system, composed by the 8 Bk1B111T thermal fusers activated, has a maximum power consumption of 44w.
15	Electrical	The melting temperature of about 160C°, is reached by the 8 Bk1B111T thermal fusers in 10s.
16	Electrical	The entire opening system, composed by the 8 Bk1B111T thermal fusers activated, has a maximum energy consumption in 10s of 440J.
17	Electrical	The Bk1B213A1 tile is electrically compatible with the 1B111E structure connection.

Figure 19: Bk1B213A Electrical Specifications .

2.3.1 Solar Cells

The solar cells used for tiles are GaAs CESI-TJ-CTJH-SolarCell-70x40 with an efficiency of 26%. From the specifics, each cell generate approximately 2.2V, so their series provides an output voltage of about 4.4V. The bypass diode is connected in parallel to each solar cell which ensures proper operation of the single cell in case, one of them is damaged or, due to the relative movements of the satellite, one of the cells is obscured by the shadow cast by other parts of the satellite. About the cells, with the increase in temperature, the performance of a single solar cell degrades in terms of output voltage and power [7]. The Figure 20 shows the power/voltage (P-V) characteristics of a single solar cell, plotted at two different temperatures (25°C & 45°C).

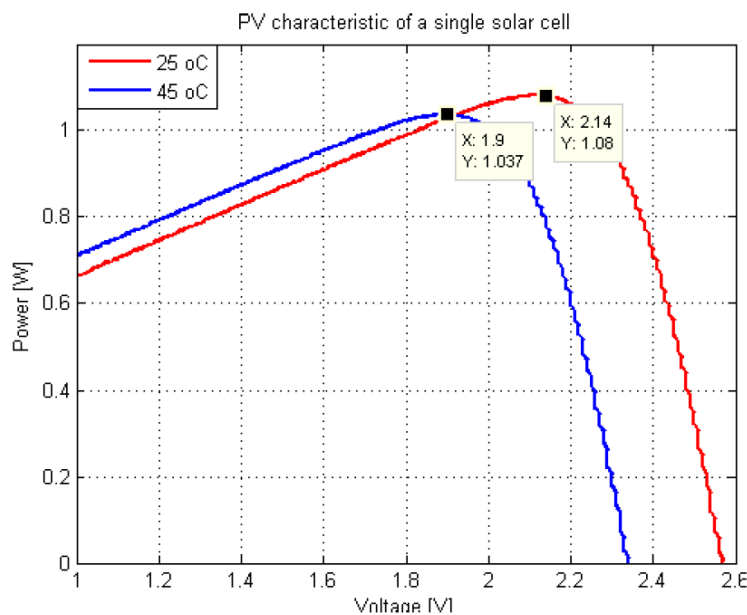


Figure 20: Singe solar cell P-V characteristics.

Using the Mentor simulation tool (HSPICE), a DC simulation analysis is performed on a first circuit with two cells in series (Figure 22 (a)) in order to analyse the electric characteristics of a single tile. The simulation models of each components are attached to the section 9.5. The simulation is performed applying a voltage sweep on the net VPOS with respect to VNEG. In this way it is possible to get a curve of the current absorption of the cells. Whith this analysis the cells are simulated as if they are lighted by sun. The current equal to 0 means absence of light. For better understand the simulation model, is good to observe a graph that plots the voltage/current characteristic of a single cell. The Figure 21 is used for this purpose. It is to note that if the voltage is inverted and it decreases until reverse breakdown voltage is reached, just as it happens in the diodes, the junction of the cells is perforated. In this way a short circuit is obtained and then an increase of current. The Figure 21 shows this situation over about -0,3V for a single cell simulated.

Now, after a first analysis of a single cell, will be analysed the characteristics of the series of more cells, starting from the simple situation of two cells in series. In Table 1 are summarized all simulation parameters of the circuit model in Figure 22 (a). In Figure 22 (b) are shown instead simulation results in two curves: one is the power vs voltage relation, and the other is the current vs voltage relation. Two marks are taken on curves in 4,4V that corresponds to a maximum peak power. So with a single tile and one channel fully lighted it is possible to obtain about 1.97W of power with a current of 450mA.

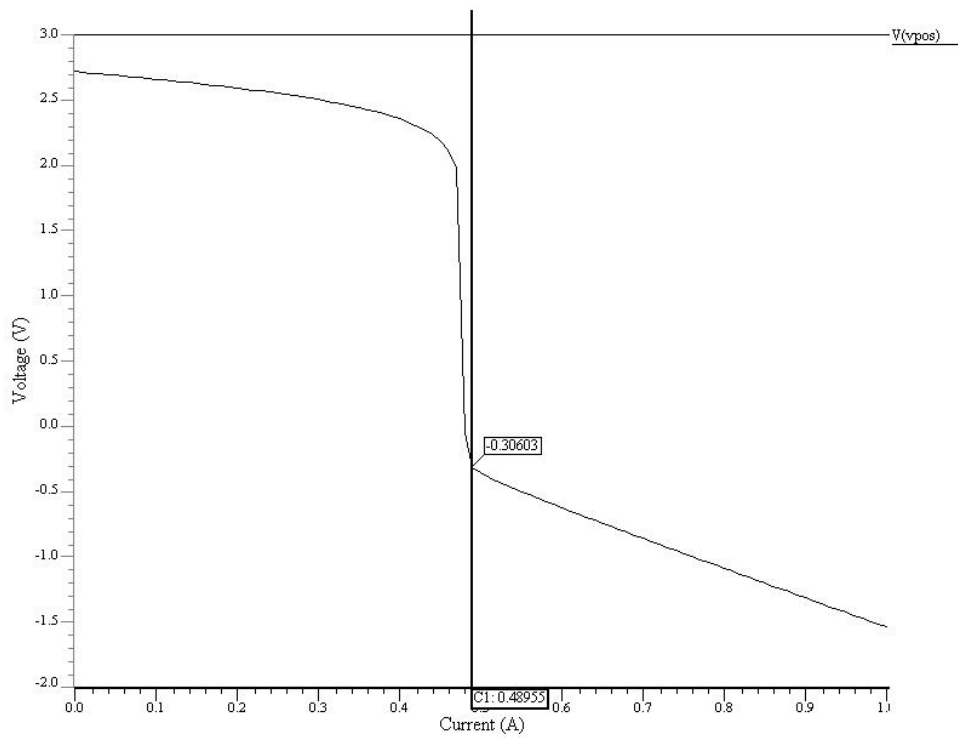
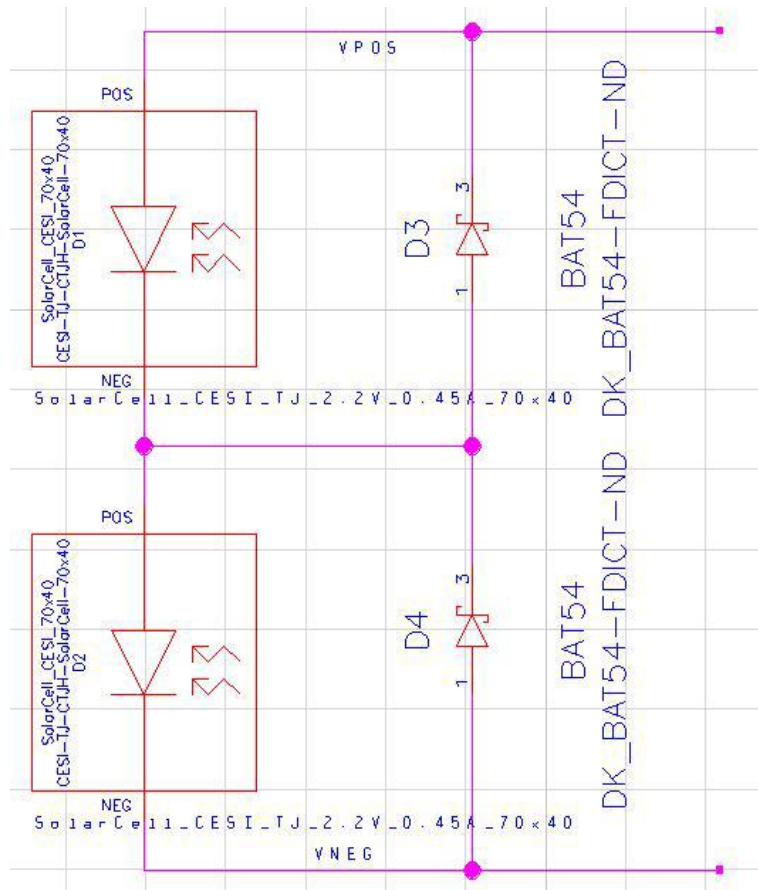
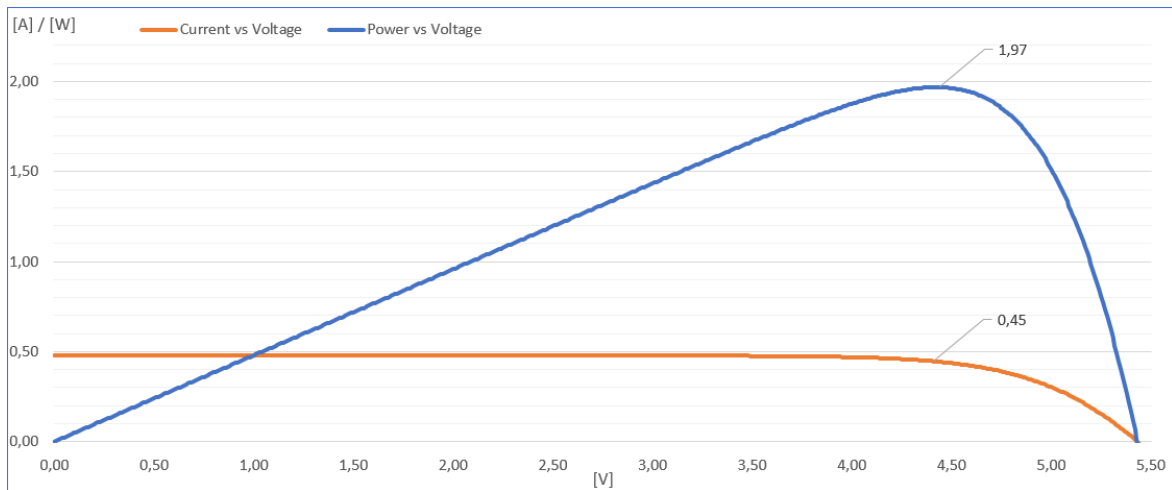


Figure 21: Current-Voltage characteristic of a single cell.



(a)



(b)

Figure 22: Two solar cells connected in series (a) Schematic (b) Current and power vs voltage.

Source	VPOS Voltage: Node+=VPOS, Node-=0; DC=1
Type	DC Analysis
Operating point Analysis	Enabled
Parametric sweep	.dc VVPOS 0 5.5 0.01 lin

Table 1: Simulation parameters of two cells in series.

Adding two more cells to the circuit model of Figure 22 (a), it is possible to simulate a channel with 4 cells in series. The same parameters of Table 1 are used with exception of sweep interval. The results are shown in Figure 23. Finally, a complete channel of three tiles, with six cells, it is simulated at the same manner, adding four more cells to the circuit model of Figure 22 (a). The results are shown in Figure 24.

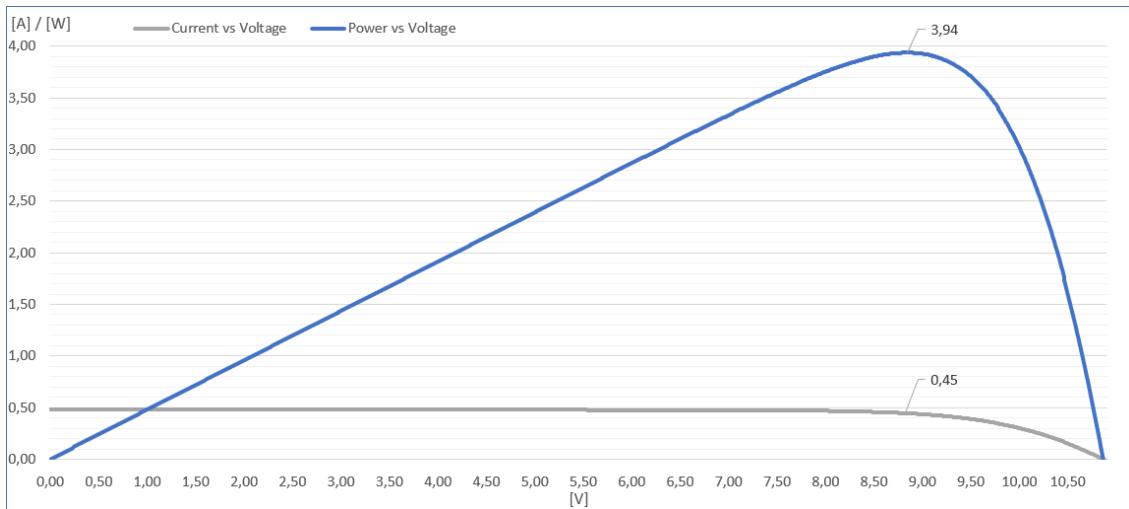


Figure 23: Current and Power vs Voltage of 4 cells connected in series.

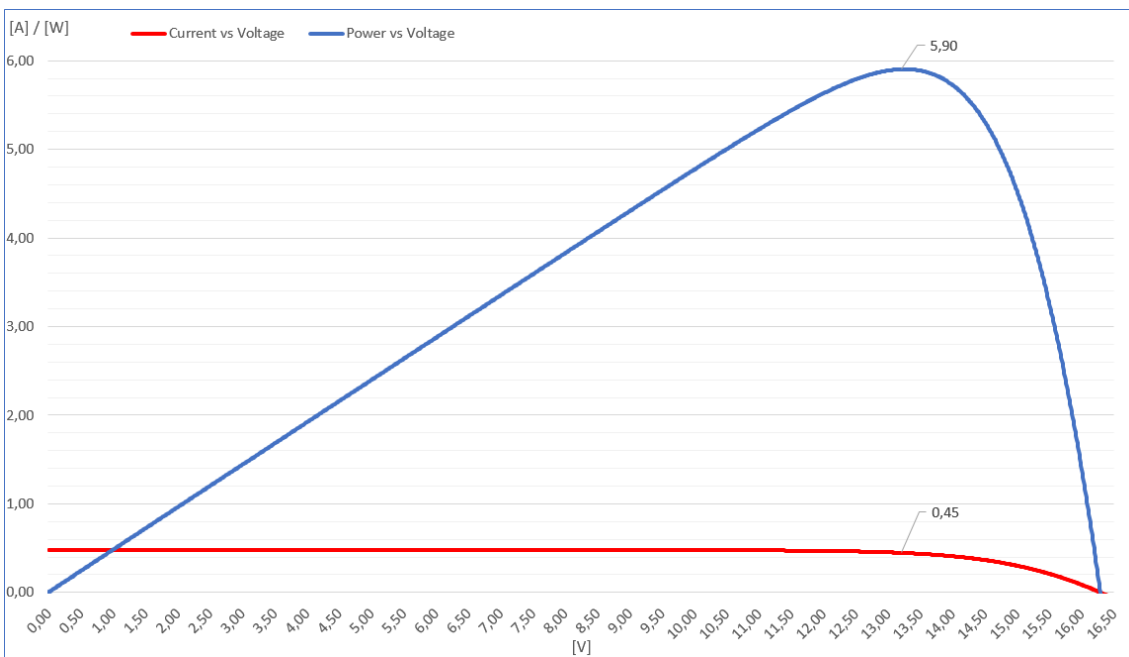


Figure 24: Current and Power vs Voltage of 6 cells connected in series.

As the Figure 23 shows, for a voltage of 8,8V the peak of power is 3,94W so the advantage in power is greater than only two cells in series. With three tiles (Figure 24) the power it is still greater because power has tripled, 5,9W for 13,2V. In conclusion, with a structure of three tiles it is possible to generate a power of nearly 6W, and since it is possible to fix a 1B111E structure on at least four faces of a single 1U CubeSat (Figure 42 (a)), the maximum power that such a system can provide to the entire satellite is about 24W. The Table 2 shows a summary of the maximum power obtainable with the three possible structures with different number of tiles.

STRUCTURE CONFIGURATION	MAX OUTPUT POWER
1x tile	1,97 W

2x tile	3,94 W
3x tile	5.9 W

Table 2: Max output power summery table.

2.4 Thermal & Attitude Specifications

The Thermal specifications involves all the specifics related to the thermal behaviour of the 1B111E deployable structure the space environment. The table Figure 25 shows the thermal specifics of the 1B111E.

Thermal specifications of the 1B111E.		
Enumeration of specification	Specification Type	Specification
30	Thermal	The Bk1B111E20 reaches an equilibrium temperature less than 90C°, at an altitude of 800km in LEO orbit.
31	Thermal	The Bk1B111E20 reaches an equilibrium temperature in less than 8 minutes, at an altitude of 800km in LEO orbit
1	Attitude	A satellite, with two 1B111E structure mounted and completely deployed, reach 1 rpm of spin in about 7 days.

Figure 25: 1B111E Thermal & Attitude Specifications.

3 Deployable Solar Panels System Architecture

The description of the thesis work is condensed in the System Architecture diagram of the entire Deployable Solar Panels System in Figure 26.

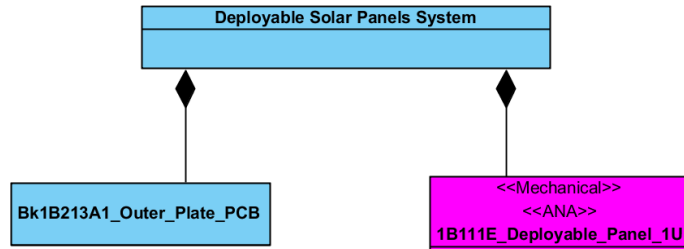


Figure 26: Deployable Solar Panels System Architecture.

The Deployable Solar Panels System is a complete satellite element, composed by two subsystems connected together: The Bk1B213A1 that represent an outer plate element of a reaction wheel tile, and the 1B111E deployable structure of three 1U tiles. The Bk1B213A1 represent a base tile where the 1B111E deployable structure is fixed. The opening system employed to deploy the 1B111E structure is implemented on the Bk1B213A1 tile. In the following paragraphs are described each subsystem in detail.

3.1 1B111E Deployable Panel 1U

The 1B111E is the system that characterises the deployable structure of tiles. Its main system architecture is shown in Figure 27.

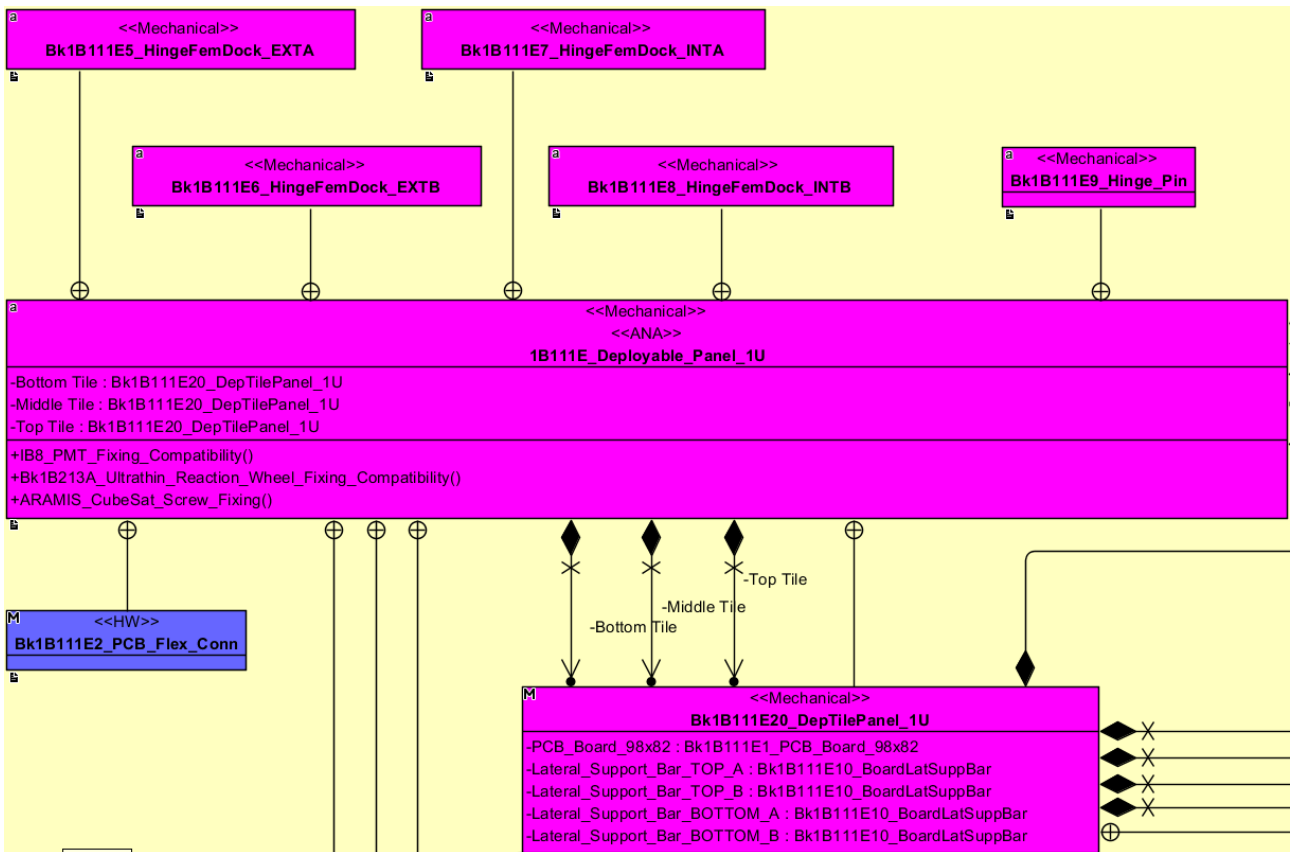


Figure 27: 1B111E Deployable Panel 1U.

The IB111E is a modular structure conceived for the structures realized with the ARAMIS approach. In such a way, the tiles that composes the structure are designed taking into account their mounting on a side tile of an ARAMIS CubeSat. The Bk1B111E20 tiles have to be compatibles also with the standards P PDO module and so they have to follow strict requirements of volume occupation. A good device of a space application is also characterized by low weight, and in such a way the tiles of the deployable solar panels are realized using small mechanical components realized with materials lightweights but strong. The structure is composed by three Bk1B111E20 tiles connected in order to compose a single mechanical structure.

The main goal of mechanical system is that in order to maintain low thickness, weight and space occupation, the mechanical tiles themselves consist directly of the Bk1B111E1 PCBs where solar panels and other electrical components are placed. The Bk1B111E2 flex board PCB is used to connect electrically each Bk1B111E20 to the others. A set of hinges are used to connect mechanically the Bk1B111E structure to the Bk1B213A1. These hinges are the Bk1B111E5, the Bk1B111E6, the Bk1B111E7, and the Bk1B111E8.

Each couple of hinges is hinged together by means of a Bk1B1119 Hinge pin. It is made in copper material like the hinges.

Since each Bk1B111E20 tile, mounts a couple of solar panels for both sides, the Bk1B111E structure of three tails exposes on its output connector two separated power channels, one for each structure side. This feature is designed because only one side at time can be efficiently exposed to sun and in such a way there is the possibility of deactivate the shady side of the structure. A double side covered by solar panels gives the possibility to maintain a constant spin for a continuous pointing of the earth surface, just because at least one side of solar panels will be always sunlit.

3.1.1 Bk1B111E20 Standard Tile

Bk1B111E20_DepTilePanel is the base standard tile used as mechanical structure to assemble each type of configuration of the deployable tiles.

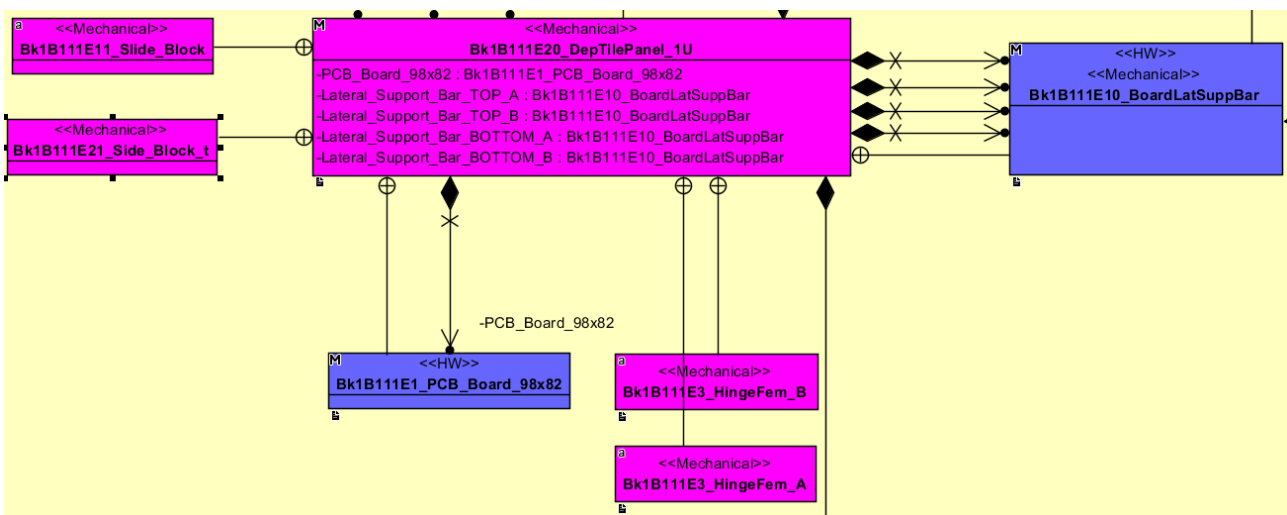


Figure 28: Bk1B111E20 Standard Tile

It is composed by: a Bk1B111E1_PCB_Board_98x82 that represents both the PCB and the mechanical structure of tile; and four Bk1B111E10_BoardLatSuppBar that represent a mechanical reinforcement of the structure and that have also a role in the opening system. The tile is considered standard because, following the ARAMIS approach, it is completely configurable depending on how the hinges are soldered on the top or bottom side of the Bk1B111E20. These hinges are of two type: the Bk1B111E3_HingeFem_A and the Bk1B111E3_HingeFem_B. Top and bottom labels are placed on Bk1B111E1 PCB sides, just to distinguish the two side of the Bk1B111E20 tail to help the fixing of the configuration of the hinges. The label “k” it is used

to distinguish the edge of the TOP side and the TOP side itself, corresponding to the starting connection of the series of the BK1B111E20 tails (This correspond to the anode of the series of solar cells, see Figure 60 (b)).

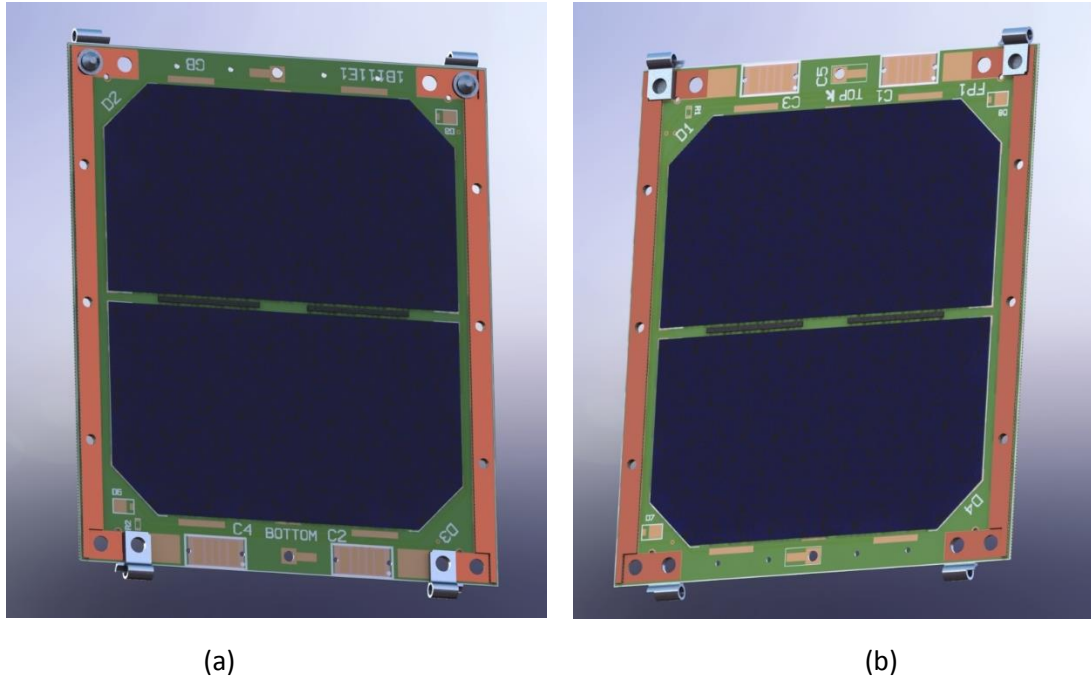


Figure 29: Example of standard tile with hinges already fixed (a) Bottom of the Bk1B111E12_A configuration (b) Top of the Bk1B111E12_A configuration.

The Bk1B111E1 PCB board is so used also for support. It is a board in FR4 standard, with a thickness of 0.4mm. It contains two solar panels on both sides, placed in order to permit fixing of at least two solar panels at side.

A couple of holes on each angle of the tile are present. These have two purposes: these are alignment holes for the hinges but they are also used as interlocking for appropriate mechanical elements called side blocks (Bk1B111E11). This one is useful when the deployable solar panels structure is completely closed to avoid small slides that can lead to the damaging. In this situation, when deployable solar panel structure is subjected to the vibrations of launch, the side blocks are wedged inside their alignment holes placed on near tile. In this condition the interlocking system acts as a block anti sliding, keeping stable the entire structure during the vibrations.

3.2 Bk1B213A1 Outer Plate

The Outer Plate element of a reaction wheel is used to implement the Bk1B111T Thermal fusers of the opening system. The Figure 30 shown the Outer Plate system.

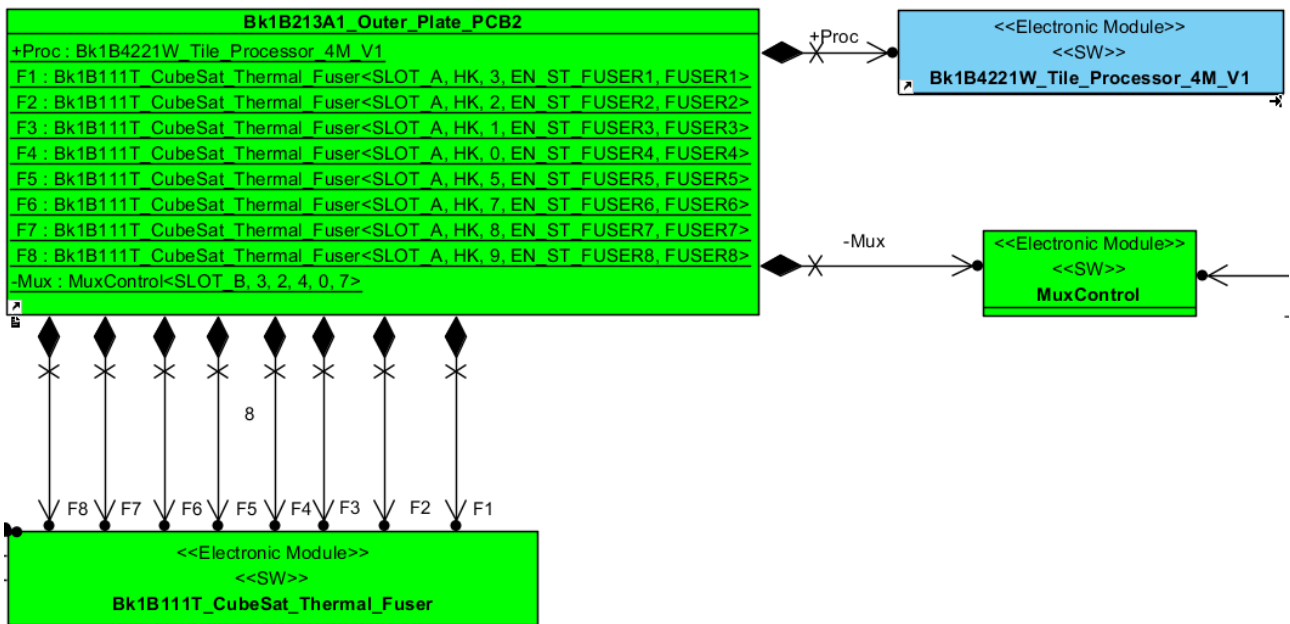


Figure 30: Bk1B213A1 Outer Plate.

The Outer Plate is used by a reaction wheel tile as part of its mechanical structure. The outer Plate mounts a magnetic circuit ring for the coils of the reaction wheels and a Teflon ring, both on the same side. When the Outer Plate is fixed to the reaction when, the other exposed side remains completely void, without devices mounted. This part of the Outer Plate board is used to implement the Bk1B111T Thermal fusers for the opening system of the 1B111E. Obviously the Bk1B111T needs a complete MCU based system in order to be managed.

The main component for the control system of the Outer Plate is the Bk1B4221W Tile Processor. It handles all the operations of the Bk1B213A1. The MuxControl is an analog multiplexer that supports the Tile Processor to selects all the analog channels from the NTC sensors implemented in the Bk1B111T thermal fusers. These latter are implemented in number of eight on the Outer Plate. The Bk1B111T is completely described in the section 7.

The Bk1B213A1 is made with a PCB of 0,5mm, it is a simple double layer of copper. The complexity of the Bk2B213A1 PCB layout is not high, but all the components of the board are placed trying to place them in compact way as much as possible.

4 1B111E Mechanical Design

4.1 Introduction

The main step of the 1B111E design is to meet the mechanical constraints, in relation to the ARAMIS structures with which the 1B111E has to be connected. The mechanical design covers the shape and size of the Bk1B111E20 tile, the materials chosen and their features, in order to meet constraints of strength and weight. That, allows safety operation after a launch and in space environment. The second goal is the designing of the Bk1B111E20 as a reconfigurable standard tile, with which is easily possible to realize different configurations and increasing as much as possible number of solar panels. In this way it is possible to increase maximum power provided by the entire 1B111E structure. The configurations are particularly useful when the 1B111E structure has to be connected to different types of ARAMIS CubeSat side tiles.

The deployment system of the 1B111E must not pose a danger for orbital environment, avoiding the detachment of small parts which would remain floating in orbit and would represent a danger for other orbital systems in orbit on its same trajectory. In addition to, the deployment system has to be designed in order to reduce as much as possible its power consumption during opening phase

This chapter initially starts with the designing of the Bk111E20 standard tile. Afterwards the description is focused on the 1B111E mechanical operation, meaning its deployment system. Finally it is analysed the behaviour of the 1B111E to the launch vibrations. The study is enriched with simulations by means of the appropriate Tools of SolidWorks.

4.2 Bk1B111E20 & Bk1B111E10 Design

The Bk1B111E20 is characterised by the implementation of two main elements, the Bk1B111E1 PCB that represents also the base mechanical structure of the Bk1B111E20, and 4 Bk1B111E10 that are fixed on the Bk1B111E20 to improve its strength properties. The main system is shown in Figure 31.

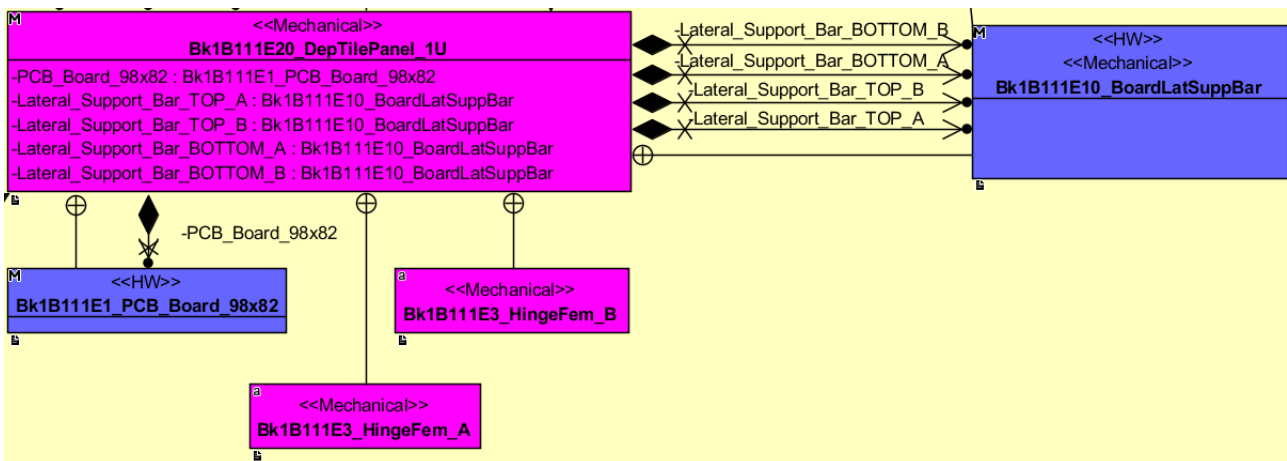
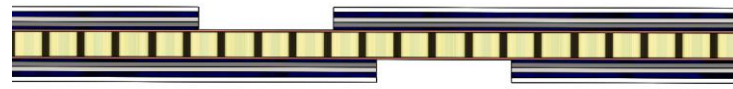


Figure 31: Bk1B111E20 Deployable Standard Tile.

The designing of the Bk1B111E20 starts with a first consideration on the placement of the solar cells.

As explained in the 3.1.1 the Bk1B111E20 contains two solar cells on both sides, placed in order to permit fixing of at least two solar cells at side. Really, the Bk1B111E20 can be configured also with different number of solar cells. Since one Bk1B111E20 has four couple of solar cells that are connected in series in couple, it is possible to realise two type of solar cells configurations, as it is described in section 2.2.3. In this type of analysis, it is considered only the full configuration of solar cells. This is done because the intent of this analysis is to verify that an asymmetric placement for the two cells in couple, is the better choice from the

strength point of view. In this way the solar cells are not symmetrically mounted between the top layout and the bottom one.



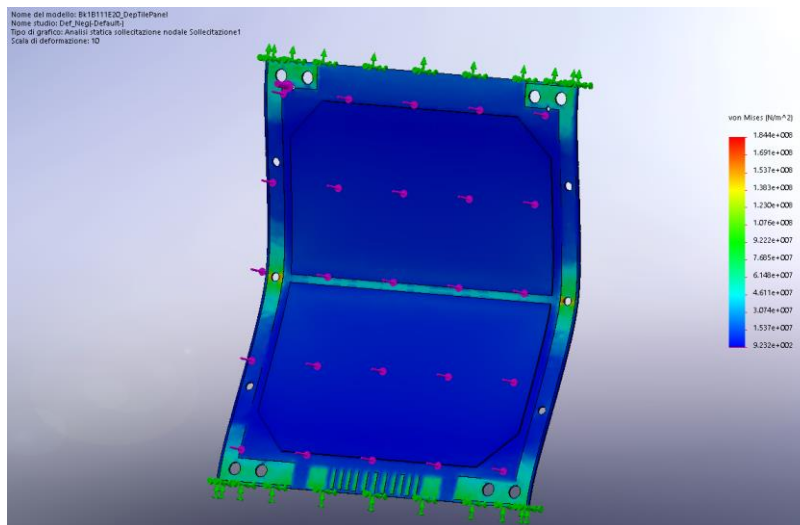
(a)



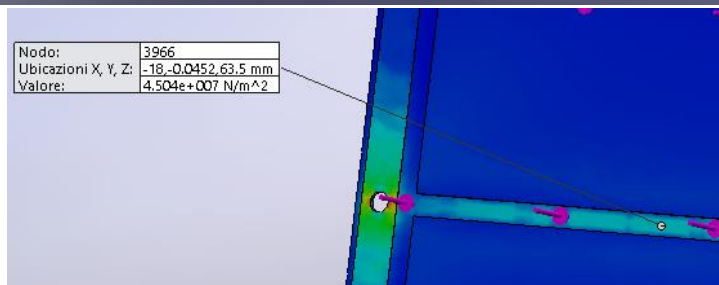
(b)

Figure 32: Cross section of a centre of a standard tile (a) Solar cells placed in asymmetric layout (b) Solar cells placed in symmetric layout.

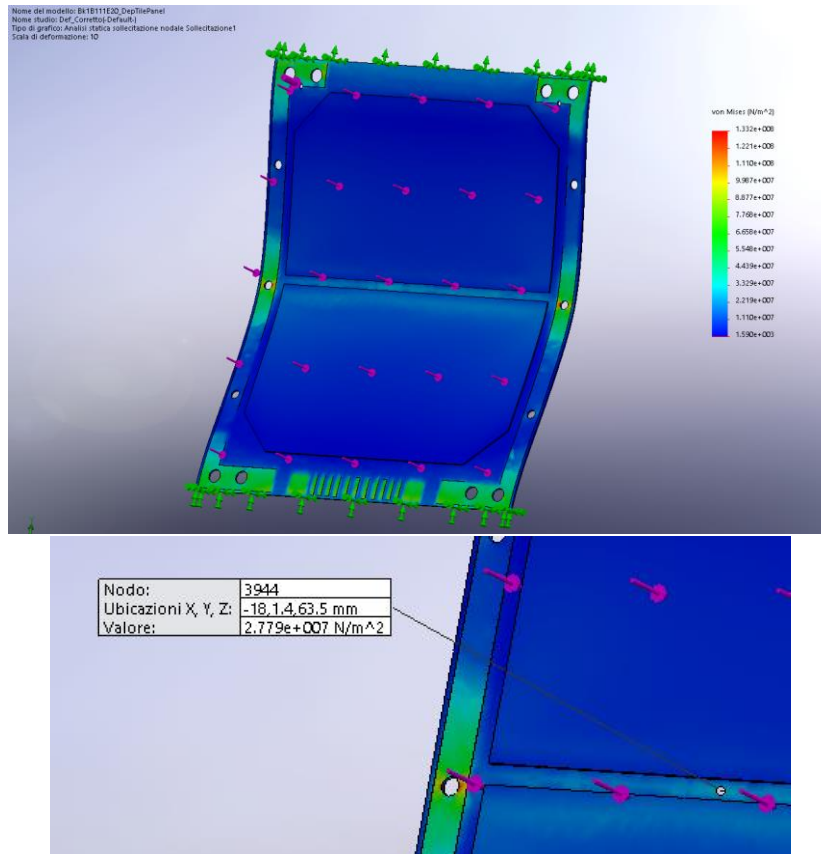
This is also due to the custom surface connectors, C1, C2, C3, and C4 that occupy space and in this way the cells are shifted toward the borders. In first approximation, this configuration increase the total stiffness of the board. In order to understand this choice two stress simulations are provided.



Nodo:	3966
Ubicazioni X, Y, Z:	-18,-0,0452,63.5 mm
Valore:	4.504e+007 N/m^2



(a)



(b)

Figure 33: Von Mises stress plot and standard tile Bk1B1120 deformation (a) Solar cells in symmetric layout (b) Solar cells in asymmetric layout.

Figure 33 shows a von Mises stress plot and the diagram of deformation amplified of 10 times with respect to the real deformation. The Von Mises stress is a strength criterion. According to that criterion, the yield strength of the material is achieved when the strain energy distorting reaches a limit value. In this way the simulation gives the pressure at which the structure is subjected and this one has to be intended as stress index of the structure. The Figure 33 (a) shows a simulation under 15N of force (violet arrows) distributed on surface of the tile with a symmetric layout of solar panels. The 15N of force is an estimated value of force near to the vibrations conditions of launch. In this evaluation its value has no purpose to give precise results, it is used only to verify in which condition the structure results more resistant. Fixed constrains are applied to the upper and to the bottom of the tile (yellow arrows) so as to bend the tile along the most critical axis, that is the weaker direction of bending. The Figure 33 (b) shows a simulation under the same simulation condition of the structure with asymmetric layout.

As it can be seen, structure with panels symmetric has a higher maximum value of Von Mises stress. $1,844 \cdot 10^8$ N/m² of maximum as visible on the scale in gradient of colour. Instead the structure with an asymmetric layout of solar cells, results to be less stressed under the same force with a maximum of scale of $1,333 \cdot 10^8$ N/m². The maximum value to the scale is related to the holes, because these are the mechanicals elements most stressed of a structure. However, mine intent it is instead to see what happens to the stress between two solar cells. In both Figure 33 (a) and (b) are highlighted the values of stress taken in the same point of the structure between the two solar panels. This values (indicated in both the Figure 33 (a) and in the (b) with the probe tool available in SolidWorks) show how in the symmetric layout, the stress is double ($4,5 \cdot 10^7$ N/m²) with respect to the asymmetric layout ($2,77 \cdot 10^7$ N/m²). So, in conclusion asymmetric disposition of solar panels is also a better choice for structure strength.

The pad of the solar cells is realized with an appropriate shape in order to distribute the gluing surface along the whole contact of the bottom of the cell. In this way the pressure of fixing of the cell is better distributed on the surface and the delicate structure of the cell is more resistant to the slight deformations due to thermal expansions/retractions or vibrations.

To increase global structure strength, are inserted lateral mechanicals reinforcements (Bk1B111E10). The same stress simulation is performed again.

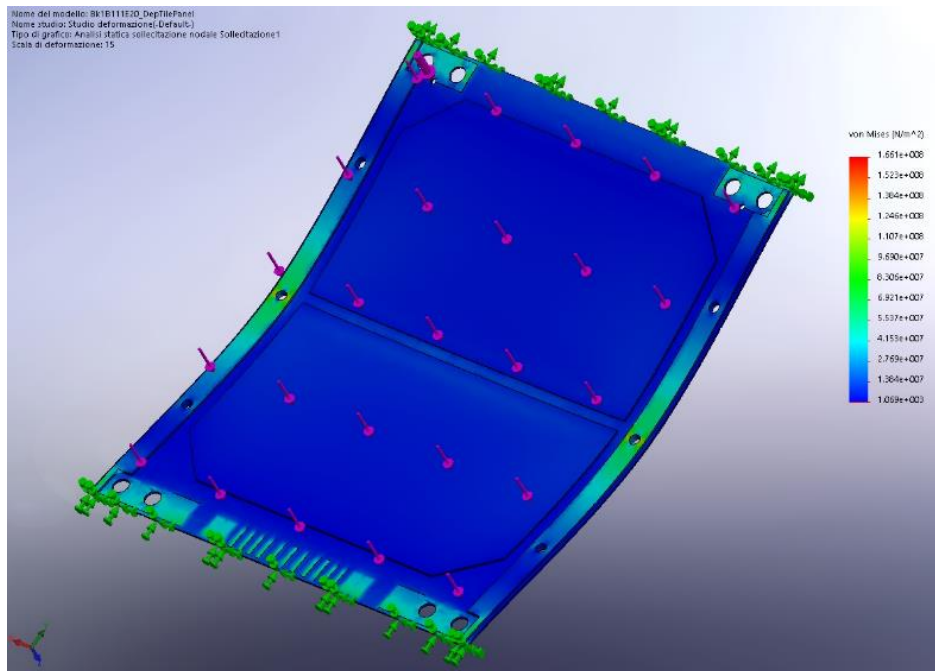


Figure 34: Von Mises stress plot and standard tile Bk1B11120 deformation using lateral supports Bk1B111E10.

The Figure 34 shows clearly how the lateral reinforcements are useful to increase the uniformity in the deformation of the structure. The deformation of Figure 34 is exaggerated of 15 times respect to the real deformation. Despite being more exaggerated with respect to the first simulation without lateral reinforcements (Figure 33 (b)), bending of tile is noticeably less. The value of stress to the same point on the tail between two solar cells is $1,5 \cdot 10^7$ N/m², almost half of the same value observed on the tile without reinforcements of Figure 33 (b). In conclusion using lateral supports increase global strength of the structure of the tile. The Bk1B111E10 lateral supports are designed as PCB board type. These ones are 0.4mm of thickness and they are covered on each side by a uniform layer of copper of 35um of thickness.

Once that the lateral supports and other components are soldered on the both the Bk1B111E1 sides, the Bk1B111E20 structure becomes a standard part. It will become a defined configuration only depending on how the hinges are oriented and fixed.

In order to estimate total weight of a single tile, the SolidWorks tool called Mass properties is used to get the weight of a single tile configuration starting from its real proprieties of the materials provided in chapter 9. The weight of a single tile in configuration A is about 25g (with 4 solar cells, the lateral supports, the side blocks and the hinges already fixed). The other types of configurations for the tiles are the same from the weight point of view. In this way a complete 1B111E structure of three tile is about 80g. The materials of the hinges and the other mechanical components will be addressed in the following paragraphs.

4.3 Side Blocks Design

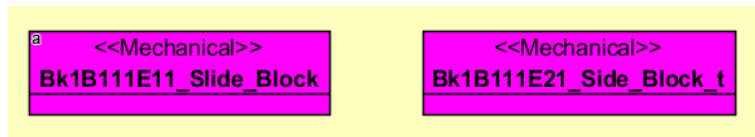


Figure 35: Side Blocks elements.

The side blocks are useful when the 1B111E structure is completely closed to avoid small slides that can lead to the damaging.

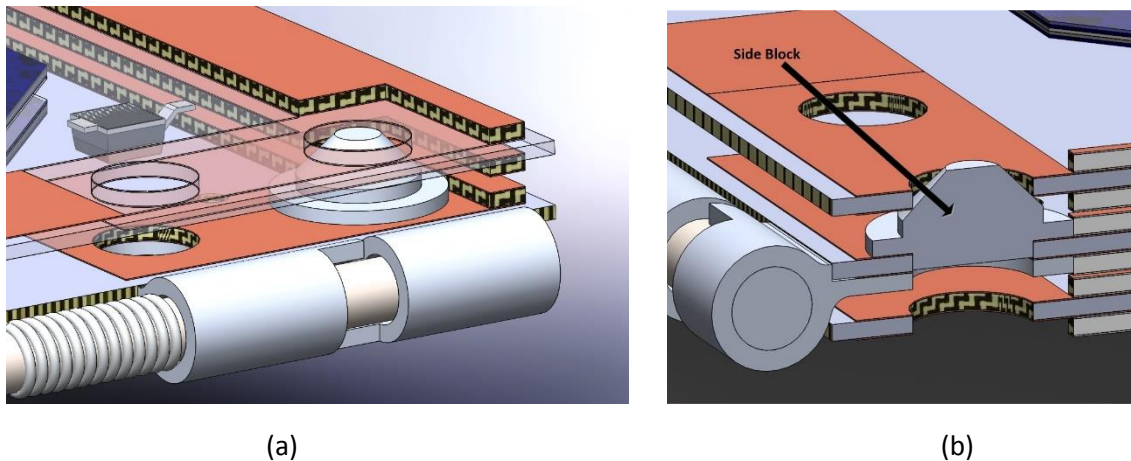


Figure 36: Side block (a) Example of a side block on tiles (b) Cross section of a side block on tiles.

The side blocks present a bottom extrusion used for its aligning and interlocking during soldering on board. The extrusion is designed in order to be interlocked into the holes of the standard tile (this extrusion it is clearly visible in the Figure 36 (b)). The upper part of the side block is the physical extrusion employed in the interlocking with the other tile. It is in wedge shaped in order to avoid that small thermal expansions, and consequently the volume growth of the component, can block folded the entire structure. For the space problems the structure is designed in such a way that a bottom tile, blocks the upper tile by means of the slide blocks. In this way a bottom tile mounts the slide blocks used to block an upper tail. This choice is functional because in this way the final tile does not needs to block other upper tiles. So there are not need of the side blocks on the upper tile and then they are not mounted. The global thickness of a structure of tiles is so reduced by the lack of the thickness of the side block. The problem of this solution is that an appropriate side block, has to be designed for an ARAMIS CubeSat side tile that constitutes the base tile for an entire 1B111E structure. The Bk1B111E21 side block is designed for this purpose. To simplify alignment, it has an alignment hole of 1mm.

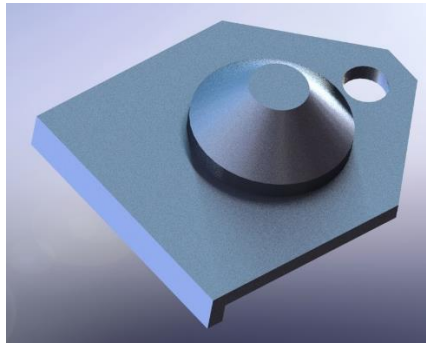


Figure 37: Side Block for base support tile.

Being the Bk1B213A1 a base tile for the 1B111E structure, it implements two of the Bk1B111E21.

4.4 Hinges Design

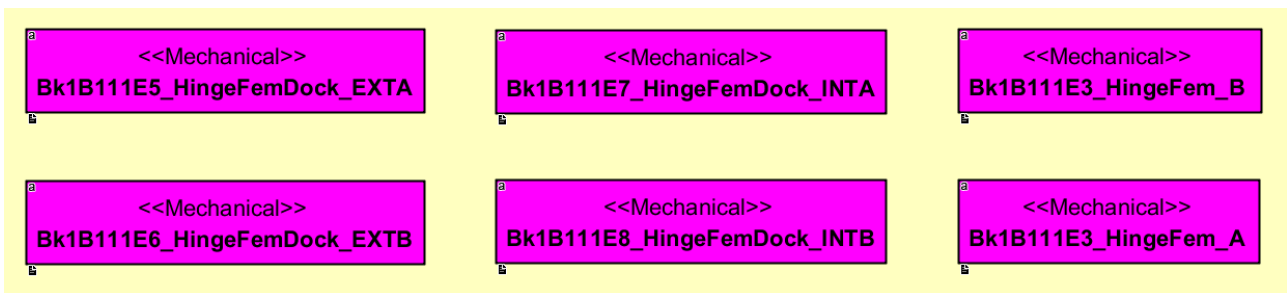


Figure 38: Types of Hinges.

The mechanical system of deployment of the 1B111E is hinge based. Each joint between two tiles is done using a couple of two hinges on the two ends of the tiles. The use of two hinge points at the two opposite ends of the folding edge of a tile, is chosen to improve the stability of the structure. The high stability is needed both for the opening phase that when the structure will be completely opened.

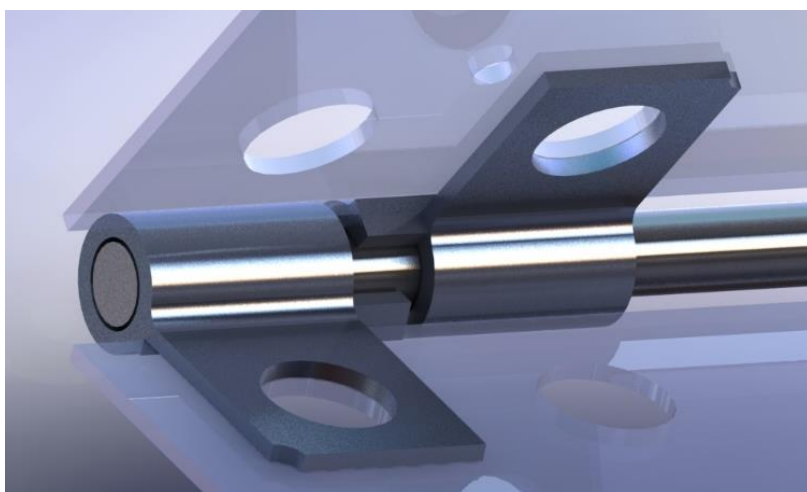


Figure 39: Two hinges connected between them.

A hinge is a single mechanical component in Aluminium or Copper material⁵, designed in order to be easy manufactured using burs and drills. Each angularity is carefully analysed in order to identify weaknesses and so to create fittings on it. One Hinge presents two holes, one is for the rotation axes of the hinge, the other it is used for alignment and for the interlocking purposes with the side blocks. Each hinge is designed taking into account the small available spaces into P POD module, in such a way, its diameter is chosen following strict requirements and so it has a small external diameter of 3mm. The hinges present a mechanical stop as it can be seen in Figure 40 (a). Each hinge is soldered, aligning its alignment hole to the tile correspondent. If the alignment is correct, between the two connected hinges there is a small space of 0.5mm. This is done in order to allow a mechanical tolerance against the thermal expansions, avoiding a possible locking of the hinges. Moreover the extrusion of the mechanical locking tab is 1.5mm, in this way, a worst case of a complete shift to the side of a tile, permits to every hinge of expose always a surface of beating on the mechanical tabs of at least 0.5mm.

The mechanical stops are used to control the rotations of the hinges in order to know the final position of the hinges. This choice is considered in order to avoid that the inertia of tiles during opening phase can cause an extra rotation in degrees, bringing the tiles in wrong positions and such of hitting others satellite components. In particular the mechanical stops have the task to stop rotation once that a board has completed a 180° rotation with respect to the other connected tile. The two type of hinges for the tails are realized in two different shapes, the A and the B. Each one differs from each other by the side where the mechanical stop is extruded, with the reference to the side of soldering. This latter is distinguishable because is present a board stop. For details about how the hinges types are used in relation to the configurations see chapter 2.2.3.

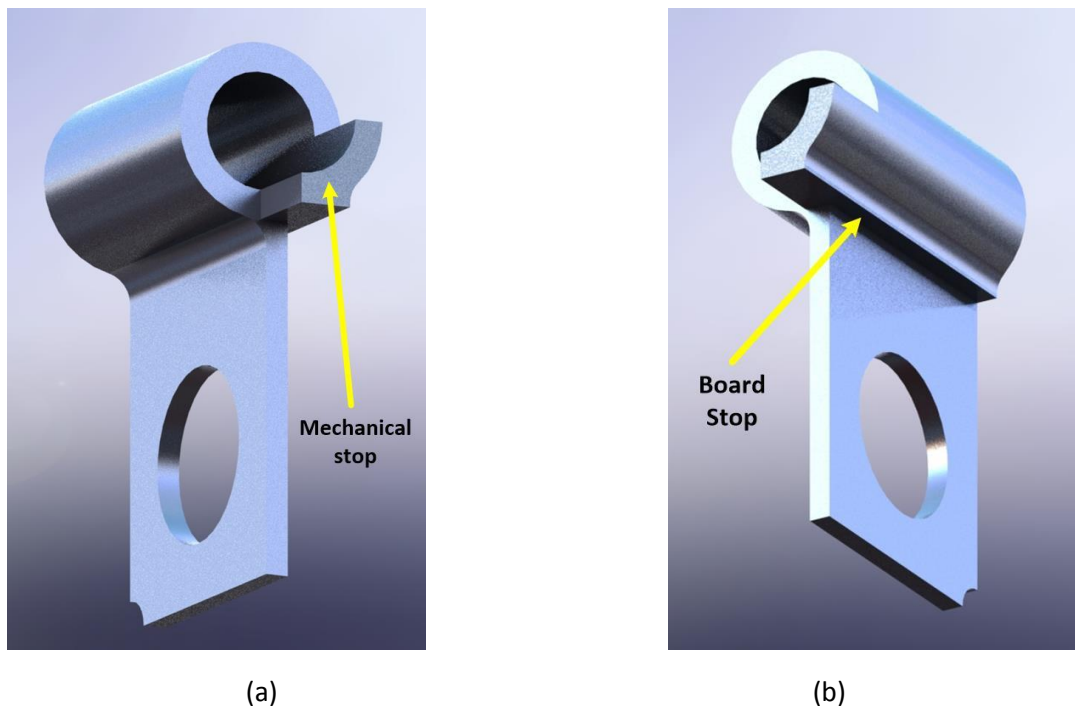
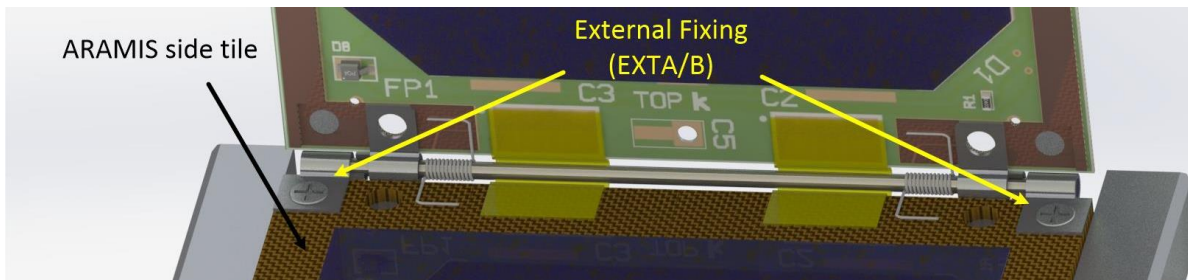


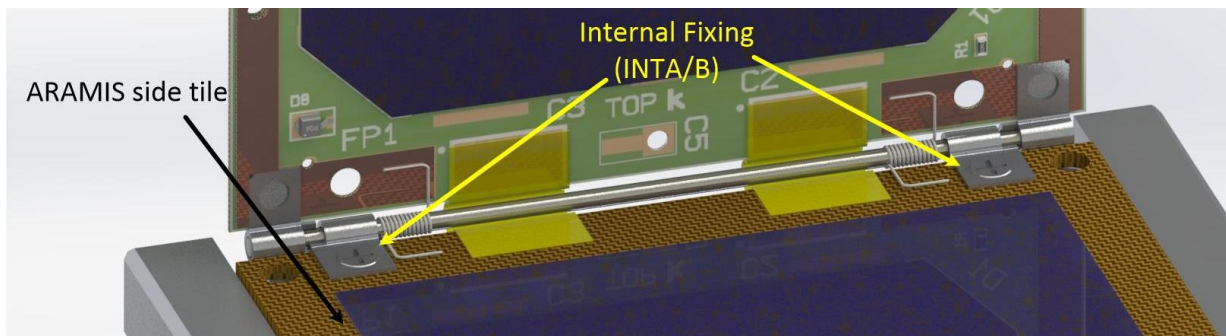
Figure 40: Tile Hinge (a) Mechanical locking of rotation (b) Mechanical board stop

⁵ The material of the hinges can be or Aluminium or Copper. The aluminium has good strength proprieties but it is not easy to solder to the copper pad of the RST. The Copper has not good strength proprieties, but it is better soldered on the copper PAD of the RST. For the simulation purpose, I used the aluminium.

The Bk1B111E3 and the Bk1B111E4 are respectively the hinge type A and B. These ones are used for the mechanical connections between 1B111E tile and others 1B111E tile. These are soldered only to the Bk1B111E20 standard tiles. Obviously the A and B types must have the possibility to be connected and fixed to a 1U ARAMIS side tile (Figure 41). In order to do that, other kinds of hinges are appropriately designed to be soldered on 1U ARAMIS side tiles. Since on the faces of the CubeSat it is possible to use three kinds of fixing holes (and these hinges must to be as well as soldered also screwed), everyone with different spacings, these new hinges have to be compatible with each one of the holes. The chapter 2.2.3 and 2.2.5 explain better this issue. In such a way are designed four types of hinges for the 1U ARAMIS side tiles: Bk1B111E5, Bk1B111E6, Bk1B111E7 and Bk1B111E8, that are called in easy manner respectively EXTA, EXTB, INTA and INTB types. In Figure 41 are shown how these hinges are used and how they are fixed to 1U side tile of an ARAMIS satellite, also by means of screws.



(a)



(b)

Figure 41: ARAMIS side tile hinges fixing example (a) INTA & INTB (b) EXTA & EXTB

A main difference from the hinges A and B is the mechanical stop. In these hinges the mechanical stop is designed in such a way that a rotation of a standard tile connected performs a rotation of 90 degrees. This is done in order to stop the first tile of the array of the 1B111E structure, to 90 degrees with respect to the 1U side tile surface of the ARAMIS CubeSat. In this way keeping a perpendicular position, the solar panels can be easily oriented to the sun.

The Figure 42 shows the shape of the 1B111E structure after a deployment. The perpendicular position of the Bk1B111R20 tiles is possible to the mechanical stops of the hinges. The Figure 42 (b) represent instead the 1B111E structure completely closed. In this position the mechanical stops of the hinges are involved in structure stability, because they are to the end rotation limit, in opposite situation respect to the opening.

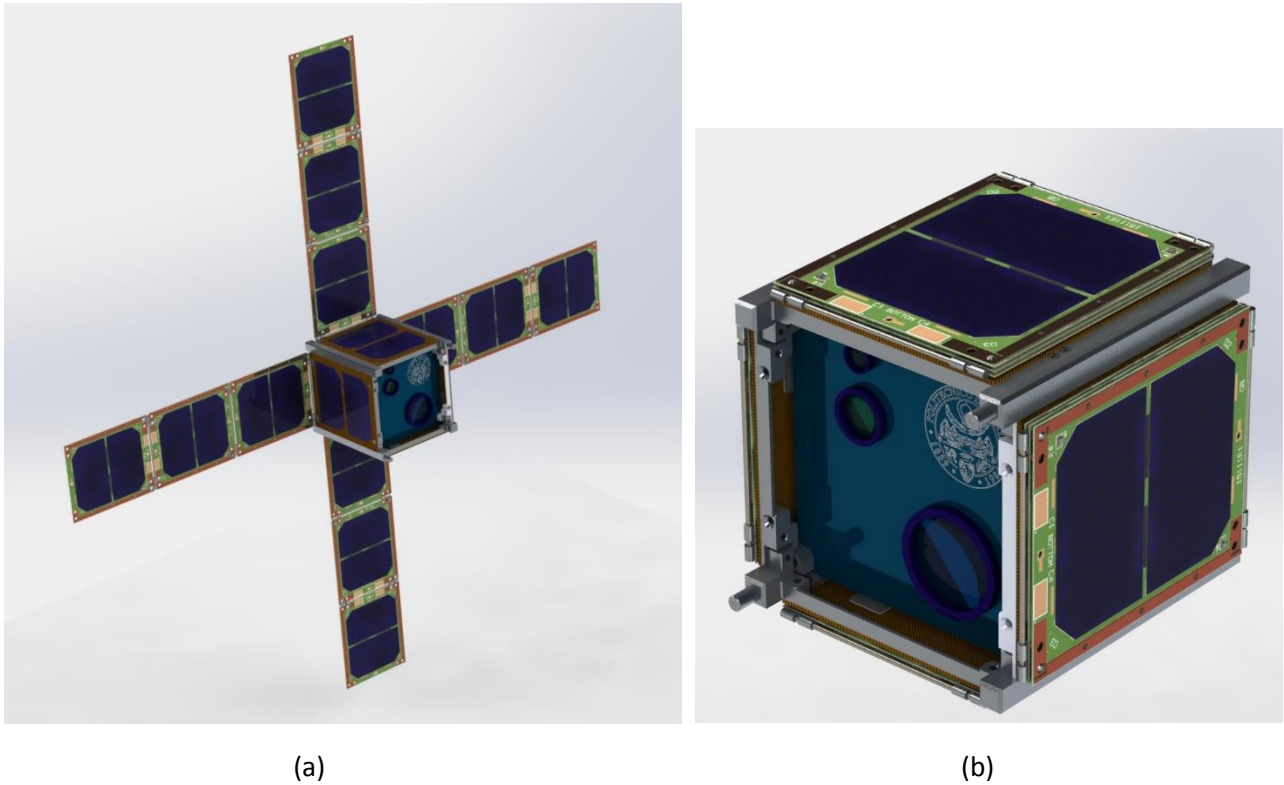


Figure 42: CubeSat 1U (a) 1U with 4 1B111E structures completely deployed (b) 1U 1B111E structures completely folded

4.5 Bk1B111E9 Hinges Pin Design

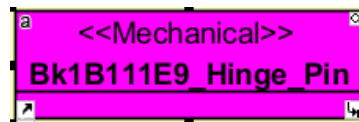


Figure 43: Bk1B111E9 Hinge Pin.

The hinges are fixed to each other by means of a pin called (Bk1B111E9). It is manufactured with the same kind of material of the hinges (Aluminium or copper). It is a simple cylindrical shape with a diameter slight less to the diameter of the axis hole of the hinges, in this way is allowed the rotation of the hinges around the pin, also in case the thermal expansion increase the volume of the pin. The pin is simply wedged into the hinges of two tiles already aligned and thus, it is soldered on one between the external hinges or on both.

4.6 1B111E Deployment System

A set of mechanical elements preloaded are employed to obtain the physical openings during deployment phase. The whole structure starts folded on launch, so it is charged by these mechanical elastic elements that consist of a couple of torsion springs for each bending angle and directly fixed on the pins of the hinges. Along its axis, the hinge pin is then hinged together to the springs. An appropriate PCB pad placed on both two connected Bk1B111E20 tails, is used to fix by soldering the two ends of the spring. In this way the spring has only the possibility of twist. The mechanism is clearly shown in the Figure 59 and Figure 41. The system is very simply from the mechanical point of view, and this allows the possibility to easy redesign of the mechanical element. Furthermore, being the system simple, it can be easily controlled giving more reliability.

4.6.1 Springs Design

The springs are torsional. Their main diameter when the springs are closed, must be less than the diameter of the pin of the hinges. The two ends must be sized so as to not exceed the size of the welding pad. The springs were chosen by springs present on the market, according to the characteristics of size and elastic constant desired. However, there is the possibility of being able to design the springs according to the desired specifications. To do this, the design parameter that you want to derive by a spring is the torsion constant.

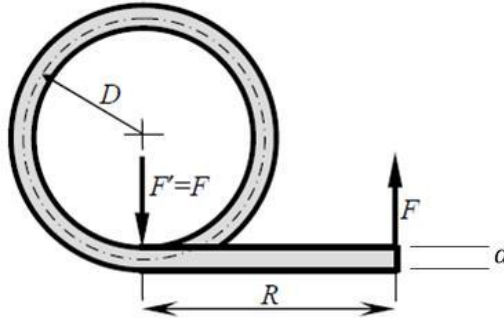


Figure 44: Torsion Spring scheme.

Referring to Figure 44, the torsion constant is equal to:

$$K = E \frac{d^4}{64 \cdot D \cdot n} \quad (1)$$

Where E is normal elastic modulus of the material⁶, D is the main diameter, d is the diameter of the wire of the spring and n is the number of turns. Thus depending on constrains involved and the material chosen, the spring can be designed with the appropriate elastic constant. A good solution evaluated for this thesis was the Copper Beryllium material for the springs. It has good properties of strength and elasticity. Furthermore, the springs in CuBe can be used as electric contact because its electric conductivity is similar to that of Copper⁷.

4.7 Mechanical Model

The opening of deployment for the 1B111E needs to be analysed from a mechanical point of view. For the analysis purpose a case of three tiles is considered. During deployment, the three tiles can assume wrong positions, meaning that some tile can hit to the 1U CubeSat structure or to other external elements of the satellite. This can be easily possible just because the 1B111E structure is conceived for not having any kind of mechanical guide for the opening. At first supposing the bodies stiff, these unwanted positions may be reached because there are not impacts completely inelastic between the mechanical stops of the hinges. In this way the oscillations can produce backward returns for the tiles. In order to avoid that, it is important to understand how the tiles could move. Its opening occurs thanks to the thrust given by the torsion torque applied to each movement angle and respect to the hinges constraints.

The Figure 45 provides a 2D mechanical model of the 1B111E structure composed of three Bk1B111E20 tiles.

⁶ The elastic modulus is a mechanical property of linear elastic solid materials. It defines the relationship between stress (force per unit area) and strain (proportional deformation) in a material.

⁷ Generally the alloy used for the application of elastics electric contacts is at 3% of Beryllium.

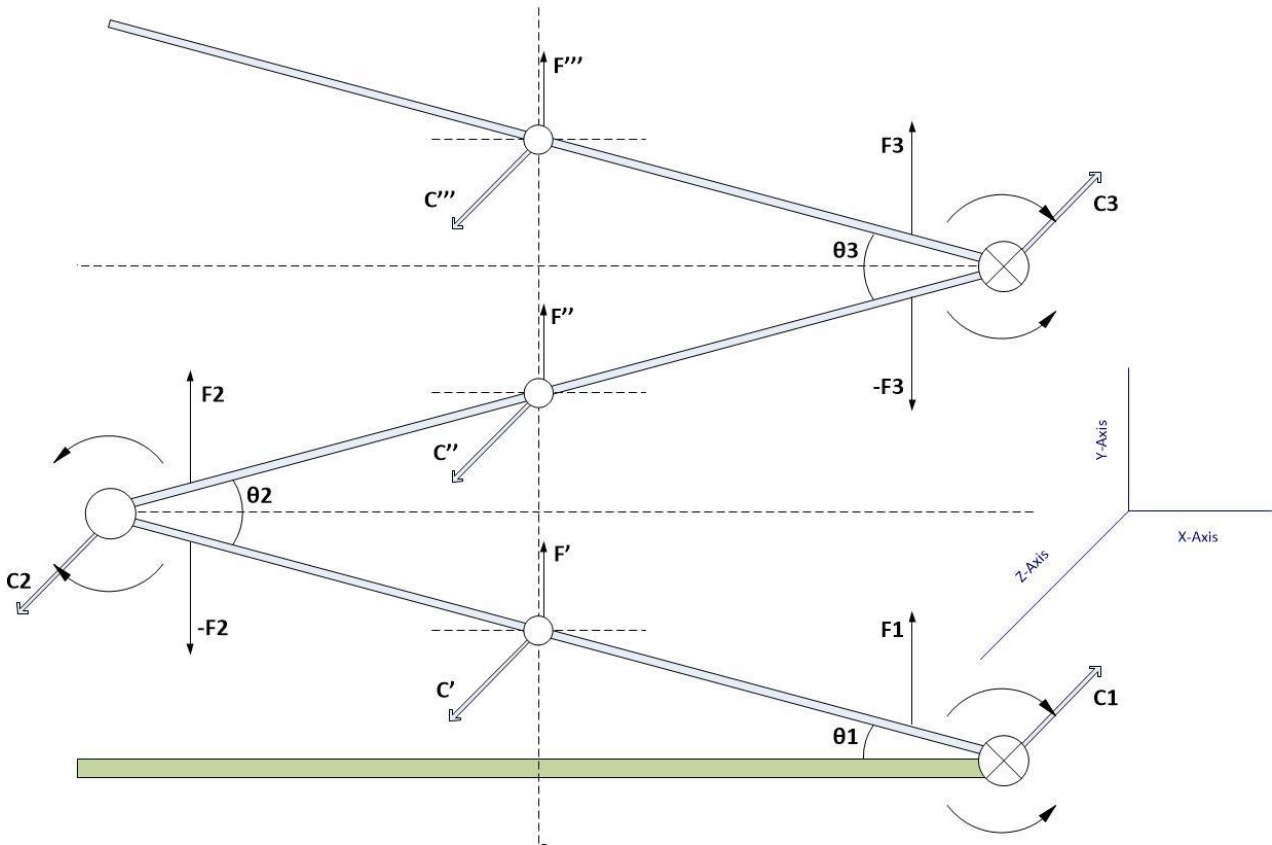


Figure 45: 1B111E Structure Mechanical Model

In the model above, C_1 , C_2 , and C_3 are three torques relative to the three torsion springs that open the tiles. These torques are shown with their conventional direction (arrows along z axis) and for each one are also shown the action and reaction torques using circular arrows. θ_1 , θ_2 , θ_3 , are angles between tiles. F_1 , F_2 , F_3 are the resultant forces of each tile. The movement is analysed always considering that the tiles movements are referred to their centre of mass. In these points the global torques C' , C'' , C''' and the global forces F' , F'' , F''' are defined. In first approximation is simple to guess that the upper tile drags less inertia, so its opening is fast. The second tile drags more inertia, that is its and the inertia of the upper tile, so its opening is slower. Even slower will be the bottom tile. Obviously its opening motion it is very difficult to guess and thus there is the needing of an analysis of the motion. The analysis has to consider the types of the impacts between the mechanical stops of the hinges, the frictions, the damping and the inertias. In this way, since the number of the variables is very high, with a set of parameters too complex and approximated to be used into an analytic analysis, the model of Figure 45 is used to build a simulation model, where the real parameters of the materials are further considered. The simulation of the mechanical model is described in section 4.8.1.

4.8 Mechanical Simulations

The Mechanical structure is analysed in detail from different point of view. Based on the model of paragraph 4.7, the model of a 1B111E structure is realized in SolidWorks and the opening simulation and the analysis are performed. Other studies using other tools are performed. A single standard tile of the 1B111E structure is analysed from vibration point of view: the natural frequencies are identified and the simulations of the vibrations are performed to the natural resonant frequencies. All parts in SolidWorks are considered with their real properties of the materials, inserted into a SolidWorks material library specially created. The library of the materials is provided in final chapter of the thesis (section 9.7). For all types of simulations that involve the SolidWorks tools, all simulations are performed taking into account all parameters and the aspects of all simulators. Before starting with the descriptions of the simulations, it is good to explain what is the meaning of mashing. This because the mashing is the basic principle of the FEA algorithms, used by the simulations of

SolidWorks. The process starts with the creation of a geometric model. Then, the program subdivides the model into small pieces of simple shapes (elements) connected at common points (nodes). This process is called mashing. For more information see the online help of SolidWorks mashing [8]. The meshing is a very crucial step in design analysis, it may affect heavily the result of simulation. Increase the number of mesh, means increasing of simulation accuracy but it means also the increasing of the time simulation. If the number of the mesh is too high, the simulation time may grows so much that it may take several days. So it is important to find the right trade-off between accuracy and simulation time. A rule of thumb generally is to create mesh curved based, in order to densify the mesh in correspondence of small parts and create larger mesh on larger parts. This can be done manually or automatically using the simulator options.

4.8.1 Opening Simulation

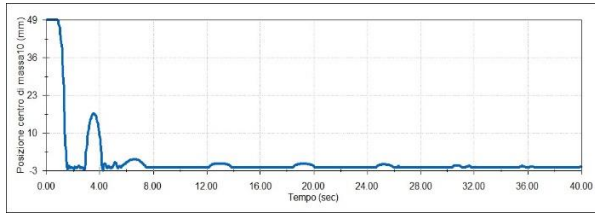
Since the opening system does not use any type of mechanical guide, the entire system is meticulously analysed in such a way to suitably choice the torsion springs and so reduce the resulting dumping of the opening phase. This permits to avoid that the tails can hit against other satellite components. The complex mechanical model of Figure 45 is translated into a SolidWorks model. The software gives the possibility to apply torsion forces that simulate the torsion torques of springs and verify how the opening system moves during the evolving of the time. The employed software tool is SolidWorks Motion Study. The case of study is a structure modelled in the configuration AAAf. The other configurations of three tiles are equivalents from the openings analysis point of view. On each angle of bending, the two torsion springs are substituted with a dummy torsion spring that simulates a torque applied on the centre between two hinges. In order to use correctly these torsion forces, have to be defined the two ends of two bodies (in my case the two tiles) where the torque has to applied and a third body element used to define the axis of rotation of these forces (in my case, I use a hinge because it is oriented to the same axis of rotation obviously). In this way three linear torques are inserted. The elastic constant k and the angle of rest of the spring are defined for each torsion spring. The bodies are considered rigid to simplify the analysis. The groups of contacts are used for the contacts of the hinges, both to define the physical contacts that realize the collisions either to give them the proprieties of the type of impact and the frictions. Furthermore the manual selection of contacts ensure the correct detection of contacts by the solver, because it can happens that in case the manual contacts are not manually forced, the solver excludes from computation all parts with two contact faces in contact along a point or an edge or else if the contact area is extremely small [9], In this situation, some particular contacts required may not be revealed. It is always advisable to add contacts manually. On the contacts are used the elastic proprieties of the real materials and in particular for hinges is selected the standard type of impact of the "Aluminium dry"; while for the friction of the hinges are used both the static and the dynamic friction whose values are those ones of the Aluminium dry:

- *Dynamic friction*
 $V_k = 10,16 \text{ mm/s}$ (dynamic friction speed)
 $\mu_k = 0,2$ (dynamic friction coefficient)
- *Static friction*
 $V_k = 0,1 \text{ mm/s}$ (static friction speed)
 $\mu_k = 0,25$ (static friction coefficient)

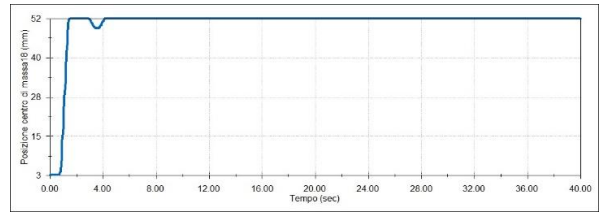
The entire structure is analysed in absence of gravity and in vacuum. Once all parameters have been defined, the structure composed of three tiles is folded and the simulation is performed for different values of elastic constant for the springs. The Figure 46 and The Figure 47 show the results.

	Rest Angle [deg]	k1 [N*mm/deg]	k2 [N*mm/deg]	k3 [N*mm/deg]	Complete Damping Swings [s]
Bad Opening	190	0,003	0,003	0,003	>80
Good Opening	270	0,058592593	0,038925926	0,019666667	<5

Table 3: Torsion springs simulation parameters

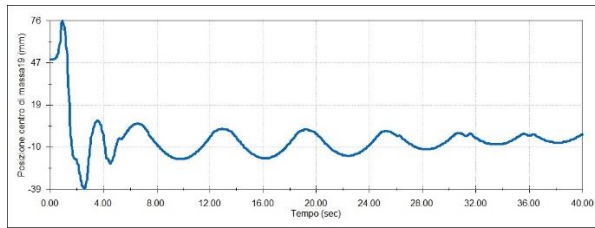


X

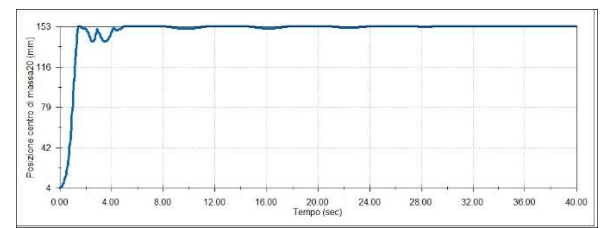


Z

(a)

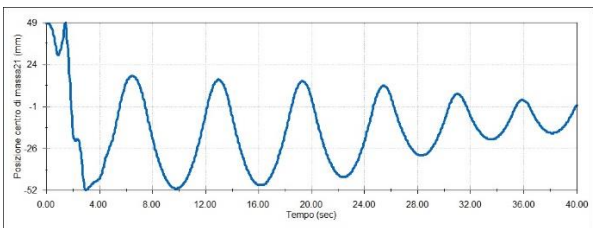


X

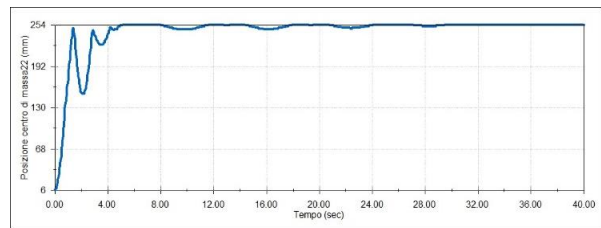


Z

(b)



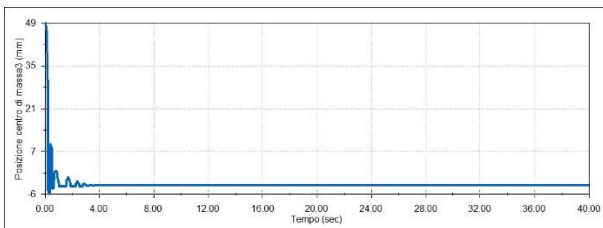
X



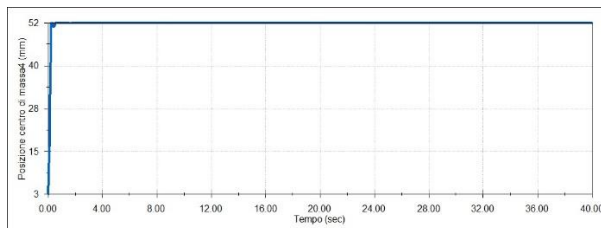
Z

(c)

Figure 46: "Bad Opening" displacements of tails due to damping (a) Bottom tile (b) Central tile (c) Upper tile.



X



Z

(a)

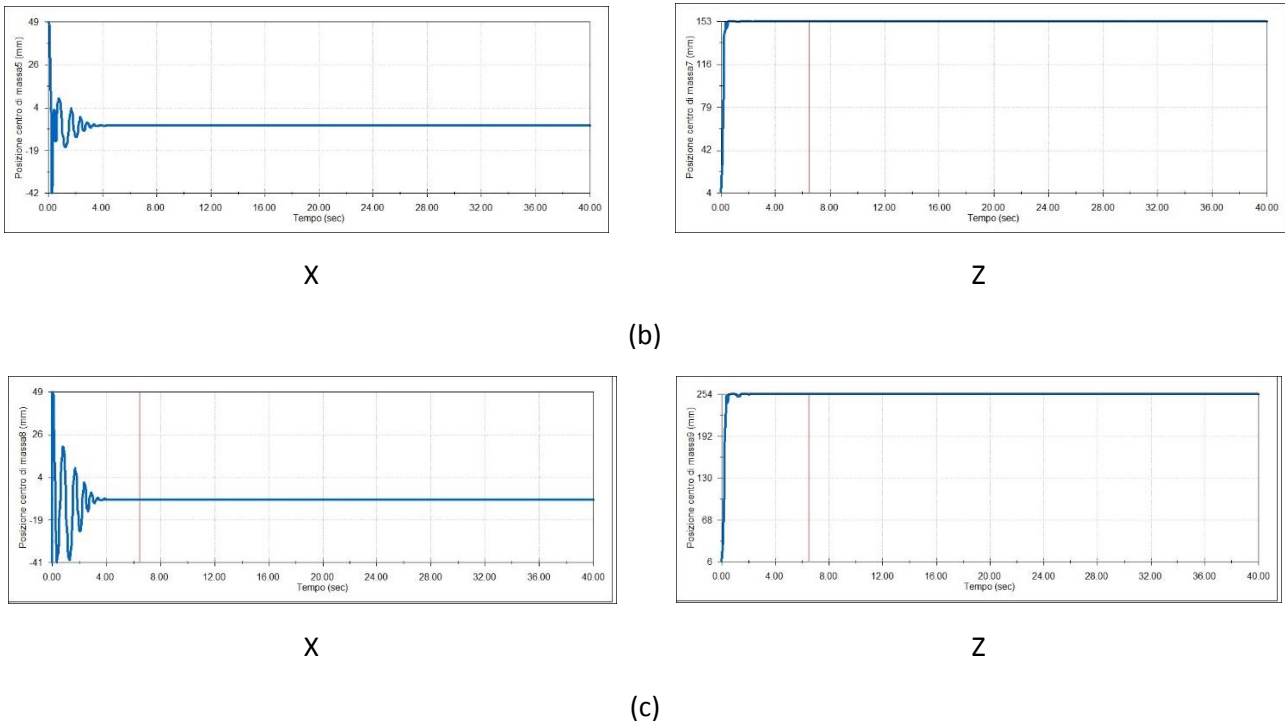


Figure 47: “Good Opening” displacements of tails due to damping (a) Bottom tile (b) Central tile (c) Upper tile.

Several simulation have been performed, but I show only two of them in order to provide good basis of comparison: one simulation named as “Bad Opening” that gives bad results (Figure 46) and another one named “Good Opening” that gives good performances of damping (Figure 47). The graphs show the displacements in mm of each tail of the structure in function of the time. The displacements are taken both in horizontal (X) and vertical (Z) direction, using the centre of mass of each tile with respect to an origin placed just at the base of the three tile structure and coincident with the axis of deployment. The Figure 48 shows an example of the two displacements in x and z for the upper tile. Each graph has the same x scale with a maximum of 40 sec. Their starting points coincide with the initial position of the relative tile. The graphs are auto scaled on z axis by SolidWorks. In order to avoid the impacts of the tiles against the satellite structure, in first approximation is enough to observe the z displacements. Along the vertical axis, the tiles move away from the satellite, thus much less is dumping and much less is the probability to have impacts. As it is observable from Figure 47 the good opening presents vertical movements almost perfect without damping. For the performance in terms of damping adjustment, instead, is enough observe what happens in horizontal direction where the dumping is worst. In the “Bad Opening”, the X dumping is too low, in this way the structure stabilization time along the deployment axis is too high. It exceed the 40 seconds⁸. For the “good opening simulation” the results are widely better. The dumping for each tile does not exceeds the 5 seconds, more of 10 times less of the case of the “Bad Opening”. The main condition in order to obtain the dumping reduction is obviously the elastic constant of the springs. Increasing the constants of the springs means increasing its torques and thus it means decreasing the restitution force to the impact of the mechanical stops. This means reduction of the damping effect. During simulations, another improvement was clear. If the three springs have different elastic constants, the damping is heavily reduced, this is the case of the “Good Opening”. The concept is that bottom springs have to push more weight of inertia, it related to the entire structure. Instead the upper springs have to push much less inertia, practically only that one of the upper tile. In such a way, an unbalanced chosen of the spring constants gives best results for opening. The best choice analysed, uses springs with elastic constants greater for the bottom springs. Obviously, since the derivative of the space with respect to the time is the velocity, the strong slopes of the graphs of Figure 47

⁸ Really the graph shows only 40 seconds, because in a complete simulation are exceeded also 80 seconds

highlight very high derivatives and thus it means a high velocity of deployment. High speed for the opening means also high forces of impact. The values of elastic constants in Table 3 for “Good Opening” are real values of springs chosen by a real manufacturer in order to understand which performances is possible to reach with the springs in the market. Their constants values are chosen in order to do not exaggerate too much with the forces of impact, even if the structure can endures at strong impacts. This resistance is due to absence of aging on the mechanical hinges, because the opening and the impacts will occur only once at the deployment phase. Furthermore, the using of high torques is a good choice because after a deployment, much more torque from the springs means much more stability (and so less vibrations) of the 1B111E structure during attitude manoeuvres. The springs are also chosen in order to be compatibles with requirements of the standard tile and with the requirements of the pin of the hinges. However, the springs can be designed according to the (1). Finally, using SolidWorks Motion Study, a motion simulation is performed for the “Good opening”. A small sequence of frames in Figure 49 shows the mains phases of the opening.

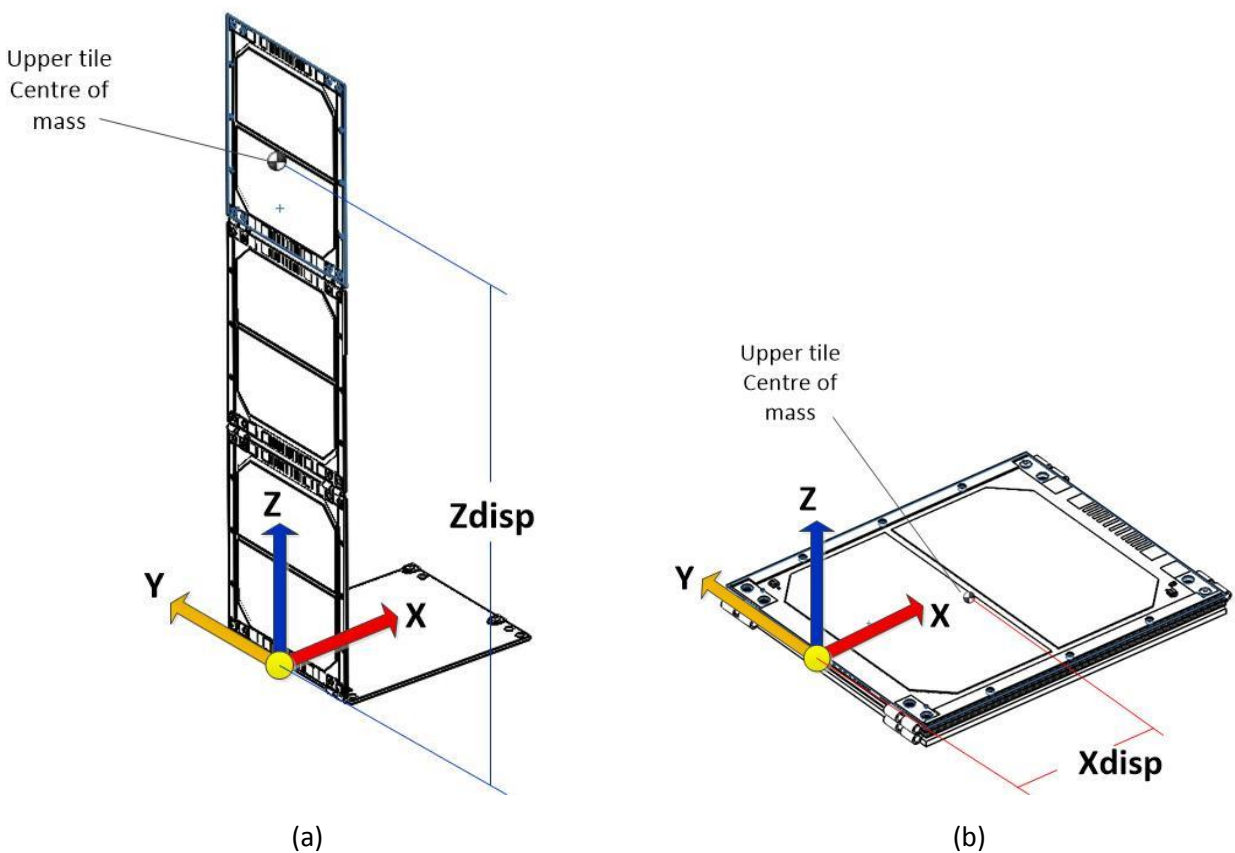


Figure 48: X and Y displacements from centre of mass (a) Vertical displacement (b) Horizontal displacement.

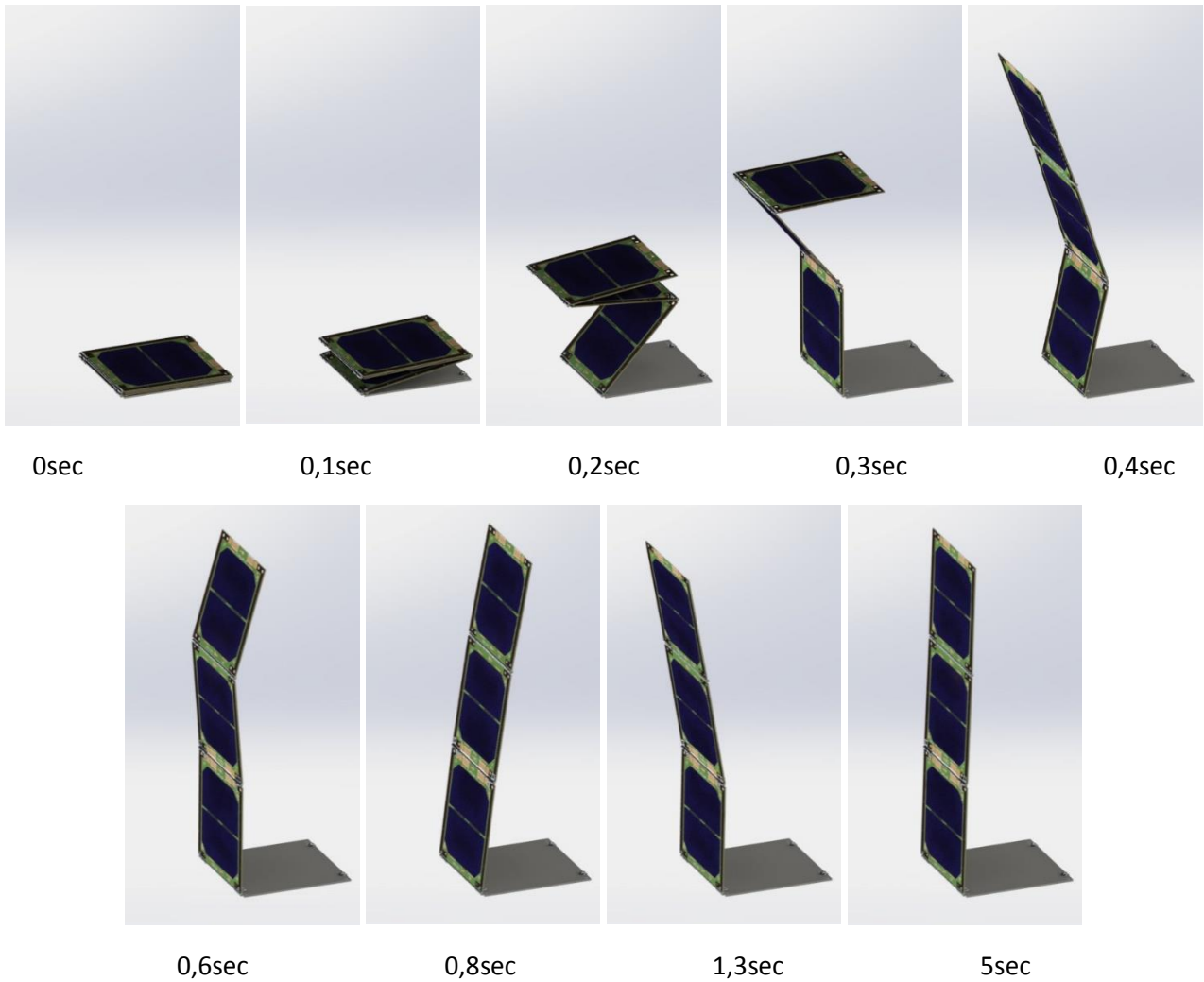


Figure 49: Main frames of the opening phase.

4.8.2 Natural Frequency

The SolidWorks Frequency Study provides a quickly and efficiently tool to investigate the natural frequencies of a design, with and without loads and boundary conditions. Understanding the natural frequency is important in predicting possible failure modes or the types of analysis required to best understand performance. Every structure has its preferred frequencies of vibration, called resonant frequencies, and each of them is characterized by a specific shape (or mode) of vibration. The frequency analysis with SolidWorks Simulation uses an Eigen value approach to determine the natural modes of vibration for any geometry. If a design's natural modes and its expected service vibration environment are closely matched, a harmonic resonance may occur and lead to excessive loads which will result in failure [10].

The Figure 50 show the model of simulation. It contains all components considered not negligible from the natural frequencies investigation. This simulation does not need external loads because the resonances frequencies are determinate on constrains imposed on the structure. In my model the only constrains imposed (yellow arrows) are: a fix body on the base tile (Figure 50 (b)), and the concentric surfaces on the holes of the fixing wires (Figure 50 (a)).

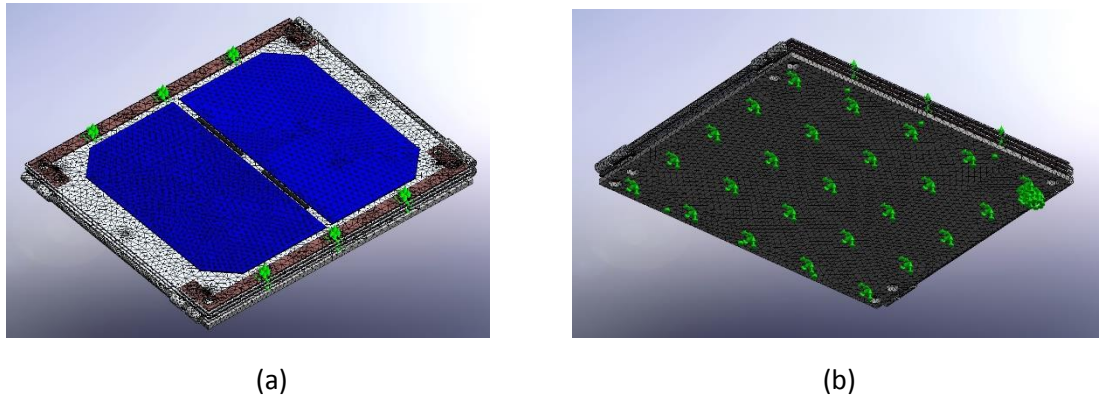


Figure 50: 1B111E structure model of natural frequencies simulation (a) Top view (b) Bottom view.

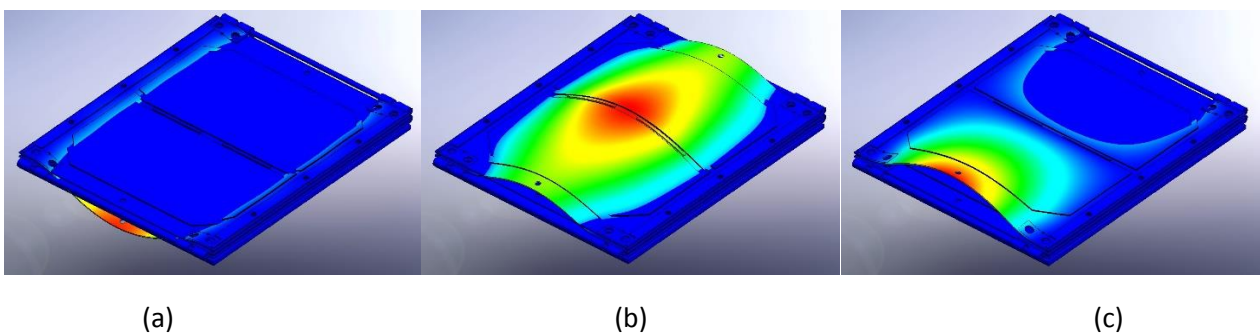
The base tile is configured with the properties of a perfect stiff material, in this way it can transmit vibrations to the tiles without deforming. The free contacts are inserted manually, in order to allow to the simulator the detection of the small contact surfaces otherwise not considered (see 4.8.1 for more details about the types of contacts). The real parameters of the materials are considered. Following a summary table with main simulation parameters is shown.

Nome studio	Natural_Frequencies(-Default-)
Tipo di analisi	Frequenza
Tipo di Mesh	Mesh di elementi solidi
Frequency range	0 – 1500 Hz
Tipo di solver	FFEPlus
Molla morbida	Disattivo
Migliora precision per portare a contatto le superfici con la mesh incongruente (lento)	Attivo

Table 4: Natural Frequencies Simulation Details.

The meshing is manually created, considering a minimum element of 400 μ m (for the smallest parts of the model), and a larger mesh of maximum 2mm. It is a good trade-off between accuracy and simulation time. For parts whose meshing gave failures, was made a mesh incongruent. The results of simulation are shown in Figure 51, where are depicted the deformations exaggerated for some of the resonance frequencies, in particular those frequencies that change completely the shape of deformation are shown.

Table 5 shows instead the summarization of the first natural frequencies of the structure until 1500 Hz.



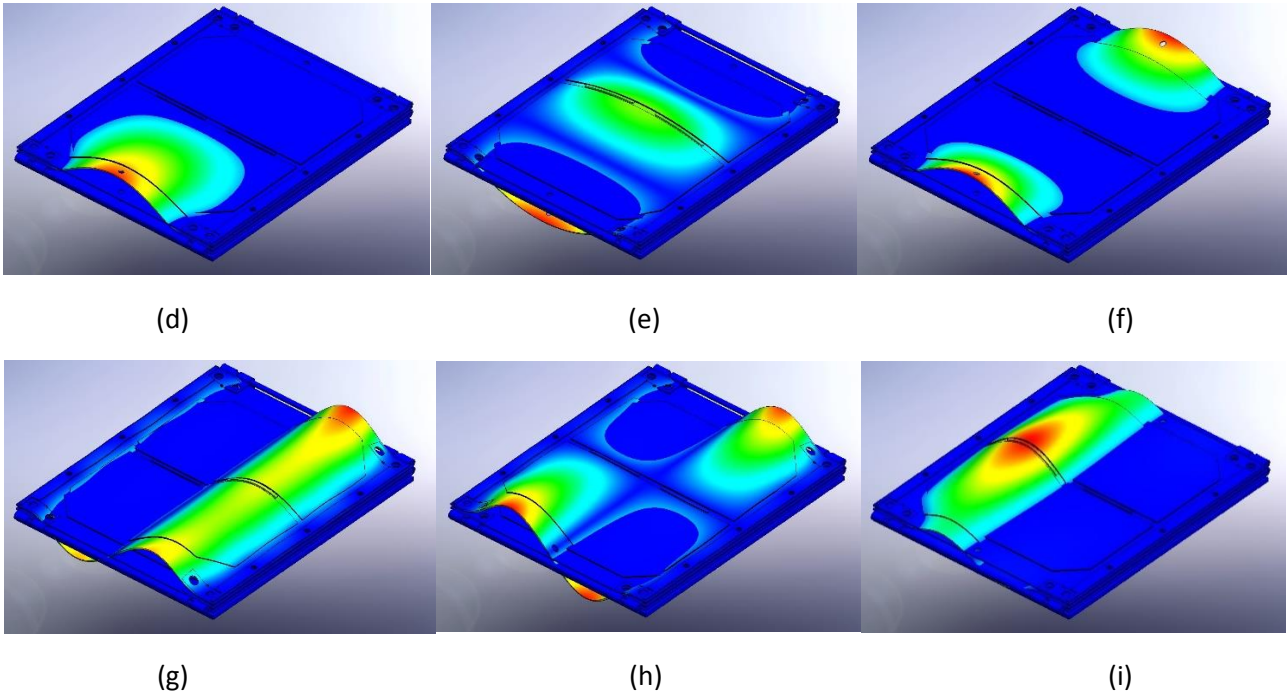


Figure 51: Plots of deformations exaggerated at resonance frequencies (a) Freq 1 (b) Freq 3 (c) Freq 4 (d) Freq 6 (e) Freq 7 (f) Freq 9 (g) Freq 10 (h) Freq 11 (i) Freq 13.

Natural Frequency	Frequency [Hz]
1	441.54
2	482.23
3	482.75
4	529.84
5	653.98
6	656.59
7	761.21
8	891.26
9	892.77
10	1223.5
11	1303.4
12	1322.8
13	1325

Table 5: Natural frequencies of the structure.

Plots of Figure 51 are exaggerated and so they results in a penetration of bodies. The exaggeration highlights better the shape of deformation at resonance frequency. The scale has no meaning, SolidWorks uses for this kind of simulation an arbitrary unit, the only meaning of this simulation is the finding of which are the natural frequencies and show the shape of deformation. The 13 natural modes had been found in the range of 1.5 kHz that is the spectre region of vibrations at launch that can gives significant results. Analyse the higher frequencies is good to explore what happens at those frequencies even if the deformations decrease quadratically with increasing frequency. A first conclusion can be easy deduced: referring to the Figure 53 that represents the spectrum of frequencies that will be evaluated, it is important to note that no one resonance frequency is present in the most dangerous range of frequencies (20-60 Hz) where the acceleration reaches the maximum of 11g. So, in first approximation the structure seems to have a good

response from the natural frequencies point of view. In 4.8.3 a single tile instead, is simulated at the natural frequencies in such a way to estimate a displacement of deformation.

4.8.3 Vibrations analysis

This simulation allows to calculate oscillations of the structure subjected to variable load. This is possible through the application of dynamic loads, the possibility to carry out simulations of stress on moving components, the analysis of the forces of impact over time, the vibration test shaker and seismic simulations [11]. In such a way this study is used as a shaker for simulate of vibrations. Since the entire structure of three tiles now results too heavy for the simulator solver⁹, only one single standard tile is simulated under vibrations. Furthermore it is difficult to apply external loads with respect to constrains in right manner. The simulation has to be intended as the verification that the resulting deformations do not exceed the half of the minimum distance between the two solar cells placed on different tiles when the 1B111E structure is folded. About the distance, I considered just half distance between two cells because both tiles, the upper one and the bottom one, they can be deformed at the same time as is shown for some frequencies in Figure 51. In this way if the minimum distance is about 0,3 mm (this is a value already over-estimated in order to maintain a certain tolerance), the half distance is 0,15mm. Furthermore, in order to maintain the compatibility with the model of the entire structure simulated for the natural frequencies investigation (Figure 50), constrains for the single tile must to be applied in the right manner and as much as possible equals to the same constrains that are applied to the tile when is interlocked in the side blocks inside a 1B111E structure folded. Even the constrains related to the presence of the fixing wires have to be considered.

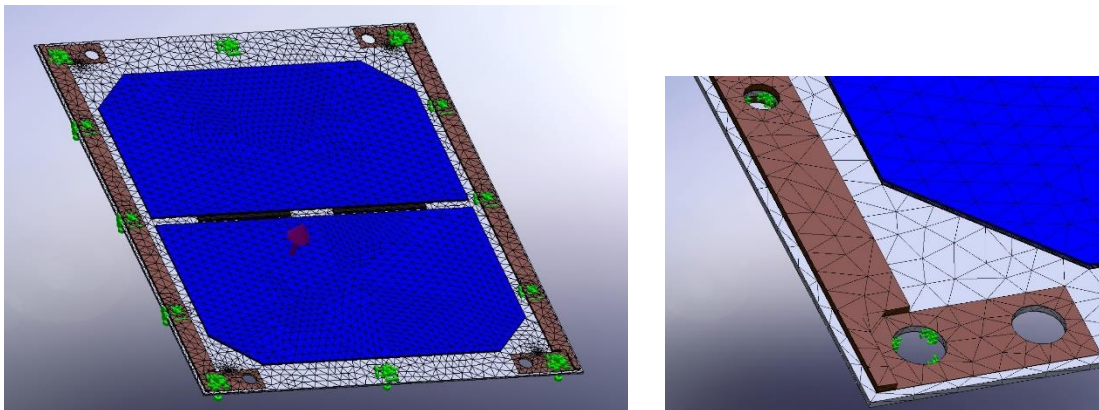


Figure 52: Standard tile model of dynamic harmonic simulation.

In Figure 52 are shown constrains: the yellow arrows are geometry constrains fixed and placed on each angular hole where the tile will be interlocked with the correspondent side blocks. The fixing constrains are placed also in correspondence of the holes where the fixing wires will be inserted and soldered, and where thanks to appropriate systems of mechanic shims, the tails result in a maintaining position. Those mechanic shims so are useful for the stabilization and the fixing of the structure reducing the displacements of deformation. The vertical axis represents the most critical direction from the vibrations point of view, because it is the axis where the structure bends more easily. In fact, the natural frequencies investigation had shown as all the resonances frequencies did deform the structure mainly along the vertical axis (Figure 51). In this way the violet arrow applied at the bottom of the base tile, represents the acceleration force for vibrations along vertical axis. The lateral vibrations can be neglected. The acceleration is performed applying a curve of acceleration in function of the frequencies. A worst case function is defined putting together the limits of the POLITO, of the ESA and of the Dnepr+50% [12]. The Figure 53 shows that curve in logarithmic scales. Since vibration analysis is strictly related to the dumping of the structure, in the simulation is used an

⁹ The number of base excitation has to increase at one for each tile increasing the global complexity of the model.

estimated value of 0.01 of modal damping. The modal damping is defined as the ratio of critical damping for each mode, where the critical damping is the lower damping that causes the return of a system to its equilibrium position without oscillation. Generally the modal damping is determinate experimentally, but when a test cannot be performed the data from a system or class similar are used to estimate the damping properties. The ratio varies from 0.01 for lightly damped systems to 0.15 or greater value for highly damped systems. Generally they are used smaller ratios, since that the higher ratios reduce the vibration amplitudes, in this way 0.01 is a worst case and a good choice of analysis [13]. The Table 6 shows a summary table with main simulation parameters.

Nome studio	Dynamic_Harmonic (-Default-)
Tipo di analisi	Analisi dinamica lineare (Armonica)
Tipo di mesh	Mesh di elementi solidi
Tipo di solver	Automatica
Molla morbida	Disattivo
Smorzamento	(-Modale -) [0.01] Su tutto il range modale
Migliora precisione per portare a contatto le superfici con la mesh incongruente (lento)	Attivo
Limite di bassa frequenza	0 Hz
Limite superiore di frequenza	1500 Hz
Num. Di frequenze risultato	15
Interpolazione	Lineare

Table 6: Vibration analysis simulation details.

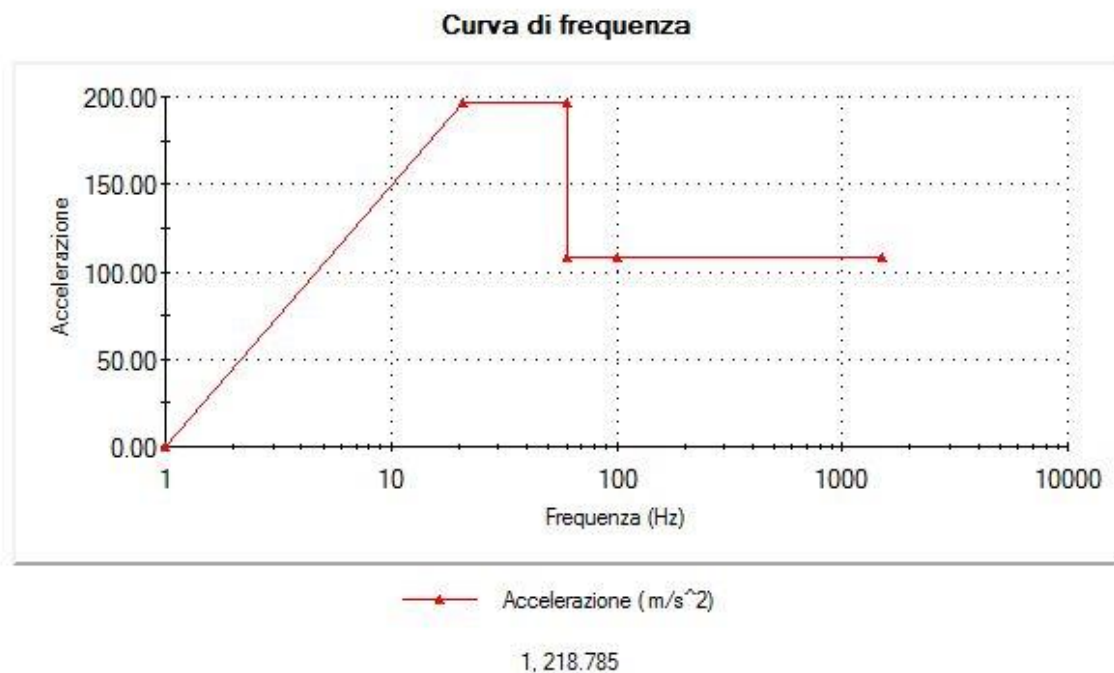


Figure 53: Vibrations stress spectrum during launch.

Taking into account that the external load that provides the vibrations follows the curve of Figure 53 using harmonics. This is done in order to simplify the analysis¹⁰. Once the simulation has been performed, results are evaluated using the displacement plot (in exaggerated format in order to show better the deformations) in the worst cases that means at the resonant frequencies obtained during the natural frequencies

¹⁰ Even if in a real launch the vibrations are random in their range, the use of harmonics gives the same results.

investigation (Table 5). Since that this simulation works exploiting all frequencies in the range in discrete manner, are selected the frequencies as much as possible nears to the frequencies in Table 5. The Table 7 is provided and shows the maximum displacements at the various resonance frequencies, highlighting in red the dangerous frequencies that make to exceed the maximum displacement tolerance estimated of 0.15mm. In Figure 54 are shown some of the main resonance frequencies of a single standard tile.

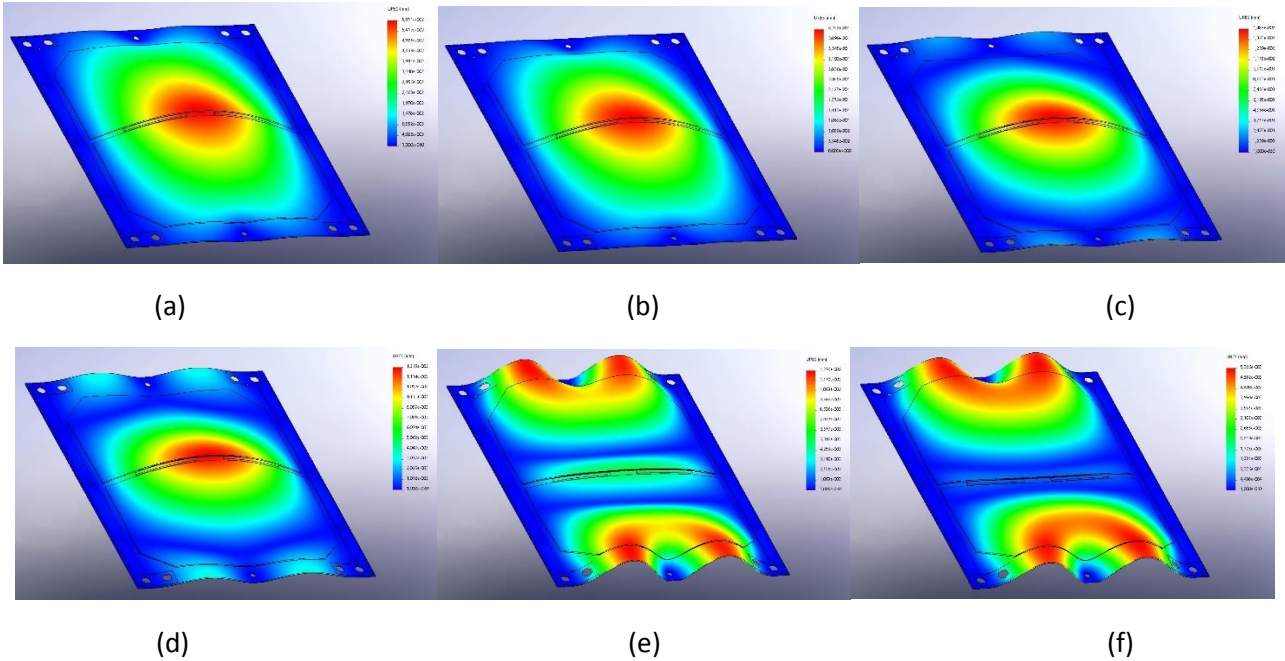


Figure 54: Plots of deformations exaggerated at resonance frequencies (a) Freq 1 (b) Freq 4 (c) Freq 7 (d) Freq 8, 9 (e) Freq 10 (f) Freq 12, 13.

Resonance frequencies	Frequencies	Max Displacement [mm]
1	436,328 Hz	0,059
2, 3	477,883 Hz	0,11
4	528,911 Hz	0,42
5, 6	697,058 Hz	0,024
7	808,366 Hz	0,014
8, 9	889,541 Hz	0,012
10	1224,4 Hz	0,012
11	1289,25 Hz	0,006
12, 13	1324,14 Hz	0,005

Table 7: Resonance frequencies of the standard tile.

In conclusion, while the investigation of the natural frequencies, gives me an estimation of natural frequencies and the shape of deformation of the entire structure, the deformations of Figure 54 represent the real deformation of each single tile subjected to vertical vibrations. Considering approximately the same resonance frequencies estimated in the 4.8.2, the results are interesting: along all the considered spectrum of vibrations, the standard tile behaves good avoiding to exceed the 0.15 mm. The only one exception is for the 4th frequency. This means that for the supposed conditions of simulation, the structure exceeds the constrain of 0.15mm. Taking into account that the damping is estimated for an extremely worst case, I refined the analysis, focusing to the critical frequency 4. In this way I increased the damping value and I performed again the same simulation, as long as the critical frequency is not fallen under the 0.15mm. This situation is achieved for a modal dumping of 0.04. Since it is not possible to find the dumping without an experiment of test of the structure, this last analysis gives the estimated lower limit for the damping of the tile. In other

words, if a real test, ensures that the damping of the structure of the tile is greater or equal of 0.04, it possible to assert that the 1B111E structure composed of three tiles, is robust to the launch vibrations within the spectre of Figure 53. This because with 0.04 of damping, the most critical frequency is under the tolerance margin of displacement of 0.15mm. The Figure 55 and the Table 8 show the final results for the mechanical analysis at the most critical frequency of one 1B111E structure composed of three tiles.

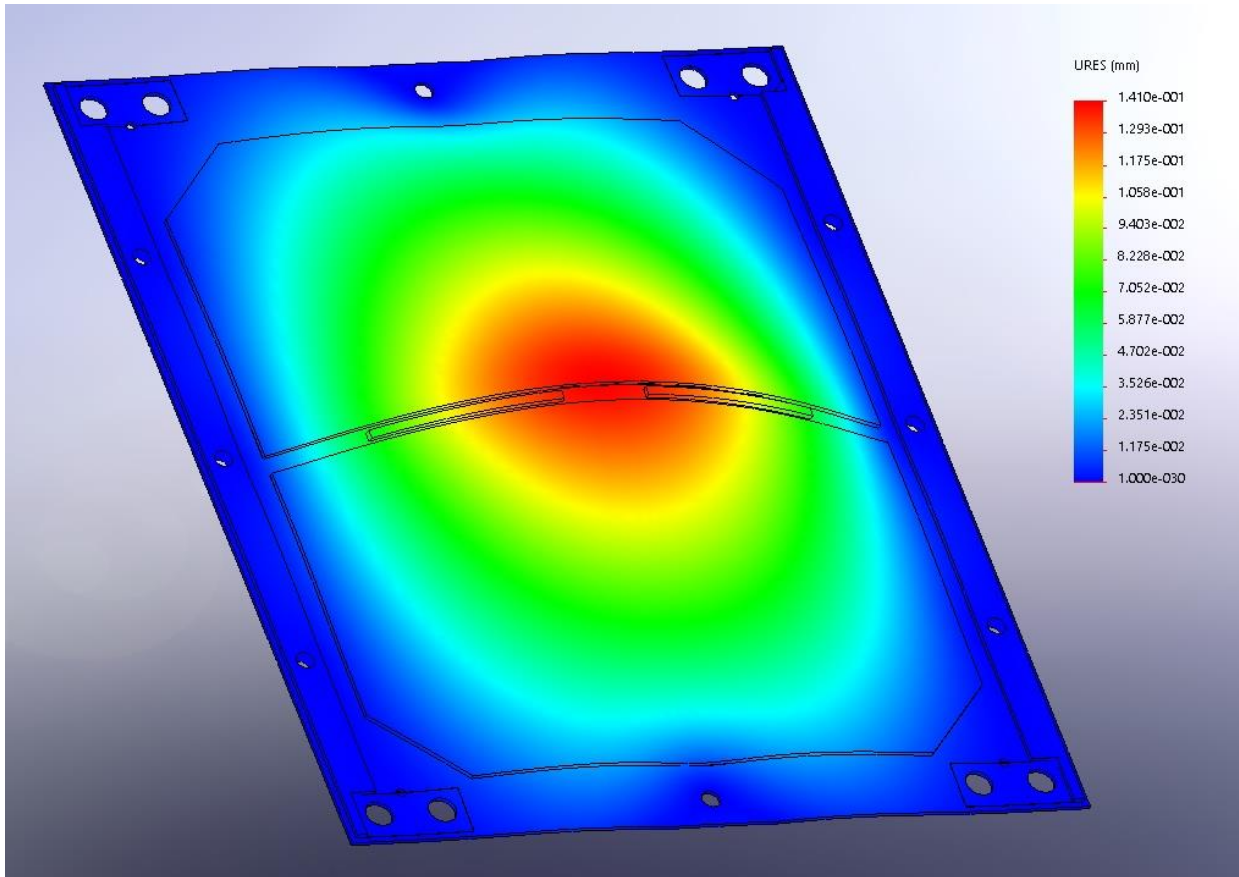


Figure 55: Plot of deformation exaggerated at resonance frequency 4.

Resonance frequencies	Frequencies	Max Displacement [mm]	Min Modal Damping
4	528,031 Hz	0,14	0,04

Table 8: Summary of the final result for the vibration analysis.

A further improvement was made to increase the reliability of the structure. As can be seen from Figure 55, the part of the tail more subject to the deformation is in the central one. The central point, however, has not the possibility to house sealing wires, since the asymmetric positioning of the four cells does not allow the realization of a through hole. In this way to deaden any possible slamming among the tiles, are realised two rubber shims for gaskets. These are inserted in in the gaps between the two solar cells and have the task of acting as mechanical stop with the solar cells, in the case the deformations exceed the margins of safety. The rubber gasket is choice since it can be easily machined and because some compounds are made to withstand to wide ranges of temperature. Furthermore, the rubber is a softer material of the glass of the solar cells, and if they flap against the solar cells do not cause injury or scratches on the surface of the delicate cells. These gasket are clearly visible in all the figures that depict a Bk1B111E20. These are the small black bars between two cells.

5 Bk1B111E1 Electrical Design

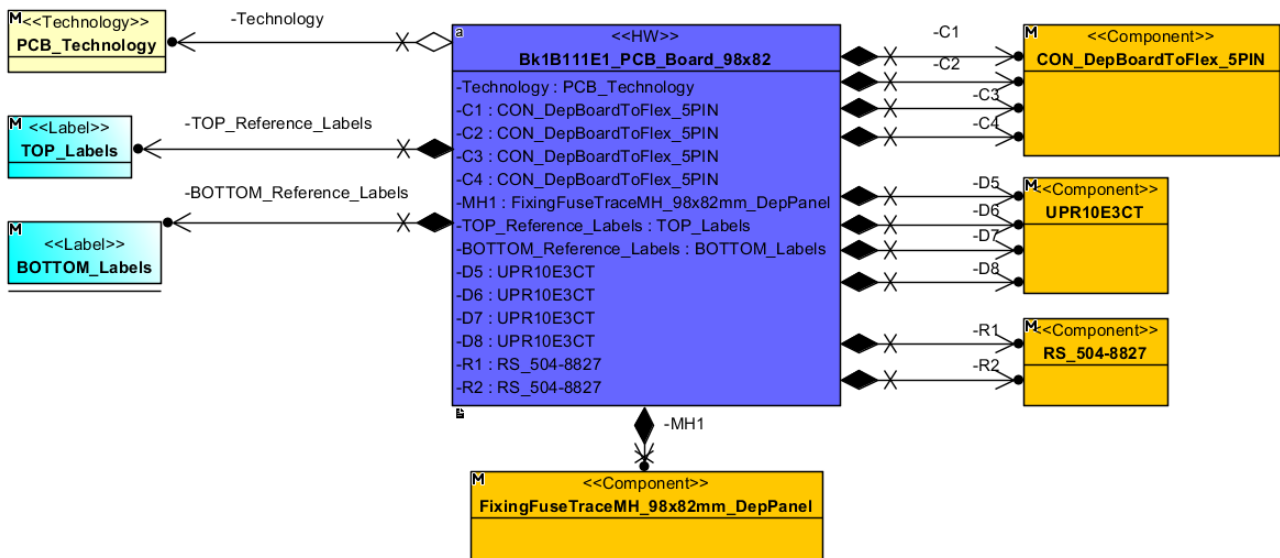


Figure 56: Bk1B111E1 PCB of the standard tile.

5.1 Introduction

The 1B111E structure, from an electronic point of view, is a power source of solar arrays in double channel. The structure is completely modular also from the electronic point of view. If the trace of the electric power do not become too long to represent a high resistance, the structure can be heightened adding further standard tiles. Once deployed, two different opposite sides of solar panels can be exposed and thus there are two possible cases of solar lighting, shown in Figure 57.

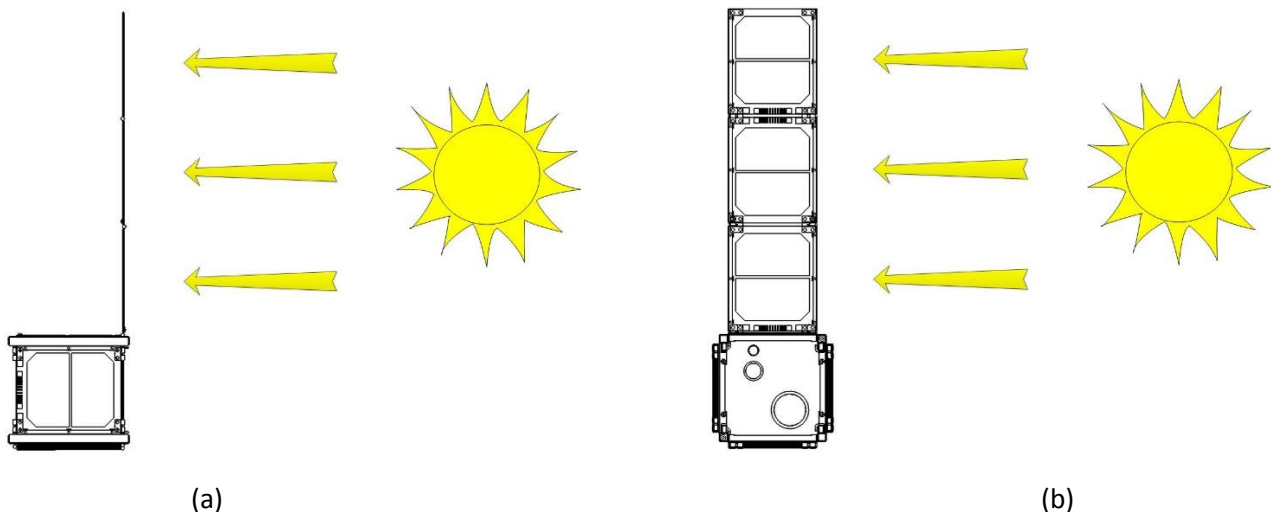


Figure 57: 1B111E structure sun exposures (a) Full side exposure (b) Partial side exposure.

The first type of orientation, the Figure 57 (a), exposes only one side of the 1B111E structure to the sun, while opposite side is in shadow. The double channel is used just to manage this situation, because the side in shadow makes the system inefficient, solar panels are open circuits and the drop voltages of bypass diodes are source of lost. In this way there is the possibility to switch and activate only the illuminated side channel. The other type of orientation, the Figure 57 (b), is relative to the situation where each side is partially exposed to sun. In this condition it is possible to choose to use both channels in order to increase the performance.

As said before, the Bk1B111E20 is a standard tile used to compose a 1B111E structure, and the tile itself is realised with a PCB. So, being a standard element, the PCB has the main requirements to be symmetrically compatible with serial and multiple connection with other identical tiles.

With respect to the electric sheet attached to chapter 9, the PCB tile contains two solar cells for both sides of the board. Considering that for each tile the two cells of one side will be connected to a different channel with respect the other two cells, it is reasonable to analyse electrically one channel at a time, since the other channel on the other side of the PCB is symmetrical. In chapter 2.3.1 are analysed the electric characteristics of a single channel, composed by a single, by a double and by a triple tile. The latter configurations is the maximum number of composition of the tiles for the P-POD standards compatibility.

5.2 Bk1B111E20 connector & resistances of configuration

A Standard tile presents also two couples of connectors, two on top side and the others on bottom one. As better described in Chapter 5, the layouts of the tail are designed in such a way that all kinds of the configurations of a deployable structure (see 2.2.5) permit a simple connection between tile and tile. This is possible because the connectors are exposed in couple on the same side folding, maintaining symmetry in the electric connection between tiles. This feature gives to the Bk1B111E20 Standard Tile the maximum of flexibility, modularity and versatility (Figure 60 (b)). The connections are realized in flexible PCB.

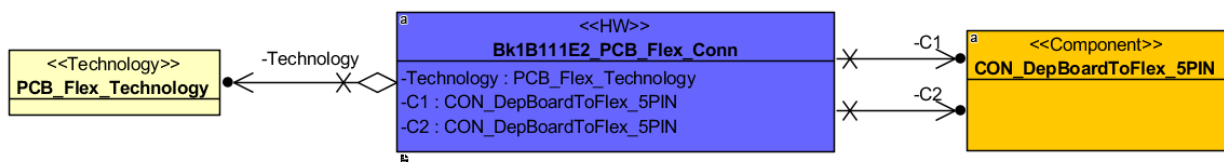
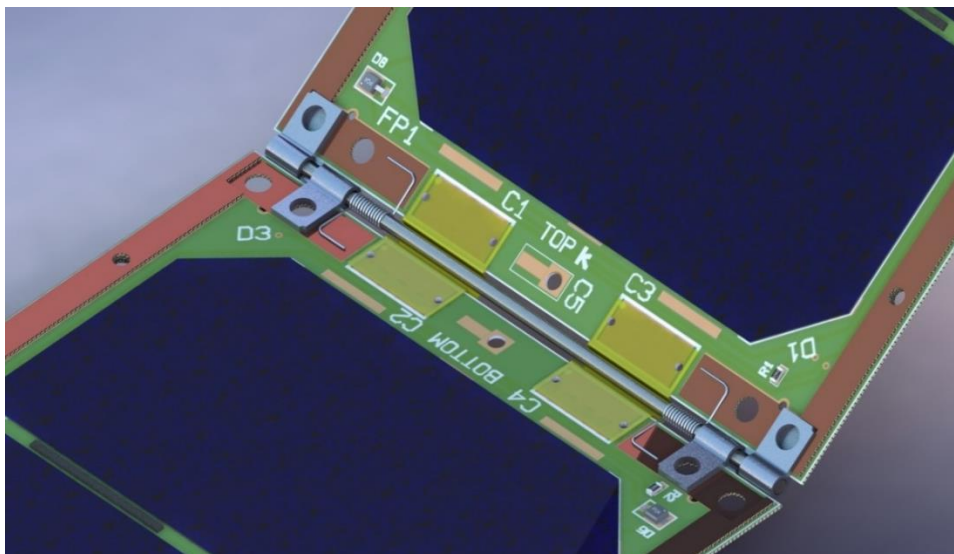
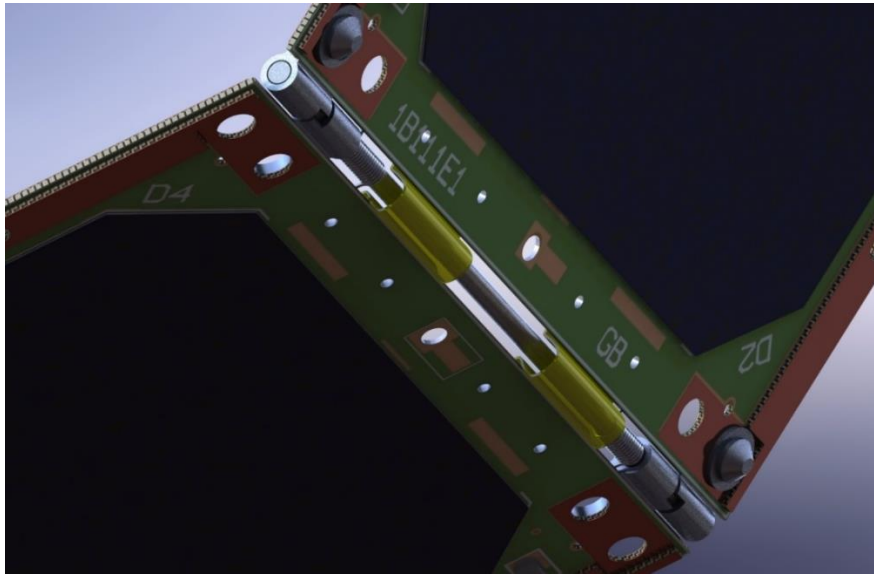


Figure 58: Bk1B111E2 Flexible PCB.

They implement simple connection traces that connect a connector of a tile to a connector of another. Since the connectors are SMD, the flexible connections are soldered directly on PCB of the tile. Also the flexible PCBs implement two alignment holes for each ends. This simplify their soldering on board.



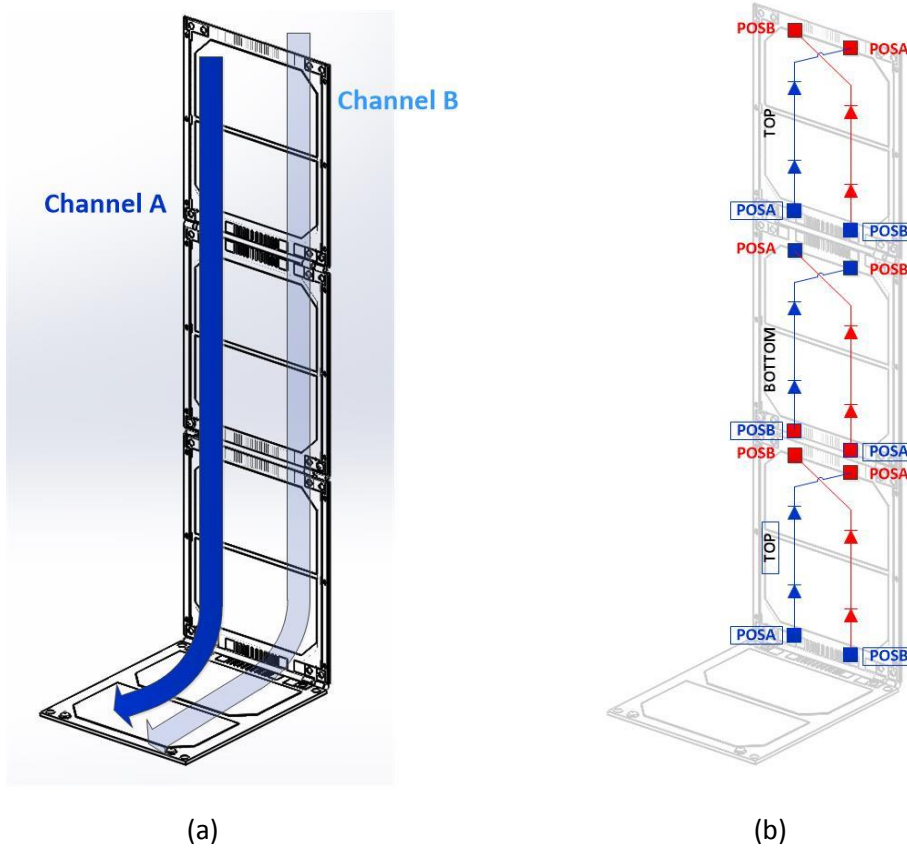
(a)



(b)

Figure 59: Flexible PCB 1B111E2 connected (a) Front (b) Back.

Finally, as described in chapter 2.2.5, the PCBs of the Bk1B111E1, are designed in such a way that when these will be connected together, each side of a 1B111E side represents a single power channel with its own solar cells (see chapter 5). This feature is shown in Figure 60.



(a)

(b)

Figure 60: 1B111E Structure Power channels (a) The two channels (b) Cells connections along two channels (In Red the side of channel B).

The standard tiles are designed to be an extremely symmetric. This symmetry has an impact not only on mechanical shape but in particular on the PCB layouts. From the Figure 16 this issue is particularly clear. One

connector on the bottom of a tile has to be connected to a connector on the top of another tile. Since the tiles are completely identical, from the point of view of the PCB layout, means that the electrical layouts of PCB have to be coincided in order to establish the electrical continuity of the serial circuits of the two side channels, both if the connection is between central and upper tile, either the connection is between central tile and the bottom one. The connectors and traces are designed in order to reflect this symmetry. In this way the serial circuit of solar cells is realized. The electrical connections from tile to tile, are realized with a flexible PCB, without using annoying cables. The connectors on the tails are designed in order to be SMD, in such a way the flexible PCB can be simply soldered on it, without using uncomfortable and bulky connectors. This solution is perfect to minimize as much as possible the overall dimensions of cables that can be a hindrance during the deployment phase. Furthermore, since the flexibles PCB are made in a very subtle way, they can be folded on themselves in a small space, so meeting the strict requirements of the P-POD module.

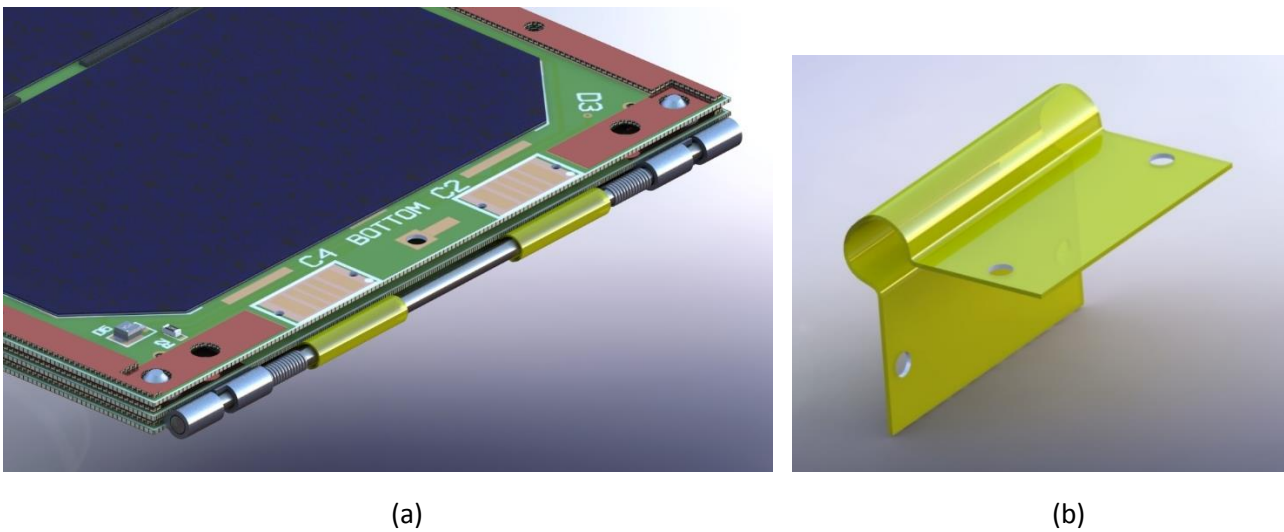


Figure 61: Flexible PCB (a) PCB folded (b) Single flexible PCB connection.

Since the circuit is designed in serial manner, the PCB layout of a standard tile, must to have the possibility to close the power line when it is fixed the last tile of the array of the 1B111E structure. This is another feature that identify a tile as a configuration Af or Bf. Resistances 0 Ohm, are employed to close the circuit in the Af and Bf configurations. When these resistances are soldered, the two side channels of a complete 1B111E structure will be closed and the system is ready to be connected to a side tile of a 1U ARAMIS CubeSat. The mechanism is shown in Figure 62.

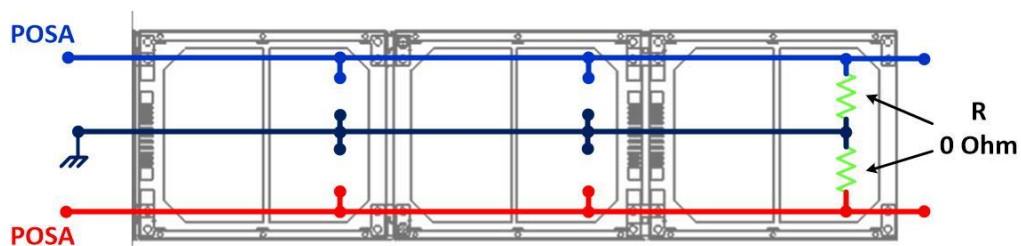


Figure 62: One side power channel closed on 0 Ohm resistor.

During the designing of the PCB of the tile, some others precautions have to be taken into account when electronics components are placed into the layout. When a 1B111E structure is folded, the spaces between tiles are so narrow, that the components of the upper tile can make contact with the components of the bottom tile. In order to avoid this, components are placed in order to be interlocked with a small space

tolerance once the tiles are folded. The Figure 63 shows an example of placement of the components, showing a cross section of a three tiles structure along a point of high density of components.

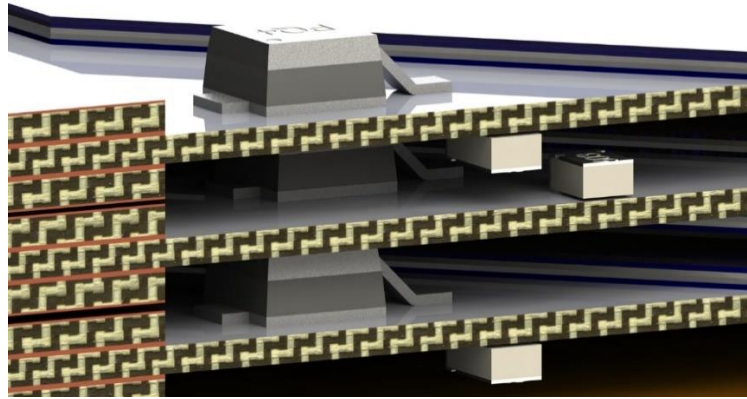


Figure 63: Cross section of a three tile structure along a points of high density of components.

5.3 Bk1b111E1 Traces design

A channel of a 1B111E structure is composed by an appropriate PCB trace that runs through all tiles of the structure and the connections of the flexibles PCBs. Such a trace has to carry a current of about half ampere, considering the solar cells used to design Bk1B111E20. So is there needs to make sure that the power channel traces do not exceed dangerous temperatures when they are crossed by current. In first approximation can be considered only power irradiated from the copper trace since the system will in vacuum, without consider its thermal conduction into the FR4. This because the FR4 has a low thermal conductivity. In this way is obtained a worst case, useful to make the system reliable. The analysis starts from the electric power dissipated by the trace:

$$Pd = \rho \cdot \frac{L}{S} \cdot I^2 \quad (2)$$

Where ρ is the copper resistivity ($1.72 \times 10^{-8} \Omega \cdot m$), L is copper length and S its cross section. I is current that cross the conductor. From the Stefan–Boltzmann law is obtained the radiated output power:

$$Pirr = \epsilon \cdot \sigma \cdot A \cdot T^4 \quad (3)$$

Where σ is the constant of proportionality or also the Stefan–Boltzmann constant ($5.670373 \times 10^{-8} W \cdot m^{-2} \cdot K^{-4}$). Since copper is considered as grey body with a certain absorption coefficient, ϵ is the emissivity. T is the temperature and A is the radiating surface area. In order to estimate final temperature of a trace crossed by current, the electric power dissipated by the trace has to be equal to output radiation power.

$$Pd = Pirr$$

If T is substituted with a temperature difference that corresponds to an increase in temperature, the equality becomes:

$$\rho \cdot \frac{L}{S} \cdot I^2 = \epsilon \cdot \sigma \cdot A \cdot [Tf^4 - T0^4]$$

Where Tf and $T0$ are respectively final and initial temperatures. Solving in function of the final temperature Tf , the (4) is obtained.

$$Tf = \sqrt[4]{\frac{\rho \cdot L \cdot I^2}{S \cdot A \cdot \epsilon \cdot \sigma} + T0^4} \quad (4)$$

With reference to Figure 64, the total surface A is obtained considering all extended faces of the trace $A = (t \cdot L \cdot 2) + (W \cdot L \cdot 2)$, where t is 35um. Finally, substituting $S = t \cdot W$ and A into (4), the dependence of Tf from L disappears and the (4) becomes:

$$Tf = \sqrt[4]{\frac{\rho \cdot I^2}{t \cdot 2 \cdot W \cdot (W + t) \cdot \epsilon \cdot \sigma} + T0^4}$$

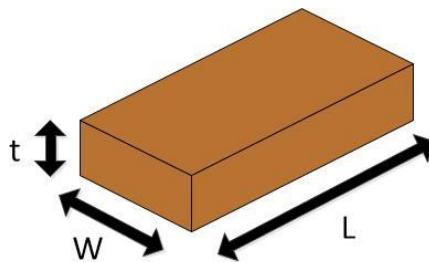


Figure 64: PCB copper trace.

In order to design the width W of the copper trace in function of the final temperature, a curve Tf(W) for the function (4) it is plotted. To do this it is used MatLab. The MatLab script is attached to the section 9.6.

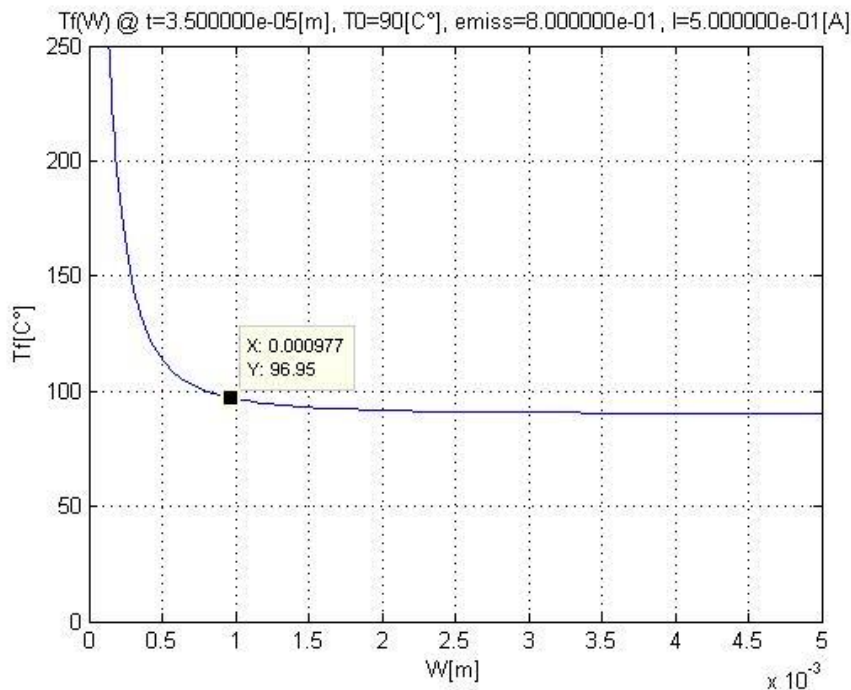


Figure 65: Tf of a copper trace as function of its width W.

The Figure 65 is obtained taking into account a worst case of an initial temperature of the tile of 90 C°. The difference of temperature with a trace of 1mm, is about 6C° (worst case). It is noticeable how for less of 0,5mm of width, the temperature of the trace increase exponentially. So in order to maintain temperature at least under 100C° in safety margins, a good choice is to design channel trace with a width of 1mm. But, for

reason of space on the PCB of the standard tile, it is impossible to use trace with 1mm of width. In this way a reasonable value of width is 0,5mm¹¹. Eventually, in order to improve the situation, the thickness of the copper traces can be increased. In this way the PCB can be realized with copper thickness of 2oz (70µm).

¹¹ The graph of Figure 65 is considered in a worst case for the dissipation, because conduction in the FR4 is not considered. Furthermore, the maximum current is approximated for tolerance to 5A, while maximum current from solar cells is 0,45A. Thus 0,5mm of width is a good choice of the trace of the power line.

6 1B111E Thermal and Orbital Spin Analysis

6.1 Introduction

Space represents a harsh environment not only for humans but also for machines that they send into it. The mechanical structures, the electronics components, the fluids, all suffers each in its own way for the harsh thermal environment and filled with radiations that the space over our atmosphere has. On a satellite the heat is generated internally from electronics systems and is absorbed externally from environment radiations incoming from sun, earth and deep space. In this way the satellite thermal control is required for structure and the electronic components integrity. The thermal study starts from the identification of thermal sources of heat and it is used to minimizing their effect. Normally radiators are used to release the heat that continuously increase satellite temperature, but in the Nano satellites the radiators are elements too heavy and too bulky to be used. So the main goal is to design a system that maintains a balance between heat absorbed from outside or internally generated and heat emitted toward the environment from satellite itself. In this manner the temperature is maintained in a range acceptable to ensure the operational conditions of the system. From the 1B111E structure point of view, the thermal study has the same purpose, verify that the tile temperature does not reach critical temperatures that may cause problems to soldering tin or problems to the efficiency of the solar cells. Furthermore the radiations present another drawback, their pressure. In space there are not frictions with the environment, thus the effects of the radiation pressure on a wide surfaces may be considerable because small differences in colour gradients of satellites elements may cause a spin. A preliminary analysis on spin gives an idea on how much the LEO orbits radiations may affects the spin of 1U satellite that mount a 1B111E structure of three tiles.

6.2 1B111E Thermal Model

From mechanical point of view, the 1B111E is a mechanical system quite independent from the rest of CubeSat satellite, both because once deployed it can no longer be controlled mechanically, either because contacts between its structure and that of the satellite are confined to a small area. Only the negligible areas of the contacts of the hinges and the connection of the very thin flexible PCB they realize the physical contacts between satellite and 1B111E structure. So in first approximation in the thermal system of the 1B111E, the tiles can be analysed separately from the CubeSat thermal model because the phenomenon of the radial conduction is very low. Furthermore the thermal conduction is further reduced by the presence of the thermal resistance of the contacts between the hinges and the copper, both on the tile of the 1B111E structure either on the side tile of the CubeSat. The same situation is presents between tile and tile on the same 1B111E structure. Thanks to this approximation, the thermal analysis can be simplified to a single tile.

6.2.1 Single tile Thermal Resistance

The thermal model can be obtained in two ways: the first from the top face to bottom face of the tile, providing thermal resistance along the top-bottom direction of heat; the second from the centre to the border of a tile face, providing thermal resistance along the radial direction of heat. In order to simplify the model can be considered that the conduction between tile and tile is very low, because there is a small mechanical contact between them and then the radial model that provide the thermal resistance employed to analyse heat conduction toward the near tiles is neglected. The top-bottom model instead is useful because it gives an idea of how the heat spreads due to the external radiation sources incidents on the surfaces. Even if in first approximation it is possible to assert that the thermal resistance will be likely very low due to the very thin structure of the tile.

A detailed thermal model is done: all mains components and layer are considered. The Figure 66 (a) shows the cross section of the tile used for thermal model from side to side. It is chosen this section because since the solar panels are much closer to each other, the space between them may be neglected. Furthermore,

this section results more accurate, because the lateral supports are considered. The Figure 66 (b) shows the equivalent thermal circuit of the model. The value of the thermal resistance depends on the length, width and material type of the respective subsection. θ_S and θ_R are the thermal resistances of a solar cell and of the resin. θ_{Cu} is the thermal resistance of the copper layer, θ_{FR4_S} and θ_{FR4_T} are the thermal resistances of the FR4 of the lateral supports and of the tile board. The total resistance between top and bottom layer is written:

$$\theta_{th} = 2 \cdot \left(\frac{2 \cdot \theta_{Cu} + \theta_{FR4_S}}{2} // (\theta_S + \theta_R) \right) + \theta_{FR4_T} \quad (5)$$

Each thermal resistance is calculated using the relation (6) provided by the Fourier's Law for the heat conduction:

$$\theta_{th} = \frac{L}{K \cdot S} \quad (6)$$

Where K is the material thermal conductivity, S it is the cross section surface, L is its length parallel to the heat flow.

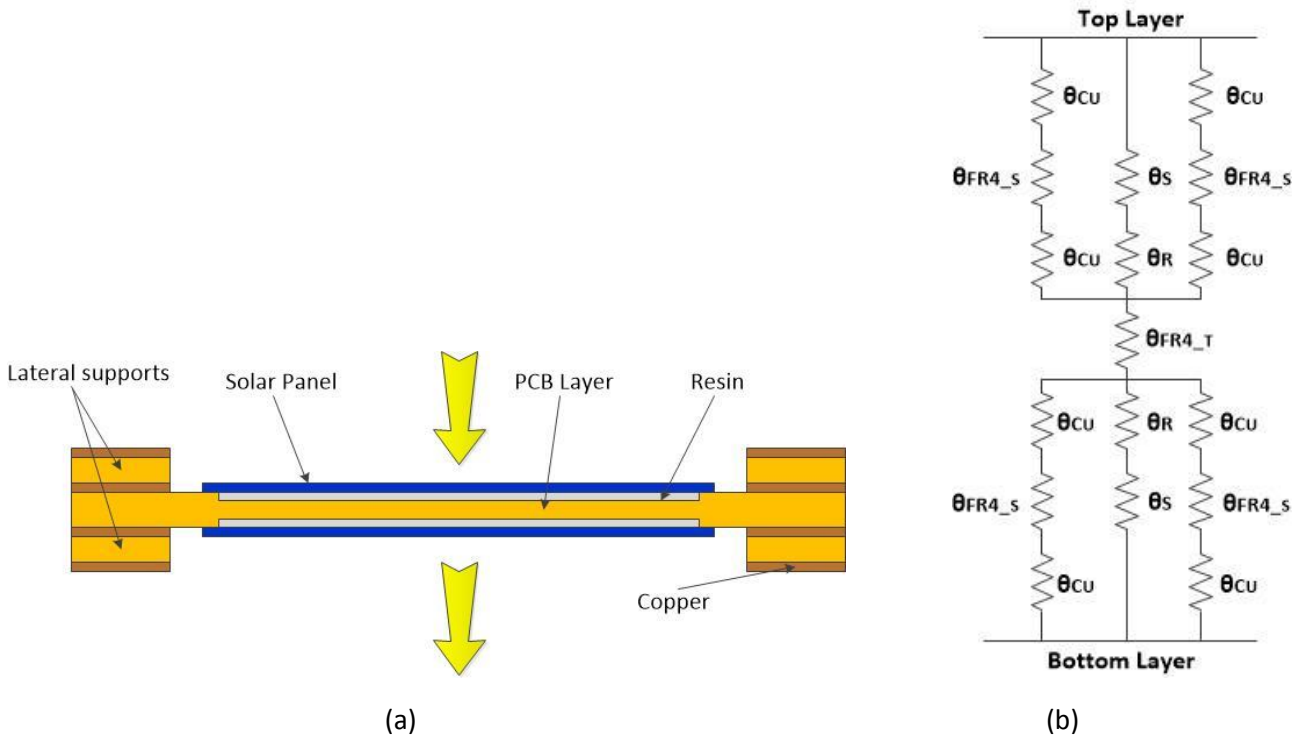


Figure 66: Single tile model (a) Cross section (b) Thermal circuit model.

$$\theta_{Cu} = \frac{L}{K_{Cu} \cdot S} = \frac{0,035 [mm]}{390 \cdot 10^{-3} [W/mm \cdot K] \cdot 4 \cdot 96,8 [mm^2]} = 2,3 \cdot 10^{-4} [K/W]$$

$$\theta_{FR4_S} = \frac{L}{K_{FR4_S} \cdot S} = \frac{0.4 [mm]}{0,5 \cdot 10^{-3} [W/mm \cdot K] \cdot 4 \cdot 96,8 [mm^2]} = 2,066 [K/W]$$

$$\theta_S = \frac{L}{(K_{glass} + K_{Ge} + K_{GaAs} + K_R) \cdot S} = \frac{0.32 [mm]}{(64 + 59,9 + 46 + 1) \cdot 10^{-3} [W/mm \cdot K] \cdot 68,96 \cdot 81,96 [mm^2]} = 3,3 \cdot 10^{-4} [K/W]$$

$$\theta_R = \frac{L}{K_R \cdot S} = \frac{0,08 [mm]}{1 \cdot 10^{-3} [W/mm \cdot K] \cdot 65 \cdot 67 [mm^2]} = 1,8 \cdot 10^{-2} [K/W]$$

$$\theta_{FR4,T} = \frac{L}{K_{FR4,T} \cdot S} = \frac{0,4[mm]}{0,5 \cdot 10^{-3} [W/mm \cdot K] \cdot 82,6 \cdot 98 [mm^2]} = 9,9 \cdot 10^{-2} [K/W]$$

Substituting all thermal resistances of all materials into the (5), the θ_{th} from the top to the bottom tile is given:

$$\theta_{th} = 0,135 [K/W]$$

Obviously, thermal resistance is very low, because the heat cross the tile along its very thin thickness.

6.3 1B111E Thermal Analysis

After obtained the thermal resistance, in order to get a temperature of the tile at the equilibrium, a specific analysis about the incident power radiation has to be defined.

6.3.1 Absorbed Radiation into the tile

The 1B111E structure is supposed to be exposed to sunlight with only one side at a time. In this way, two different cases can be distinguished for a single tile:

- CASE 1: THE EXPOSED SOLAR CELLS GENERATE ELECTRIC POWER

When a tile is hit by radiation, a portion of it (P_s) is absorbed by the material while the remaining power is reflected from the surface (P_r). The relation between P_s and P_r is given by the absorption coefficient α of the materials of the exposed surface. A further portion of the P_s is converted to useful energy by solar cells (P_c). The amount of P_c depends on the efficiency η of the cells. All the remaining absorbed power is transmitted to the tile where is transformed into heat increasing the tile temperature. This energy is so obtained as:

$$\phi = P_s - P_r - P_c \quad (7)$$

Since $P_s - P_r = \alpha \cdot F_d \cdot S$ and $P_c = \eta \cdot (P_s - P_r) = \eta \cdot \alpha \cdot F_d \cdot S$, the (7) becomes:

$$\phi = \alpha \cdot F_d \cdot S \cdot (1 - \eta) \quad (8)$$

Where F_d is the incident power density at LEO (1366 W/m^2) and S is the area of the exposed surface.

- CASE 2: THE EXPOSED SOLARE CELLS DO NOT GENERATE ELECTRIC POWER

When the solar cells are not used, obviously $P_c = 0$, no energy is translated into electric power end so the (7) becomes:

$$\phi = \alpha \cdot F_d \cdot S \quad (9)$$

The ϕ so represents an unwonted energy because it grows the tile temperature.

6.3.2 Radiation sources

The (9) obviously depends from incident power density of radiation F_d that in LEO orbits is relative to different factors. Three mains sources of radiations act on a satellite, the sun radiation (F_{sun}), the Earth's albedo (F_{Albedo}) and the radiation emitted by earth ($F_{Infrared}$). The sun radiation F_{sun} at LEO orbit has a typical value equal to $F_{sun} = 1366 \text{ W/m}^2$, instead F_{Albedo} and $F_{Infrared}$ depend from the orbit elevation. The albedo radiation has approximately the same spectral distribution as that of the Sun. The Albedo is highly variable

across the globe and depends by the surface properties and by the cloud cover. It also depends by the solar zenith angle. The average terrestrial albedo is slightly lower than 0.4 of F_{sun} for distances less than 1/5 of Earth's radius, thus in first approximation it is possible to say that albedo radiation is 0.4 of the sun radiation.

$$F_{Albedo} = F_{Sun} \cdot 0.4 = 546 \text{ [W/m}^2\text{]} \quad (10)$$

This value is further reduced approximately at the 80% at an altitude of 800km because it decrease with the square of the distance ($\left(\frac{R}{R+h}\right)^2$), so supposing just a satellite orbiting at an altitude of 800km, I have $F_{Albedo} = 437 \text{ [W/m}^2\text{]}$. $F_{Infrared}$ is the Earth infrared radiation. The Earth-emitted thermal radiation has a spectrum of a black body with a characteristic average temperature of 288K. The Earth infrared radiation also varies across the globe but less than the albedo. It also shows a diurnal variation which is small over the ocean but can amount to 20% for desert areas. Furthermore its power density, decrease with the square of distance respect the centre of the earth and thus the power density reduces of a factor $\left(\frac{R}{R+h}\right)^2$ with altitude. Earth's radiation at altitude h is so given by:

$$F_{EInfrared} = \sigma \cdot \alpha_T \cdot T_T^4 \cdot \left(\frac{R}{R+h}\right)^2 = 160 \text{ [W/m}^2\text{]} \quad (11)$$

Where T_T is the temperature of earth supposed 288 K, α_T is the absorption coefficient of earth obtained from the albedo, in fact if reflectivity of albedo is 0.4 so the absorption coefficient is $\alpha_T = 1 - 0.4 = 0.6$. R is the earth radius of $R = 6371\text{km}$ and h is the satellite altitude supposed $h = 800 \text{ km}$. $\sigma = 5.78 \cdot 10^{-8} \text{ [W/m}^2\text{/K}^4\text{]}$ is the Stefan-Boltzmann's constant.

Once defined all radiations sources, an estimation of the radiation environment in a worst case is given. Since only one face at time can be fully exposed to sun, the Figure 67 provides a worst case to the exposition to radiations sources.

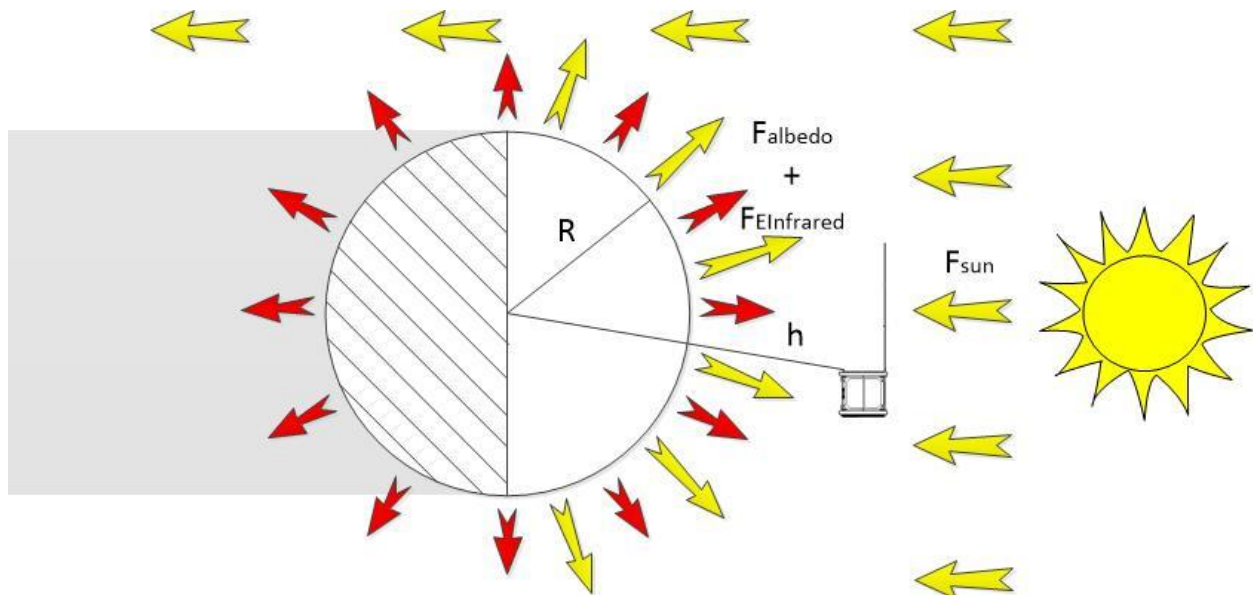


Figure 67: CubeSat worst case of exposition to radiations in LEO orbits.

The CubeSat position in Figure 67 (the satellite orbit is not in scale) for a worst case of exposure to radiations is obtained taking into account that the main contribution of radiation, is received from sun when the solar cells are perpendicular to its rays. So with a satellite oriented in order to expose cells in perpendicular way toward the sun, the other side of the satellite is exposed to the earth albedo and to the earth infrared

radiation. So the global radiation from earth contributes to increase temperature on satellite. The worst case of the total radiation from earth is estimated as:

$$F_{Earth} = F_{Albedo} + F_{Infrared} = 597 \text{ [W/m}^2\text{]}$$

Really, infrared radiation being into the infrared radiation spectrum, it acts on the materials with a different absorption coefficients. So, the addition of the infrared radiation to F_{Albedo} is an approximation, but it is possible because the absorption coefficient in the infrared spectre is about the same of the visible light one¹².

6.3.3 Thermal equilibrium equation

Since I am considering only one tile, I have only two surfaces, one exposed to F_{sun} radiation and the other that is exposed to F_{Earth} .

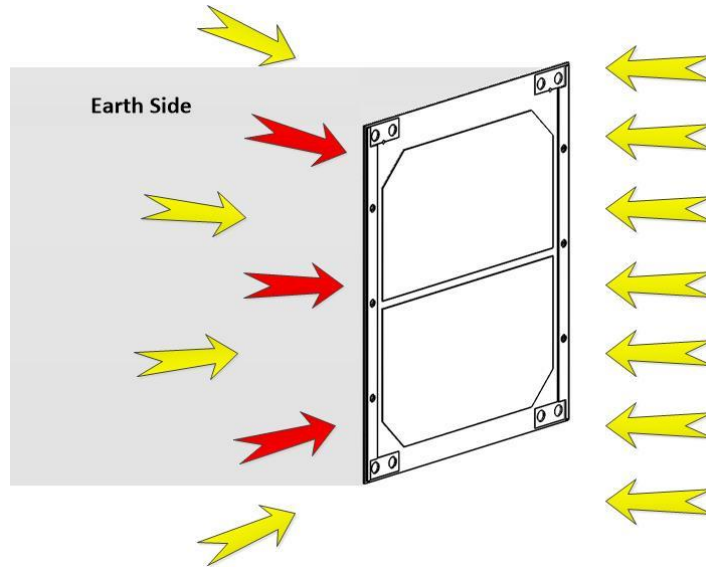


Figure 68: Radiated Energy from tile.

I consider a worst case of the tile where the two surfaces exposed to the sun and the earth radiations are considered as a grey body: the surface faced to the sun with an emissivity to the visible light of $\alpha_{sun\ side} = 0.9$ (in [7] is described as this coefficient is experimentally estimated) and the surface exposed to the earth with an equal emissivity of $\alpha_{earth\ side} = 0.9$ (the earth radiation is composed by visible radiation from the albedo and from the infrared one, generally a material exposed to infrared radiation reacts with a different emissivity with respect the visible light but experimentally from [7] is demonstrated as the emissivity at infrared radiation for this type of tile is about the same of the emissivity at visible light). In this way the total energy emitted from all tile surfaces is:

$$\sum_{i}^{all\ surfaces} (P_{E_i}(T)) = P_{E_{sun\ side}} + P_{E_{earth\ side}} = \quad (12)$$

$$(\sigma \cdot \alpha_{sun\ side} \cdot T^4 \cdot S) + (\sigma \cdot \alpha_{earth\ side} \cdot T^4 \cdot S) = 2 \cdot \sigma \cdot \alpha \cdot T^4 \cdot S$$

¹² This assumption can be done, because a structure with tiles similar was been experimentally tested on a real device [12]. The experiments were intended to find the emissivity of the structure, both for the visible radiation either for that infrared one. The result was that the two value of emissivity were about the same.

Where the energies P_E are deduced from Stefan-Boltzmann's law using the (3). S is the surface exposed, it equals for each side. The energy accumulated as heat inside the tile depends by its mass m , its specific heat and its temperature T :

$$P_C(t) = \frac{d}{dt} \cdot m \cdot c \cdot T(t) = m \cdot c \cdot \frac{d}{dt} \cdot T(t) \quad (13)$$

Where t is the time. As is shown, the energy accumulated depends from mass. Since the mass of tile is very low, the P_C is approximately zero. Now, with some parameters already defined, the equation of thermal equilibrium is introduced:

$$\sum_i^{\text{sun irradiated surfaces}} (P_{\text{sun}_i} - P_{P_i}) + P_J + P_{\text{Earth}} - \sum_i^{\text{all surfaces}} P_{E_i}(T) = P_C(T) \quad (14)$$

In relation the (14), $P_C(T)$ and $P_E(T)$ are already defined, instead P_J is the internal heat generated by the electronic components that since the system is supposed turned off, it is $P_J = 0$. If the cells are off and so they do not convert the energy of radiation into electric power, also P_p , the electric power generated from the cells is $P_p = 0$. P_{sun} and P_{Earth} are respectively the power radiation from the sun and the power radiation from the earth. In such a way for a single tile and considering only the two wide faces, the (14) becomes:

$$\begin{aligned} P_{\text{sun}} + P_{\text{Earth}} - P_E &= 0 \\ P_{\text{sun}} + P_{\text{Earth}} &= P_E \\ (\alpha_{\text{sun side}} \cdot F_S \cdot S) + (\alpha_{\text{earth side}} \cdot F_{\text{Earth}} \cdot S) &= 2 \cdot \sigma \cdot \alpha \cdot T^4 \cdot S \end{aligned} \quad (15)$$

All the emissivity and the surfaces are equals, then:

$$(F_{\text{sun}} + F_{\text{Earth}}) = 2 \cdot \sigma \cdot T^4 \quad (16)$$

Substituting all values we obtain the temperature at equilibrium for a tile structure:

$$T = \sqrt[4]{\frac{F_{\text{sun}} + F_{\text{Earth}}}{\sigma}} = \sqrt[4]{\frac{1963 \text{ [W/m}^2\text{]}}{2 \cdot 5,78 \cdot 10^{-8} \text{ [W/m}^2\text{/K}^4\text{]}}} = 361 \text{ [K]} = 88 \text{ [C}^\circ\text{]} \quad (17)$$

From the (17), it is possible to see how the maximum temperature is well below the critical temperatures that could hamper the correct working operation of the system. Finally, using the worst case of the (9), I estimate the value of the absorbed power unwanted into the tile, considering always an emissivity of $\alpha = 0.9$:

$$\phi = \alpha \cdot F_d \cdot S = \alpha \cdot (F_{\text{sun}} + F_{\text{Earth}}) \cdot S = 0,9 \cdot 1963 \left[\frac{\text{W}}{\text{m}^2} \right] \cdot 82,6 \cdot 98 \text{ [mm}^2\text{]} = 14,3 \text{ [W]}$$

From the power absorbed by the tile, it is also possible give an estimation of difference temperature between the illuminated surface and that one exposed to the earth. The total thermal resistance provided from the (5) is now useful:

$$\Delta T = \phi \cdot \theta_{th} = 14,3 \text{ [W]} \cdot 0,135 \text{ [K/W]} = 1,93 \text{ [K]} \quad (18)$$

This low value of temperature difference is correct, because the structure of the tile is so thin that has a low thermal resistance and then a low difference of temperature between two sides. So it is also possible to assert that the temperature of the two faces are the same.

6.4 1B111E Thermal Simulation

The value of temperature from with the (17) is obtained analytically. In this section, a double check using the tool Flow Simulation of SolidWorks is performed. The simulation proposed is quite complex because it concerns the radiation properties that are more difficult to manage. The model reproduce the same worst conditions for a single standard tile analysed analytically in 6.3.3: a single tile with one side exposed to the sun end the other side exposed to the earth albedo and the infrared radiation.

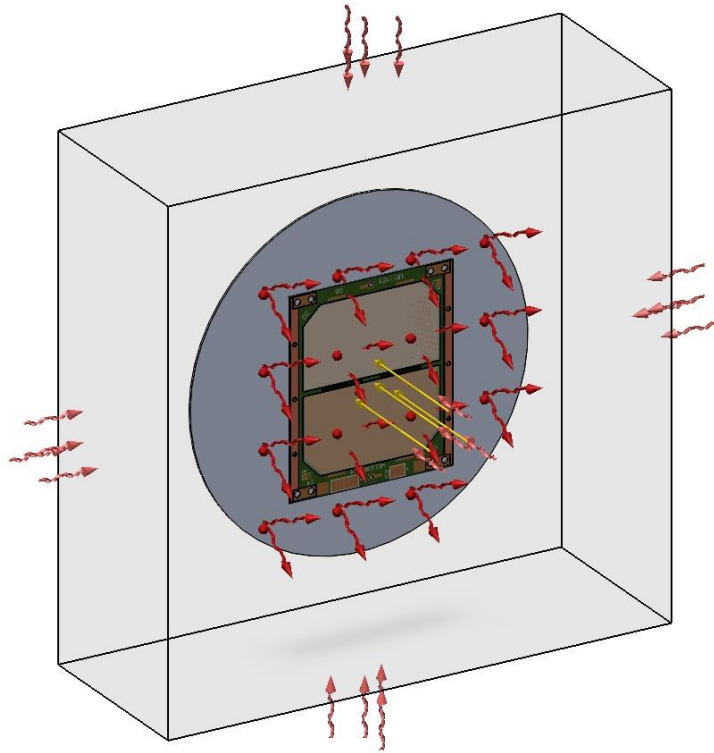


Figure 69: Radiation Model.

The model is composed by the tile under test with real proprieties of materials and a disk that models the earth sphere seen by a single 1U tile in orbit. The diameter and the distance between the earth disk and the tile, are estimated performing some trigonometrical calculations, considering the satellite and so the tile under test orbiting an altitude of 800km. What I want to find is the angle between the earth horizon seen by the satellite and the perpendicular axis from the satellite to the centre of the earth. For the estimation of the correct diameter of the disk, the tile and thus the satellite is firstly approximated to a single point. The Figure 70 shows the geometrical model used to calculate the angle of the horizon:

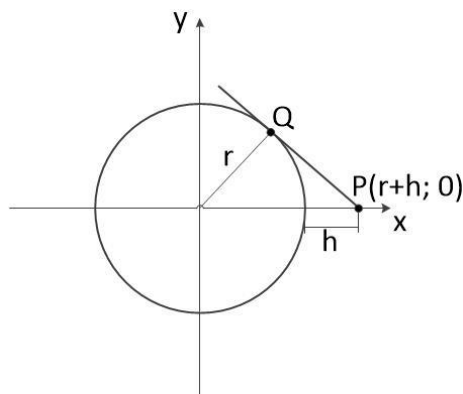


Figure 70: Orbit elevation.

The circle is the model of the Earth. The two equations of the circle and the straight line are:

$$\begin{cases} x^2 + y^2 - r^2 = 0 \\ y = m(x - r - h) \end{cases}$$

Substituting the straight line equation into the circle equation I obtain a second degree equation that is function of the angular coefficient of the straight line m and function of x :

$$(1 + m^2) \cdot x^2 - 2 \cdot m^2 \cdot d \cdot x + (m^2 \cdot d^2 - r^2) = 0$$

Where $d = r + h$. In order to find the angular coefficient of the straight line it is used the technique of the delta. Delta is imposed to 0 because if the straight line is tangent to the circumference, the two solutions have to be coincident.

$$\Delta = b^2 - 4ac = (2 \cdot m^2 \cdot d)^2 - 4 \cdot (1 + m^2) \cdot (m^2 \cdot d^2 - r^2) = 0$$

Solving with respect to m , I get two angular coefficients, respectively of the two possible straight line tangents to the circle and passing through the point P.

$$m = \pm \sqrt{\frac{-r^2}{r^2 - d^2}}$$

If I consider $r=6371\text{km}$ and $h=800\text{km}$ I obtain $m_1 = 1.935625$ and $m_2 = -1.935625$. Since I refer to Figure 70, I chose the negative coefficient m_2 and then now I have to find the coordinates of the point Q. The system of equations becomes:

$$\begin{cases} x^2 + y^2 - r^2 = 0 \\ y = -1.935625(x - r - h) \end{cases}$$

Solving this system in function of x and y I obtain $X_q = 5660,248\text{km}$ and $Y_q = 2924,24\text{km}$, that are the two coordinates of Q(X_q , Y_q). Using the Figure 71 it is possible to obtain the angle of view (α) of the earth from satellite.

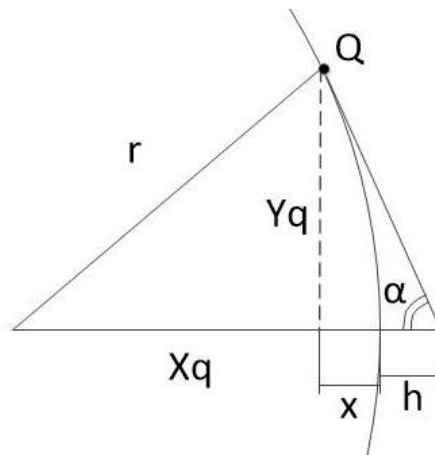


Figure 71: Horizon view angle.

$$x = r - X_q = 6371\text{km} - 5660,248\text{km} = 711\text{km}$$

$$x + h = 711\text{km} + 800\text{km} = 1511\text{km}$$

$$\alpha = \tan^{-1}\left(\frac{Y_q}{x + h}\right) = \tan^{-1}\left(\frac{2924,24\text{km}}{1511\text{km}}\right) \approx 63^\circ$$

In the simulation model obviously the distances in km cannot be reproduced, in this way an approximation is performed. Since the only parameter that I want to keep real is the angle of view of the horizon, I have supposed to approach the disk to the tile at a distance of 10mm. This step is shown in Figure 72.

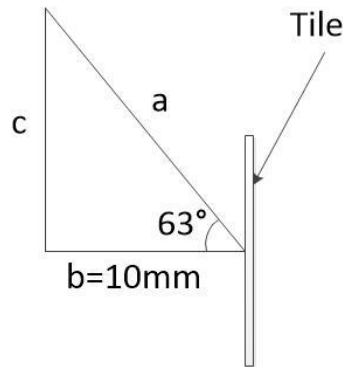


Figure 72: Approximation of the distances.

$$a = \frac{b}{\cos 63^\circ} = 22\text{mm}$$

$$c = \sqrt{a^2 - b^2} = 19\text{mm}$$

Since I want avoid a strong approximation so I can consider the tile not like a single point. I have added to c also the size h of the tile, as is shown in Figure 73.

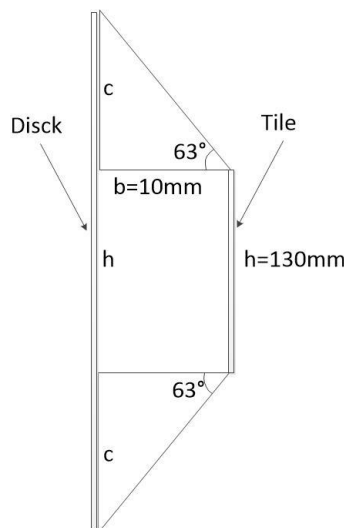


Figure 73: Final diameter of disk.

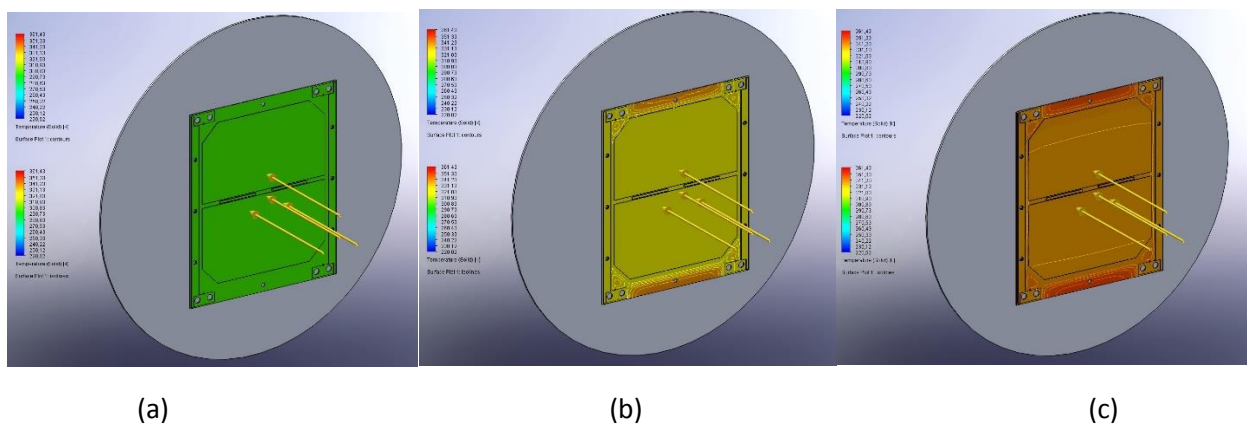
In conclusion the final diameter estimated for the earth disk is $2 \cdot c + h \approx 170\text{mm}$, where h, is the maximum vertical size of a tile that corresponds to the diagonal dimension.

Once the all shapes are defined and the model of simulation is complete, the boundaries conditions and the radiation sources are placed. All simulation conditions are listed:

- The materials of the tail are considered with real proprieties.
- The analysis type is "External", selecting heat conduction in solid only. This means that the outer space is considered empty (vacuum condition), thus only conduction into the solid is considered.
- The Radiation proprieties consider the absorption in solid. In this way, if a radiative surface with different emissivity from a black body is used, the value of the emissivity can be applied to the bodies of the surface.

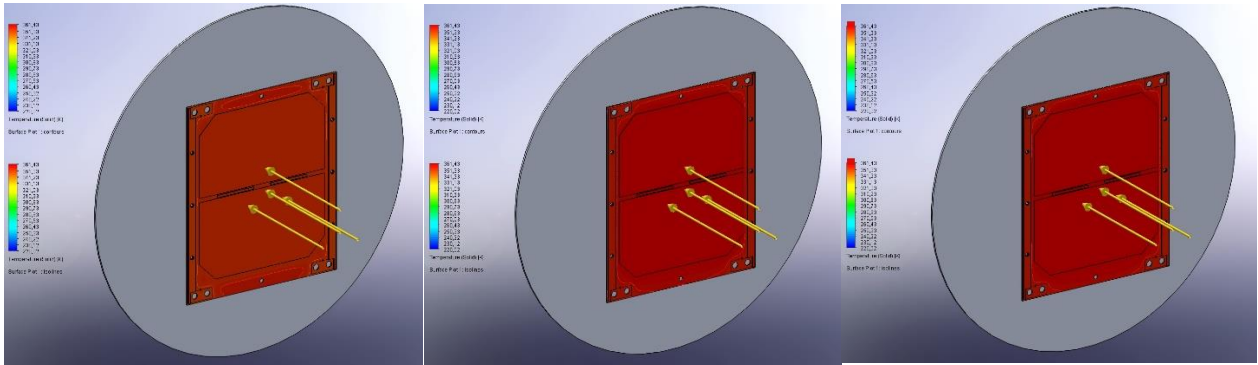
- A custom radiative surface is applied as wall condition for all surfaces of the tile bodies: in order to obtain the same condition of the analytic calculation, this radiative surface is considered with an emissivity of 0.9, in this way all bodies under study are considered as a grey bodies. The absorbance of the sun is considered also 0.9. The specularity coefficient gives an indication of how the rays are reflected, so in order to be closer to a real situation its value is kept 0 (it means a diffusive reflection, because materials are not completely smooth). The Radiative surface type is set to “wall”, this means that also rays reflected from a body surface can affect other surfaces that these reflected rays hit, increasing the reality of simulation.
- All bodies of the tail are considered opaque to radiation, in this way the simulator knows that has to consider only the global radiative surface, imposed with its parameter of emissivity.
- The external sources are: the external radiation from deep space of 3k¹³, direct rays from sun with a power density of 1366 w/m². The sun rays are automatically simulated by the simulator as a directive source.
- A further radiative surface condition is applied to the earth disk. The disk is considered as black body and its material is defined transparent to sun radiation. In this way the disk can only emit its intrinsic radiation defined without absorb and thus emit the sun radiation eventually reflected on the disk¹⁴. The radiation defined is diffusive type with a power density of 597 w/m².
- The initial temperature of the bodies is 298k.

The Figure 69 shows the complete model. The external rectangle represents the computational domain. The yellow arrows represents the direct sun radiation. The Red arrows that spread from earth disk represent the earth radiation and the infrared one. The Pink arrows incoming from outside of the computational domain, represent the radiation of 3k of the environment background. A simulation is performed for about 15 minutes. The Figure 74 shows 15 minutes of simulation, divided into some significant time instants. In order to better understand the evolution of the temperature, the Figure 75 provides the temperature profile in function of time for 15 minutes of simulation. The point measured is the symmetric centre of the tail.



¹³ This is the background radiation of the space. Generally can be neglected since it is too low but to increase the accuracy of the simulation, it has been taken into account.

¹⁴ The radiation generated from the disk, already takes into account the albedo radiation. In this way the body of the disk has to be completely transparent to the sun radiation, otherwise the sun rays reflected by its surface, will be added again to the radiation that it emits. The result would result in a exceeding of the radiation estimated.



(d) (f) (g)

Figure 74: Heating phases (a) Initial Condition (b) 1 min (c) 2min (d) 4 min (f) 8 min (g) 15 min.

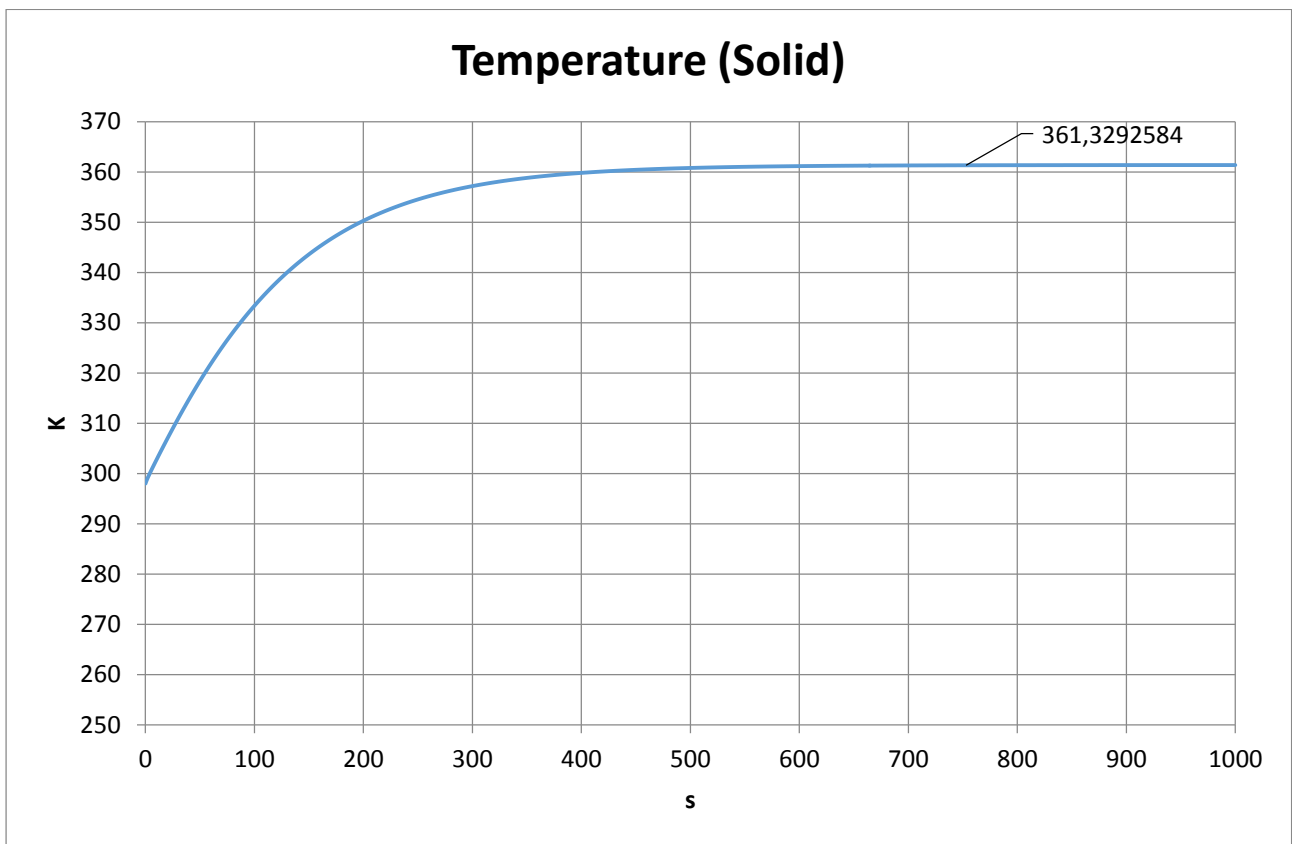


Figure 75: Temperature profile in the symmetric centre of the tile.

As we can see, the temperature of the solid reaches a value of convergence to around 10 minutes, and it is remarkable how the final temperature at steady state ($361,32k \approx 88C^\circ$), is identical to the analytic value of the (17). In this way it is possible to validate the simulation model used. The side of the tile exposed to earth surface is not shown because practically it reaches the same temperature of the sun exposed side. There is only a slight difference less than $0.5C^\circ$ between two sides. This is also conform to the analytic result of the (18), where a small difference of temperature was expected. The slight higher temperature of the (18) with respect to the simulation result, is due to the more approximated thermal model of the analytic analysis and thus to the approximated value of θ_{th} .

6.5 1B111E Spin Analysis

When a flow of radiation hits a surface of a material, it applies to the surface a pressure that obviously is directly proportional to the incident radiation power density and depends also by the absorption coefficient of the material. When power density of the radiation is high or the surface is high, the effect of the relative force applied, increases and in space, in absence of frictions the object can be pushed significantly. If the same surface has a different gradient of colour between two surfaces parts placed on the two opposite sides of the centre of mass of the object, this one can acquire a spin due to the relative momentum. In LEO orbit is more important the analysis of the spin, because its estimation gives the possibility to understand in how much time the satellite needs an attitude correction. For the analysis I considered the same worst case for power density of radiation of $F_d = 1554 \text{ [W/m}_2\text{]}^{15}$. A simplified model for a single standard tile is provided in Figure 76, where the centre of the tile has an absorption coefficient α , instead the two lateral strips represent the two portions of surfaces with different gradient of colour that means different absorption coefficients α_1 and α_2 .

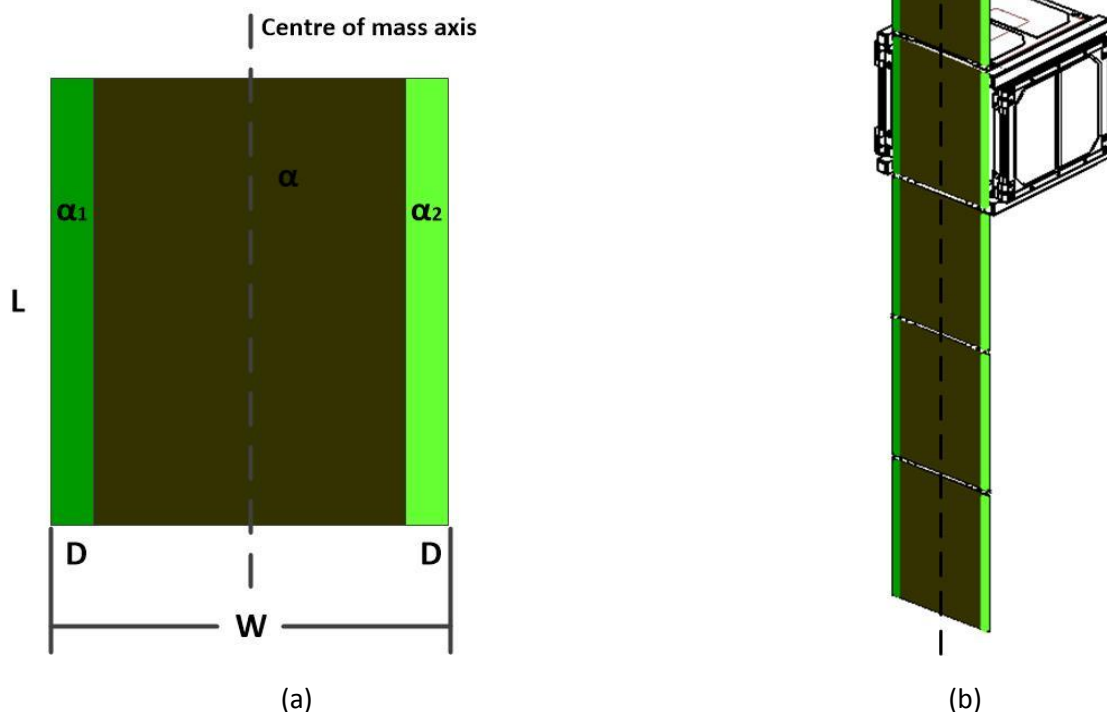


Figure 76: Standard tile model with two different gradient of colours between the edges (a) Single tile (b) Entire model structure

¹⁵ The worst case involves both the radiation from the sun either the radiation from the earth. This can be asserted because also the side exposed to the earth has the same gradient of colour between the two edges. In this way the two contributions of the momentum, can be added together.

The Figure 76 shows also the axis of symmetry respect the centre of mass of the model. Thus, the parallel axis that cross the centre of mass represent the axis of rotation when a momentum is applied due to a radiation pressure. The pressure is given by:

$$p = \frac{Fd}{c} \cdot (2 - \alpha)$$

Where c is the speed of light ($3 \cdot 10^8$ [m/s]). The pressure is considered for solar panels off and for a transmittance of the tile $\tau = 0$. This means, a material not transparent. In order to obtain a force, the pressure has to be multiplied by the surface where it acts, in such a way are obtained the two forces that create a momentum and that act on the lateral strips:

$$F_1 = \frac{Fd}{c} \cdot (2 - \alpha_1) \cdot L \cdot D$$

$$F_2 = \frac{Fd}{c} \cdot (2 - \alpha_2) \cdot L \cdot D$$

These forces are obtained for one single tile, but the goal of this analysis is to estimate the spin associated at least to a couple of complete structures of three tiles, fixed along the same axis. With only two structure, the spin can be analysed along one axis because the structure becomes symmetric with respect to the centre of mass of the CubeSat. In this way is avoided that the spin can acquires another components on another axis and the satellite rotates also with respect to an axis different from the longitudinal one. As is shown in Figure 76 (b) and considered also the side tile of the CubeSat. Now the two forces become:

$$F_1 = \frac{Fd}{c} \cdot (2 - \alpha_1) \cdot (7 \cdot L) \cdot D$$

$$F_2 = \frac{Fd}{c} \cdot (2 - \alpha_2) \cdot (7 \cdot L) \cdot D$$

So, the two momentum that are supposed to be imposed on the geometric centre of each lateral strip are given:

$$M_1 = \frac{Fd}{c} \cdot (2 - \alpha_1) \cdot (7 \cdot L) \cdot D \cdot (W - D)$$

$$M_2 = \frac{Fd}{c} \cdot (2 - \alpha_2) \cdot (7 \cdot L) \cdot D \cdot (W - D)$$

The total momentum is then defined as the difference between the momentums associated to each force:

$$M = M_1 - M_2 = \frac{Fd}{c} \cdot (\alpha_2 - \alpha_1) \cdot (7 \cdot L) \cdot D \cdot (W - D) \quad (19)$$

The angular acceleration provided by the momentum M is:

$$\dot{\omega} = \frac{M}{J} \quad (20)$$

J is the scalar momentum of inertia with respect to the axis of rotation. The rotation is performed only with respect to one axis since the structure is completely symmetric and thus balanced around to its centre of mass¹⁶. The analytic estimation of J with respect to the axis of rotation crossing the centre of mass is very complex and anyway the computation will lead to an approximated value. For this reason, J is obtained using

¹⁶ In lack of gravity, the axis of spin crosses the structure in its centre of mass.

the tool property of mass of SolidWorks. For estimation of J, the structure of Figure 77 is used. A dummy payload is used to reach a weight of about 1,5g for the entire satellite.

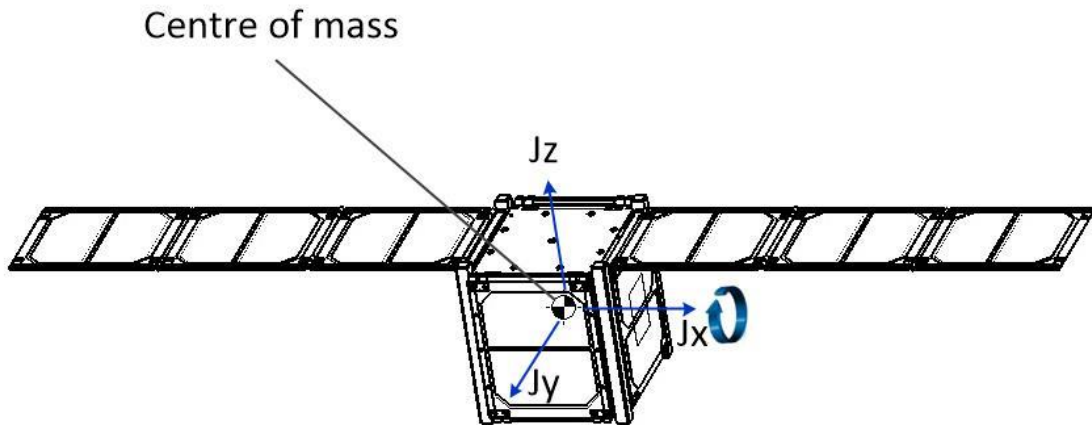


Figure 77: Centre of mass of a satellite with two 1B111E structure deployed.

The axis of rotation is the x axis with respect to the origin of the centre of mass. Momentum of inertia calculated by the software is $J = 3353516.95 \text{ [g}\cdot\text{mm}^2]$. Finally, in order to know how much time is needed to reach a certain spin, calculated in rpm, the following formula has been used:

$$T = \frac{\omega_0}{\dot{\omega}} = \omega_0 \cdot \frac{J}{M} \quad (21)$$

Where ω_0 is the angular velocity. Supposing to have $D = 10\text{mm}$, a real size of tiles with $L = 98 \text{ mm}$ and $W = 82,6 \text{ mm}$ a difference of colour gradient of $\alpha_2 - \alpha_1 = 0.3$ and a density of radiation of $Fd = F_{Earth} + F_{Sun}$ (considering that each tile side can contribute to increase satellite momentum in the same spin direction), the angular velocity ω_0 is so drawn as function of T (the inverse of the (21)). This is done using MatLab. The Figure 78 shows this graph.

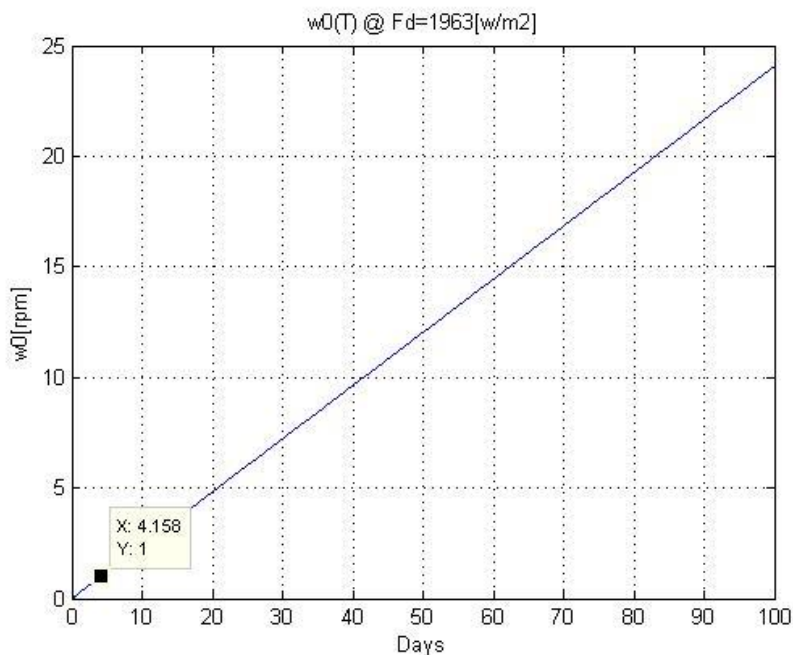


Figure 78: Time to reach ω_0 spin.

In the other directions is intuitive that momentum of inertia will be higher respect to the x direction, because the mass is distributed more distant with respect the axis of rotation. In fact from the software, the estimations of the momentum of inertia of the z and y axis, are $J_y = 9652375.89 \text{ [g}\cdot\text{mm}^2]$, $J_z = 10189222.45 \text{ [g}\cdot\text{mm}^2]$. In this way is obvious that supposing the same gradient of colour for the effect of spin along the z and y axis, the angular momentums in these axis are lower respect to the x axis. So, the rotation along x represents a worst case. In Figure 78 is shown a mark that highlights that the satellite reaches 1rpm in about 4 days. But this happens if it is continuously illuminated, then considering an altitude of 800km with an orbit of about 100 minutes, there are only 60 minutes of sun exposition for each orbit. Using those parameters it is simple to calculate the total minutes of exposition in a single day, because the total number of the orbits is $24\text{h}/100\text{m} = 14,4 \text{ [orbits/day]}$. Now since only 60 minutes of an orbit allow the exposition to the sun (and albedo approximately) of the satellite, the total number of minutes of exposition at day is $14,4[\text{orbits/day}]\cdot 60\text{m}[\text{exposition/orbit}]=864\text{m}[\text{exposition/day}]$. Using the curve of Figure 78, is obtained that in 864m are reached 0.144rpm¹⁷. This value thus is the real rpm reached in a day. In this way, the real situation of 1rpm can be reached in about $1[\text{rpm}]/0,144[\text{rpm/day}] \approx 7\text{days}$.

¹⁷ Since the (21) is a straight line, the rpm in 864m can estimated easily with a mathematical proportion, knowing the days to reach 1 rpm (the mark of Figure 78).

7 Bk1B111T Thermal Fusers Design

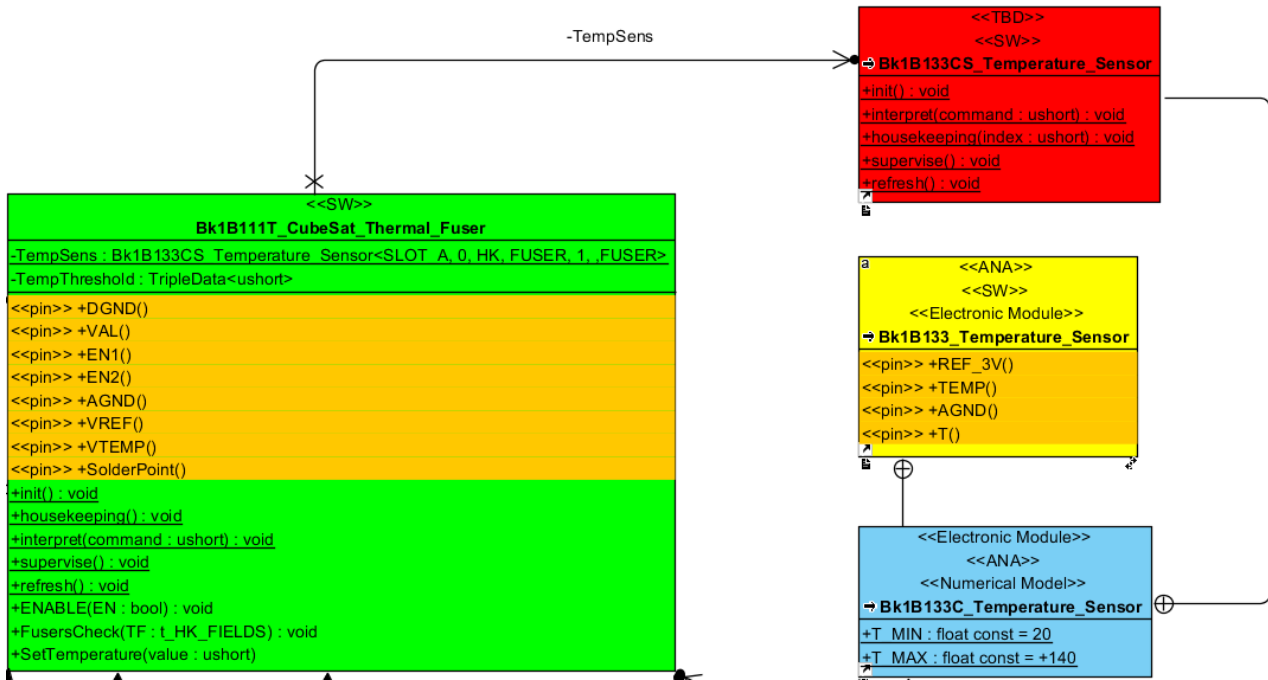


Figure 79: Bk1B111T Thermal Fuser.

7.1 Introduction

When the 1B111E structure is folded, the entire system has to be maintained steady in a fix position in order to guarantee that tiles do not deploy during launch. A system of eight wires is designed just to keep the structure closed and to provide high stability during the vibrations of launch. Once in orbit these wires have to be detached permitting so the deployment of the tiles. The detachment is performed with the use of specific thermal fusers that act on the tin soldering of the wires. The goal of the electronic opening system is to satisfy strict requirements: the tensile strength of the wires has to be enough to withstand the high acceleration of the launch and they have to guarantee that they do not detach from the satellite transforming themselves into dangerous space debris. Other requirements must be complied about the electric and thermal specifics: the Bk1B111T must not have high power consumption during its activity, and its hot points must not to reach too high temperatures. Also space occupation and weight follow strict requirements. Finally, the Bk1B111T system is further improved increasing its reliability to failures.

7.2 Sealing Wire

The sealing wire is the main element involved in the maintenance of the 1B111E structure folded. The wires are fixed both to the Bk1B213A1 base tile, either to the last Bk1B111E20 tile of the 1B111E array of tiles. The choice of the wire material and its diameter is not trivial. Is to be noted that the diameter of the wires affect the thermal proprieties of the thermal fusers, and the tensile strength of the material of the wires, affect the total sealing force. The best trade-off between the material type and the wire diameter has to be founded.

7.2.1 Strength Analysis

During a launch, the wires have the purpose to maintain steady the tiles when the structure is subjected to vibrations. The material of the wires and their sizes have to be analysed carefully in order to resist the big launch acceleration. Following are described all steps that led me to the chosen of the type of wire. The strength of a wire depends by the tensile strength of the material used, and by the surface where the force is applied:

$$F_{st} = T_{st} \cdot S \quad (22)$$

T_{st} is the tensile strength of the material and S in our case is the area of the circular cross section of a wire. With respect to the vibration spectre of Figure 53, I use the worst case of the maximum acceleration of 20g. About the weight of the structure instead, using the tool proprieties of mass of SolidWorks, I estimate the total weight of a 1B111E structure of three tiles that is of about 100g. Then, if the satellite is considered as a fix body (with a mass much larger with respect to the 1B111E structure) under 20g of acceleration, the structure of tiles can be subjected to an estimated force of about $F = m \cdot a = m \cdot 20g = 0,1\text{kg} \cdot 20 \cdot 9,81\text{m/s}^2 \approx 20 \text{ [N]}$. Actually this is a heavy approximation and so it is convenient to use fixing wires that are able of withstanding a much greater force. In this way, the Table 9 shows the analysis on different types of materials with different tensile strength.

	Cu	CuBe	Nylon 6	Nylon 6/6
d (diameter) [m]	3,00E-04	3,00E-04	3,00E-04	3,00E-04
S (section/surface) [m ²]	7,07E-08	7,07E-08	7,07E-08	7,07E-08
Tensile Strength [Pa]	7,00E+07	1,30E+09	7,80E+07	8,50E+07
F strength [N]	4,95E+00	9,19E+01	5,51E+00	6,01E+00

Table 9: Wire Material analysis.

The diameter chosen is 0,3mm. The comparison of different materials with the same diameter of wire shows as a single wire of CuBe is already enough to withstand over 20 N. The CuBe is so a good choice, but the 1B111E structure is designed in order to be fixed with 8 fixing wires, for a global tensile strength of about 735 N. The use of eight anchor points of the structure is not only for increase the resistance to the force of acceleration, but it increases the margins of safety in case one or more wires are broken during the launch. In addition, they distribute the tension on more points, avoiding that it falls on a single soldering point. Another advantage is related to the vibration frequencies: if these points are appropriately joint with mechanical shims, they act as fixed constrains points during vibrations thus becoming stabilization points for the structure.

7.3 Bk1B111T Thermal Fuser Analysis

The thermal fuser is considered an electronic element suitable to produce energy and concentrate the same in a small part. The point that needs this energy is the pad where the CuBe wire is soldered to the base tile. In first approximation a structure that concentrates the heat in small area can be characterized by two near resistors among which there is placed the soldering point of the wire (Figure 17 (b)). Obviously in order to choose the right resistors and estimate the current needed to heat them, a thermal model has to be defined. Starting from the structure of Figure 17, the thermal model of the fuser is realized and shown in Figure 80. Three main direction of spread for the heat are considered: the longitudinal direction where the heat flows through θ_1 , θ_2 and θ_4 , the vertical direction where the heat spread into the wire through θ_w and θ_5 and the laterals directions where the heat spreads through θ_6 ¹⁸.

¹⁸ It 'should be noted that the laterals directions were inserted to improve the accuracy of the thermal model. From a first simulation using SolidWork and without having considered the θ_6 resistances, was clear that the lateral spread has a considerable contribute to the heat spread. Furthermore, in order to further improve the model accuracy, the "Wlat" (see Figure 80) used for calculations is used slight greater (3.3mm) than the real size (3mm). This because after simulation was seen that lateral spread of heat cover an area slightly greater then 3mm). This techniques of improving of the analytic model is a typical example of iteration between numeric simulators and analytic computations

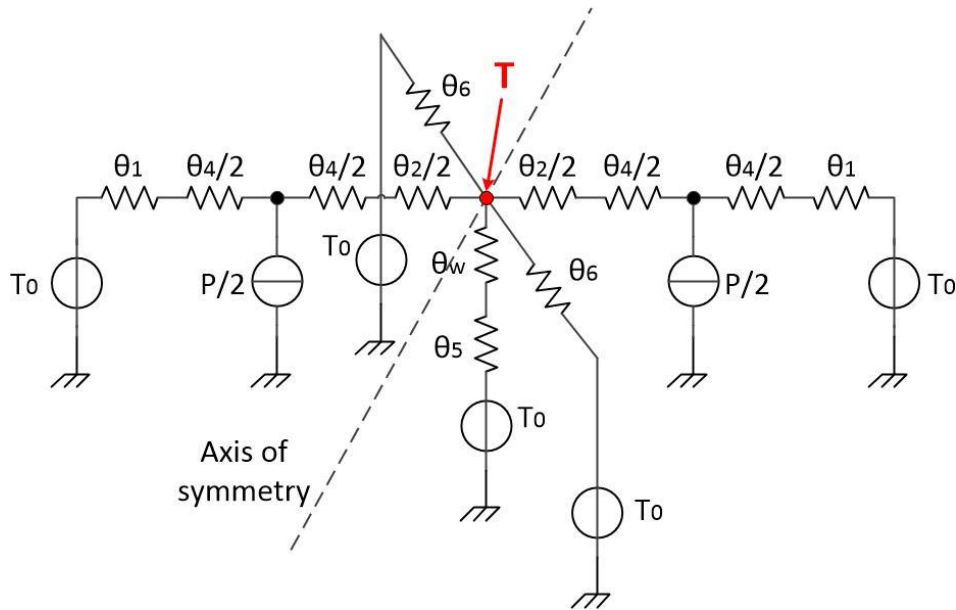


Figure 81: Thermal circuit of the thermal fuser.

Where, all elements are:

- T_0 is the environment temperature, considered in a worst case of -25°C .
- P represents the total electric power of both the two resistors.
- θ_1 and θ_2 are respectively the thermal resistance of the external copper traces and the central trace.
- θ_4 is the thermal resistance between two traces.
- θ_6 is the thermal resistance of the two laterals gap of FR4.
- θ_w is thermal resistance of the CyBe wire.
- θ_5 is the thermal radial resistance of the upper tile.
- T is the temperature of the soldering point, and since the tin has a low thermal resistance, T is considered also the temperature of the whole volume of the soldering tin. This temperature is the parameter to be find.

In order to find T , the circuit has to be simplified. The first simplification is performed taking into account the circuit symmetry (with respect to the axis of symmetry shown in Figure 81). If the circuit is symmetric, all parameters of the two semi-sections of the circuit will be the same. In this way, the circuit is reduced to one semi-section with the resistances exactly half value, while power generators with the double value.

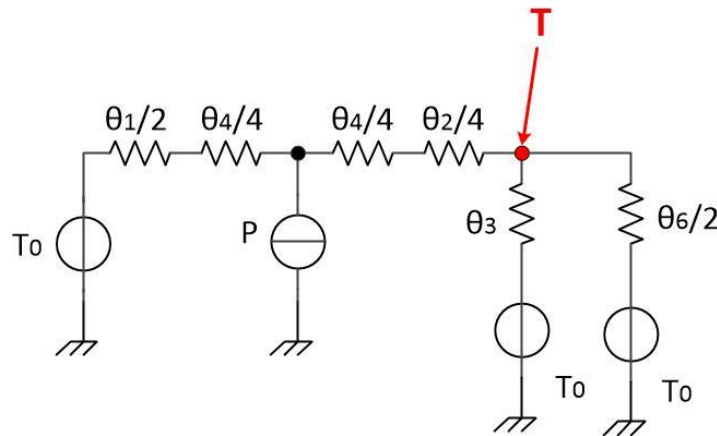


Figure 82: Simplification due to symmetry

Where $\theta_3 = \theta_w + \theta_5$. Now, can be performed two simplifications: the first is the Norton equivalence (Figure 83 (a)) and the second is the Thevenin equivalence (Figure 83 (b)).

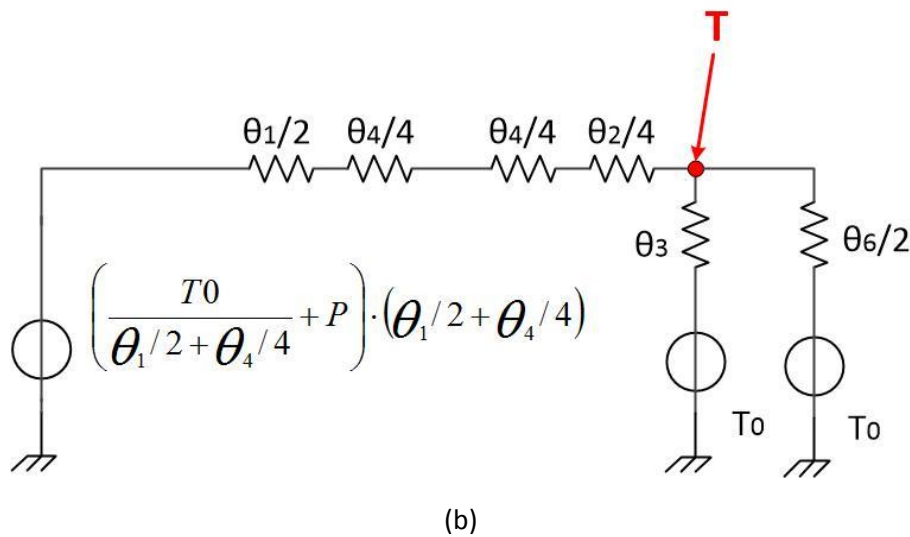
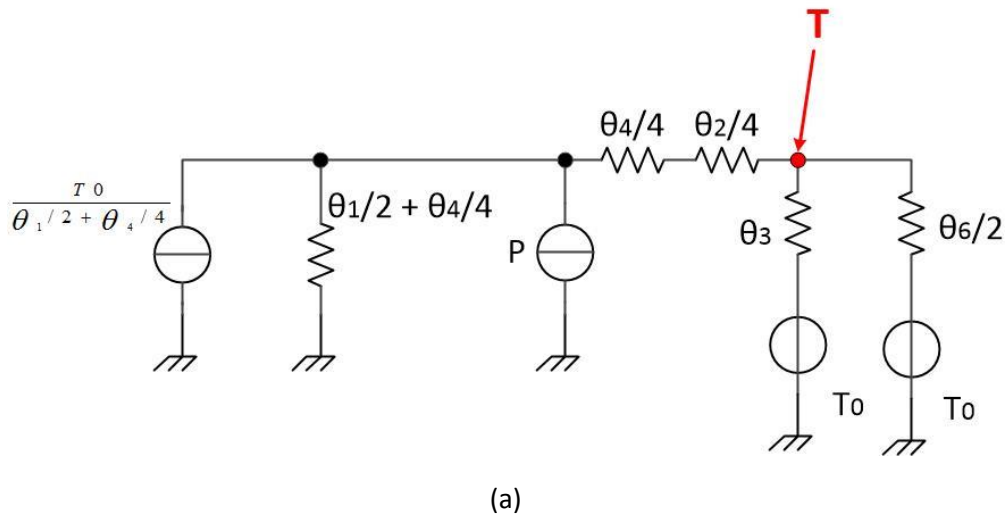


Figure 83: Circuit reduction (a) Equivalent Norton (b) Equivalent Thevenin.

With the circuit of Figure 83 (b) it is possible to apply the Millman theorem to find T:

$$T = \frac{\left(\frac{T_0}{\theta_1/2 + \theta_4/4} + P\right) \cdot (\theta_1/2 + \theta_4/4)}{\theta_1/2 + \theta_4/4 + \theta_4/4 + \theta_2/4} + \frac{T_0}{\theta_3} + \frac{T_0}{\theta_6/2}$$

$$T = \frac{1}{\theta_1/2 + \theta_4/4 + \theta_4/4 + \theta_2/4} + \frac{1}{\theta_3} + \frac{1}{\theta_6/2}$$

$$T = T_0 + P \cdot \left(\frac{\theta_1/2 + \theta_4/4}{\theta_1/2 + \theta_4/2 + \theta_2/4} \cdot \frac{(\theta_1/2 + \theta_4/2 + \theta_2/4) \cdot \theta_3 \cdot \theta_6/2}{(\theta_3 \cdot \theta_6/2) + (\theta_1/2 + \theta_4/2 + \theta_2/4) \cdot \theta_6/2 + (\theta_1/2 + \theta_4/2 + \theta_2/4) \cdot \theta_3} \right) \quad (23)$$

The (23) can be written highlighting the total thermal resistance.

$$\theta_{tot} = \left(\frac{\theta_1/2 + \theta_4/4}{\theta_1/2 + \theta_4/2 + \theta_2/4} \cdot \frac{(\theta_1/2 + \theta_4/2 + \theta_2/4) \cdot \theta_3 \cdot \theta_6/2}{(\theta_3 \cdot \theta_6/2) + (\theta_1/2 + \theta_4/2 + \theta_2/4) \cdot \theta_6/2 + (\theta_1/2 + \theta_4/2 + \theta_2/4) \cdot \theta_3} \right) \quad (24)$$

$$T = T_0 + P \cdot \theta_{tot} \quad (25)$$

The (25) shows a clear result: the main goal in the designing of a thermal fuser is to achieve the desired temperature with the lowest possible power consumed. Thus, supposing a defined final temperature T, if P decreases and T₀ is a constant, θ_{tot} must increase. This is obvious, because greater thermal resistance means a much more isolation for the hot point: the heat is much more confined to the soldering point, permitting to reach the desired temperature at low power consumption. The concept is quite simple, but designing a structure in order to expose a low thermal resistance is much more difficult. A good trade-off is reached with the following parameters:

Lw	5,00E-03 [m]	d	3,00E-04 [m]
L	3,00E-03 [m]	σ_{Cu}	4,00E+02 [W·m ⁻¹ ·K ⁻¹]
LR	3,00E-03 [m]	σ_{FR4}	5,00E-01 [W·m ⁻¹ ·K ⁻¹]
Llat	2,00E-03 [m]	σ_{CuBe}	1,01E+00 [W·m ⁻¹ ·K ⁻¹]
Wcu	1,00E-03 [m]	tCu	3,50E-05 [m]
Wb	4,00E-03 [m]	tu	1,60E-03 [m]
Wlat	3,30E-03 [m]	tb	4,00E-04 [m]
R	1,50E-03 [m]		
r	5,00E-04 [m]		
R/r	3		

Table 10: Parameters used for thermal fuser.

Where σ is the conductivity of the materials.

In order to complete the calculation of θ_{tot} all single thermal resistances will be defined. Their values are obtained, referring to the model of Figure 80.

$$\theta_1 = \frac{L}{\sigma_{FR4} \cdot (w_b \cdot t_b) + \sigma_{Cu} \cdot (w_{Cu} \cdot t_{Cu})} = 174 [K/W]$$

$$\theta_2 = \frac{L_R}{\sigma_{FR4} \cdot (w_b \cdot t_b) + \sigma_{Cu} \cdot (w_{Cu} \cdot t_{Cu})} = 174 [K/W]$$

$$\theta_4 = \frac{L_h}{\sigma_{FR4} \cdot (w_b \cdot t_b)} = 969 [K/W]$$

$$\theta_w = \frac{L_w}{\sigma_{CuBe} \cdot \left(\pi \cdot \frac{d^2}{4} \right)} = 70000 [K/W]$$

$$\theta_5 = \frac{\ln\left(\frac{R}{r}\right)}{\sigma_{FR4} \cdot t_u} = 5490 [K/W]$$

$$\theta_3 = \theta_w + \theta_5 = 75490 [K/W]$$

$$\theta_6 = \frac{L_{lat}}{\sigma_{FRA} \cdot (w_{lat} \cdot t_b)} = 758 [K/W]$$

Substituting all thermal resistances into the (24), the total thermal resistance obtained is: $\theta_{tot} = 125 [K/W]$. Once the thermal model is defined, the type of the tin for the soldering of the wires has to be chosen. The correct working of the BK1B111T is based to the use of a tin in low melting temperature. If it is not used this type of tin and is chosen a standard tin, the melting temperature of about 220C°, it risks to melt also the tin of soldering of the resistors. So, causing a disastrous detachment of the components. In such a way the tin chosen for the wires, has a melting temperature of about T = 120 C°.

Once defined a temperature that I want to reach, given the boundary temperatures of T₀ = -25C° (worst case) and inverting the (25), I obtain a minimum power of P = 1,16w to be dissipated, in order to reach the melting temperature in the hot point of T=120C°.

Taking into account a minimal tolerance to guarantee the achieving of the melting temperature, I use a total power of P = 1.5w (This consideration is done because T₀ is considered as worst case of low temperature in LEO orbit, but really this value may be lower). Using this power, the temperature that I aspect is T = 163C°. Before design the driver circuit that provide power to the two resistors, the value of temperature T generated by a total power of 1.5w will be verified in paragraph 7.4 using a simulation of the thermal model by means of SolidWorks.

7.4 Bk1B111T Thermal Simulation

The model of Figure 80 is fully translated into a SolidWorks simulation model. The tool Flow Simulation is used to perform the analysis. The real proprieties of materials are used and all sizes and shapes of the employed bodies are defined (Table 10). With respect to the analytic model, in the simulation one it is inserted the tin of soldering. This chosen is functional since the tin is used to ensure the physical contact between the trace of the board and the wire. Obviously the real proprieties of the tin are used. Since the tin has a low thermal resistance, the thermal model does not stray far from the analytical model. Once the all shapes are defined, are placed the boundaries conditions and heat sources. All simulation conditions are listed:

- The bodies of the materials are considered with real proprieties.
- The analysis type is "External", selecting heat conduction in solid only. This means that the outer space is considered empty (vacuum condition), thus only conduction into the solid is considered.
- For the entire body is considered a blackbody wall.
- A real wall is applied on lateral surfaces of the upper and bottom board of the model. The temperature applied to real wall is -25C°.
- The external source is only radiation from deep space of 3k.
- The two heat sources are applied to the two volumes of the resistors. The value of generation is 0,75w for each resistor. In this way the total amount of power generated is 1,5w.
- The initial temperature of the bodies is 293k.
- The goals for simulation are set on the convergence of the results. This means that the simulation is stopped automatically by the solver when the results values reach a convergence.

The Figure 84 shows the complete model of a fuser. The picture is slightly zoomed to see all applied constrains. The external rectangle represents the computational domain. The Pink arrows incoming from outside of the computational domain represent the environment radiation of 3k. The spirals on the resistors indicate the power generators, while the squares on lateral surfaces of the boards indicate the real walls.

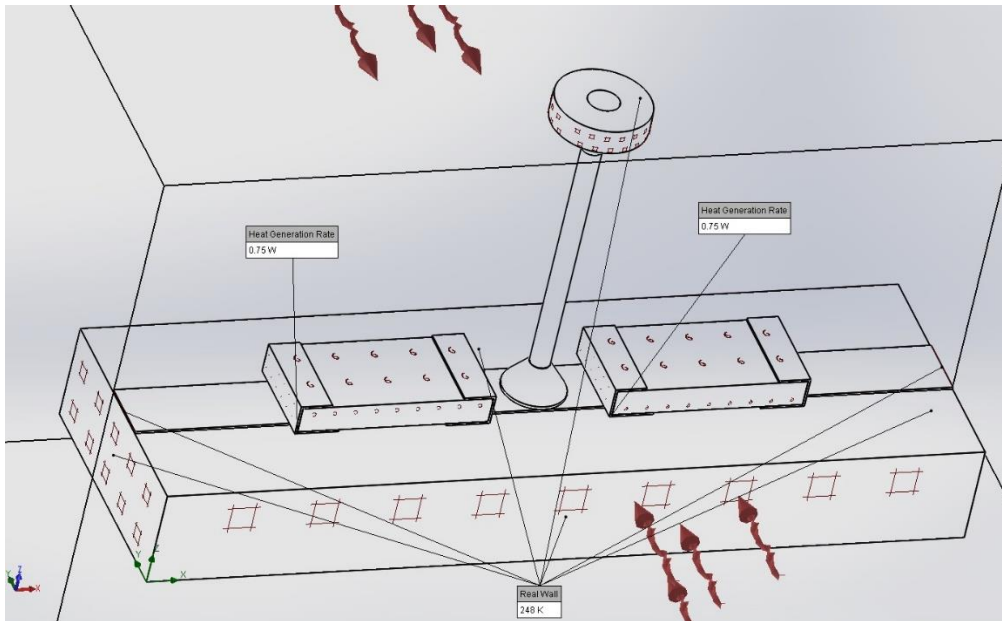


Figure 84: Simulation thermal model structure of a fuser.

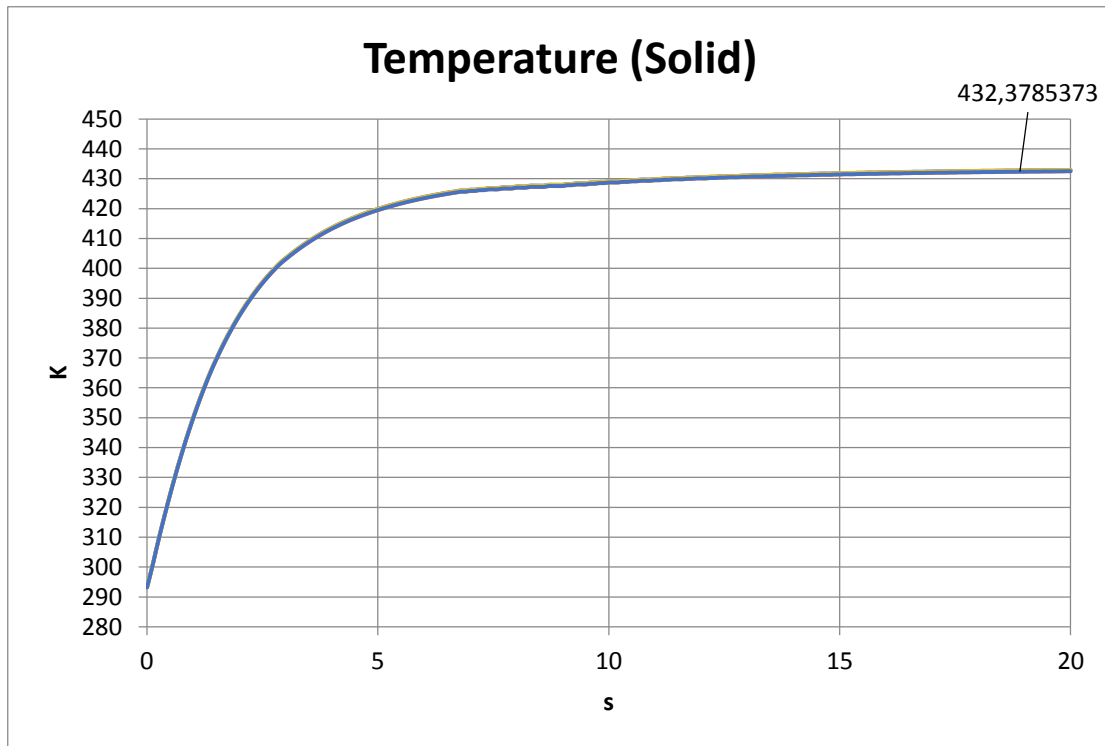


Figure 85: Temperature profile of the tin of soldering.

Figure 85 shows the temperature in function of time that the tin of soldering reaches. The temperature is about 159 °C at equilibrium. This value is quite near to the analytic value of 161 °C and so the simulation model can be validated. The slightly difference between the temperature calculated in analytic way and the simulated one is likely due to the low accuracy of the analytic model. In fact, the analytic model does not considers the vertical conduction, deep into the base board (this is not considered in order to avoid to makes the analytic model too complex, because the purpose of thermal analytic analysis is not the determination

of a precise temperature, but its estimation¹⁹). And so the temperature results slightly higher. The Figure 86 shows the heating phases in some pictures. The Figure 87 shows the same phases but with a slice chart along the horizontal central axis. The slice charts highlight better how the vertical spread of heat into the board is not so much negligible as it is done in the analytic model.

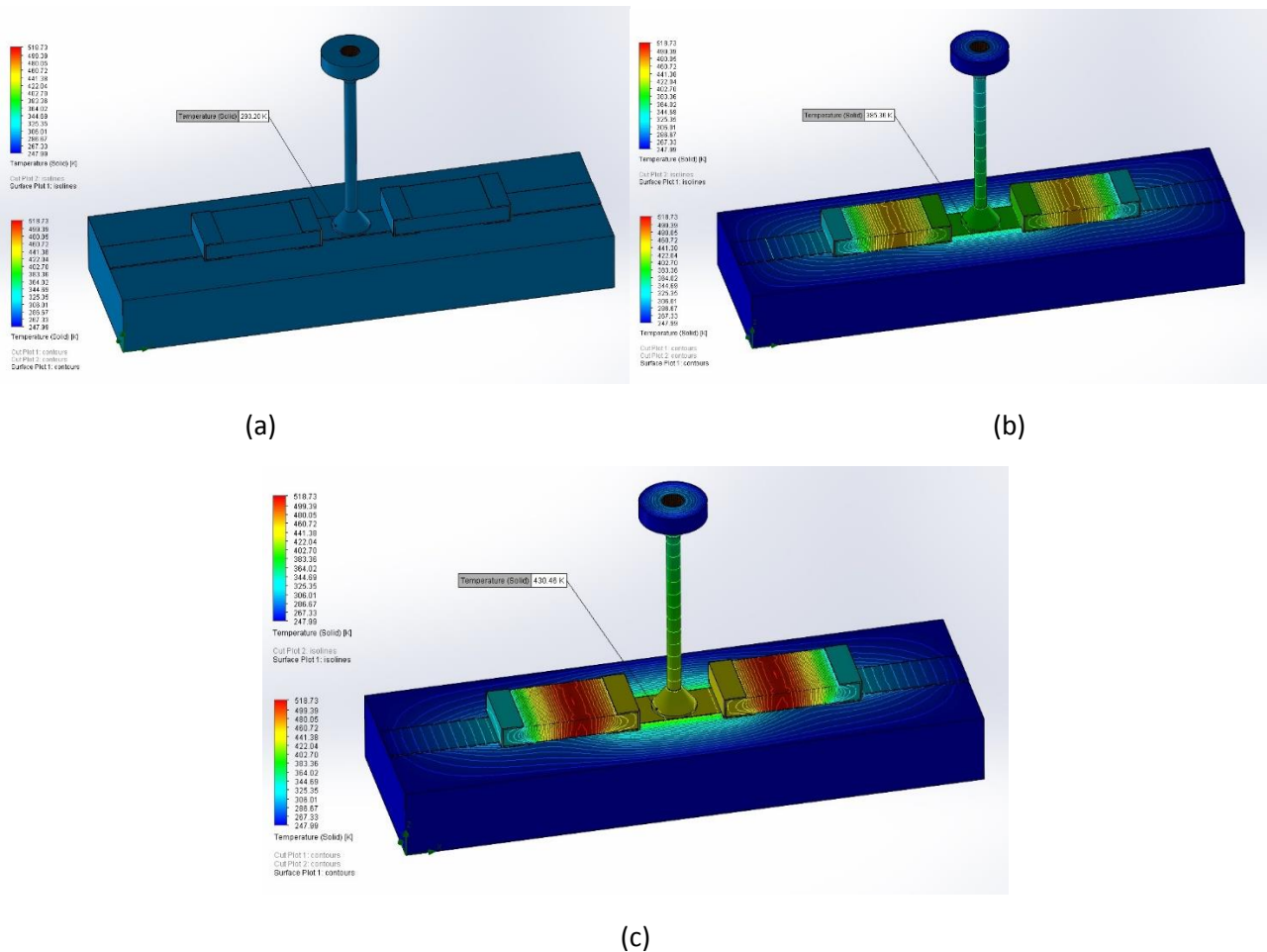
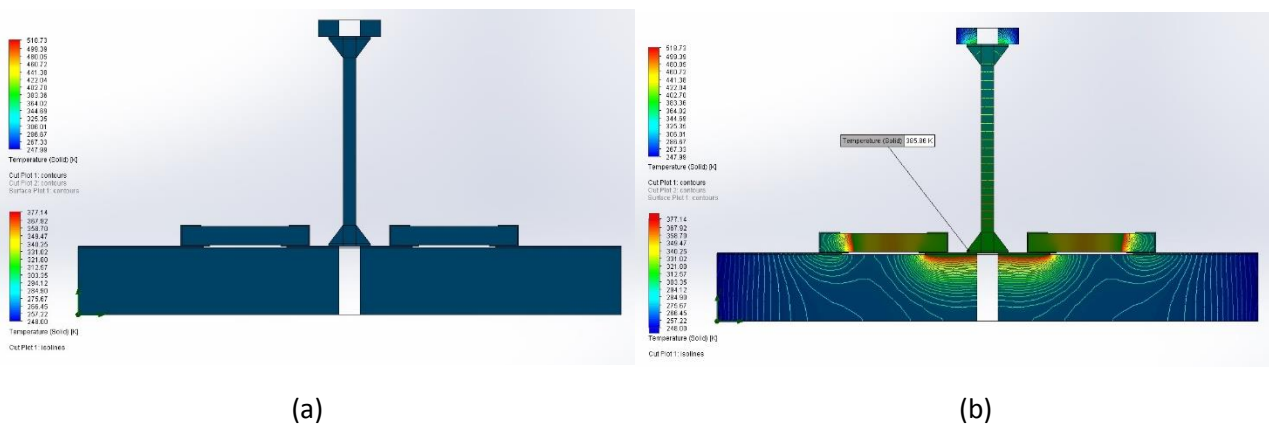
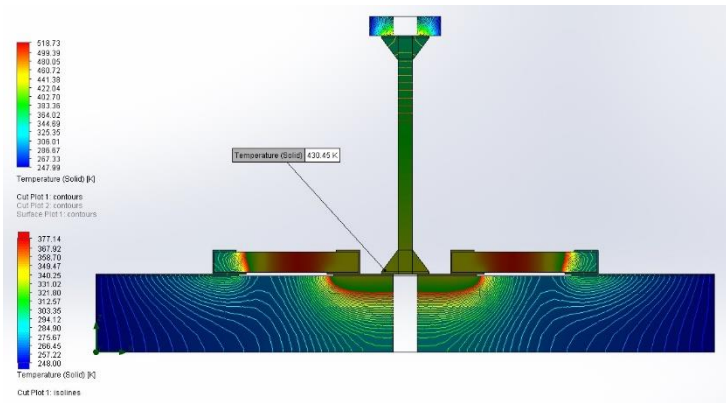


Figure 86: Heating phases of the thermal fuser (a) Initial conditions (b) 2 sec (c) 10 sec.



¹⁹ The analytic model is good techniques to easily estimate a value of temperature. Obviously, the techniques based on FEA algorithms are much more accurate.



(c)

Figure 87: Heating phases of the thermal fuser along the horizontal central axis (a) Initial conditions (b) 2 sec (c) 10 sec.

7.5 Bk1B111T Electrical Design

A single thermal fuser is first of all an electronic element, essentially composed by two resistors that generate heat and a copper trace with a shape appositely designed. The single fuser element analysed in paragraph 7.3 and 7.4 is entire integrated in the PCB that will constitute the base tile of a 1B111E structure. In order to produce heat, the employed technique is the conversion of electric energy into heat energy by means of the Joule effect. This is done using two resistor components connected into the same serial circuit. In this way a single current is used to generate the electric power needed. With respect to results obtained in 7.3, in order to reach the melting temperature of the tin of soldering, the power desired is $P = 1,5w$. Moreover, since this is a typical application that requires a relative high power and currents (especially when more fusers have to be used simultaneously), the circuit is designed considering the high voltage bus of 14V. This one, according to the ARAMIS specifications, it is available on its PDB. The Figure 88 shows the circuit designed.

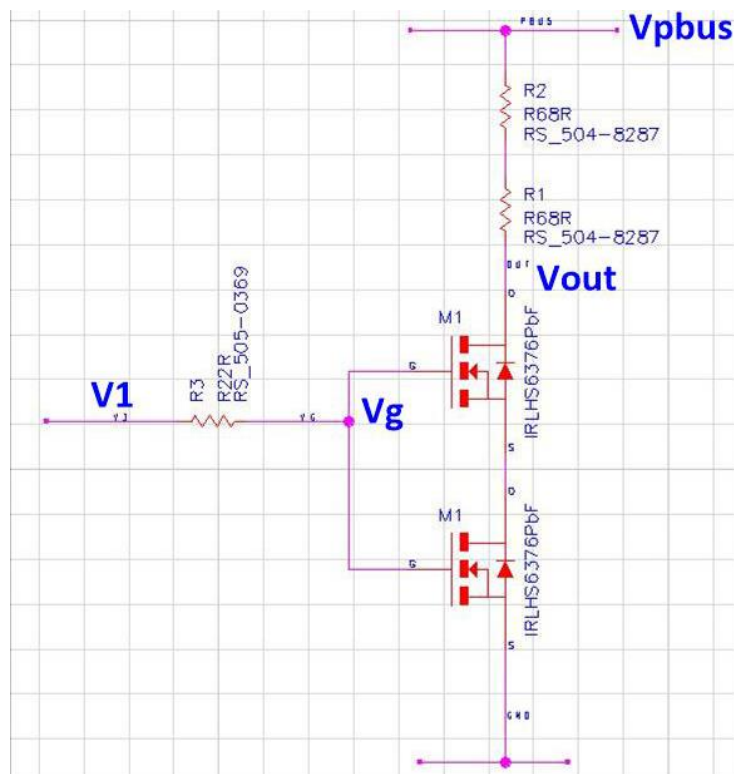


Figure 88: Driver circuit of the Thermal Fuser.

Since I want an electric power supply of 1.5w and I have a power bus from the PDB of 14V, the current needed is:

$$I_{min} = \frac{P}{V} = \frac{1.5w}{14V} = 107mA \quad (26)$$

Whit this current, the total amount of resistance needed is $R = \frac{P}{I_{min}^2} \approx 131 [\Omega]$. This latter is related to the entire load. But in order to design the fuser these resistances have to be split into two equal resistances connected in series, each one that will dissipate half of the power supply P. Using the standard resistors value I chosen to consider two resistances of 68 Ω each one. Each resistance is chosen in order to be a small component, in my case a 0603 resistor. About power consumption, these are chosen in order to have a max power dissipation of 0.75w²⁰.

Since the commands of the deployment that will come from a microcontroller cannot directly supply a current of 107mA, a drive circuit has to be designed. The best choice is using transistors MOS as switches. The resistances are so electrically considered as a single load. The current flowing inside the load is driven by means of a couple of transistors MOSFET. The chosen of a couple of transistor is done to increase the reliability to failures. In fact, if one between the two MOSFET will be damaged and will creates a short circuit, the second transistor avoids that the PDB goes in short circuit, causing a catastrophic failure that can compromise the mission. Furthermore, in order to reduce as much as possible space occupation of the MOSEFT, I chosen to use a double channel MOS integrated inside the same package. Obviously, the type of transistors are chosen taking into account a tolerance for the maximum current (1A in my case) and a much low possible ON resistance (few m Ω in my case). The working principle is simple, the two transistors are in common gate²¹. Once the common gate exceeds the Vth voltage of the MOS, these enter in conduction and since they expose a low drain-source ON resistance, the ground potential is as if it were applied directly to the load. In this way the drop voltage on MOS are negligible and the entire voltage of 14V is directly applied to the load. The Figure 89 shows the Spice simulation of the circuit of Figure 88. The real Spice models are used for the two MOSFET. In the simulation, a transition 0-1-0 is performed on the control input V1. The gate resistor is inserted to increase the MOS input resistance and so eliminate the oscillations on the gate. The latter are due to the parasitic capacitances on the input of the gate. Since the gate current in negligible, the V1 voltage is exactly the same on common gate Vg. The simulation shows as once the Vg voltage reaches 2.8V (the output voltage of the high level from the low power microcontroller), the two transistors switch practically instantaneously. Vout is the low drop voltage, on the two series of MOS and its much low value is related to the very much low ON resistance of the two transistors in conduction. Ivbus is the current in the load, then its value of about 103mA is about the same estimated in analytic way of 107mA (taking into account the in analytic estimation are considered the resistance not normalised and are not considered the low ON resistances of the two MOS in conduction). In the simulation the value of the current is negative for the convention of generators in SPICE environment. The waveform wf2 represents the power consumption of the entire circuit, because is the multiplication between load current and Vpbus. Its value is 1,44w during conduction.

²⁰ Generally this is a high value for resistors 0603, but in the datasheet of the resistors there are indications about how much power the resistor can dissipate and for how much time it can does it. Generally the resistors can be subjected to much more power with respect its maximum power dissipation, provided that the conduction not exceeds a certain time. In this way, since the fusers are not intended to be used for a long time but only for the phase of deployment that can take few seconds, the resistors can be chosen also with a much more low maximum power dissipation, but always according to the datasheet indications.

²¹ The common gate is a solution used to simplify the simulation. In the real circuit the two input of enable are separated.

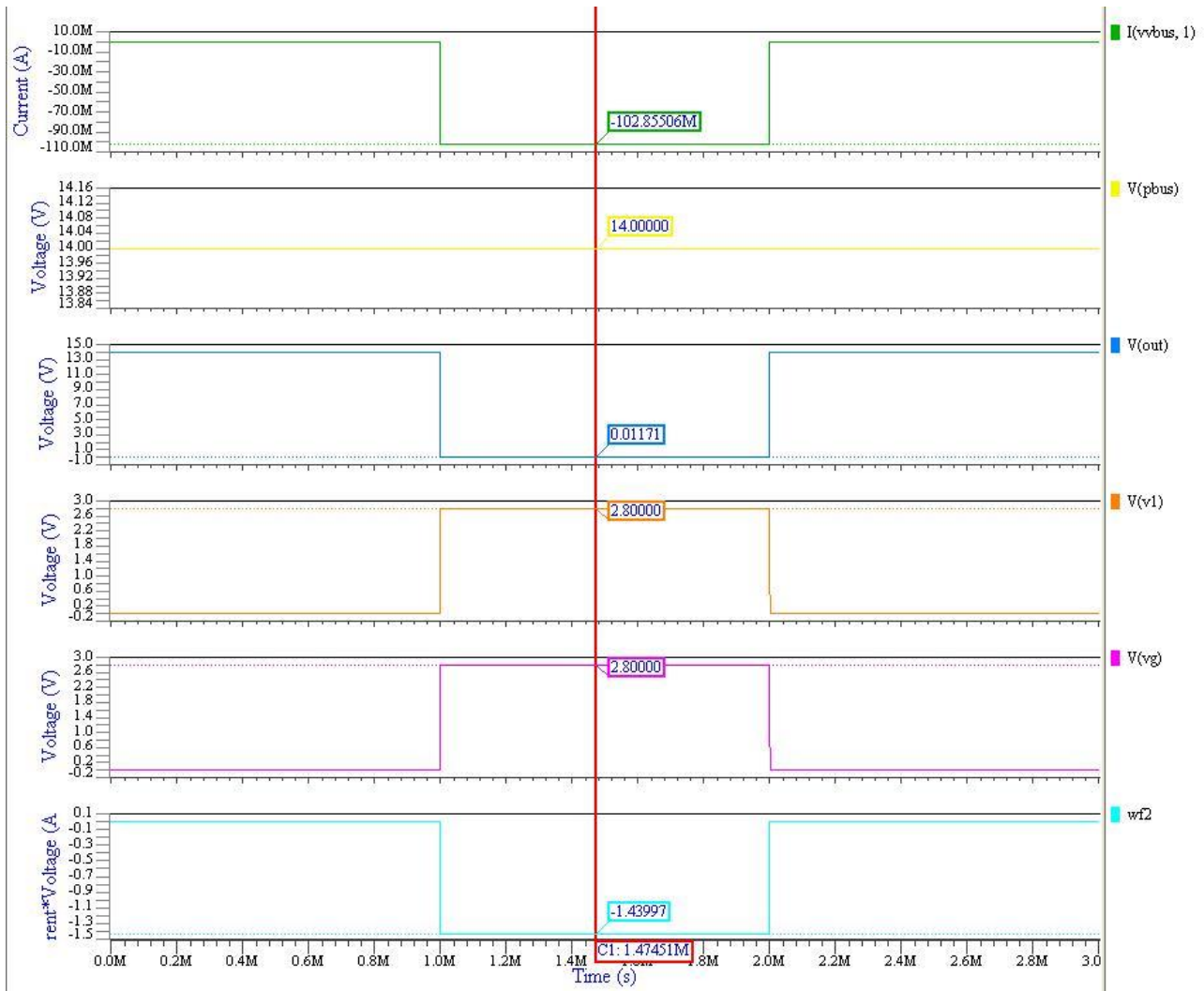


Figure 89: Thermal fuser circuit SPICE simulation.

The space environment often presents conditions that are difficult to predict with absolute precision. All thermal analytics analysis and simulations provide an estimation of what happens once the resistors of the thermal fuser will be powered. Analytics calculations and simulations are done, considering as worst case, a boundary temperature condition of $T_0 = -25^\circ\text{C}$. Unfortunately this temperature can variate. For low temperature there are no many problems because in the 7.3, P is chosen with a greater margin of tolerance²².

If T_0 increase, the problem is instead different: for the same power supplied P, if T_0 increases, also the final temperature T, increases. This can produce catastrophic failures because it may be achieved the melting temperature of the soldering tin of the near resistors (the soldering tin of the resistors is the “normal type”, with a melting temperature of about 220°C). It may cause a detachment of the resistances by producing debris and causing a series of shorts circuits. To avoid this situation, the maximum temperature has to be controlled. This is done using a temperature sensor. In this way the fuser system has a feedback control, as the Figure 90 shows.

²² In fact if T_0 drops and none margins of tolerance are considered, the power P may be not enough to reach the melting temperature.

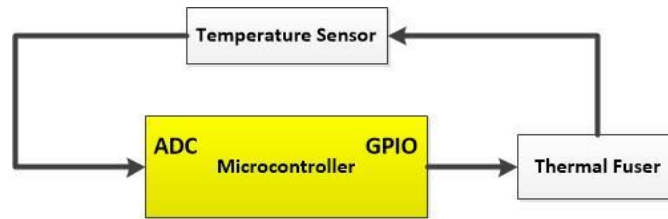


Figure 90: Temperature control of the thermal fuser.

A microcontroller provides the control signal to activate the fuser, but it realizes also the feedback control on the fuser. The microcontroller reads the value of temperature using the sensor and then it can deactivate the fuser if the temperature exceeds a certain threshold. The sensor used is a simple NTC, operating in the range of $-40-150^{\circ}\text{C}$. The component used is chosen for its small size features, in this way they are particularly suited for the placement very closer to the fuser. This sensor has a 0603 package and is placed very close to the pad of the fuser, but not so much as to interfere with the thermal characteristics of the fuser. Figure 91 shows the layout of the pad of the fuser component. The real layout is slight different from the layout analysed in section 7.3 of Figure 80. This difference is due to the different shape of the pads of the real components found and used. Fortunately, even if the distance between the two pads of the two resistors of heating is lower, the two lateral traces have been reduced in width and extended in length. As it is possible to see in Figure 80, these traces correspond to the thermal resistance θ_1 . If the width is decreased and the length is increased, the thermal behaviour improves, because θ_1 increase and then it is possible to reach the melting point using less power. In this way the layout of Figure 91 represents a thermal fuser improved, respect to theoretical model of the section 7.3. Obviously the width of the trace of the two heating resistors is verified using the (4). This is done to see if the current of about 100mA estimated with the (26) may be a problem. As the Figure 92 shows, with a width of 0,4mm the temperature does not exceed 100°C , thus these lateral traces do not represent a thermal problem for the components.

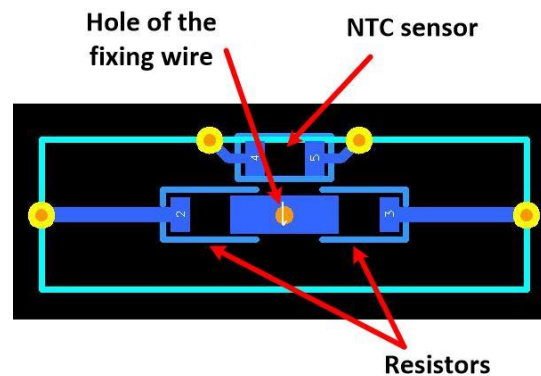


Figure 91: Thermal fuser layout.

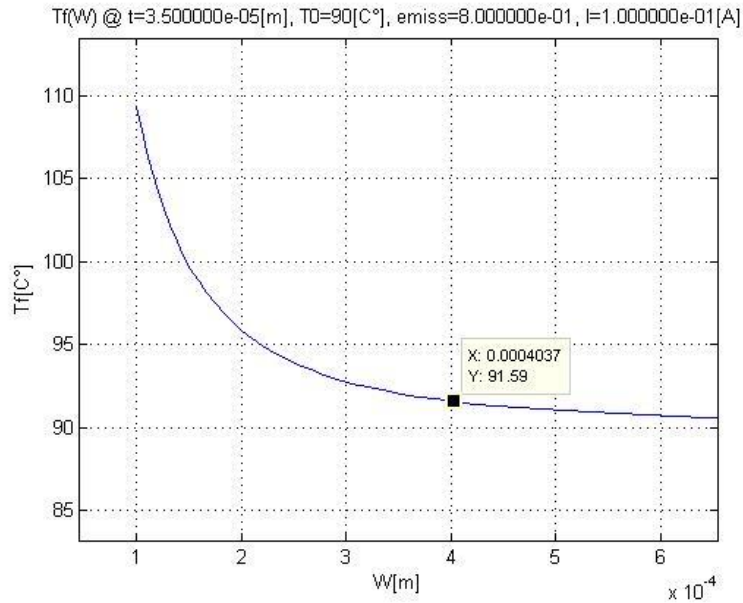
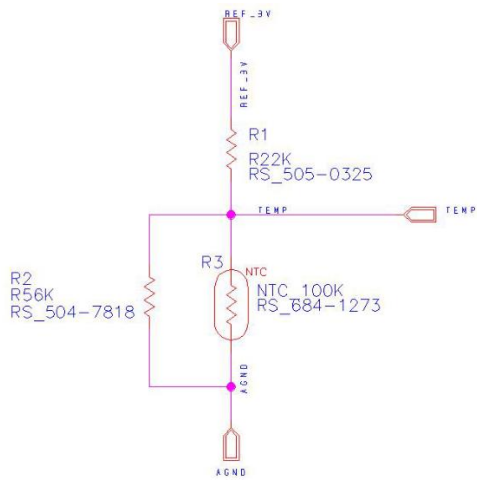


Figure 92: Worst case of the temperature reached by the trace of heating due to current of the thermal fuser.

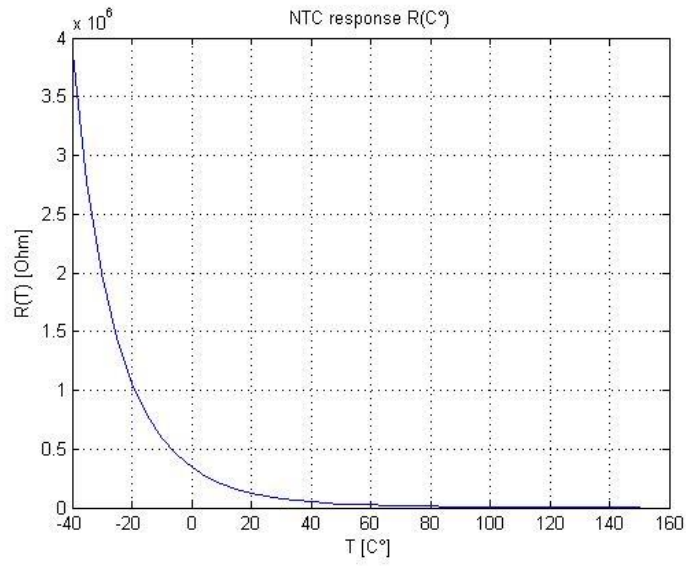
The NTC sensor is a thermistor sensor type. It means that the sensor varies its parameter of electric resistance according to the variations of the temperature. The NTC class is a category of thermistors that decrease its resistance to the increase of temperature. Unfortunately a big problem with these types of sensor is its nonlinear behaviour (Figure 93 (b)). To avoid this, a circuit of linearization is designed. There are different types of linearization circuits, each one with different improvements in the linearization. Since I have no particular needs of high precision measurements of the temperature, the most simple linearization circuit is used. It consists of a simple voltage divider, and the NTC sensor is inserted in parallel to one of the two resistances of the voltage divider. Referring to the circuit in Figure 93 (a), it is used an NTC of 100k with two resistances $R_2 = 56\text{k}\Omega$ and $R_3 = 22\text{k}\Omega$. The V_{temp} is the output voltage of the voltage divider and is given by:

$$V_{temp} = V_{ref} \cdot \frac{R_2 // R_{NTC}}{R_1 + R_2 // R_{NTC}} = V_{ref} \cdot \frac{R_2 \cdot R_{NTC}}{R_1 \cdot R_2 + (R_1 + R_2) \cdot R_{NTC}} \quad (27)$$

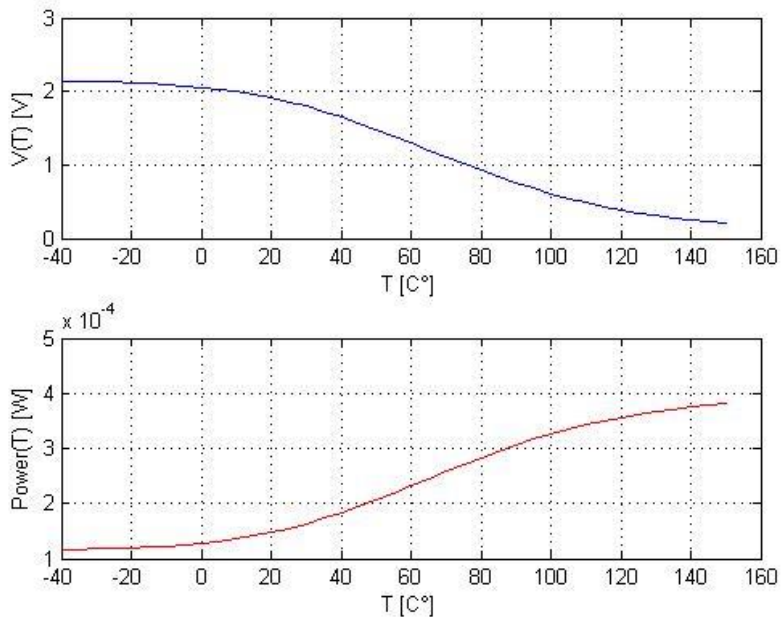
For V_{ref} is used 3V. The output voltage V_{temp} represents then the linearized response of the sensor output. Combining the relation of linearization (27) and the curve $R_{NTC}(T)$ from the datasheet of the NTC (Figure 93 (b)), the $V_{temp}(T)$ is obtained. An appropriate MatLab script is used to plot the NTC component response and the linearized output response of the circuit of linearization. The script is available in section 9.6. The two responses are plotted in Figure 93. From Figure 93 (c) it is possible to observe that the curve response is quite linear from 20C° to about 140C° . For the working operation of the thermal fuser, it is more interesting the maximum temperature of the range. In this condition, the range of linearization of the circuit, is good, because the maximum temperature that I want to measure is around $140 - 150\text{C}^\circ$. The Figure 93 (c) shows also the power consumption of the linearization circuit of the NTC. The power consumption is useful for the total estimation of the power consumption of the entire system.



(a)



(b)



(c)

Figure 93: Linearization circuit of the NTC (a) Linearization circuit scheme (b) $R(T)$ response of the NTC (c) Output response $V(T)$ and $P(T)$ of the linearized circuit.

8 Bk1B213A1 Outer Plate board Desing

8.1 Introduction

The configurations of the tiles described in chapter 2.4 are all compatibles with the holes of the 1U ARAMIS CubeSat. This means that the configurations of the standard tiles can be fixed to other ARAMIS side tiles (Figure 41). EXTA, EXTB, INTA and INTB hinges types are employed to realize the mechanical connection interface between the Bk1B111E20 tile of a 1B111E structure and a side tile of 1U ARAMIS CubeSat. This side tiles, represent a primary element for the implementation of the 1B111E system, because is the base where the deployment system is fixed. This section deals of the realization of the tile Bk1B213A1 outer plate that is considered as a test board for a 1B111E structure of three tiles. The compatibility between the test board and the 1B111E structure does not mean only mechanically, but means also electrically. Furthermore the electronic opening system has to be realized just on the base tile itself. So if an engineer wants to realize a side tile for a 1U ARAMIS CubeSat, compatible with the 1B111E, has to follows strict requirements and has to realize the BK1B111T fusers on the ARAMIS side tile.

The following paragraph gives the description of the design of the outer plate board that has to be intended as a test board. This one will be a reference design to realize the BK1B111T fusers system in other base tiles.

8.2 Bk1B213A1 System Design

The entire system of the BK1B213A1, is a typical embedded application. A suitable microcontroller is used to control and monitor the status of the eight thermal fusers. These ones, have to be activated simultaneously for some seconds. In this way all fixing wires can be correctly detached. The thermal fusers are realized electronically with the same circuits described in section 7.5. The only difference is that the input gates of the two driver MOS are decoupled. In this way, one input of the all fusers will represent a single enable signal (EN1-1 to EN1-8 of Figure 94) for all fusers, connecting all these inputs together. The other inputs will constitute the enable signal of each single fuser (EN2-2 to EN2-8). The total amount of enable signals for the BK1B111T fusers is nine. The use of the enable signals is very important. These types of subsystems will be operatives only one time in the mission and also for a small time, in this way it results essential disable them in order to avoid that these circuits continue to consume power uselessly.

Each electronic fuser has also a NTC sensor connected. This sensor is used with the linearization circuit seen in section 7.5. Thus, the whole circuit provides an analog output signal that from the NTC has to be read by the microcontroller to obtain the temperature of each fuser (TEMP). Since the microcontrollers generally don't have many ADCs (Analog to Digital Converter) respect to the large amount of sensors present on a satellite, all the eight analog outputs from the eight fusers are multiplexed by means of an analog multiplexer. This chosen is efficient for the electronic opening system because it is conceived to be implemented by another system of the CubeSat, and in particular the system realized on the base tile of the 1B111E structure. In this way the BK1B111T will be part of a system that probably will contain other sensors or subsystems that will require the use of ADCs. Thanks to the multiplexer, the analog outputs of the NTCs have need only of one ADC. Obviously the microcontroller have to provide three logic input signals of selection (A0, A1, A2) to the analog MUX. These inputs allow to switch from an analog input to another (S1 to S8). The multiplexer has also an enable signal that is connected to the same global signal enable of the driver MOSs of the thermal fusers. All enable and control signals will be connected to the microcontroller, where a suitable firmware will be implemented to manage them. The microcontroller needs also an opposite connector of JTAG. This is used to test and upload the firmware into the flash inner memory of the MCU.

The main system previously described is shown in the scheme of Figure 94.

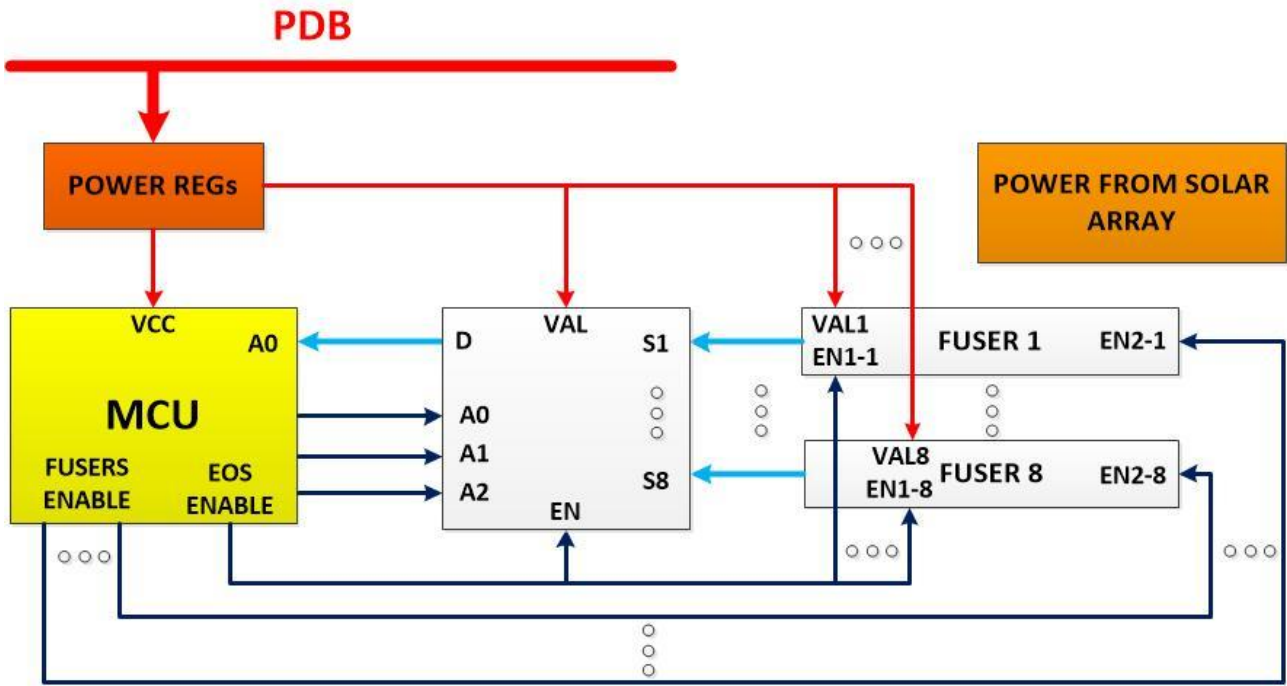


Figure 94: Block diagram of the BK1B213A1.

In the diagram of Figure 94, the red arrows represent the power supply line. From the regulators, the power is distributed on the various devices. The blue arrows represent the analog signals from the NTC. The dark arrows represent instead the digital control signals. The complete electric sheet of the outer plate test board is attached to the section 9.2. It's should be noted that the complete electronic sheet is divided into more pages. In this way it is more easy their consultation. Due to the large number of connections from the MCU, the modules are used. These are electronic buses, used to simplify the design and the management of the circuits.

8.2.1 Bk1B4221W Tile Processor 4M

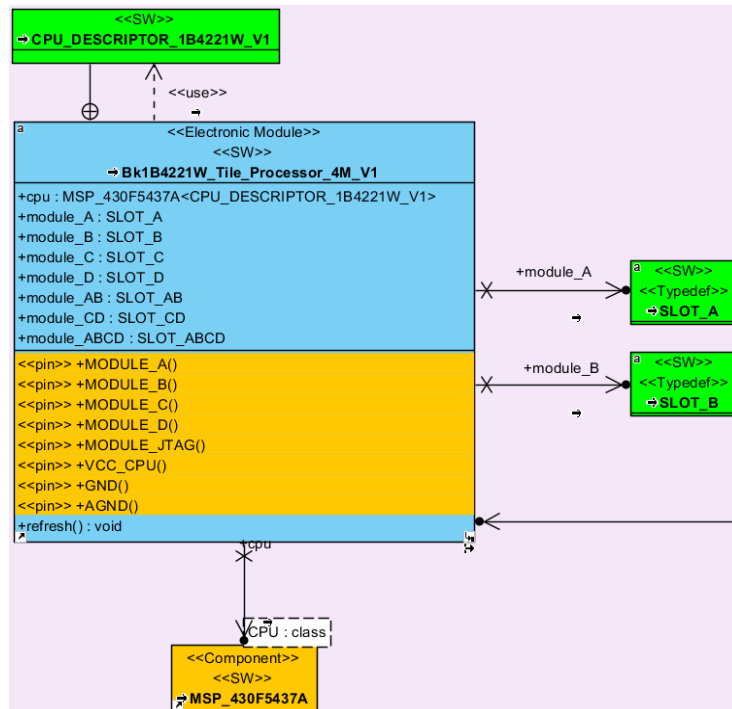


Figure 95: Bk1B4221W Time Processor 4M V1.

The microcontroller is the element employed in the management of the Bk1B111T. In the test board, it will be employed only for this purpose since the BK1B111T is conceived to be integrated with other systems and it will not have its own MCU (MicroController Unit). The microcontroller used for the test board is the same used for other types of subsystems of ARAMIS (MSP430 [14]). It is a 16-bit RISC architecture and a low power MCU. The system clock can works up to 18 MHz. Among all the MCU features, only two are important for the BK1B111T: the ADC and the timers. The MCU has a 12-bit ADC with 14 external channels and two internal ones, and it has also three different 16-bit timers that will be useful during the switching among the input signals from the NTC sensors. For the purpose of the correct working, the MCU needs of bulk and coupling capacitors to filter the power supply noise. It needs also of quartz oscillators for the main system clock (8Mhz) and for the correct synchronization of the timers (32,768kHz). All values of the capacitors are taken from those ones advised in the datasheet of the component. Even from datasheet a resistance of 47kΩ is placed to the reset pin (RST). The MCU circuit configuration is attached to the section 9.2. The Table 11 shows instead the summarization of the MCU pins mapping, and for which purpose they are used²³. The unused pins, those used for power supply, those used for JTAG or those ones not connected are not listed.

Module Pin	Module	Conn	Pin Name	Function
3	A	D4/CLK	P3.0/UCA0CLK	BK1B111T global enable. When this pin is low, the MUX, the linearization circuits and the drivers of the fusers are all disabled. When this pin is high, all the normal functions of the BK1B111T are enable.
5	A	D3/SDA /SIMO	P3.1/UCB0SDA	Individual enable of Thermal Fuser Driver 1. When this pin is low the Fuser 1 is disabled. When this pin is high the Fuser 1 is enabled.
7	A	D2/SCL/ SOMI	P3.2/UCB0SCL	Individual enable of Thermal Fuser Driver 2. When this pin is low the Fuser 2 is disabled. When this pin is high the Fuser 2 is enabled.
9	A	D1/TX/S IMO	P3.4/UCA0SIMO/ UCA0TXD	Individual enable of Thermal Fuser Driver 3. When this pin is low the Fuser 3 is disabled. When this pin is high the Fuser 3 is enabled.
11	A	D0/RX/S OMI	P3.5/UCA0SOMI/ UCA0RXD	Individual enable of Thermal Fuser Driver 4. When this pin is low the Fuser 4 is disabled. When this pin is high the Fuser 4 is enabled
1	A	D5/PW M	P4.6/TB0.6	Individual enable of Thermal Fuser Driver 5. When this pin is low the Fuser 5 is disabled. When this pin is high the Fuser 5 is enabled
10	A	D7/A1	P6.1/A1	Individual enable of Thermal Fuser Driver 6. When this pin is low the Fuser 6 is disabled. When this pin is high the Fuser 6 is enabled
4	A	D8/ID/I NT	P1.0/TA0CLK/ ACLK	Individual enable of Thermal Fuser Driver 7. When this pin is low the Fuser 7 is disabled. When this pin is high the Fuser 7 is enabled
2	A	D9/EN/ PWM2/I NT	P1.3/TA0.2	Individual enable of Thermal Fuser Driver 8. When this pin is low the Fuser 8 is disabled. When this pin is high the Fuser 8 is enabled
12	A	D6/A0	P6.0/A0	Analog input Pin of the ADC used for the conversion of the output D of the MUX.
5	B	D3/SDA /SIMO	P3.1/UCB0SDA	Digital output pin for the input selection A0 of the MUX.

²³ All of the table reference names, refer to the nomenclature used in ARAMIS project for the MCU used.

7	B	D2/SCL/ SOMI	P3.2/UCB0SCL	Digital output pin for the input selection A1 of the MUX
3	B	D4/CLK	P3.3/UCA0STE	Digital output pin for the input selection A3 of the MUX

Table 11: MCU pin configuration.

8.2.2 Analog Multiplexer

The analog multiplexer is employed in the multiplexing of the output signals from the NTC sensors. It has exactly eight analog inputs, each one connected to the outputs of the NTC circuits. The analog output is instead connected to one ADC channel of the MCU (A0). For a multiplexing of eight input there is need of at least $\log_2(8)$ inputs of selection: the analog device has three digital input signals connected to a port of the MCU and employed in the switching among the various 8 analog inputs. The Figure 96 shows the functional block of the MUX [15]. The device is operated in single ended mode, because the output signal from the NTC (Figure 93 (c)) has a range between 0 and 2,2V. The output dynamic of the MUX is rail-to-rail. It means that the output can reach the voltage supply of the device. In this way since the output range of the NTC has a maximum value of about 2,2V, the supply voltage of the MUX is chosen 3V. The same 3V voltage is so used for both the linearization circuits of the NYC either for the MUX. Also the MUX device needs bulk and coupling capacitors. These are chosen and inserted according to the datasheet of the component.

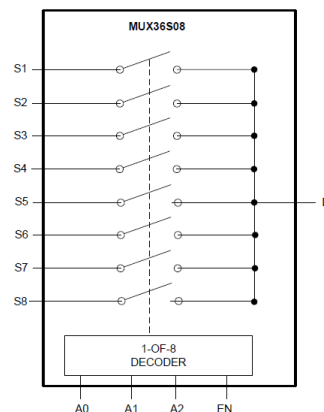


Figure 96: Functional block of the MUX.

8.2.3 Circuit Power Management

The test board is designed with the aim to test all the functionality of the BK1B111T. From an energy point of view, in a future implementation the BK1B111T will be powered by the main power bus of the satellite, the PDB. In the test board the PDB is provided through the connector J1. The voltage that has to be applied to simulate the PDB is 14V. This voltage is subsequently adjusted, by means of a set of voltage regulators. The system of voltage distribution has been designed using three regulators: the first regulator (LT1761 [16]) fetches the input voltage of 14V and provides the output 3.3V. This first voltage is used to power the MCU. Always the 14V input voltage is used by a second voltage regulator (LTC3631 [17]) that generates an output of 5V. This voltage is not directly used by a BK1B213A1 device, but it is necessary for the operation of the third regulator (LM4128AMF [18]). The latter in fact provides the voltage of 3V to the MUX and to the circuits of NTC. Since the LM4128AMF cannot be connected to an input voltage higher than 5,5V, the 5V regulator LTC3631 is useful and is used to provide the input voltage to the 3V regulator. Thus, the last two regulators are connected in a mixed way. The mixed solution also provides a much more stable control voltage, particularly suitable for circuits involving analog signals from sensors. The voltage regulator of the MCU has its enable pin, directly connected to its input. In this way the regulator is always active. The other two

regulators instead not supply any control circuit, but they are used exclusively for the BK1B111T. In this way the enable pins of the 5V and 3V regulators, are directly controlled by the MCU. When the BK1B111T has completed its task, these regulators can be turned off. The enable signal of these regulators is the same used for the activation of the drivers of the thermal fusers and the MUX.

All regulators are mounted with bulk capacitors on the inputs and on the outputs. Their values were chosen based on the recommended configurations in the datasheet of the component from the manufacturer. Only the 5V regulator requires an inductor of 100uH because it is a switching type. All these devices have been considered as reusable blocks already verified and tested. The results of their testing are described in [7].

8.3 Bk1B213A1 Power Consumption Estimation

Once the whole system is designed, the last step is the determination of its power consumption. It is very important since the BK1B111T is a satellite application. In the system, the microcontroller is not considered in the power estimation because as it was previously explained, the BK1B111T is designed to be integrated into other subsystems, with their own MCU. The power consumption of the BK1B111T is due mainly to three elements: the thermal fusers together their drivers, the linearization circuits of the NTC sensors and power regulators that feed the previous elements. The power dissipation of the MUX is negligible because has low leakage current of some μA . The power dissipation of a single thermal fuser is analysed in section 7.5 and the power consumption can be obtained from the simulation data of Figure 89. The power dissipation of each single linearization circuit of the NTC sensors and their power consumption is obtained from the Figure 93 (c). In order to compact the data, all power consumptions of each element are summarized in the Table 12.

Element	Power @ element	Number of elements used	Power @ group of elements
Thermal fuser + Driver	1,45 [w]	8	11,6 [w]
Linearization Circuit NTC	4 [w]	8	32 [w]
3V Regulator	0,35 [w]	1	0,35 [w]
5V Regulator	0,1 [w]	1	0,1 [w]
Total Power Consumption			44 [w]

Table 12: BK1B111T total power consumption.

The power of the linearization circuits depends strictly by the temperature, as it is possible to see in Figure 93 (c). Since the range of temperature needed is around 120-150C°, it is considered the power consumption of about 4w. From Table 12 is clear as the maximum contribution in the power consumption is given by the linearization circuits. It is about the triple of the power consumption of the fusers themselves. Nevertheless, it's should be noted as the BK1B111T works at low current, about 100mA for the fusers and its drivers, and much less for the linearization circuits. So, its limit of implementation can depend exclusively of how much energy the on board batteries of the CubeSat are able to provide. Furthermore, the BK1B111T is used only once in life cycle of the mission and it is active only for some seconds, exactly the time needed to reach the melting temperature of the tin used to solder the fixing wires. The Figure 85 gives an estimation of the time needed to reach this melting temperature. It's should be noted that the Figure 85 is a worst case. Probably in the space, the melting temperature will be reached much earlier, because the energy is more retained inside the bodies due to the slowness of the radiation mechanism. In order to give an estimation of the feasibility of the BK1B111T, it has to be defined the maximum energy available at the moment of the BK1B111T activation. A typical battery for a CubeSat, has a total energy when completely charged of:

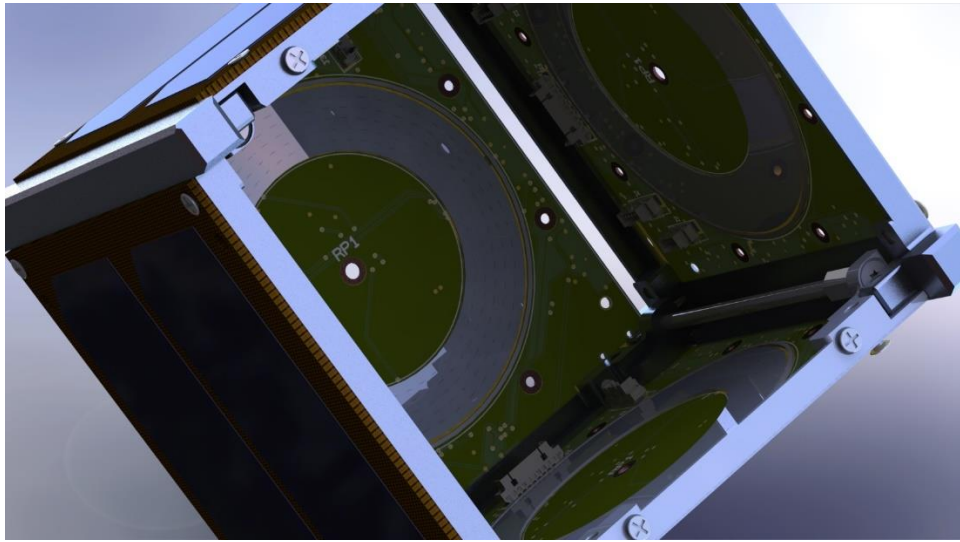
$$E_{batteries} = 3,7[V] \cdot 2[V] \cdot 3600[s] = 26640[J]$$

Considering 10 seconds of operation (Figure 85), the total energy needed by the BK1B111T system is:

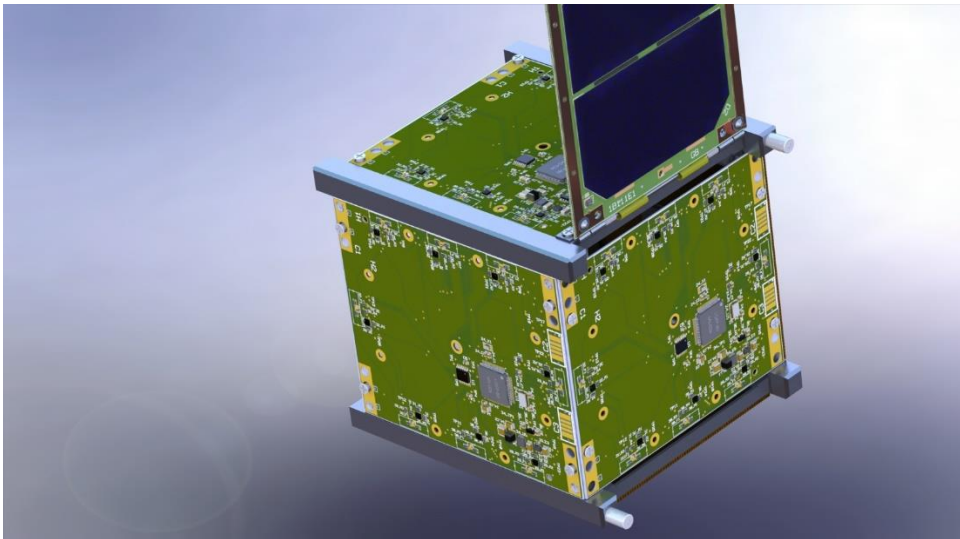
$$E_{EOS} = P_{EOS_{tot}} \cdot 10[s] = 440[J]$$

As it possible to see, the E_{EOS} is well below the $E_{batteries}$. With this result, it is possible to assert that with 26640 Joule of energy, they can be activated together four BK1B111T of four different 1B111E structures, remaining yet well below the maximum energy available from the batteries. In this way the BK1B111T system is suitable to be used also in a full configuration of four 1B111E structures for a 1U ARAMIS CubeSat (Figure 42 (a)).

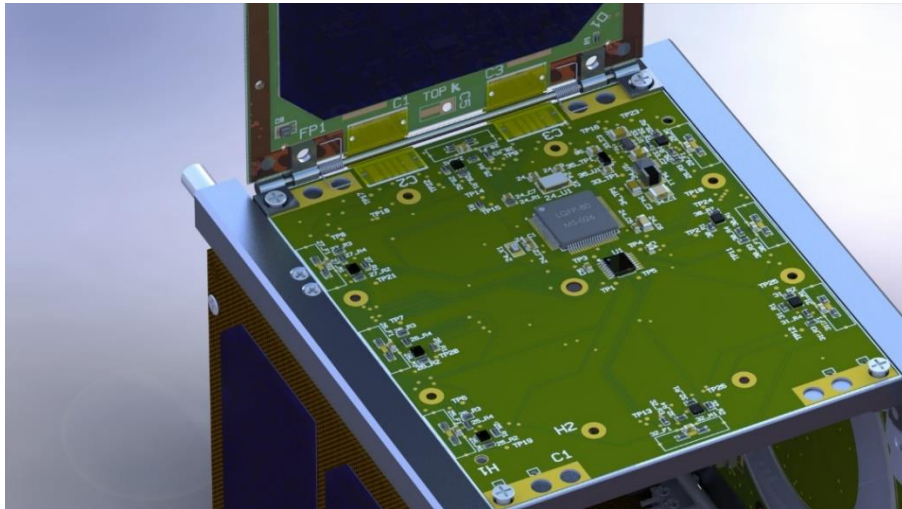
Finally two pictures that show the Outer Plate and a 1B111E structure both mounted on a 1U CubeSat are provided in Figure 97.



(a)



(b)



(c)

Figure 97: Final mounted system of an Outer Plate board and a 1B111E structure (a) Inner side (b) Back (c) Front.

8.4 Bk1B213A1 Management Software

The MCU used for the BK1B213A1 management has to be appropriately programmed to realize the correct control of all elements of the BK1B111T. For the BK1B213A1 software has been followed the approach to make the code highly versatility, because it has to be easily handled in order to be implemented and integrated into another future software system of another satellite application. The Firmware is wrote in C++ and it uses all class libraries and functions ones written for the ARAMIS project. In the in following paragraphs, the UML is used to better understand the software development.

8.4.1 Software Operation

The main task of the software is the thermal fusers management for the opening phase of the 1B111E structure. In the test board, the opening algorithm is implemented to perform a complete phase of opening. The Figure 98 shows the use case diagram of the test board. Through this diagram, are described the main operations of the management algorithm.



Figure 98: Use Case Diagram of the Outer Plate.

The main actors of the test board outer plate are a “Configurator” and a “Ground Mission Controller”. The first represents the user involved into the configuration of the outer plate. Two use cases are possible: the setting of the maximum temperature that the fusers can achieve, and the setting of the number of fusers that can be used. The setting of the max temperature, makes the BK1B111T compatible with a large amount of other applications that require lower temperatures. Also the number of Fusers can be set in order to make the BK1B111T more versatile. The second actor is the ground mission controller. This is the main element involved into the control of the entire satellite. It send commands to the OBC that interprets the instruction, interacting with the satellite subsystems. The BK1B111T is triggered by the OBC, thanks to an appropriate command sent from the ground. The firmware of the BK1B213A1 is designed taking into account a command incoming from a ground mission controller. This latter has different use cases. A "Blow Fusers" is used to start the operation of all the thermal fusers of the Outer Plate, which are enabled and attached²⁴. The temperature of all the fusers enabled, is increased to a set threshold value, and then kept constant. After a certain time from the beginning, all the thermal fusers are turned off automatically. "Get temperatures" gives the possibility to obtain the actual temperature of the fusers. “Self-test” is a useful function, because before a launch, a self-test of heating for the fusers improves the reliability of the BK1B111T. The use of "Fuser Status" is needed, because the status of the fusers has to be continuously monitored, to maintain the temperature constant and to verify the correct operation of the BK1B111T. All the use cases, "Enable" and "Disable", and the "Attach" and "Detach" are also needed to instantiate the BK1B111T. These work together a "Configuration Module". This latter acts on a configuration register, where each bit represents an enable configuration bit for a fuser. In the same register there is also an attach configuration bit. Only the Disable case and the Detach case, need the Reset Module Configuration. This is used to reset all configuration bits of the configuration register. "Blow Fusers" and "Self-Test" use Slave commands to be activated. Instead "Get Temperatures" need the Get Module Housekeeping to store the values of temperature of the thermal fusers.

Now, I focus on the main operation of the BK1B111T. The base algorithm of the opening phase is explained using a simple flow chart shown in Figure 99.

²⁴ An element is considered "attached" if it is physically present on the tile and it has not been detached. If a thermal fuser is attached and enabled, any further action of it will be carried on. The difference between "attach" and "enable" is that the former has always effect, while the latter has effects only if the subsystem is attached, therefore the former enables the latter. This Use Case is intended only in rare occasions, to recover from an erroneous Detach Fuser operation.

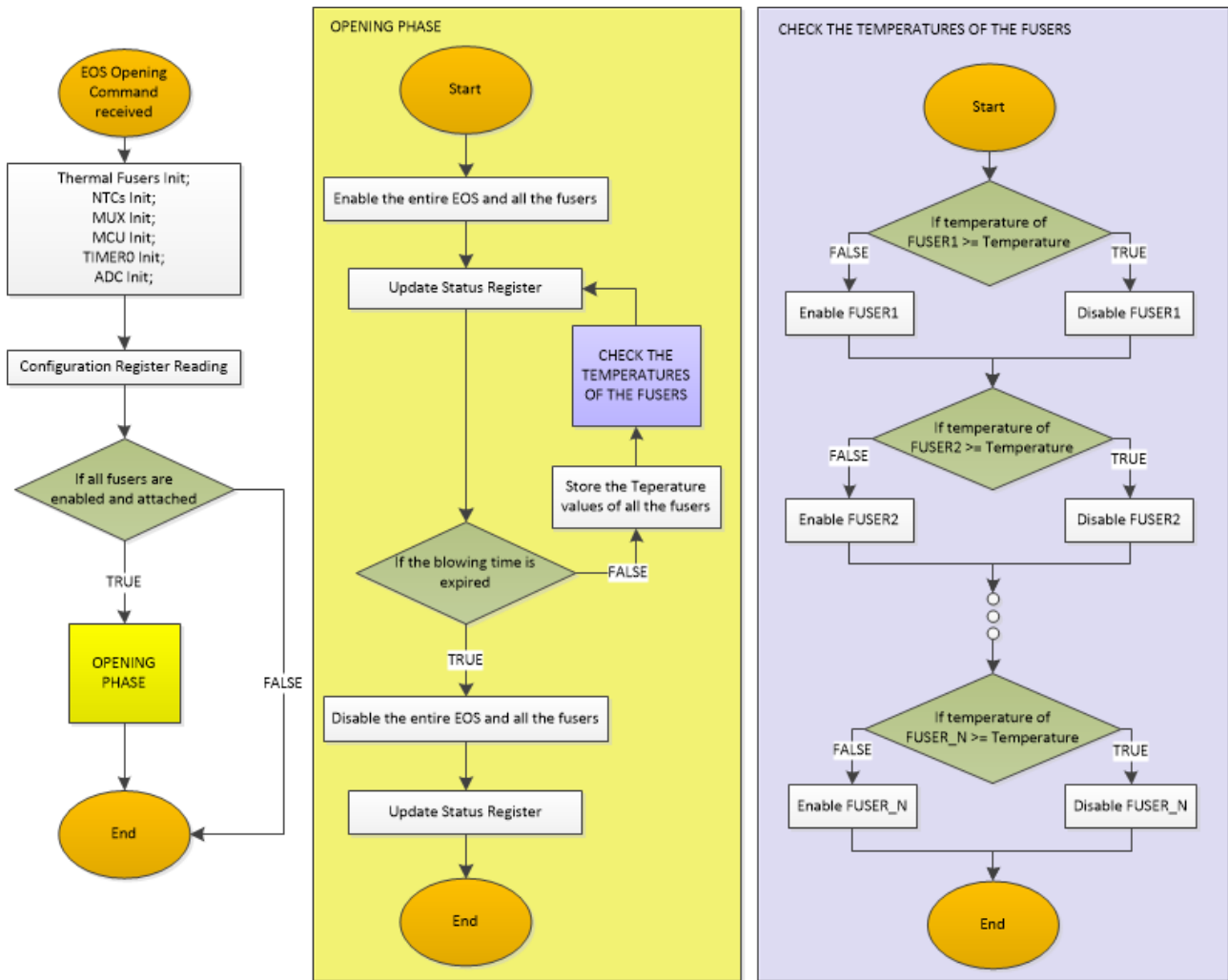


Figure 99: Opening Phase Algorithm.

The software triggers when the OBC sent the command of opening to the MCU of the BK1B213A1. The first state is the initialization of the all devices. Since the software is objects oriented, all devices represent object classes that have to be instantiated and initialised. The initialization involves also the setting of the pins of the MCU as outputs or inputs. The configuration register contains all the setting configurations for the enabling of the fusers. These information are used to physically rise or drop, the logic values of the enable pins of the BK1B213A1 (Figure 94). If all "enable" bits and the "attach" bit are true, the BK1B111T can be activated and the "OPENING PHASE" starts. Otherwise the software ends. In these conditions the fusers begin to heat up. Once the "opening phase" starts, the BK1B111T and the fusers are enabled and the software enters in a first loop. The software, cycles for a certain time. An MCU timer is used for counting the time. When a maximum time is reached, the "opening phase" ends, and the BK1B111T and all the fusers are turned off and disabled. During this time, all temperature from the NTCs sensors are stored into an appropriate vector and are also checked to avoid the exceeding of a maximum temperature threshold. In other words, what happens is that all the fusers are kept to a constant temperature. In the phase of checking, each fuser is disabled if its temperature exceed a maximum threshold, and it is enabled again if its temperature decrease below the same threshold. In this way all fusers can be maintained to a constant temperature, allowing the desoldering of the sealing wires. The time of heating can be set arbitrary as it is possible to see in section 8.4.2. But for the BK1B111T analysed in the thesis, the maximum time of heating can be obtained from the simulation graph of Figure 85 from the section 2.2.6.

8.4.2 Main classes

The section 8.4.1 has been used to introduce the main software system and the base algorithm of the opening phase. In this section all main software classes are described. The related C++ code is attached to the section 9.8. The management software is written following the use case diagram of Figure 98. Since the software is written in C++, all devices are instantiated using software classes. For the software designing, a large amount of other classes that already existed, are used. These are the main classes designed for the OBC taken from the ARAMIS project. For this reason in this section are dealt only the specific classes designed for the BK1B111T. All the support classes from the ARAMIS project are described in a marginal way.

A first classes that are implemented are the software classes of the thermal fusers and the NTC sensors (Figure 100).

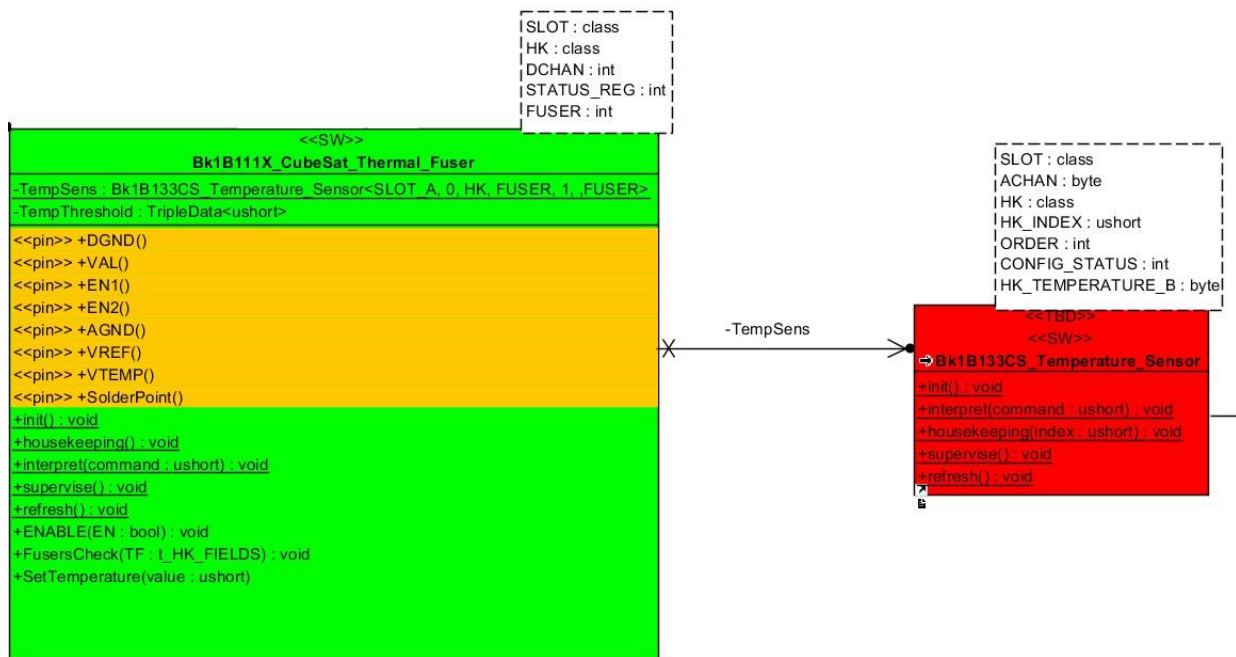


Figure 100: Thermal Fusers and NTC sensors classes.

Since each thermal fuser contains a NTC sensor, the better choice to organize the software was to instantiate the sensor class directly inside the thermal fuser class. In this way each time a fuser class is instantiated, at the same time, the related sensor class is also instantiated. Each device class is divided into attribute and methods. In the methods are always present a function of initialization (init()), a function of housekeeping (housekeeping()), an interpreter function (interpret()), a supervisor function (supervise()) and refresh function (refresh()). The init function is employed for the initialization of the device class. The housekeeping performs the main function of the class. The interpreter function has the task to decode the instruction commands. The supervise function performs monitoring tasks. Instead the refresh function is used to refresh all the variables instantiated, and in particular the variable types most interesting that are those instantiated as "TripleData". This format is part of a class appropriately designed to improve the robustness of the code to space radiations. When the environment in the space becomes harsher, and the radiations increase, all data stored in the memory elements are easily exposed to problems of switching from a logic state to another. To avoid this, a statistic technique is used to protect the data and thus reduce the possibility of failures. If a variable is instantiated as TripleData, three copies of the data of that variable are performed in memory. The statistical probability that a data changes in two of the three memory locations, for effect of radiation, is low. In this way, each time the refresh function is launched, it is performed a triple check on the three copies of the data. If one location of data is changed, the refresh function restores to all

the three memory locations the value of the other two locations not changed. The most critical data are all protected by a TripleData type. For Example, the temperature maximum threshold (TempThreshold) is a TripleData because if the temperature changes in a higher value, the fusers can reach a very high temperature thus damaging the system. All classes present also a set of template parameters, used for the instantiation of the classes. The init function of the thermal fuser class performs the enabling of the right MCU pin as output, used for the enable signal of the fuser. The housekeeping methods launch the houskeeping of the sensor class, which store the value of temperature in the "HK::housekeeping[]" vector. Furthermore, it runs the FuserCheck() method that performs the comparison of the temperature with the TempThreshold. The result of the FuserCheck() can be a fuser enabling or disabling, depending on the result of the comparison. SetTemperature() is used to give the value to the TempThreshold variable. The temperature value is passed by template parameter. ENABLE() is a function used to physically rise or drop the logic level of the MCU pin of enable of the corresponding fuser²⁵. The sensor method init() performs the initialization of the pin of the AO channel of the ADC used. The housekeeping of the same class instead performs an algorithm of conversion from the value obtained by the ADC, to the right value of temperature. The algorithm is based to the possibility of use different linearization circuits for the NTC sensors, characterized by different orders of linearization. In my case, the linearization circuit is of the 1th order, thus none equation of linearization is applied to the ADC value.

The other class used is for the MUX. The class is shown in Figure 101.



Figure 101: MUX class.

The init() function of the class is used to set the output type for the MCU pin used for the selection controls of the MUX. The housekeeping and the SELECT functions, are used together for the correct switching from a channel of the MUX to another. An incrementing index provided by the TIMER used for the counting in the MCU, is used to select the time instants where the switching between the channels of the MUX have to occur. For now, the index of the TIMER is incremented each 1ms. So the software, switches from a channel of the MUX to another each 1ms. Instead for the temperature readings of the fusers, each polling of eight sensors is performed each 1 second. Also in this case, the MUX class is designed with the maximum of versatility and portability, using the template parameters to pass the channel of the SLOTS that are following assigned to the control pins of the MUX. No other devices of the BK1B111T need to be instantiated with a separate class. Thus only two classes remain to be defined: the class of the "main()", and the Outer Plate main class. The former is shown on Figure 102, the second is shown in Figure 103.

²⁵ Generally, all methods that involves MCU pins, are treated completely in parametric way. To increase the versatility and portability of the code, the channels of the SLOTS that I want to use are passed by template parameters. The channels will be after assigned to the pins by means a "switch" instance.



Figure 102: Class of the "main()" of the software.

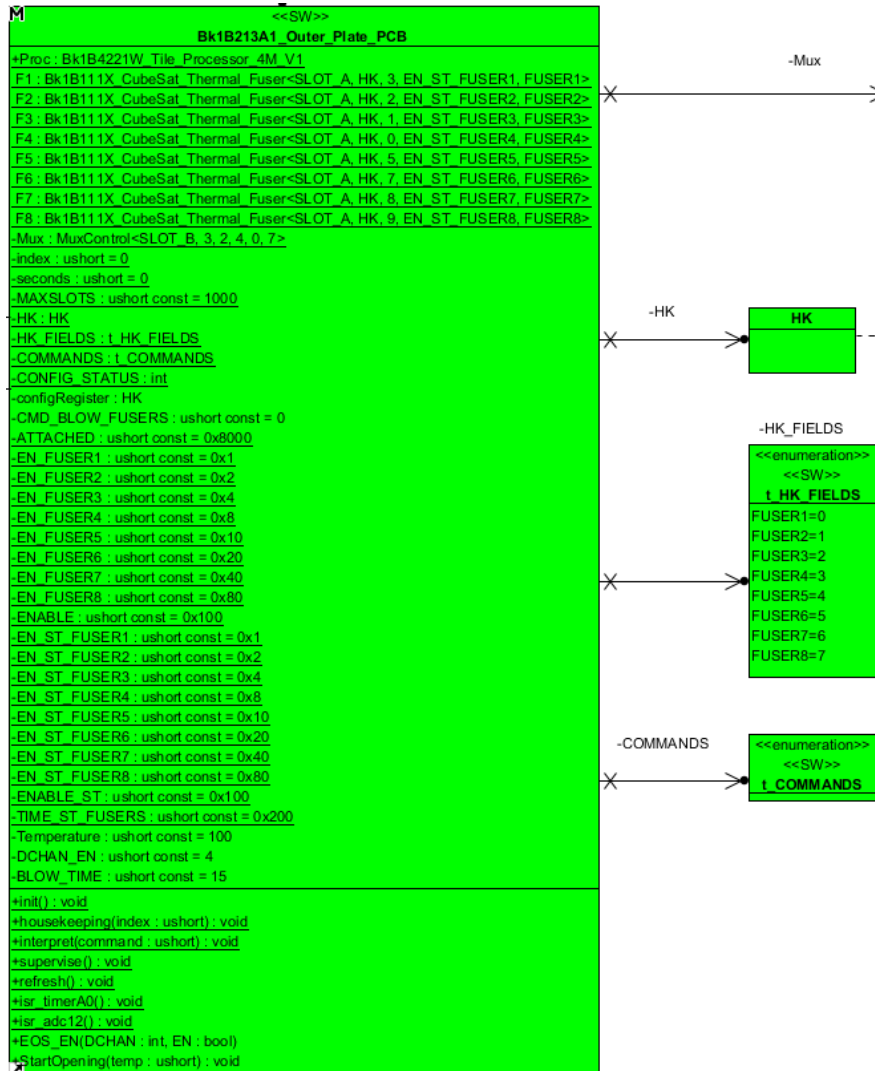


Figure 103: Outer Plate main class.

A software, must to have always a "main()". Generally, the main() is instantiated in a specific class. This class is used to instantiate the main class of the software, in my case the Outer Plate main class. In the main() are launched the initialization of all devices and the main cpu.proc initialization class for the MCU. This latter is necessary, to initialize all the peripherals of the MCU and all the main configuration registers, as that used for example for the clock frequency setting of the MCU.

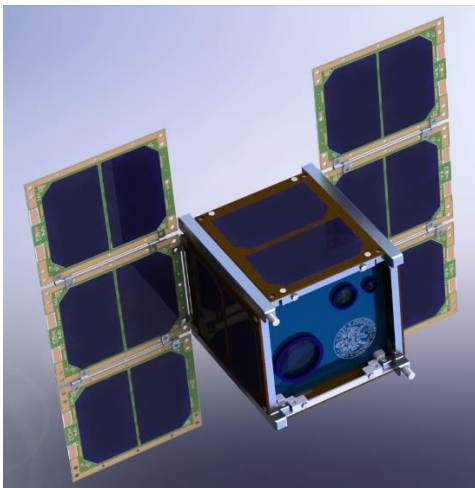
In the main class Outer Plate, all the eight instances of the fusers, the MUX class and the main variables are instantiated as attributes. A set of bits are declared for the correct pointing of the enable bits in the configuration register (EN_FUSER1 to EN_FUSER8), and in the status register (EN_ST_FUSER1 to EN_ST_FUSER8). Other bits are used for the global enable (ENABLE and ENABLE_ST), and a status bit to flag the end of the TIMER counting (TIME_ST_FUSERS). The configuration register, the status register and the housekeeping vector used, are all contained into an appropriate class called Housekeeping. This class is necessary because is used for the storing of global housekeeping, status and configuration data for AraMiS-

compatible AraModules. For this reason the Housekeeping class is also instantiated into the attributes of the main class, by means of an intermediate class called HK. In the Outer Plate class are further contained the function for the timer interrupt management (`isr_timerA0()`), the function for the ADC interrupt management (`isr_adc12`), and a function for the global enable activation (`EOS_EN()`). Its housekeeping function is employed to collect the temperature data from the fusers instances. Finally it contains a `StartOpening()` function that is employed to manage the opening phase of the BK1B111T. All codes are attached to the section 9.8.

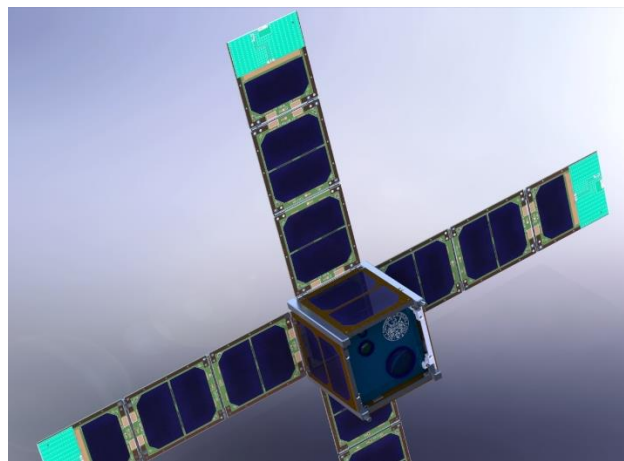
9 Chapter

9.1 Conclusion

The mechanical deployable structure discussed in the thesis is an innovative design expression. It has followed the guidelines of ARAMIS technology. In the thesis work, the 1B111E structure was developed with the lowest possible impact on the weight of the components, their dimensions and their cost. It was analysed in particular a structure consisting of three tiles, whose dimensions do not exceed 5mm in thickness when they are folded on themselves. In this way the system is fully compatible with the standard of a P-POD typical. The COTS electronic components have been selected so as to allow the operation of system within the safety limits. The mechanical components are miniaturized and extremely versatile. The proposed structure is based on a longitudinal deployment (Figure 42 (a)), but the hinges may be easily repositioned to obtain other types of deployment such the transverse ones. An example of this structure is shown in Figure 104 (a). In this way, you can reduce the effects of vibrations induced by structures extended in length, and there are not more problems of collisions in the opening phase. In the analysed structure, each individual tiles accommodate solar cells with high efficiency. Each tiles provides about 2w power, then a three tiles structure provides about 6w power. If a 1U CubeSat is configured in full way and so it mounts 4 possible 1B111E structure (Figure 42 (a)), the maximum power is therefore about 24w. This is an enormous power, if placed in relation to the overall dimensions and weight of the structure. The tile system is also completely symmetric, from the mechanical and electrical point of view. The layouts of the PCBs that realize the tiles, are characterized by interfaces of standard connections. That allows the attachment of other types of devices on different individual tiles. In Figure 104 (b) it is shown a possible implementation of antennas with micro strip technology. The systems of antennas in fact may be used and fixed in place of the solar cells, allowing the realization of complex antenna systems such as systems for SAR. Furthermore, being the tiles modular, they may also be composed in hybrid mode with tiles that hold different devices.



(a)



(b)

Figure 104: (a) Example of transversal deployment (b) Example of implantation of micro strip antennas.

The whole of three tiles structure was then completely analysed from the point of view of the opening and of the mechanical vibrations at launch. The complete deployment occurs in less than 5 seconds and the results obtained have shown that the proposed system has no problems opening and it is robust to the profile of launch vibrations of the Figure 53. Accurate thermal analysis and thermal simulations were done on individual tile highlighting how in LEO orbits, the temperature of the structure remains in the operating margins of the components. A further analysis of the spin gave results about the effect that the pressure of radiation has on a 1U CubeSat that mounts the discussed structure. These data will be useful in the process

of prediction for the management of the manoeuvres for the attitude corrections. Finally, all the considerations made for a 1U structure can easily be extended to structures 2U, 3U or even larger systems such as 2x2x2U and above. Finally, all the considerations made for a 1U structure can easily be extended to structures 2U, 3U or even larger systems such as 2x2x2U and above. It is only enough realize the tiles in different size and both the mechanical components and the opening system remain fully compatible with these structures. The fig... shows some examples of how the 1B111E structures developed will be employed in the multy-CubeSats configurations.

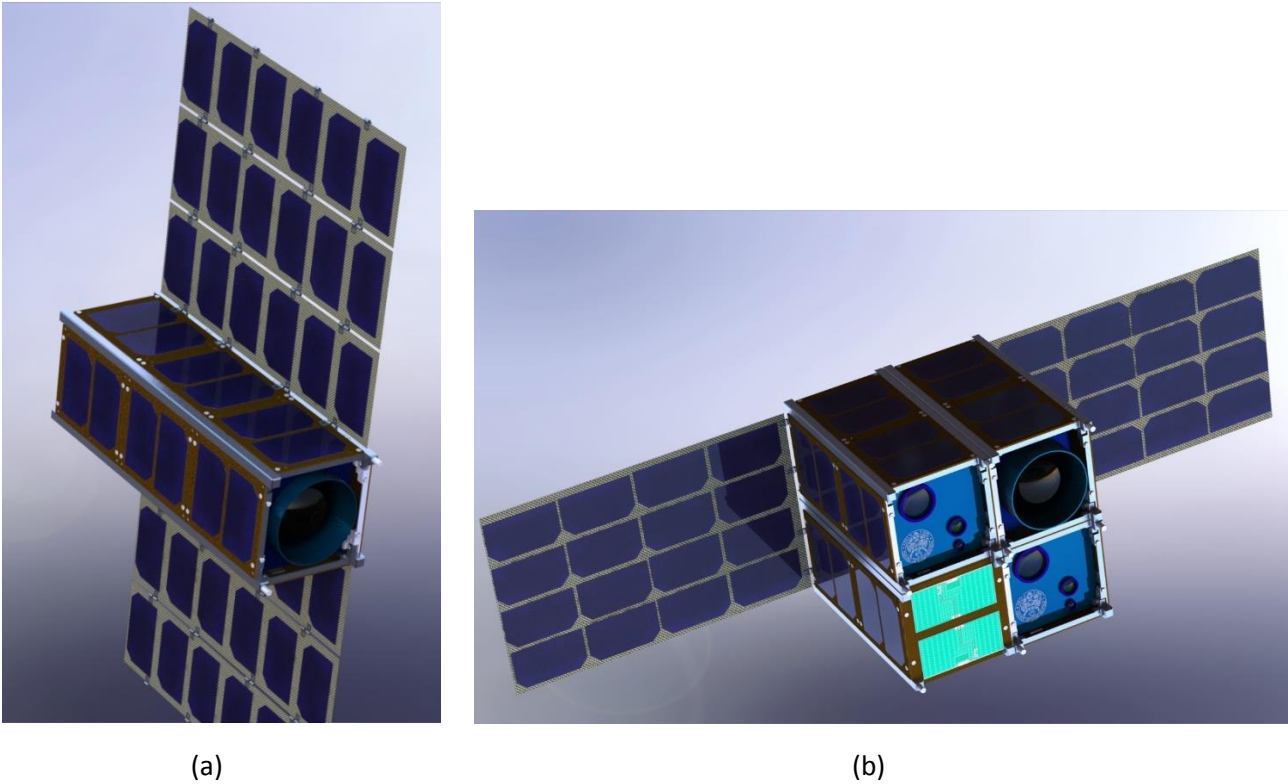


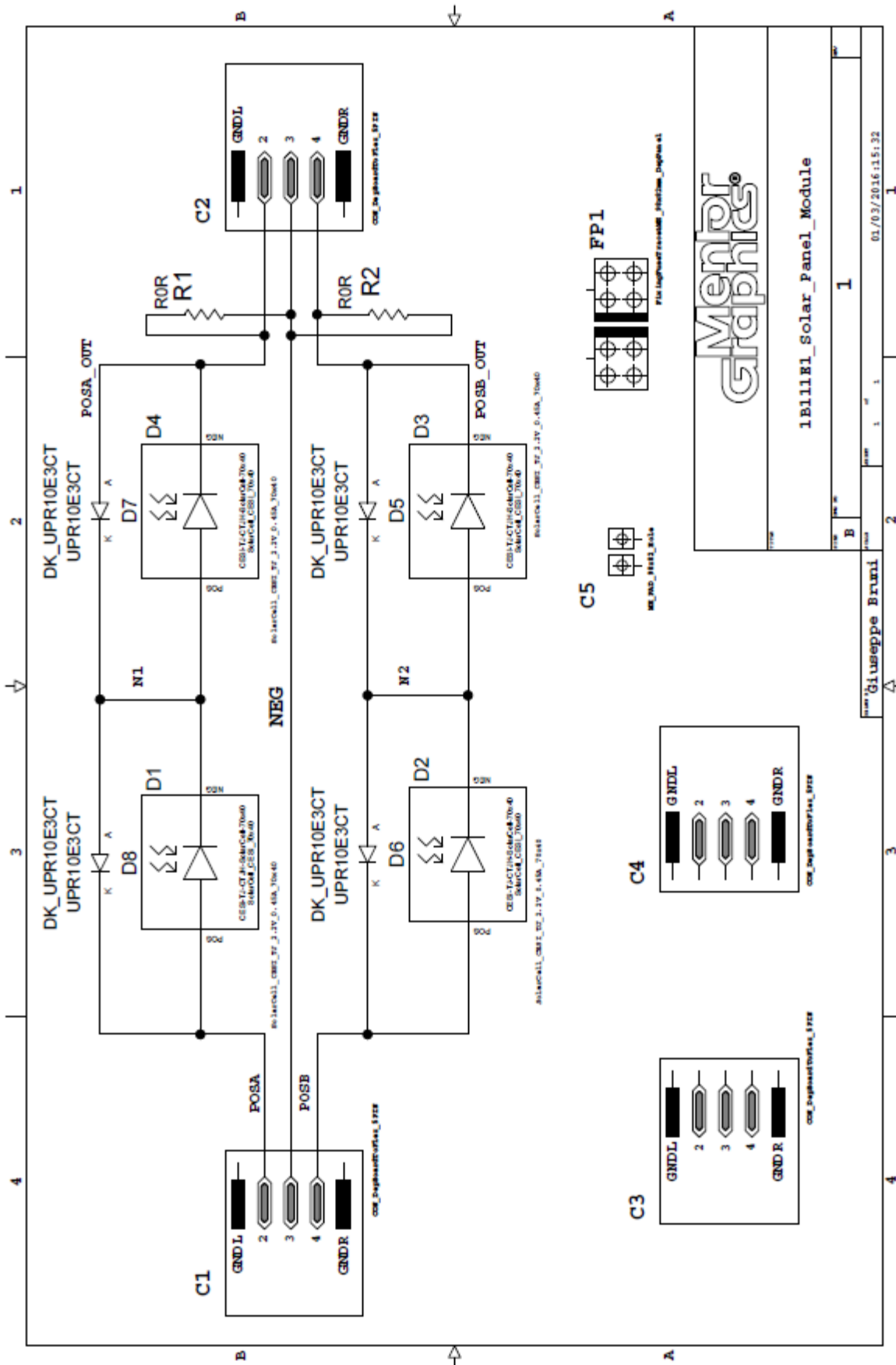
Figure 105: (a) 3U CubeSat Configuration (b) 2x2x2U CubeSat Configuration.

The technological innovations are not limited only to the dense and compact mechanical structure. The system uses a new release technology, it based on the detachment of sealing wires, through the use of thermal fusers in low energy consumption. With a strength greater of 500N for single structure, the sealing wires can be detached using less than 450 Joules of energy and with a current lower of 800mA. A thermal model is defined for the thermal fusers and a simulation is performed to predict with more accuracy their operation in the space environment. The detachment system is electronically controlled and can be easy used for the deployment of a large amount of other satellite devices. Their possible use is in the deployment of antennas. The electronic control drivers of the thermal fusers are accurately simulated with SPICE using the real simulation models of the components.

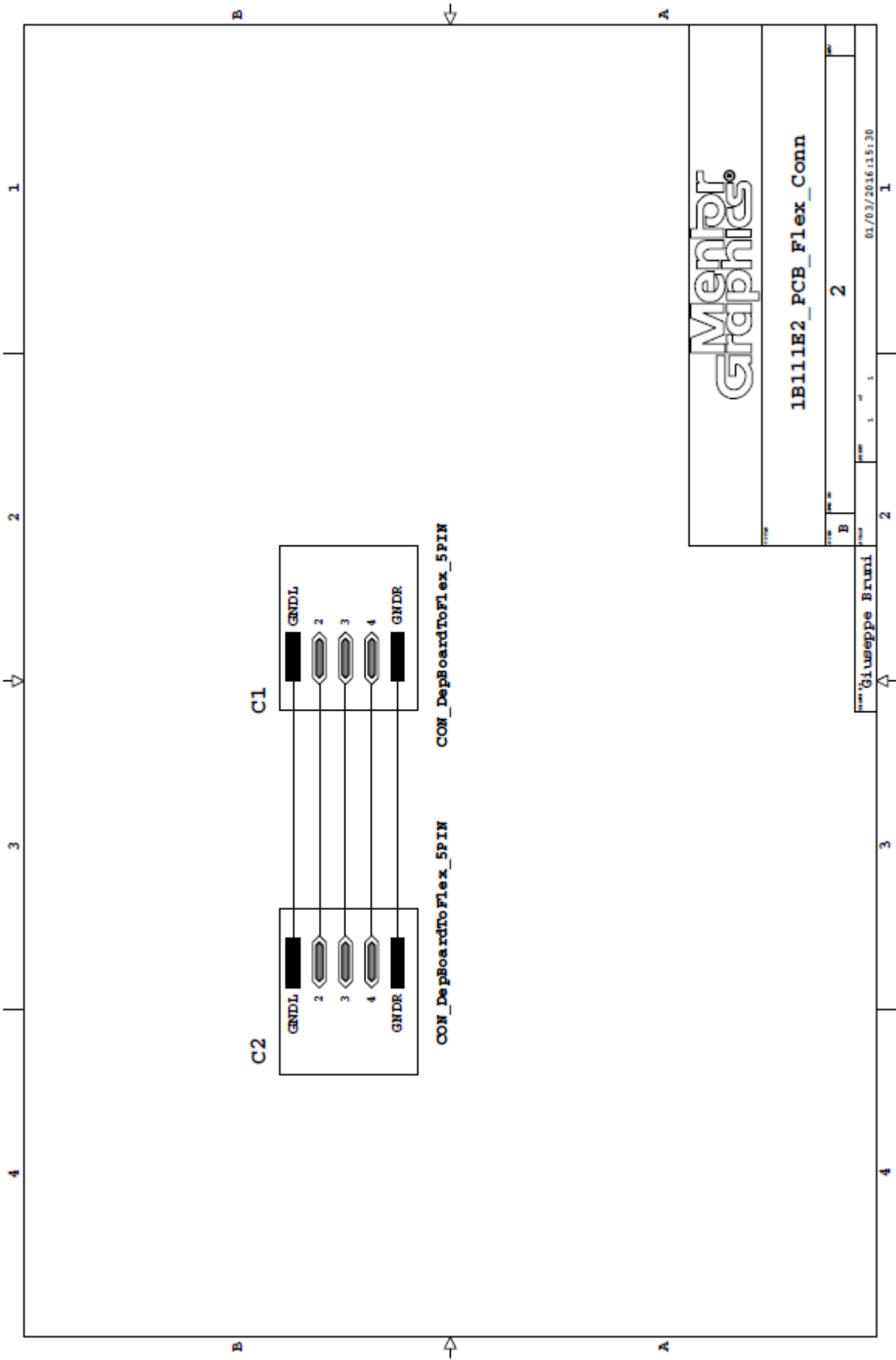
Part of the BK1B111T system and in particular its BK1B213A1, must be realized on a base tile, on which the 1B111E structure is mounted. This base tile is generally a side tile of an ARAMIS CubeSat. In the thesis, the BK1B213A1 for the BK1B111T is designed on a specific tile that will be part of another system. An outer plate of a reaction wheel is thus used to fix the thermal fusers and the microcontroller based system that manages them. In such a way, the circuit of the BK1B213A1 proposed in thesis is designed with the maximum of the versatility, just because it has to be integrated to another system. The outer plate represents a test board, used for the only purpose to test the BK1B111T system, no other embedded applications are implemented on it. As well as its circuit the firmware of the BK1B213A1 is designed with the maximum of versatility, to allow that it can be easily transported to another system with minimal impact on the software interfaces.

9.2 Circuit Diagrams

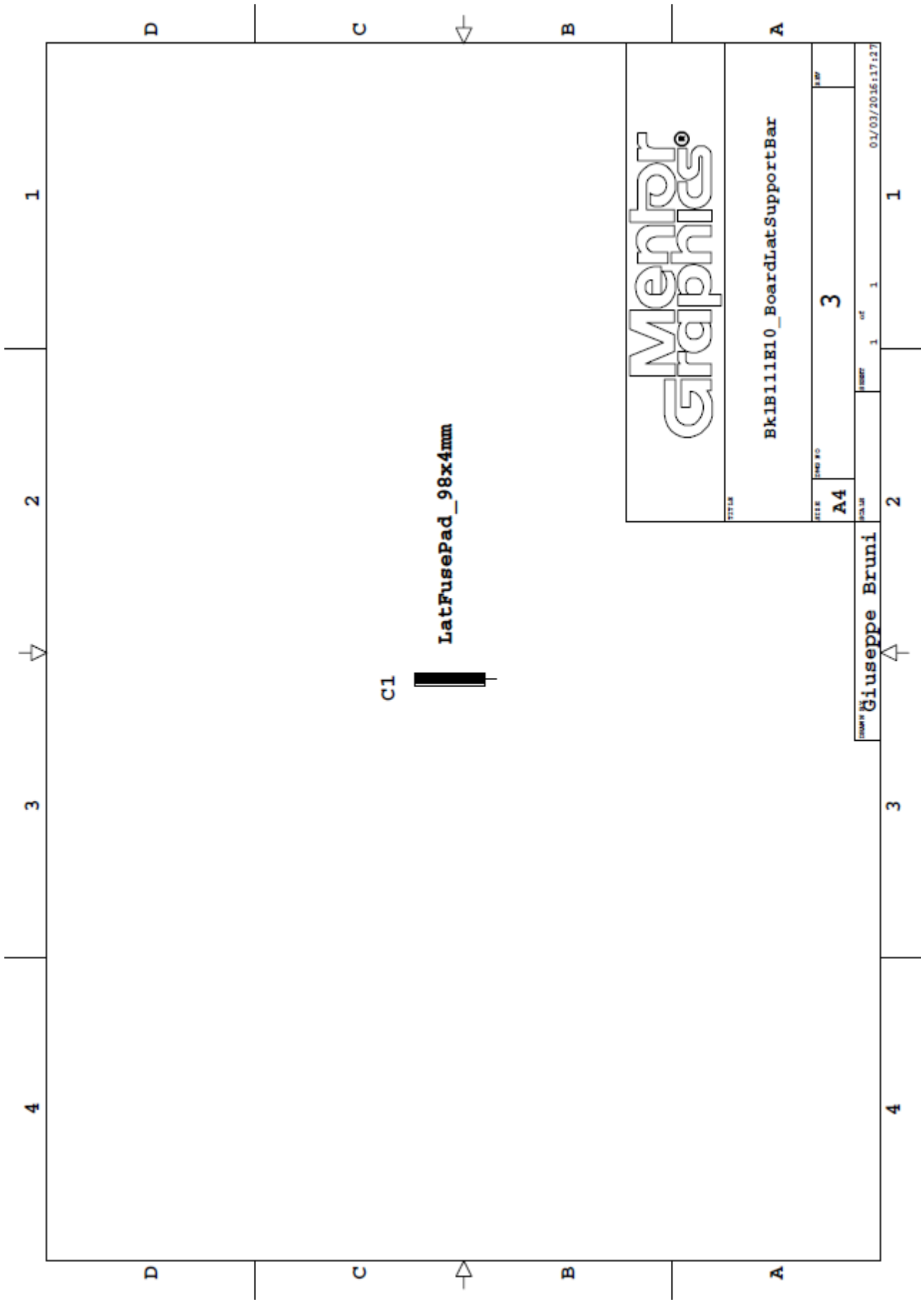
9.2.1 1B111E1 Standard Tile PCB



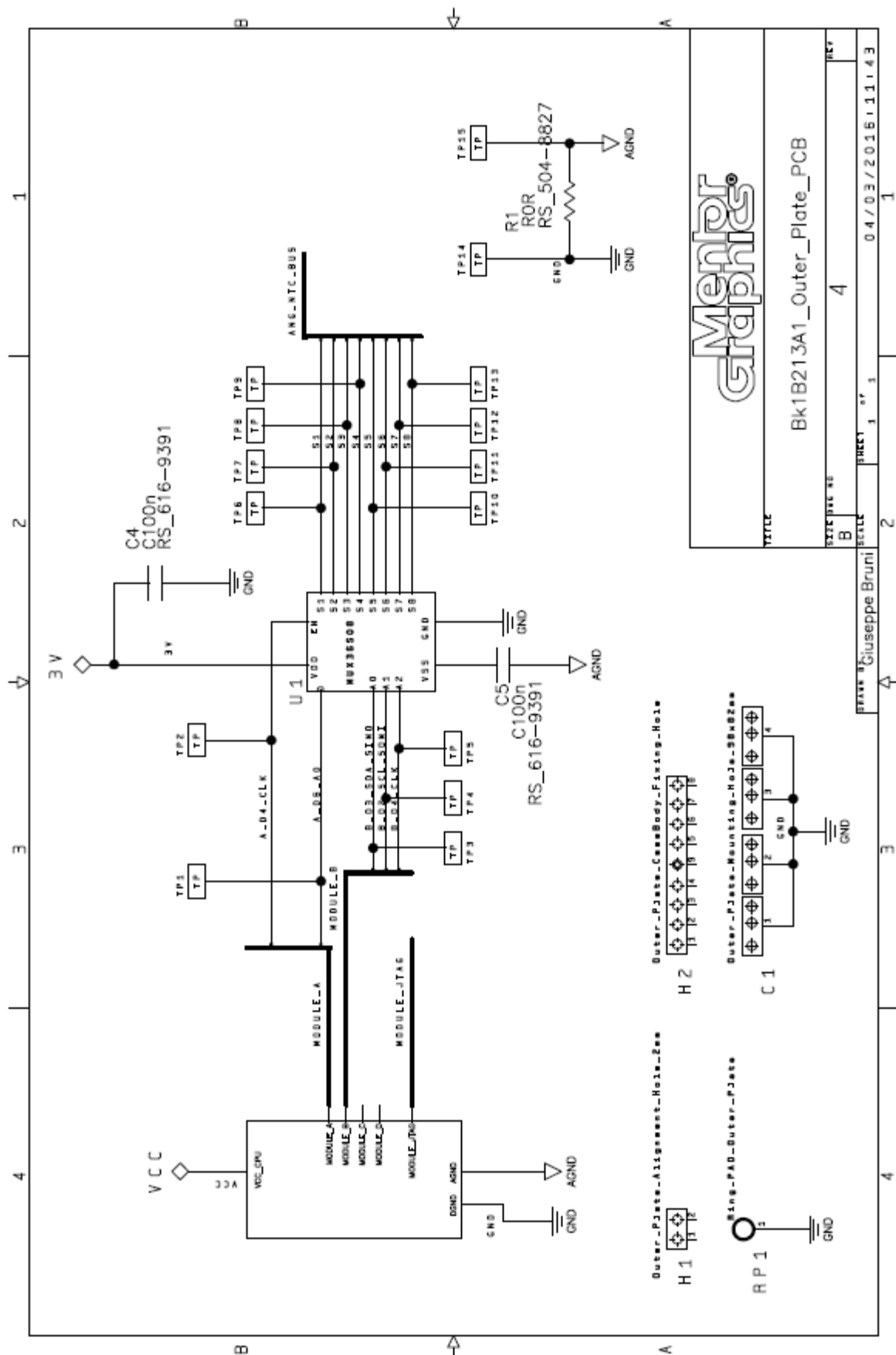
9.2.2 1B111E2 Flex PCB



9.2.3 1B11110 Lateral Support PCB

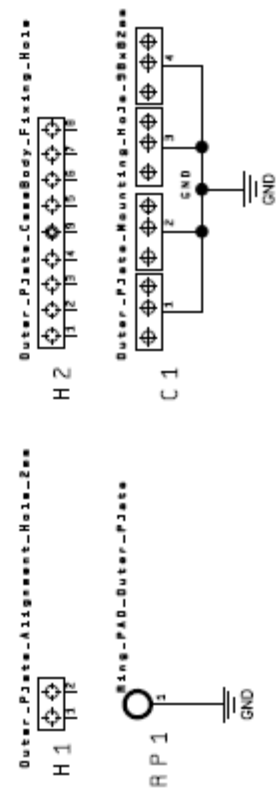


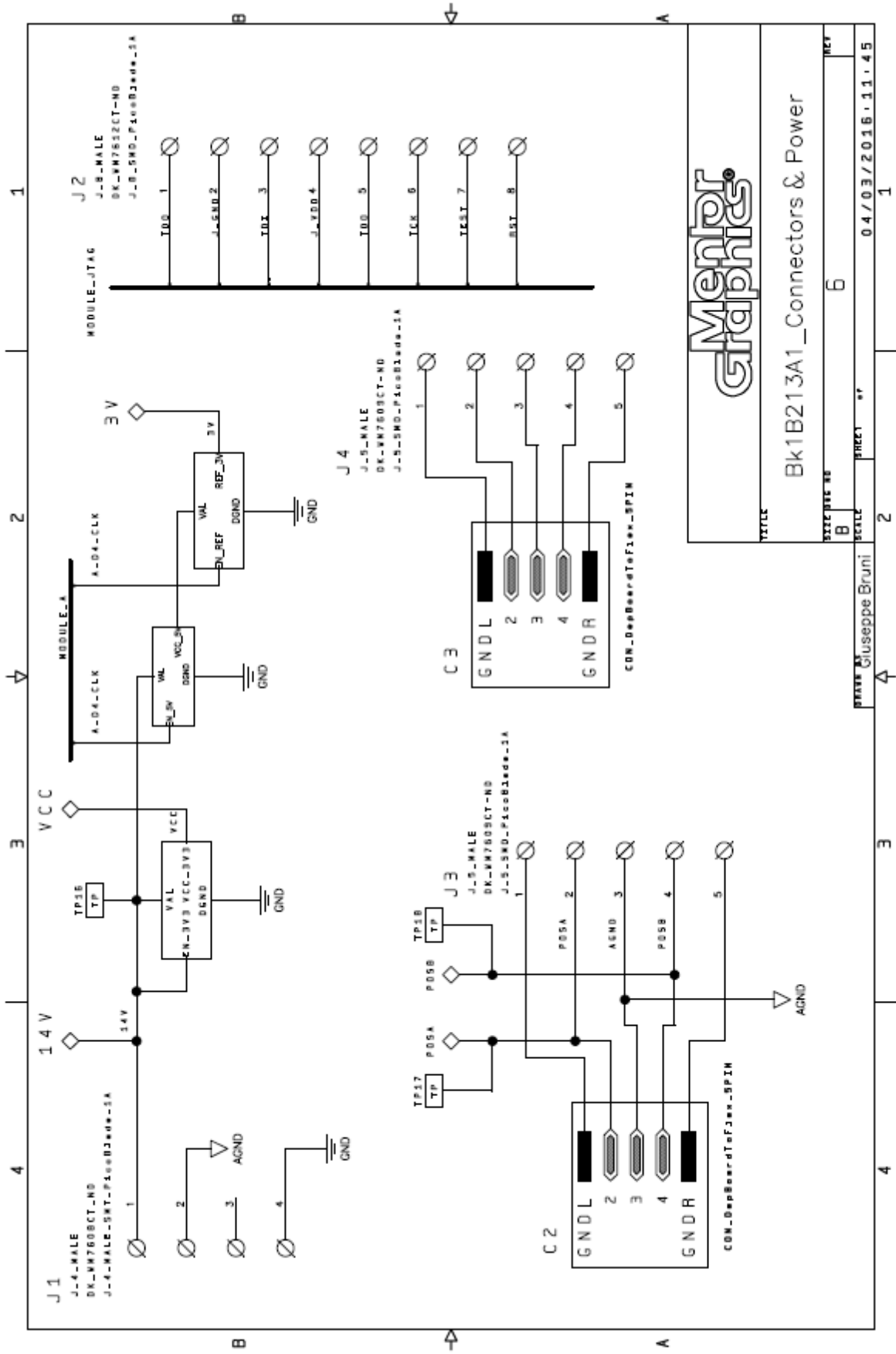
9.2.4 Bk1B213A1 Outer Plate Test Board



Bk1B213A1_Outer_Plate_PCB

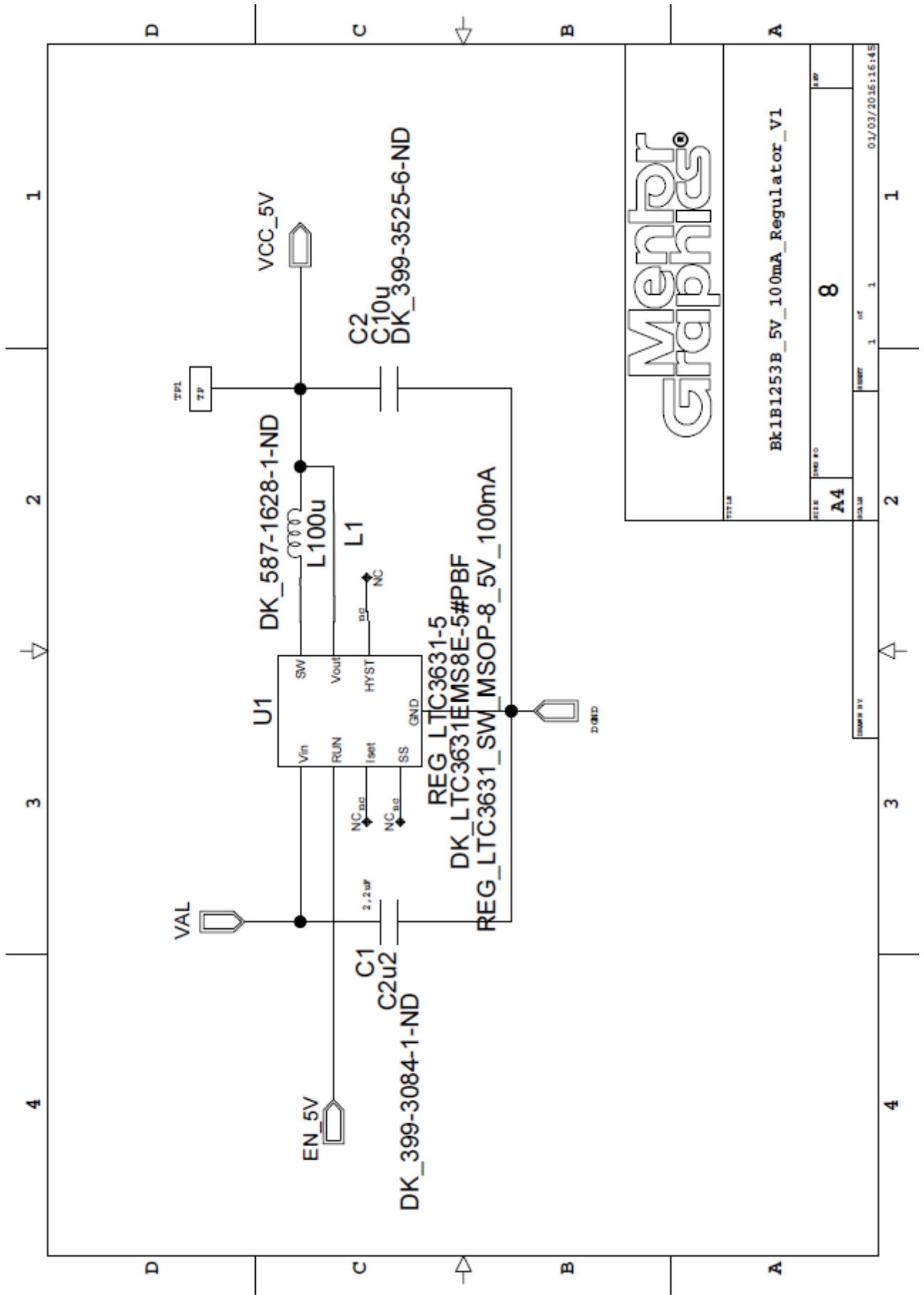
REV	1	1
DATE	04/03/2016	11:43
DESIGNER	Giuseppe Bruni	
SCALE	1:1	
SHEET	4	





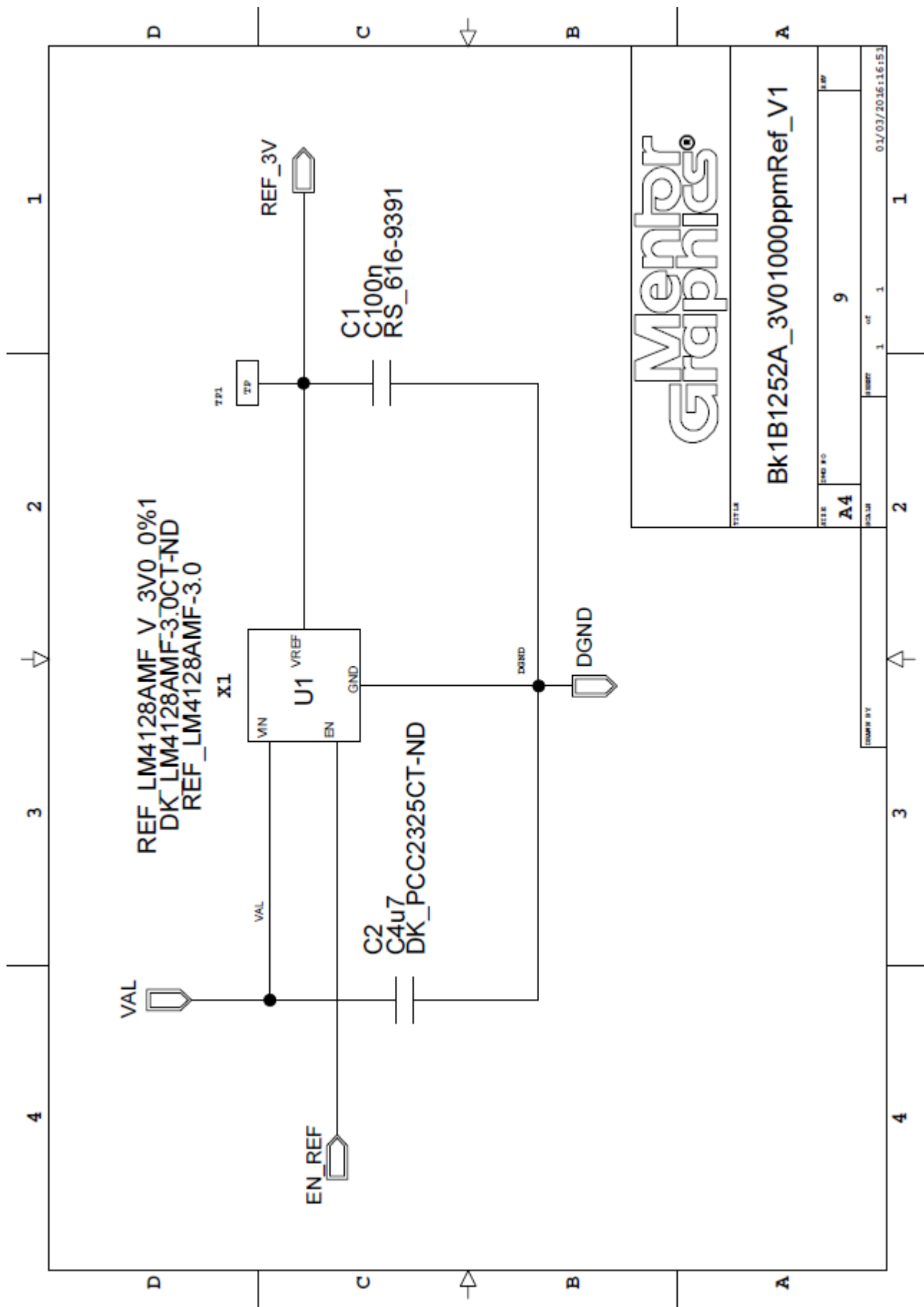
Bk1B213A1_Connectors & Power

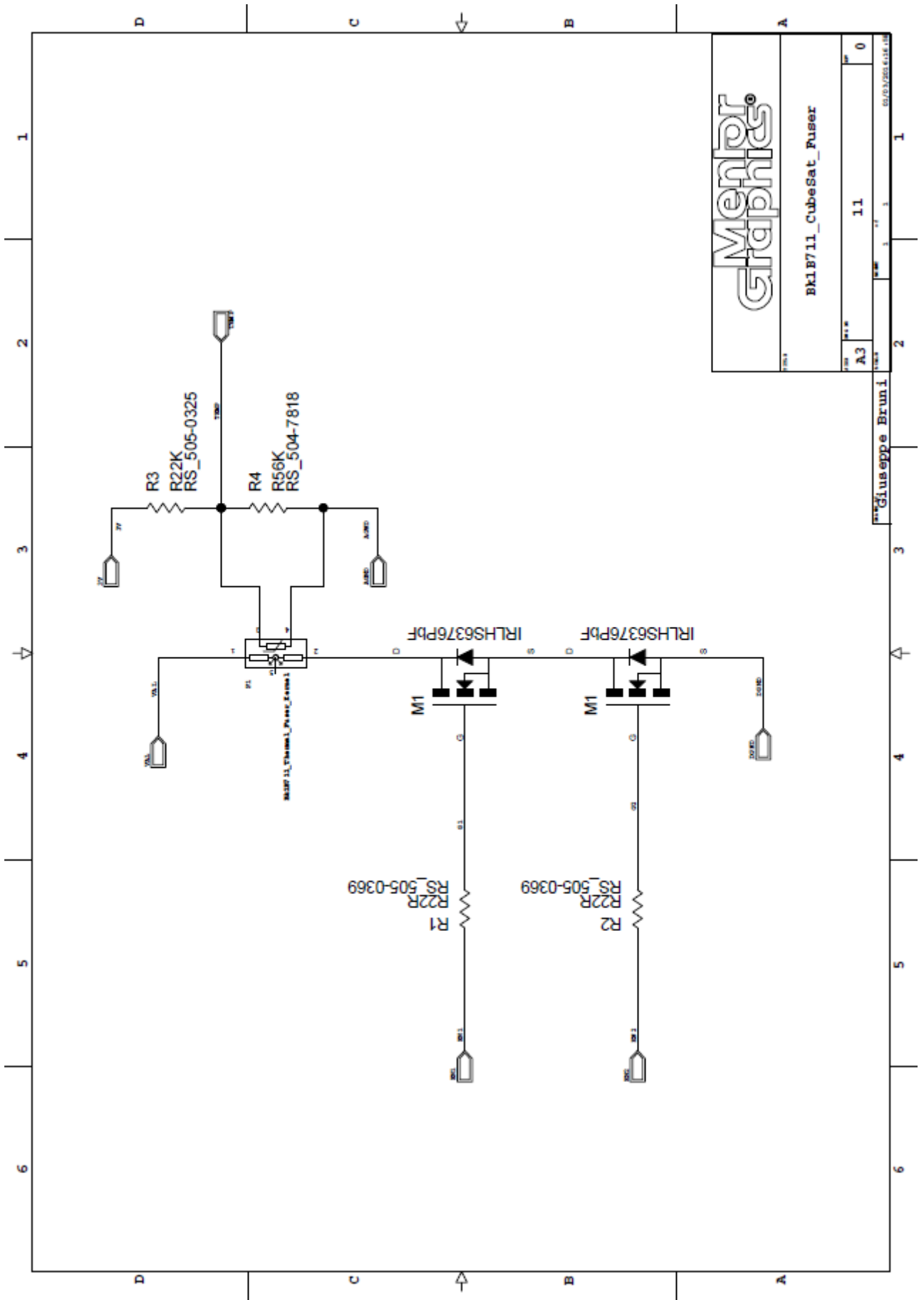
DATE	04/03/2016.11.45
DESIGNER	Giuseppe Bruni
PROJECT	97
REV	6



Bk1B1253B_5V_100mA_Regulator_V1

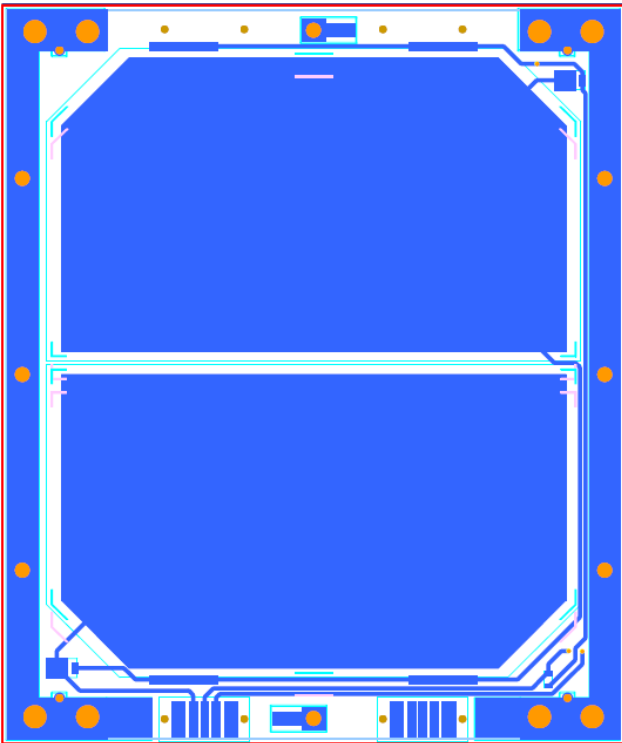
FILE	END NO	8	REV
A4			
SCALE		1	of 1
DRAWN BY			
DATE		01/03/2016	16:14:45



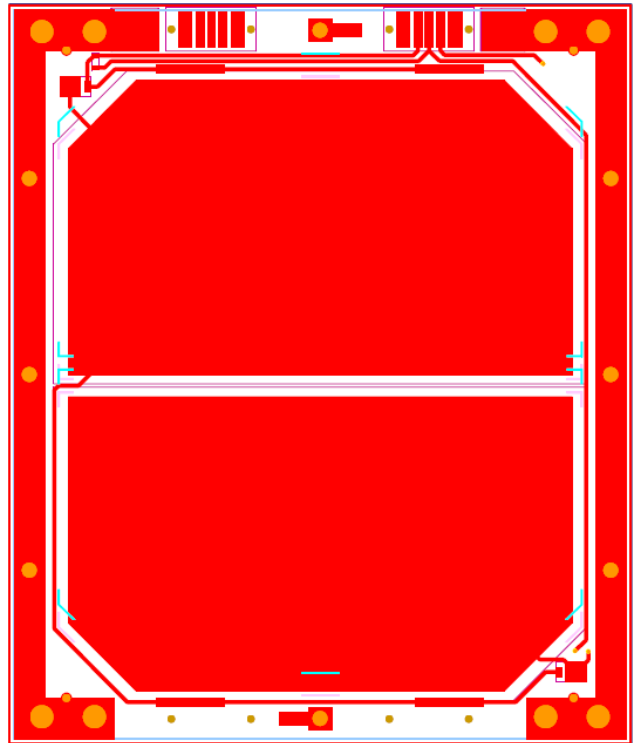


9.3 PCB Layouts

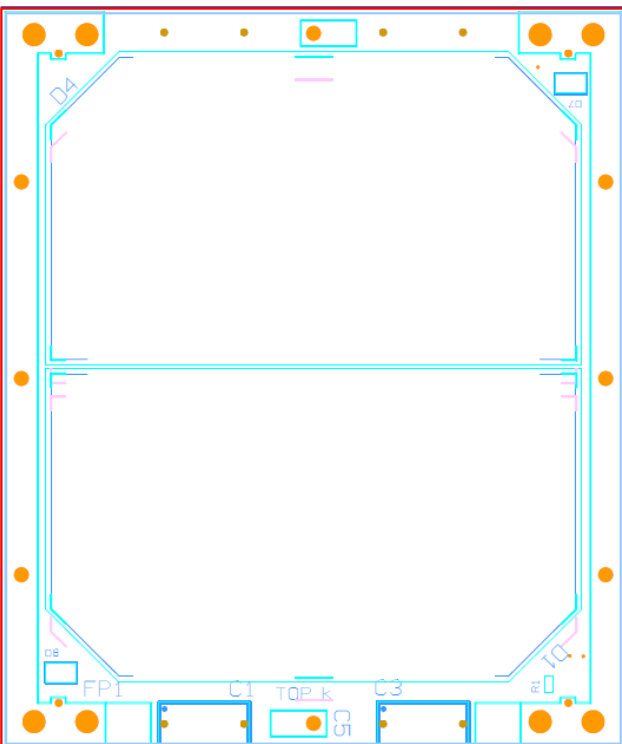
9.3.1 1B111E1 Standard Tile PCB



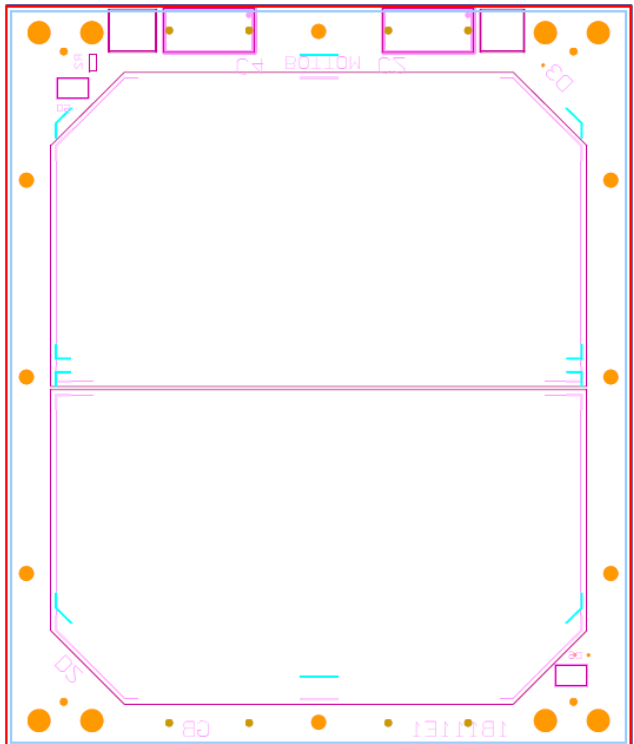
TOP LAYOUT



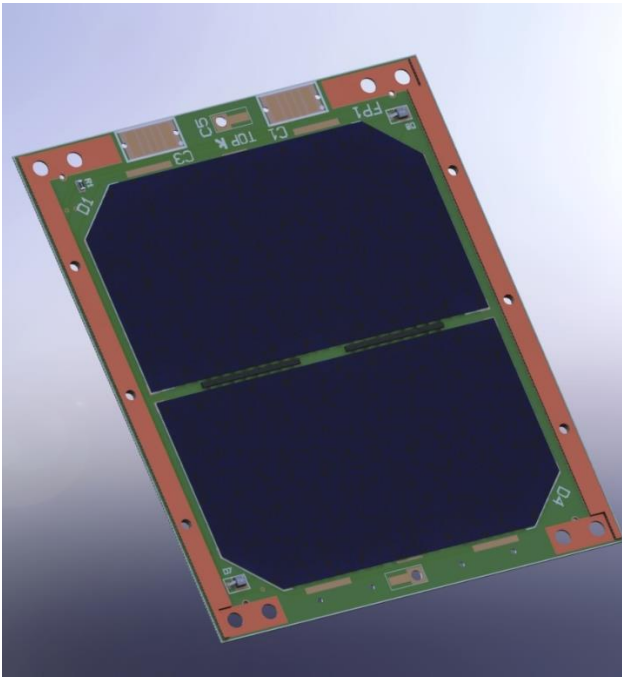
BOTTOM LAYOUT



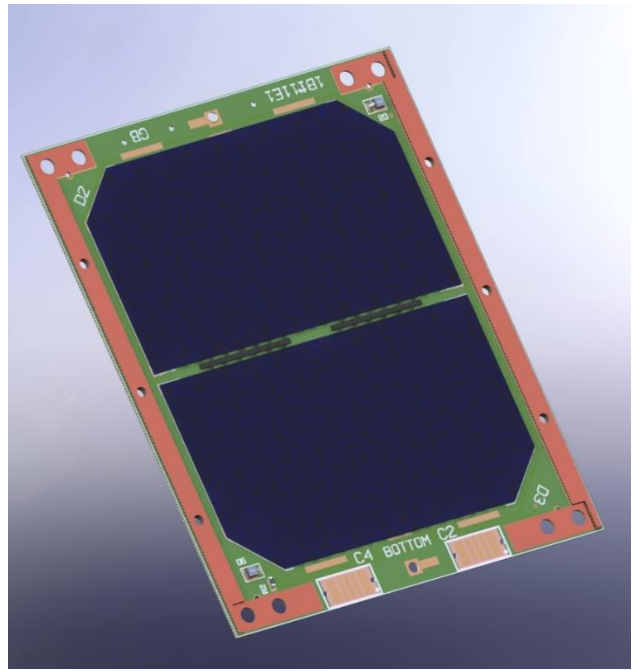
TOP COMPONENTS



BOTTOM COMPONENTS

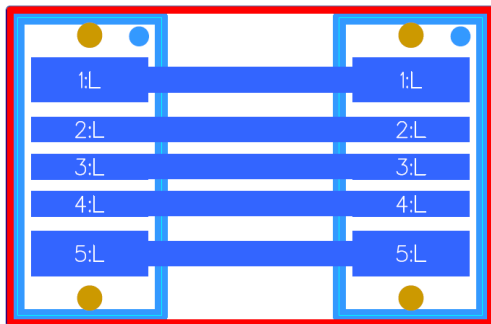


TOP 3D VIEW

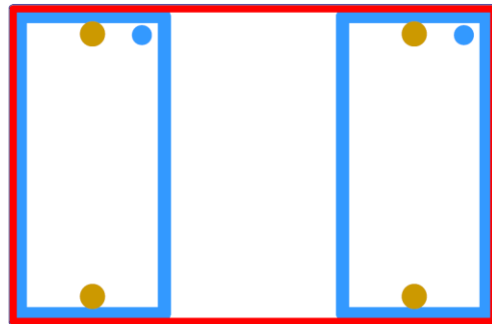


BOTTOM 3D VIEW

9.3.2 1B111E2 Flex PCB



TOP LAYOUT



BOTTOM LAYOUT

9.3.3 1B11110 Lateral Support PCB



TOP LAYOUT

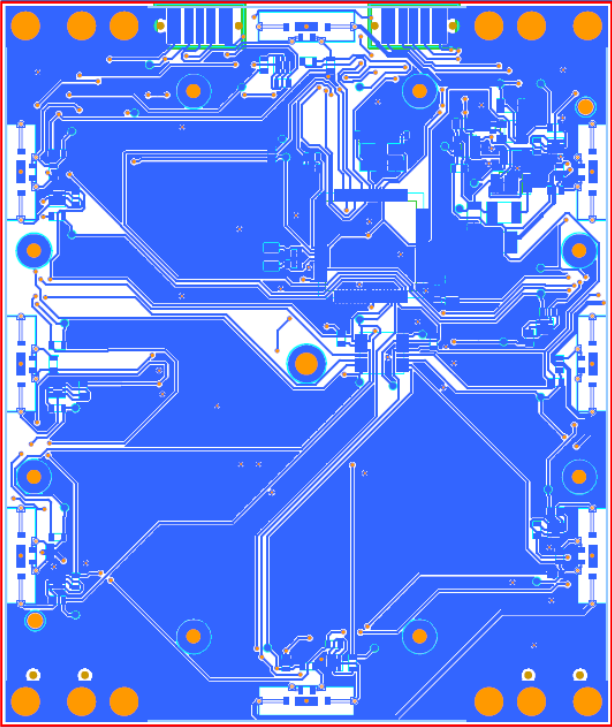


BOTTOM LAYOUT

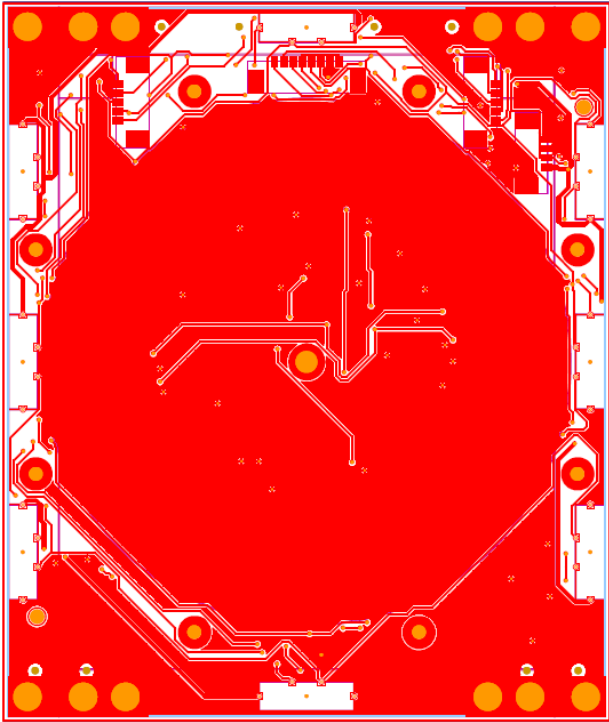


3D VIEW

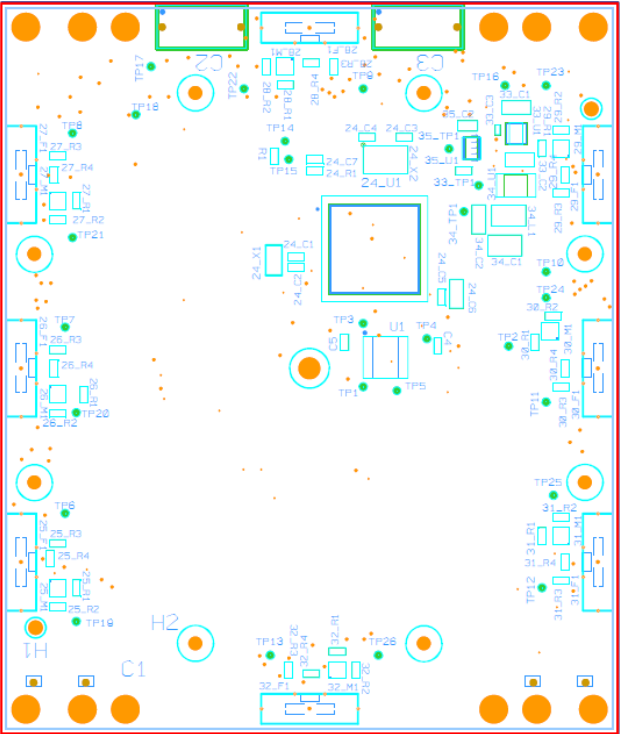
9.3.4 Bk1B213A1 Outer Plate Test Board



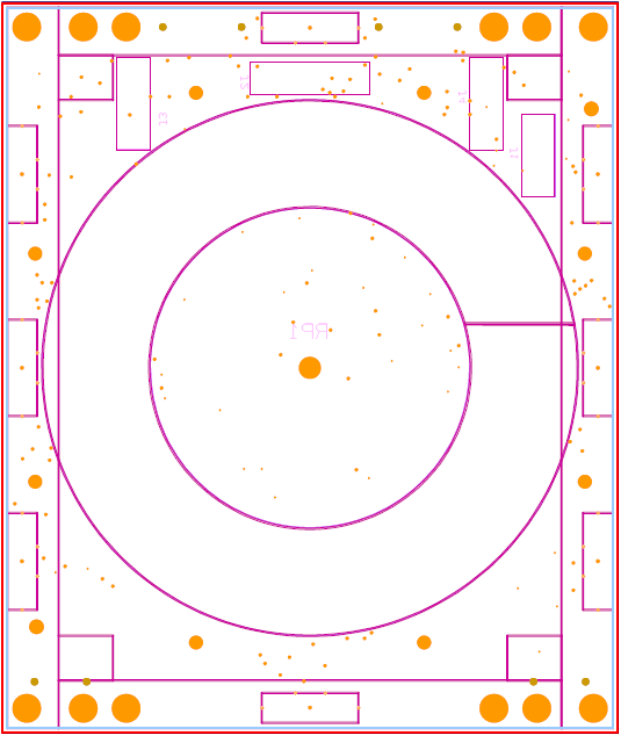
TOP LAYOUT



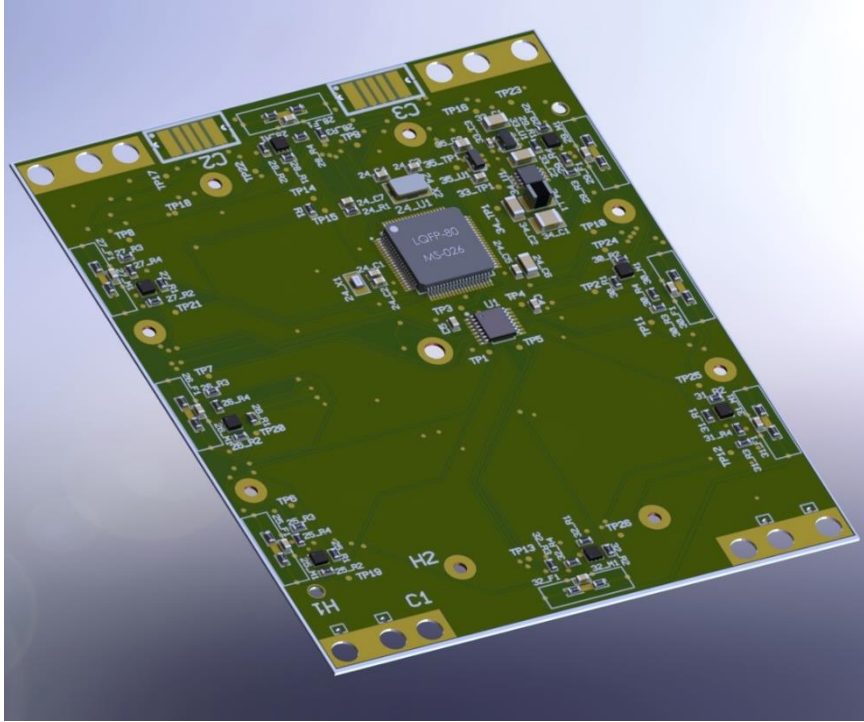
BOTTOM LAYOUT



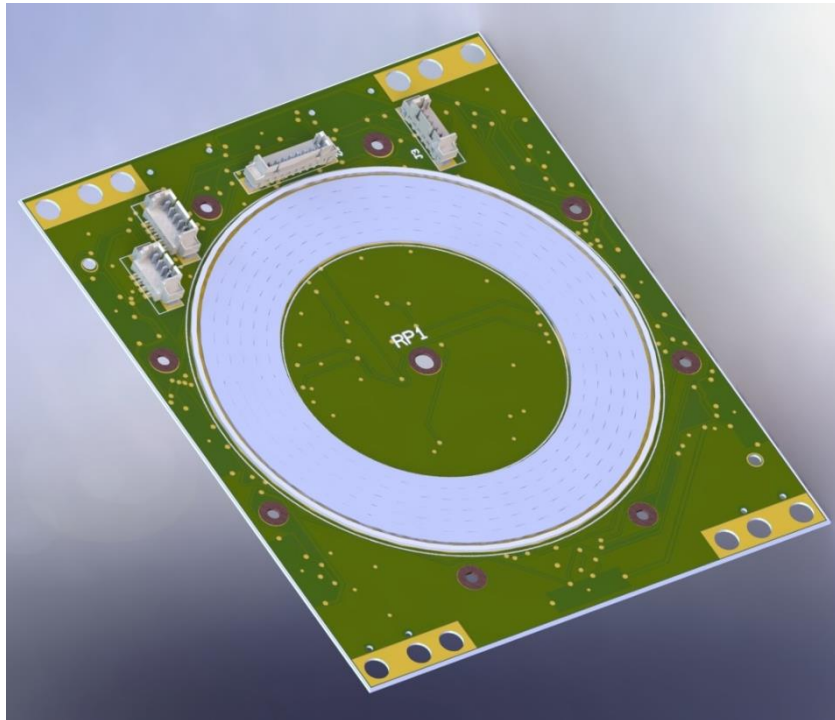
TOP COMPONENTS



BOTTOM COMPONENTS



TOP 3D VIEW



BOTTOM 3D VIEW

9.4 Mechanical Sheets

9.5 Simulation Models of the electric components for hSPICE

This section contains the scripts of electronic components models used into Mentor Simulation tool.

CESI-TJ-CTJH-SolarCell-70x40

```
.subckt solarcell 1 4
iph1 4 3 dc 0.48
d1 3 5 dln4002mod
d2 5 6 dln4002mod
d3 6 4 dln4002mod
rp 3 4 800
rs 3 1 0.1
.model dln4002mod d (is=14.11e-9 n=1.984 rs=33.89e-3 ikf=94.81 xti=3
+ eg=1.110 cjo=51.17e-12 m=.2762 vj=.3905 fc=.5 isr=100.0e-12
+ nr=2 bv=100.1 ibv=10 tt=4.761e-6)
.ends
```

BAT54

```
.model BAT54 D(Is=.1u Rs=2.2 N=1 Cjo=12p M=.3 Eg=.69 Xti=2 Iave=300m
Vpk=30)
```

IRLHS6376PbF

```
.SUBCKT irlhs6376pbf 1 2 3
* SPICE3 MODEL WITH THERMAL RC NETWORK
*****
* Model Generated by MODPEX *
* Copyright(c) Symmetry Design Systems*
* All Rights Reserved *
* UNPUBLISHED LICENSED SOFTWARE *
* Contains Proprietary Information *
* Which is The Property of *
* SYMMETRY OR ITS LICENSORS *
* Commercial Use or Resale Restricted *
* by Symmetry License Agreement *
*****
* Model generated on Nov 21, 11
* MODEL FORMAT: SPICE3
* Symmetry POWER MOS Model (Version 1.0)
* External Node Designations
* Node 1 -> Drain
* Node 2 -> Gate
* Node 3 -> Source
M1 9 7 8 8 MM L=100u W=100u
.MODEL MM NMOS LEVEL=1 IS=1e-32
+VTO=1.31248 LAMBDA=0.0497001 KP=29.3563
+CGSO=2.59003e-06 CGDO=1.45749e-07
RS 8 3 0.0338159
D1 3 1 MD
.MODEL MD D IS=1e-17 RS=0.0437879 N=0.617647 BV=30
+IBV=0.00025 EG=1.2 XTI=1 TT=1e-07
+CJO=4.69616e-11 VJ=4.99996 M=0.841611 FC=0.5
RDS 3 1 5e+07
RD 9 1 0.0001
RG 2 7 16.8802
D2 4 5 MD1
* Default values used in MD1:
* RS=0 EG=1.11 XTI=3.0 TT=0
```

```

* BV=infinite IBV=1mA
.MODEL MD1 D IS=1e-32 N=50
+CJO=1.75007e-10 VJ=0.539795 M=0.845354 FC=1e-08
D3 0 5 MD2
* Default values used in MD2:
* EG=1.11 XTI=3.0 TT=0 CJO=0
* BV=infinite IBV=1mA
.MODEL MD2 D IS=1e-10 N=0.458926 RS=3e-06
RL 5 10 1
FI2 7 9 VFI2 -1
VFI2 4 0 0
EV16 10 0 9 7 1
CAP 11 10 2.33591e-10
FI1 7 9 VFI1 -1
VFI1 11 6 0
RCAP 6 10 1
D4 0 6 MD3
* Default values used in MD3:
* EG=1.11 XTI=3.0 TT=0 CJO=0
* RS=0 BV=infinite IBV=1mA
.MODEL MD3 D IS=1e-10 N=0.458926
.ENDS irlhs6376pbf

*SPICE Thermal Model Subcircuit
.SUBCKT irlhs6376pbft 3 X

R_RTHERM1      3 2  7.406833675
R_RTHERM2      2 1  9.689893537
R_RTHERM3      1 X  1.887219931
C_CTHERM1      3 2  0.000335895
C_CTHERM2      2 1  0.001687426
C_CTHERM3      1 X  6.07579e-05

.ENDS irlhs6376pbft

```

9.6 MatLab Scripts

This section contains MatLab scripts of Thesis analysis and calculations.

Estimation of a trace minimum width with respect to final temperature

```

%%% Using only the radiation as a source of dissipation I calculate
%%% temperature reaching a conductor traversed by current I
%%% tsing Pf (radiated) = Pd (electric)

%Copper properties
rho=1.72*10^(-8); %[ohm*m]
emissivity=0.8;

%Wire shape and electrical parameters
I=0.5; %[A]
l=0.7; %[m] 10cm*3*2[forward-bacward tails]+3cm*3*2
thickness = 35E-6; %[m]
width = logspace(-4,-2,100); %[m]

%Init Temp
T0 = 90; %[C]
T2=273.14+T0; %[K]

%Stefan-Boltzmann constant
sigma=5.67E-8; %[W/M^2*K^4]

```

```

%T final
T1=nthroot(((rho*I^2)./(sigma*emissivity*thickness*2.*width.*(width+
thickness)))+T2^4,4)
figure(1)
plot(width,T1-273.14)
str=sprintf('Tf(W) @ t=%d[m], T0=%d[C°], emiss=%d, I=%d[A]', thickness,
T0, emissivity, I);
title(str)
xlabel('W[m]')
ylabel('Tf[C°]')
grid on
ylim ([0 250]);
xlim ([0 0.005]);

```

Spin Analysis

```

%Spin Analysis

gradient = 0.3; %alpha2 - alpha1
L = 0.098; %m
W = 0.0826; %m
D = 0.010; %m
Fd = 1963 %W/m2
c = 3e8 %m/s
J = 0.003353516 %kg*m2 @ massa = 1.5kg

T = linspace(0,8640000,1000); %[sec] max 100 days

M = (Fd/c)*gradient*(7*L)*D*(W-D);

w0=T*(M/J); %rad/s
figure(1)
plot(T/(3600*24),w0*9.549296596425384)
str=sprintf('w0(T) @ Fd=%d[w/m2]', Fd);
title(str)
xlabel('Days')
ylabel('w0[rpm]')
grid on

```

Linearization of the NTC Vishay model NTCS0603E3104FXT

```

%Linearization of the NTC Vishay model NTCS0603E3104FXT

% NTC Vishay model NTCS0603E3104FXT response
NTC = [-40 3921252;-35 2774565;-30 1988706;-25 1442861;-20 1058901;-15
785573;-10 588793;-5 445602;0 340346;5 262229;10 203723;15 159522;20
125851;25 100000;30 80003;35 64422;40 52200;45 42548;50 34879;55 28749;60
23820;65 19835;70 16597;75 13951;80 11780;85 9988.4;90 8504.3;95
7269.4;100 6237.5;105 5371.7;110 4642.5;115 4025.9;120 3502.7;125
3057.1;130 2676.4;135 2350.1;140 2069.5;145 1827.4;150 1617.9]

%Circuit Paramenters
R1=22e3; %[Ohm]
R2=100e3; %[Ohm]
Vref = 3; %[V]

%NTC Vishay model NTCS0603E3104FXT response plot
figure(1)
plot(NTC(:,1),NTC(:,2)), 'b';
grid on;
title('NTC response R(C°)');

```

```

xlabel('T [C°]');
ylabel('R(T) [Ohm]');

%NTC Vishay model NTCS0603E3104FXT linearized response plot
figure(2)
V0=Vref*((NTC(:,2)*R2)./(NTC(:,2)+R2))./(((NTC(:,2)*R2)./(NTC(:,2)+R2))+R1
); %output linearized voltage value
subplot(2,1,1);
plot(NTC(:,1),V0),'b';
grid on;
xlabel('T [C°]');
ylabel('V(T) [V]');

P=Vref^2./(((NTC(:,2)*R2)./(NTC(:,2)+R2))+R1); %power dissipation of the
circuit
subplot(2,1,2);
plot(NTC(:,1),P,'r');
grid on;
xlabel('T [C°]');
ylabel('Power(T) [W]');

NTC(:,3) = V0;
NTC(:,4) = P;

save NTC;

```

9.7 SolidWorks ARAMIS materials library

This section lists all materials and their proprieties used for SolidWorks models. These are contained into an appropriate SolidWorks library called ARAMIS.

Proprietà	Valore	Unità
Modulo elastico	6.9e+010	N/m ²
Coefficiente di Poisson	0.33	N/A
Modulo di taglio	2.7e+010	N/m ²
Densità di massa	2700	kg/m ³
Resistenza alla trazione	68935600	N/m ²
Resistenza a compressione		N/m ²
Snervamento	27574200	N/m ²
Coefficiente di espansione termica	2.4e-005	/K
Conducibilità termica	200	W/(m·K)
Calore specifico	900	J/(kg·K)
Rapporto di smorzamento del materiale		N/A

Table 13: Alluminuim Alloy 1060

Proprietà	Valore	Unità
Modulo elastico	1.1e+011	N/m ²
Coefficiente di Poisson	0.37	N/A
Modulo di taglio	4e+010	N/m ²
Densità di massa	8900	kg/m ³
Resistenza alla trazione	394380000	N/m ²
Resistenza a compressione		N/m ²
Snervamento	258646000	N/m ²
Coefficiente di espansione termica	2.4e-005	/K
Conducibilità termica	390	W/(m·K)
Calore specifico	390	J/(kg·K)
Rapporto di smorzamento del materiale		N/A

Table 14: Copper

Proprietà	Valore	Unità
Modulo elastico	2.3e+010	N/m ²
Coefficiente di Poisson	0.28	N/A
Modulo di taglio		N/m ²
Densità di massa	1850	kg/m ³
Resistenza alla trazione		N/m ²
Resistenza a compressione		N/m ²
Snervamento		N/m ²
Coefficiente di espansione termica	3e-005	/K
Conducibilità termica	0.5	W/(m·K)
Calore specifico	950	J/(kg·K)
Rapporto di smorzamento del materiale		N/A

Table 15: FR4

Proprietà	Valore	Unità
Modulo elastico	4609000000	N/m ²
Coefficiente di Poisson	0.34	N/A
Modulo di taglio		N/m ²
Densità di massa	1600	kg/m ³
Resistenza alla trazione		N/m ²
Resistenza a compressione		N/m ²
Snervamento		N/m ²
Coefficiente di espansione termica	2e-005	/K
Conducibilità termica	0.12	W/(m·K)
Calore specifico	1090	J/(kg·K)
Rapporto di smorzamento del materiale		N/A

Table 16: Flexible PCB polymer

Proprietà	Valore	Unità
Modulo elastico	7.5e+010	N/m ²
Coefficiente di Poisson	0.22	N/A
Modulo di taglio	2.8022e+010	N/m ²
Densità di massa	2605	kg/m ³
Resistenza alla trazione		N/m ²
Resistenza a compressione		N/m ²
Snervamento		N/m ²
Coefficiente di espansione termica	9e-006	/K
Conducibilità termica	64	W/(m·K)
Calore specifico	320	J/(kg·K)
Rapporto di smorzamento del materiale		N/A

Table 17: Solar Panel Glass

Proprietà	Valore	Unità
Modulo elastico	30000000	N/m ²
Coefficiente di Poisson	0.48	N/A
Modulo di taglio		N/m ²
Densità di massa	1730	kg/m ³
Resistenza alla trazione		N/m ²
Resistenza a compressione		N/m ²
Snervamento		N/m ²
Coefficiente di espansione termica	0.00027	/K
Conducibilità termica	1	W/(m·K)
Calore specifico	1386	J/(kg·K)
Rapporto di smorzamento del materiale		N/A

Table 18: Panel Resin

Proprietà	Valore	Unità
Modulo elastico	1.03e+011	N/m ²
Coefficiente di Poisson	0.26	N/A
Modulo di taglio		N/m ²
Densità di massa	5323	kg/m ³
Resistenza alla trazione		N/m ²
Resistenza a compressione		N/m ²
Snervamento		N/m ²
Coefficiente di espansione termica	6e-006	/K
Conducibilità termica	59.9	W/(m·K)
Calore specifico	320	J/(kg·K)
Rapporto di smorzamento del materiale		N/A

Table 19: Germanium (Ge)

Proprietà	Valore	Unità
Modulo elastico	8.5e+010	N/m ²
Coefficiente di Poisson	0.31	N/A
Modulo di taglio		N/m ²
Densità di massa	5320	kg/m ³
Resistenza alla trazione		N/m ²
Resistenza a compressione		N/m ²
Snervamento		N/m ²
Coefficiente di espansione termica		/K
Conducibilità termica	46	W/(m·K)
Calore specifico	350	J/(kg·K)
Rapporto di smorzamento del materiale		N/A

Table 20: Gallium arsenide (GaAs)

Proprietà	Valore	Unità
Modulo elastico	1.31e+011	N/m ²
Coefficiente di Poisson		N/A
Modulo di taglio		N/m ²
Densità di massa	8360	kg/m ³
Resistenza alla trazione		N/m ²
Resistenza a compressione		N/m ²
Snervamento		N/m ²
Coefficiente di espansione termica	1.7e-005	/K
Conducibilità termica	105	W/(m·K)
Calore specifico	360	J/(kg·K)
Rapporto di smorzamento del materiale		N/A

Table 21: Copper beryllium (CuBe) alloy 260

Proprietà	Valore	Unità
Modulo elastico	1.1858961e+013	N/m ²
Coefficiente di Poisson	0.4	N/A
Modulo di taglio	11238434	N/m ²
Densità di massa	7300	kg/m ³
Resistenza alla trazione	11858961	N/m ²
Resistenza a compressione		N/m ²
Snervamento		N/m ²
Coefficiente di espansione termica		/K
Conducibilità termica	34	W/(m·K)
Calore specifico	0.228	J/(kg·K)
Rapporto di smorzamento del materiale		N/A

Table 22: Low melting temperature tin, Indalloy_1E_118°C

Proprietà	Valore	Unità
Modulo elastico	2.2059e+011	N/m ²
Coefficiente di Poisson	0.22	N/A
Modulo di taglio	9.0407e+010	N/m ²
Densità di massa	2300	kg/m ³
Resistenza alla trazione	172340000	N/m ²
Resistenza a compressione	551490000	N/m ²
Snervamento		N/m ²
Coefficiente di espansione termica	1.08e-005	/K
Conducibilità termica	1.4949	W/(m·K)
Calore specifico	877.96	J/(kg·K)
Rapporto di smorzamento del materiale		N/A

Table 23: Ceramic

Proprietà	Valore	Unità
Modulo elastico	10000000	N/m ²
Coefficiente di Poisson	0.45	N/A
Modulo di taglio		N/m ²
Densità di massa	750	kg/m ³
Resistenza alla trazione	18000000	N/m ²
Resistenza a compressione		N/m ²
Snervamento		N/m ²
Coefficiente di espansione termica		/K
Conducibilità termica	0.25	W/(m·K)
Calore specifico	1737	J/(kg·K)
Rapporto di smorzamento del materiale		N/A

Table 24: Generic Rubber

Proprietà	Valore	Unità
Modulo elastico	1e+015	N/m ²
Coefficiente di Poisson		N/A
Modulo di taglio	1e+015	N/m ²
Densità di massa	100	kg/m ³
Resistenza alla trazione	1e+015	N/m ²
Resistenza a compressione	1e+015	N/m ²
Snervamento	1e+015	N/m ²
Coefficiente di espansione termica	0	/K
Conducibilità termica	1000000	W/(m·K)
Calore specifico	1000	J/(kg·K)
Rapporto di smorzamento del materiale		N/A

Table 25: Generic stiff body

9.8 BK1B213A1 Management Software

9.8.1 Bk1B111X_CubeSat_Thermal_Fuser <<SW>>

- **Init()**

```
switch (DCHAN) {
  case 0:
    SLOT::D0.output ();
    break;
  case 1:
    SLOT::D1..output ();
    break;
  case 2:
    SLOT::D2..output ();
    break;
  case 3:
    SLOT::D3..output ();
    break;
  case 4:
    SLOT::D4..output ();
    break;
  case 5:
    SLOT::D5..output ();
    break;
  case 6:
    SLOT::D6..output ();
    break;
  case 7:
    SLOT::D7..output ();
    break;
  case 8:
    SLOT::D8..output ();
    break;
  case 9:
    SLOT::D9..output ();
    break;
}
```

```
TempSensor.init ();
```

- **housekeeping()**

```
TempSensor.housekeeping (FUSER); //Save temp into housekeeping
FusersCheck (FUSER);
```

- **ENABLE (EN: bool)**

```
switch (DCHAN) {
  case 0:
    SLOT::D0.write (EN);
    break;
  case 1:
    SLOT::D1.write (EN);
    break;
  case 2:
    SLOT::D2.write (EN);
    break;
  case 3:
    SLOT::D3.write (EN);
    break;
  case 4:
```

```

        SLOT::D4.write(EN);
        break;
    case 5:
        SLOT::D5.write(EN);
        break;
    case 6:
        SLOT::D6.write(EN);
        break;
    case 7:
        SLOT::D7.write(EN);
        break;
    case 8:
        SLOT::D8.write(EN);
        break;
    case 9:
        SLOT::D9.write(EN);
        break;
}

//Update Status Register
HK::statusRegister[STATUS_REG].set(EN)

```

- **FusersCheck(TF : t HK_FIELDS)**

```

if (HK::housekeeping[TF] >= TempThreshold) {
    ENABLE(DCHAN, false);
} else
    ENABLE(DCHAN, true);
}

```

- **SetTemperature(value : ushort)**

```
TempThreshold = value;
```

9.8.2 Bk1B133CS_Temperature_Sensor <<SW>>

- **Init()**

```

switch(ACHAN) {
case 0:
    SLOT::A0.init();
    break;
case 1:
    SLOT::A1.init();
    break;
}

```

- **housekeeping(index : ushort)**

```

switch (index) {
case HK_INDEX:
    switch (ACHAN) {
        case 0:
            SLOT::A0.acquire(HK::housekeeping[HK_INDEX]);
            break;
        case 1:
            SLOT::A1.acquire(HK::housekeeping[HK_INDEX]);
            break;
    }
}

```

```
}  
}
```

```
-----  
  
switch (index) {  
case HK_INDEX:  
switch (ACHAN) {  
case 0:  
SLOT::A0.select();  
start();  
while(!IsReady());  
N=Read();  
if((N>=3826) || (N<=520)) //temperature higher then 130°C or less then 0°C  
{  
HK::statusRegister[CONFIG_STATUS].set(OVERTEMP);  
}  
  
if(ORDER==1)  
{  
Nletto=N;  
}  
elseif(ORDER==3)  
{  
mat1=(Bx_3+N*Ax_3)/C_256;  
mat2=N*mat1;  
mat3=(mat2_3/C_512);  
mat4= mat3+Cx_3;  
mat5=((N*mat4)/C_1024);  
Nletto=mat5+Dx_3;  
}  
elseif(ORDER==5)  
{  
mat1=(N*Ax_5+Bx_5)/C_1024;  
mat2=mat1*N;  
mat3=2*(mat2/C_1024);  
mat4=mat3+Cx_5;  
mat5=((N*mat4)/C_1024);  
mat6=mat5+Dx_5;  
mat7=((N*mat6)/C_1024);  
mat8=mat7+Ex_5;  
mat9=((N*mat8)/C_1024);  
Nletto=mat9+Fx_5;  
}  
Temp=Nletto/100;  
  
break;  
case 1:  
SLOT::A1.select();  
start();  
while(!IsReady());  
N=Read();  
if((N>=3826) || (N<=520)) //temperature higher then 130°C or less then 0°C  
{  
HK::statusRegister[CONFIG_STATUS].set(OVERTEMP);  
}  
  
if(ORDER==1)  
{  
Nletto=N;  
}  
}
```

```

elseif (ORDER==3)
{
    mat1=(Bx_3+N*Ax_3)/C_256;
    mat2=N*mat1;
    mat3=(mat2_3/C_512);
    mat4= mat3+Cx_3;
    mat5=((N*mat4)/C_1024);
    Nletto=mat5+Dx_3;
}
elseif (ORDER==5)
{
    mat1=(N*Ax_5+Bx_5)/C_1024;
    mat2=mat1*N;
    mat3=2*(mat2/C_1024);
    mat4=mat3+Cx_5;
    mat5=((N*mat4)/C_1024);
    mat6=mat5+Dx_5;
    mat7=((N*mat6)/C_1024);
    mat8=mat7+Ex_5;
    mat9=((N*mat8)/C_1024);
    Nletto=mat9+Fx_5;
}
Temp=Nletto/100;
HK::housekeeping[HK_TEMPERATURE_B]=Temp;
break;
}
}

```

9.8.3 MuxControl <<SW>>

- Init()

```

switch (DCHAN_SEL0) {
case 0:
    SLOT::D0.output();
    break;
case 1:
    SLOT::D1.output();
    break;
case 2:
    SLOT::D2.output();
    break;
case 3:
    SLOT::D3.output();
    break;
case 4:
    SLOT::D4.output();
    break;
case 5:
    SLOT::D5.output();
    break;
case 6:
    SLOT::D6.output();
    break;
case 7:
    SLOT::D7.output();
    break;
case 8:
    SLOT::D8..output();
    break;
case 9:

```

```

        SLOT::D9..output();
        break;
    }

switch (DCHAN_SEL1) {
    case 0:
        SLOT::D0..output();
        break;
    case 1:
        SLOT::D1..output();
        break;
    case 2:
        SLOT::D2..output();
        break;
    case 3:
        SLOT::D3..output();
        break;
    case 4:
        SLOT::D4..output();
        break;
    case 5:
        SLOT::D5..output();
        break;
    case 6:
        SLOT::D6..output();
        break;
    case 7:
        SLOT::D7..output();
        break;
    case 8:
        SLOT::D8..output();
        break;
    case 9:
        SLOT::D9..output();
        break;
}
switch (DCHAN_SEL2) {
    case 0:
        SLOT::D0..output();
        break;
    case 1:
        SLOT::D1..output();
        break;
    case 2:
        SLOT::D2..output();
        break;
    case 3:
        SLOT::D3..output();
        break;
    case 4:
        SLOT::D4..output();
        break;
    case 5:
        SLOT::D5..output();
        break;
    case 6:
        SLOT::D6..output();
        break;
    case 7:
        SLOT::D7..output();
        break;
    case 8:

```

```

    SLOT::D8..output();
    break;
case 9:
    SLOT::D9..output();
    break;
}

```

- **housekeeping(index : ushort)**

```

if ((index >= HK_FIRST_INDEX) && (index < HK_FIRST_INDEX+NUM_CHAN)) {
    SELECT (index-HK_FIRST_INDEX);
}

```

- **SELECT(CH : int)**

```

switch (DCHAN_SEL0) {
case 0:
    SLOT::D0.write(CH&0x1);
    break;
case 1:
    SLOT::D1.write(CH&0x1);
    break;
case 2:
    SLOT::D2.write(CH&0x1);
    break;
case 3:
    SLOT::D3.write(CH&0x1);
    break;
case 4:
    SLOT::D4.write(CH&0x1);
    break;
case 5:
    SLOT::D5.write(CH&0x1);
    break;
case 6:
    SLOT::D6.write(CH&0x1);
    break;
case 7:
    SLOT::D7.write(CH&0x1);
    break;
case 8:
    SLOT::D8.write(CH&0x1);
    break;
case 9:
    SLOT::D9.write(CH&0x1);
    break;
}

```

```

switch (DCHAN_SEL1) {
case 0:
    SLOT::D0.write(CH&0x2);
    break;
case 1:
    SLOT::D1.write(CH&0x2);
    break;
case 2:
    SLOT::D2.write(CH&0x2);
    break;
case 3:
    SLOT::D3.write(CH&0x2);
    break;
}

```

```

case 4:
    SLOT::D4.write(CH&0x2);
    break;
case 5:
    SLOT::D5.write(CH&0x2);
    break;
case 6:
    SLOT::D6.write(CH&0x2);
    break;
case 7:
    SLOT::D7.write(CH&0x2);
    break;
case 8:
    SLOT::D8.write(CH&0x2);
    break;
case 9:
    SLOT::D9.write(CH&0x2);
    break;
}
switch (DCHAN_SEL2) {
case 0:
    SLOT::D0.write(CH&0x4);
    break;
case 1:
    SLOT::D1.write(CH&0x4);
    break;
case 2:
    SLOT::D2.write(CH&0x4);
    break;
case 3:
    SLOT::D3.write(CH&0x4);
    break;
case 4:
    SLOT::D4.write(CH&0x4);
    break;
case 5:
    SLOT::D5.write(CH&0x4);
    break;
case 6:
    SLOT::D6.write(CH&0x4);
    break;
case 7:
    SLOT::D7.write(CH&0x4);
    break;
case 8:
    SLOT::D8.write(CH&0x4);
    break;
case 9:
    SLOT::D9.write(CH&0x4);
    break;
}

```

9.8.4 Bk1B213A1_main <<SW>> <<main>>

- **Init()**

```

Proc.cpu.init();    //MCU init

Mux.init(); //Mux Init
F1.init(); //Fusers Init
F2.init();

```

```

F3.init ();
F4.init ();
F5.init ();
F6.init ();
F7.init ();
F8.init ();

//Global Enable init
switch (DCHAN_EN) {
    case 0:
        SLOT::D0.output ();
        break;
    case 1:
        SLOT::D1..output ();
        break;
    case 2:
        SLOT::D2..output ();
        break;
    case 3:
        SLOT::D3..output ();
        break;
    case 4:
        SLOT::D4..output ();
        break;
    case 5:
        SLOT::D5..output ();
        break;
    case 6:
        SLOT::D6..output ();
        break;
    case 7:
        SLOT::D7..output ();
        break;
    case 8:
        SLOT::D8..output ();
        break;
    case 9:
        SLOT::D9..output ();
        break;
}

__enable_interrupt ();

```

- **housekeeping(index : ushort)**

```

Mux.housekeeping (index) ;
switch (index) {
    case FUSER1:
        F1.housekeeping ();
        break;
    case FUSER2:
        F2.housekeeping ();
        break;
    case FUSER3:
        F3.housekeeping ();
        break;
    case FUSER4:
        F4.housekeeping ();
        break;
    case FUSER5:
        F5.housekeeping ();

```

```

        break;
    case FUSER6:
        F6.housekeeping();
        break;
    case FUSER7:
        F7.housekeeping();
        break;
    case FUSER8:
        F8.housekeeping();
        break;
}

```

- **interpret(command : ushort)**

```

switch (command) {
    case CMD_SET_CONFIGURATION:
    case CMD_RESET_CONFIGURATION:
    case CMD_WRITE_CONFIGURATION:
        //ENABLE(HK::housekeeping[CONFIG_STATUS] &ENABLED);
        break;
    case CMD_BLOW_FUSERS:
        StartOpening(Temperature)
        break;
}

```

- **isr_timerA0()**

```

housekeeping(index);

if (index == MAXSLOTS-1) {
    HK::updateStatistics();
    HK::updateHistory();
}

index++;
if (index >= MAXSLOTS) {
    index = 0;
    seconds++;
    if (seconds >= 100)
        seconds = 0;
}

```

- **isr_adc12()**

```

// Reads value and stores into user-defined address
*Proc.cpu.adc.get_value_ptr() = Proc.cpu.adc.read();

Proc.cpu.adc.clearInterrupt();

```

- **EOS_EN(DCHAN : int, EN : bool)**

```

switch (DCHAN) {
    case 0:
        SLOT::D0.write(EN);
        break;
    case 1:
        SLOT::D1.write(EN);
        break;
}

```

```

case 2:
    SLOT::D2.write(EN);
    break;
case 3:
    SLOT::D3.write(EN);
    break;
case 4:
    SLOT::D4.write(EN);
    break;
case 5:
    SLOT::D5.write(EN);
    break;
case 6:
    SLOT::D6.write(EN);
    break;
case 7:
    SLOT::D7.write(EN);
    break;
case 8:
    SLOT::D8.write(EN);
    break;
case 9:
    SLOT::D9.write(EN);
    break;
}

//Update Status Reg
HK::statusRegister[ENABLE_ST].set(EN)

```

- **StartOpening(temp : ushort)**

```

Proc.cpu.adc.enable();

//All fuser can reach the temp temperature
F1.SetTemperature(temp);
F2.SetTemperature(temp);
F3.SetTemperature(temp);
F4.SetTemperature(temp);
F5.SetTemperature(temp);
F6.SetTemperature(temp);
F7.SetTemperature(temp);
F8.SetTemperature(temp);

//Enable all fusers
EOS_EN(DCHAN_EN, HK::configRegister[CONFIG_STATUS].test(ATTACHED & ENABLE));
F1.ENABLE(HK::configRegister[CONFIG_STATUS].test(ATTACHED & EN_FUSER1));
F2.ENABLE(HK::configRegister[CONFIG_STATUS].test(ATTACHED & EN_FUSER2));
F3.ENABLE(HK::configRegister[CONFIG_STATUS].test(ATTACHED & EN_FUSER3));
F4.ENABLE(HK::configRegister[CONFIG_STATUS].test(ATTACHED & EN_FUSER4));
F5.ENABLE(HK::configRegister[CONFIG_STATUS].test(ATTACHED & EN_FUSER5));
F6.ENABLE(HK::configRegister[CONFIG_STATUS].test(ATTACHED & EN_FUSER6));
F7.ENABLE(HK::configRegister[CONFIG_STATUS].test(ATTACHED & EN_FUSER7));
F8.ENABLE(HK::configRegister[CONFIG_STATUS].test(ATTACHED & EN_FUSER8));

while((HK::statusRegister[EN_ST_FUSER1].test(true) ||
    HK::statusRegister[EN_ST_FUSER2].test(true) ||
    HK::statusRegister[EN_ST_FUSER3].test(true) ||
    HK::statusRegister[EN_ST_FUSER4].test(true) ||
    HK::statusRegister[EN_ST_FUSER5].test(true) ||
    HK::statusRegister[EN_ST_FUSER6].test(true) ||
    HK::statusRegister[EN_ST_FUSER7].test(true) ||

```

```
HK::statusRegister[EN_ST_FUSER8].test(true) &&
seconds<20){
}

//Disable all fusers
EOS_EN(DCHAN_EN, false);
F1.ENABLE(false);
F2.ENABLE(false);
F3.ENABLE(false);
F4.ENABLE(false);
F5.ENABLE(false);
F6.ENABLE(false);
F7.ENABLE(false);
F8.ENABLE(false);

Proc.cpu.adc.disable();

Proc.cpu.timerA0.stop();
Proc.cpu.timerA0.disableInterrupt(0);
```

Bibliography

- [1] M. B. D. D. C. A. H. C. P. D. R. C. S. S. S. M. T. N. U. A. V. A. C. M. B. L. S. L.M. Reyneri, «ARAMIS – an alternative approach to CubeSats for more demanding satellite applications,» Würzburg, 2009.
- [2] C. Space, «Deployable CubeSat Solar Panels,» [Online]. Available: http://www.clyde-space.com/cubesat_shop/solar_panels_-_deployable.
- [3] C. P. State University, Poly Picosatellite Orbital Deployer, in CubeSat Design Specification (CDS).
- [4] Dassault System, Technical Reference SolidWorks Flow Simulation, 2014.
- [5] Dassault Systemes , Tutorial SolidWorks Flow Simulation, 2014.
- [6] Dassault Systemes, Dassault Systemes, [Online]. Available: <http://help.solidworks.com/>.
- [7] A. Ali, «1B111B Solar Panel,» in *Power Management, Attitude Determination and Control Systems of Small Satellites*, Turin, 2014, p. 40.
- [8] «Meshing,» Dassault Systemes, [Online]. Available: http://help.solidworks.com/2014/English/SolidWorks/cworks/c_Background_on_Meshing.htm.
- [9] Dassault Systemes, «Contatto globale,» [Online]. Available: http://help.solidworks.com/2011/Italian/SolidWorks/cworks/LegacyHelp/Simulation/Dialog_Box_Help/IDH_HELP_SET_GLOBAL_CONTACT.html.
- [10] «Frequency Analysis,» Dassault Systemes, [Online]. Available: http://help.solidworks.com/2012/English/SolidWorks/cworks/IDH_Analysis_Background_Introduction.htm?id=6613dea6b06549459dc63fe49ffff98e#Pg0&ProductType=&ProductName=.
- [11] «When to Use Dynamic Analysis,» Dassault Systemes, [Online]. Available: http://help.solidworks.com/2012/English/SolidWorks/cworks/When_to_Use_Dynamic_Analysis.htm?id=c58a9739e04f4dcc956447be0c5ff481#Pg0&ProductType=&ProductName=.
- [12] Wikipedia, «Dnepr-1,» [Online]. Available: <https://en.wikipedia.org/wiki/Dnepr-1>.
- [13] Dassault Systemes, «Smorzamento modale,» [Online]. Available: http://help.solidworks.com/2015/italian/SolidWorks/cworks/c_Modal_Damping.htm.
- [14] T. Instruments, «16-Bit Ultra-Low-Power Microcontroller, 256KB Flash, 16KB RAM, 12 Bit ADC, 2 USCs, 32-bit HW Multi,» [Online]. Available: <http://www.ti.com/product/MSP430F5437>.
- [15] T. Instruments, «MUX36xxx 36-V, Low-Capacitance, Low-Leakage-Current, Precision, Analog Multiplexers,» [Online]. Available: <http://www.ti.com/product/MUX36S08>.
- [16] L. Technology, «LT1761 - 100mA, Low Noise, LDO Micropower Regulators in TSOT-23,» [Online]. Available: <http://www.linear.com/product/LT1761>.
- [17] L. Technology, «LTC3631 - High Efficiency, High Voltage 100mA Synchronous Step-Down Converter,» [Online]. Available: <http://www.linear.com/product/LTC3631>.

- [18] T. Instruments, «SOT-23 Precision Micropower Series Voltage Reference,» [Online]. Available: <http://www.ti.com/product/LM4128/quality>.